SEDIMENTOLOGY AND TECTONICS OF THE WESTERN CAMEROS BASIN PROVINCE OF BURGOS NORTHERN SPAIN.

D. Phil. Thesis

Department of Earth Sciences

University of Oxford.

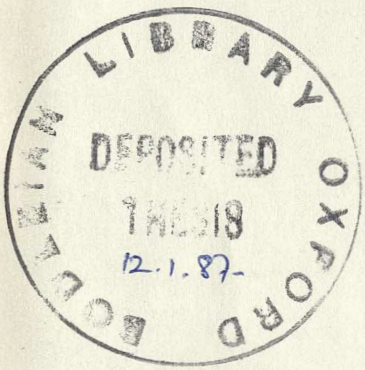

Trinity 1986.

Volume 3: Figures.

NIGEL HOWARD PLATT

Worcester College

Oxford.

Fig 4.1. Typical section through the Hortigüela Formation (younging towards camera) showing the Zurramujeres Member - alternations of 1-3m oncoidal limestone beds and marls/sands (locally micaceous; not outcropping). The base of the Formation (San Martin Member) is represented by approximately 50m of red marls (cornfield on opposite side of road). Looking N. Mambrillas de Lara.

Fig 4.2. Integrated facies model for the Hortigüela Formation. See discussion in text, section 4.2.6.

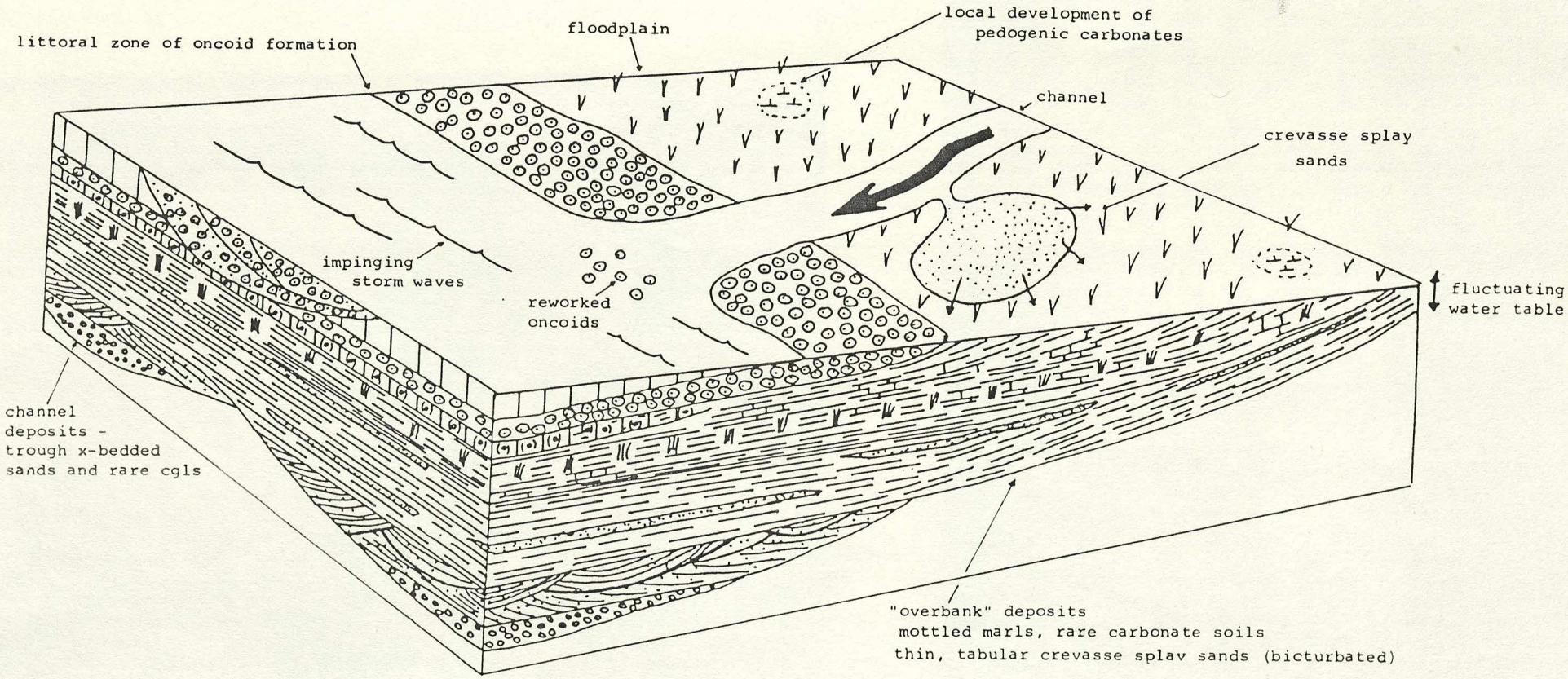

HORTIGÜELA FORMATION:

Integrated facies model.

Fig 4.3. Massive, 1m thick, oncoidal limestone bed truncating nodular and brecciated, marly, mottled, pedogenically-modified, carbonate. Oncoidal limestone has few oncoids near base (becoming more abundant towards top), and mildly erosive base; appears weakly cross-bedded near top, although this is not evident in photograph.
Interpretation: These oncoidal units are laterally very continuous (often traceable for several kilometres along strike). Their sheet-like nature argues strongly for littoral lacustrine rather than channel environments.
Zurramujeres Member. Mambrillas de Lara.

Fig 4.4. Closer view of mottled carbonate shown in fig 4.3. Weakly-developed prismatic fabric; carbonate content increasing upwards from green-purple mottled marl to white marly and nodular limestone.

Fig 4.5. Polished slab of oncoidal limestone from the Zurramujeres Member. Specimen is 20cm in length. Note: concentric structure of oncoids, although some micro-unconformities are present; some irregular nuclei, consisting of numerous oncoid fragments; one oncoid nucleated upon black clast; "bushy" growth around nuclei; spar nucleus to one oncoid (this is a common feature, especially of the larger oncoids. Oncoid may have been nucleated on vegetal material or on now-dissolved bioclast, eg bivalve or other shell fragment); some grading of oncoids; large irregular micritic limestone intraclast; abundant oncoid débris; a very little included green marl (pale blebs).

Fig 4.6. Outcrop photograph of the upper part of one oncoidal limestone unit from near the top of the Zurramujeres Member. Note: unusually thinly-bedded limestone, thicknesses varying laterally; weak cross-bedding; abundant loose oncoids resting on modern erosion surface (easily reworkable in flood events - see section 5.2). Lens cap for scale, upper left. Younging to right. Zurramujeres Member, Mambrillas de Lara.

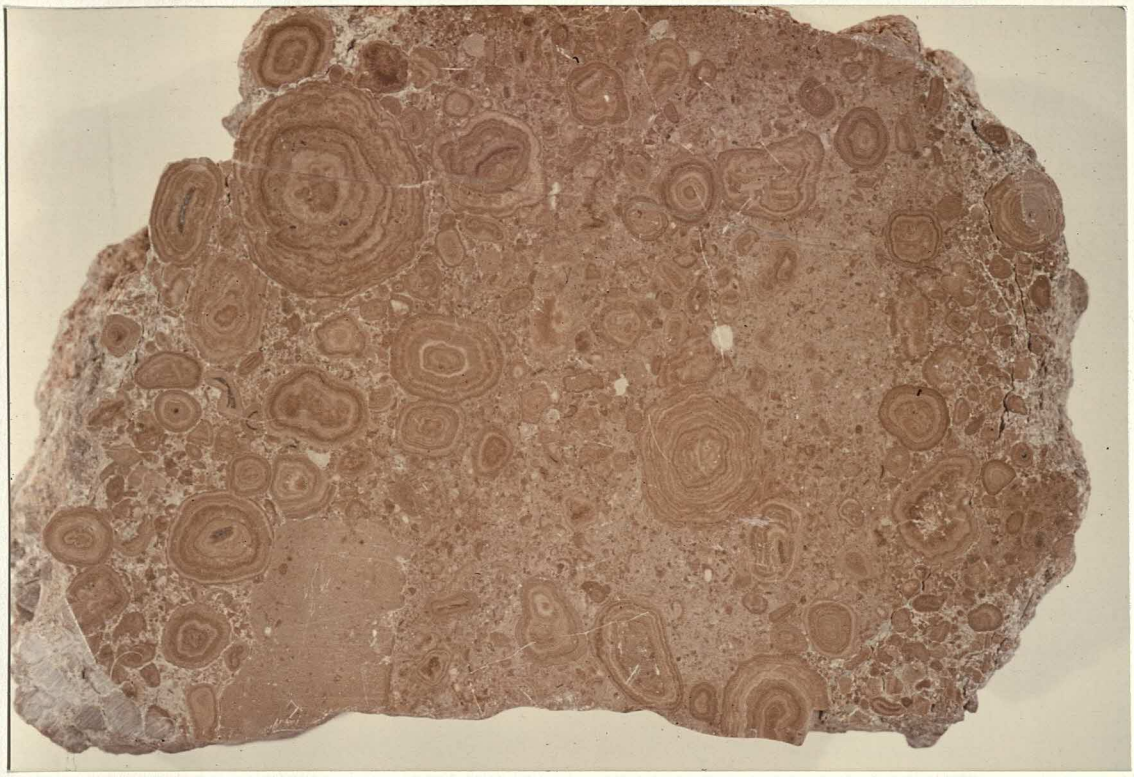

Fig 4.7. Oncoidal limestones from the same locality as fig 4.6 showing: lenticular nature of some beds (eg bed to right of hammer pick end wedges out laterally moving away from camera); large oncoids in ?weakly cross-stratified units. Younging to right.

Fig 4.8. Close-up view of the base of oncoidal limestone unit showing: very irregular, possibly erosive base; weak cross-lamination; few oncoids at base. Zurramujeres Member, Mambrillas de Lara.

Fig 4.9. Cross-bedded oncoidal limestone showing: erosive base, abundant 1-3cm rounded oncoids, especially at top of unit; intercalated coarse quartz sand with oncoid débris. Interpretation: reworking of littoral lacustrine oncoids in high energy fluvial channel. ?Zurramujeres Member. Rio Helechal, near Hortezuelos.

Fig 4.10. Same locality as fig 4.9. Cross-bedded sandy oncoidal limestone truncating weakly-mottled and -brecciated nodular, impure marly carbonate. Weakly developed prismatic fabric. Intepretation: overbank - pedogenic/ephemeral lacustrine carbonate formation in interchannel area.

Fig 4.11. Unusually large asymmetric oncoid showing: irregular oncoid fragment as nucleus; clear radial filaments; micro-unconformities; alternating layers of denser and more porous, spongy and lighter-stained micrite; some "bushy" growth at upper centre. Top surface of uppermost oncoidal limestone. Zurramujeres Member. Mambrillas de Lara. Scale bar in centimetres.

Fig 4.12. Oncoidal limestone with unusually large, moderately- to well-rounded, oncoids reaching up to 6cm at top of 1m bed. Zurramujeres Member. Valparaiso, about 2km N of Hortigüela.

Fig 4.13. Criteria for the distinction of vadoids and oncoids.

FEATURES OF ONCOIDS
USEFUL AS CRITERIA FOR THEIR DISTINCTION FROM VADOIDS.

---

1) presence of algal filaments

2) clotted, spongy texture (typical of algal structures)

3) included silt, clay etc. (suggests trapping by algal mucilage)

4) sedimentary structures indicative of high-energy environment
(vadoids are formed in situ)
eg - cross-bedding
- "cut and fill" structure

5) nuclei - reworked skeletal and non-skeletal fragments
- (vadoids are generally nucleated on vadoid fragments)

6) absence of positive indications of pedogenic origin
eg - reverse grading
- in situ downward elongation
- polygonal shapes (indicative of interference from neighbours during growth)

PLATT, N (1986)
data modified from Sbeta (1976), with additions

Fig 4.14. Classification of oncoids on the basis of internal stacking (Logan et al, 1964).

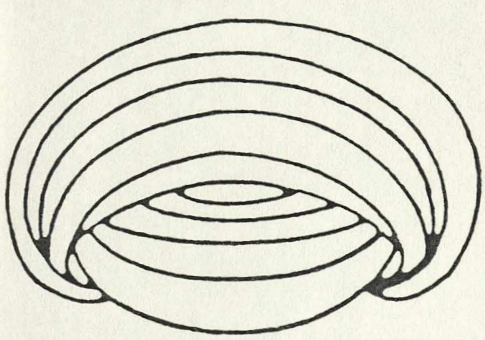

MODE "I"
INVERTED
STACKED
HEMISPHEROIDS

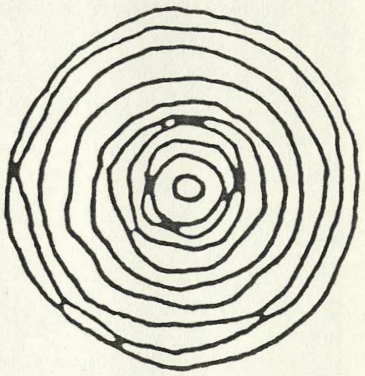

MODE "C"
CONCENTRICALLY
STACKED
SPHEROIDS

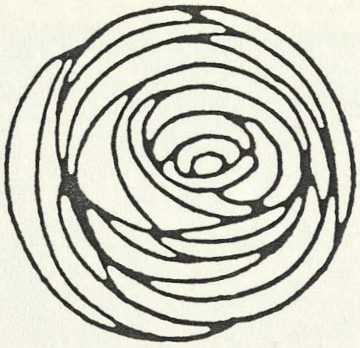

MODE "R"
RANDOMLY
STACKED
HEMISPHEROIDS

FIG. 4.—Spheroidal structures, type SS

Fig 4.15. Well-rounded, but poorly sorted, oncoids from the Hortigüela Formation (Zurramujeres Member). Concentric structure clearly visible. Interstitial finer débris of oncoid fragments. Stylolite to right of lens cap. Mambrillas de Lara.

Fig 4.16. Oncoidal limestone from the Zurramujeres Member showing concentric structure. Some irregular examples, especially the smaller ones, upper right. "Bushy" growth around nucleus, some radial filaments towards margins of oncoids. Interstitial finer débris of oncoid fragments. Stylolitisation has preferentially followed oncoid boundaries. Mambrillas de Lara.

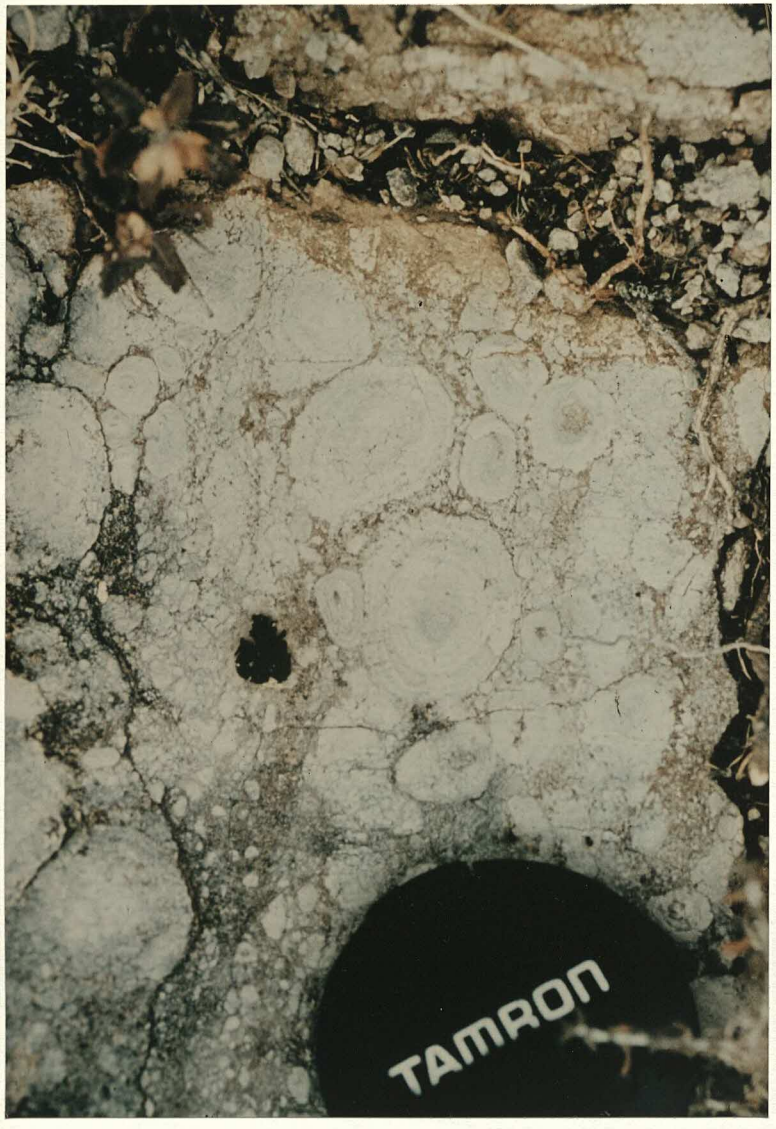
TAMRON

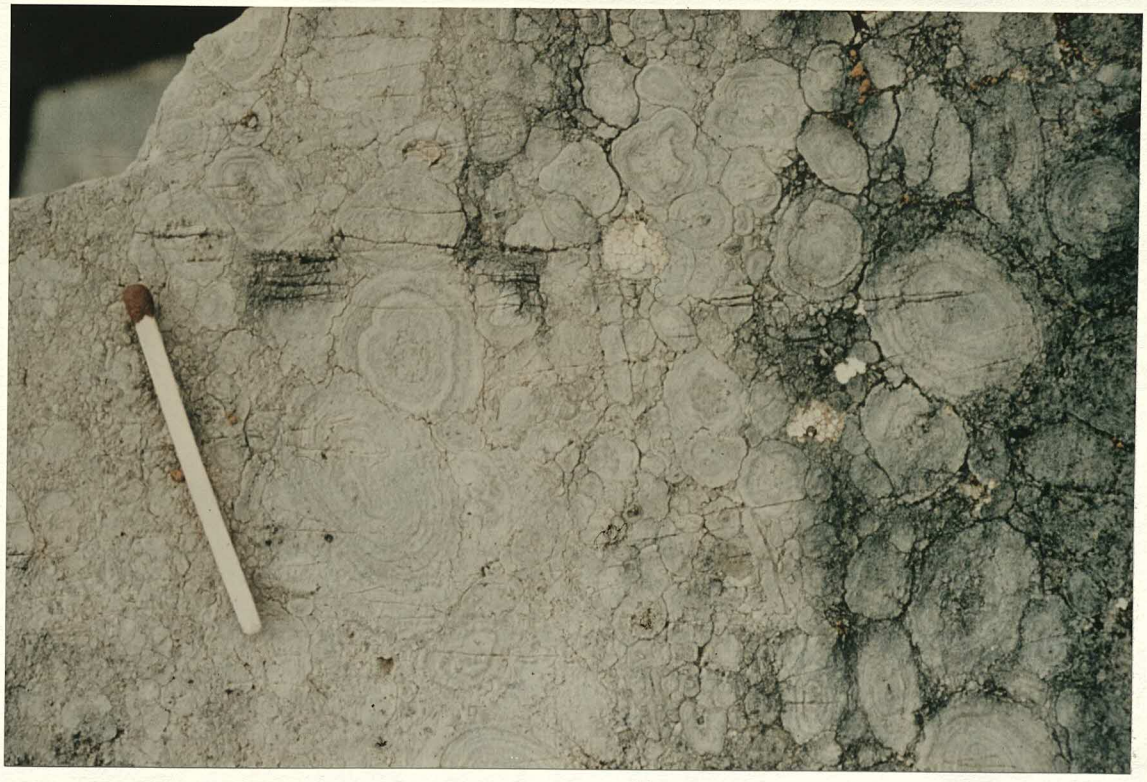

Fig 4.17. Micrograph of oncoid showing: concentric structure; radial (algal) filaments; these passing through alternating layers of spongy (poorly-calcified) and more massive carbonate; spar replacing nucleus (oncoid possibly nucleated on bivalve shell fragment); Unstained section; Field of view: 9mm. Zurramujeres Member. Mambrillas de Lara.

Fig 4.18. Similar oncoid microstructure with single filaments. Late ferroan cement-filled vein. Stained section. Field of view: 4mm. Zurramujeres Member. Mambrillas de Lara.

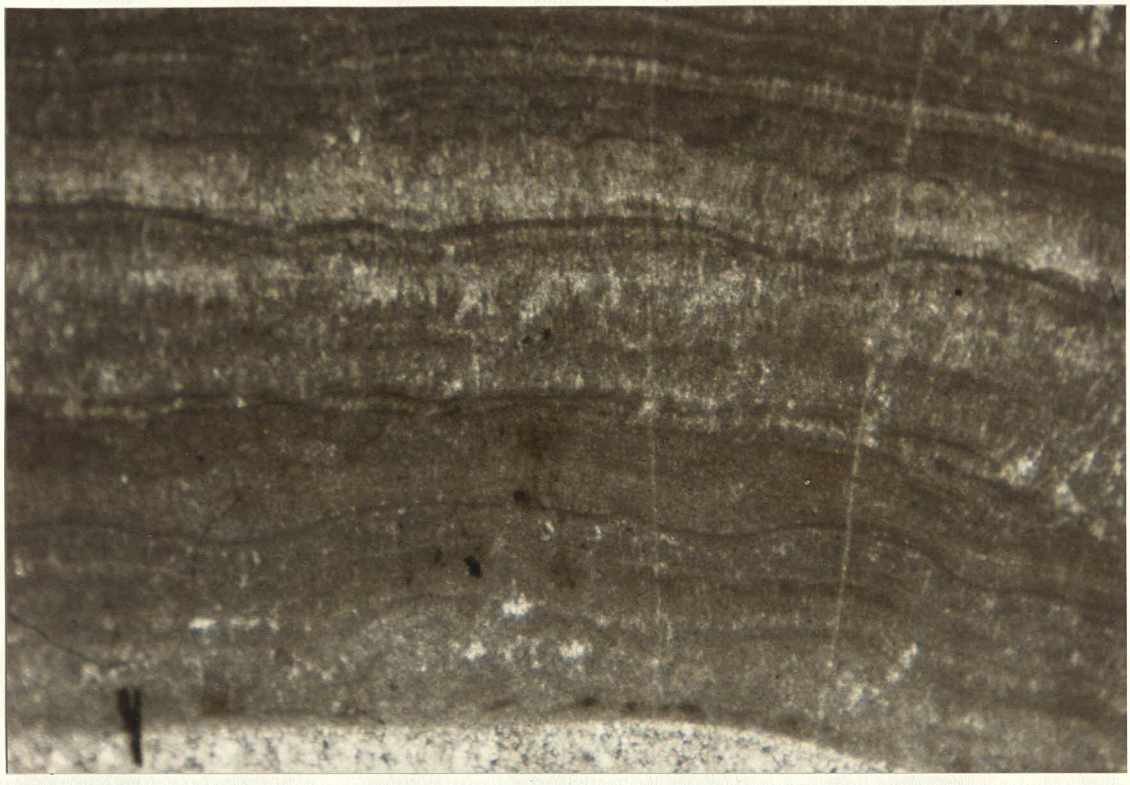

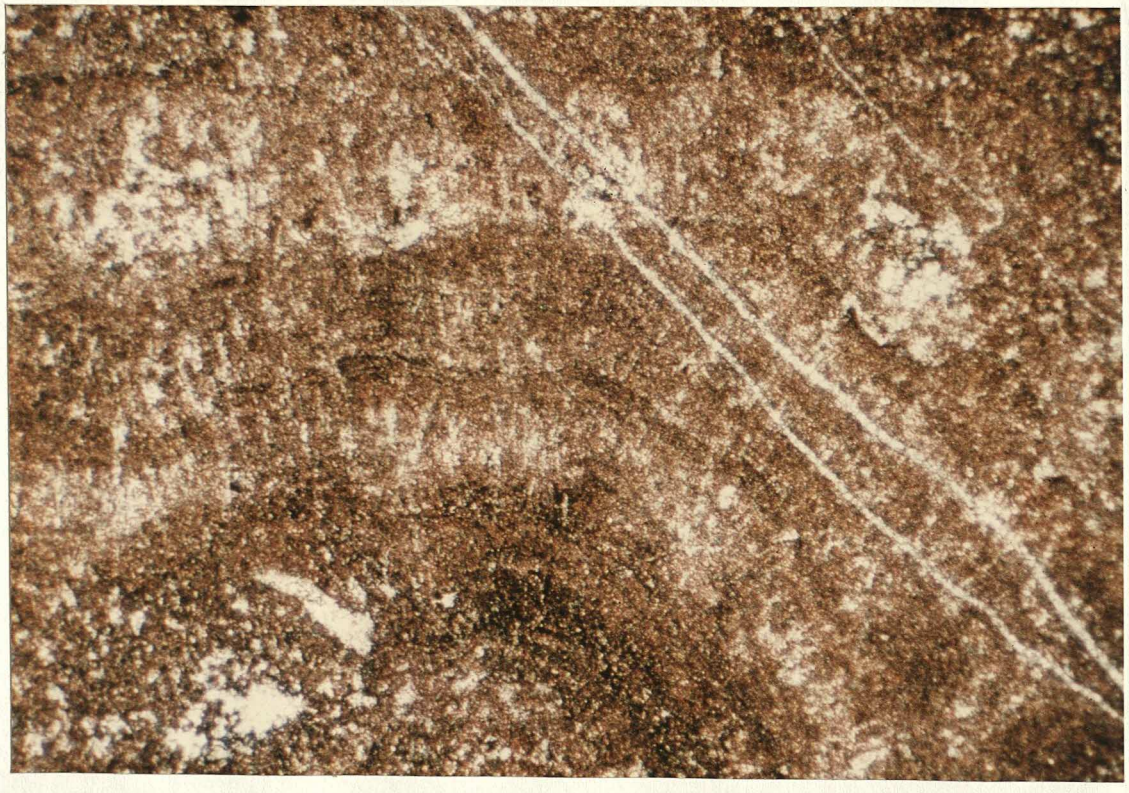

Fig 4.19. Micrograph of larger oncoid showing fan-like, bushy ("arborescent") growth of filaments. Retention of some organic matter, especially in algal filaments. Zurramujeres Member. Spongy fabric, with spar infilling cavities; this is typical of poorly-calcified oncoids. Unstained section. Field of view: 9mm. 2km N of Mambrillas de Lara.

Fig 4.20. Micrograph showing "knobbly" growth of dense micritic layers in oncoid - weakly developed "microstromatolitic" fabric. also abundant solitary filaments. Unstained section. Field of view: 9mm. Zurramujeres Member. 2km N of Mambrillas.

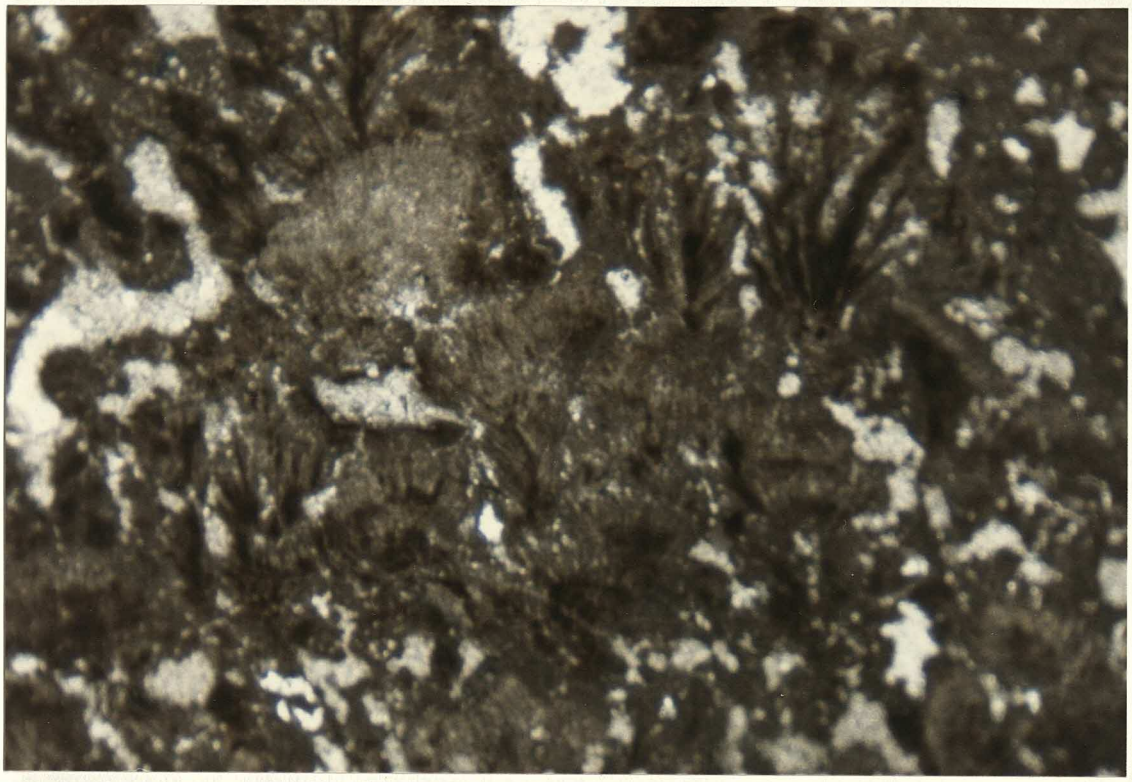

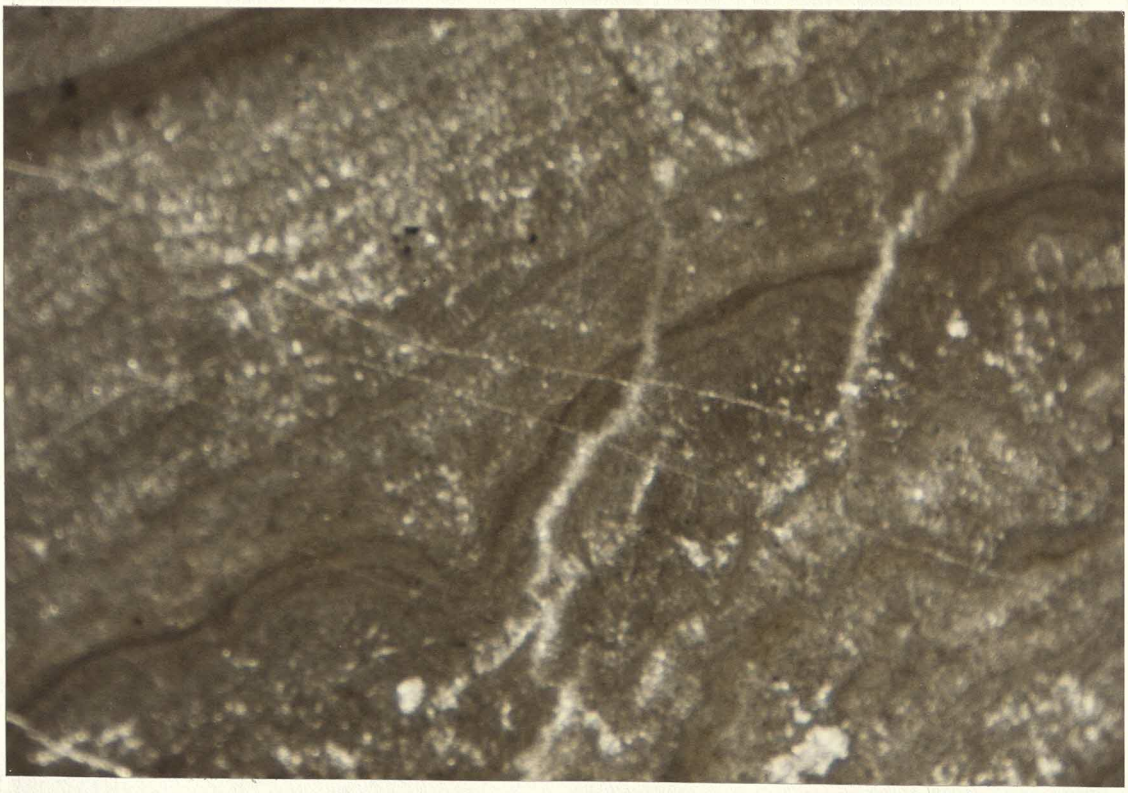

Fig 4.21. Integrated facies model for the Piedrahita de Muno Formation.

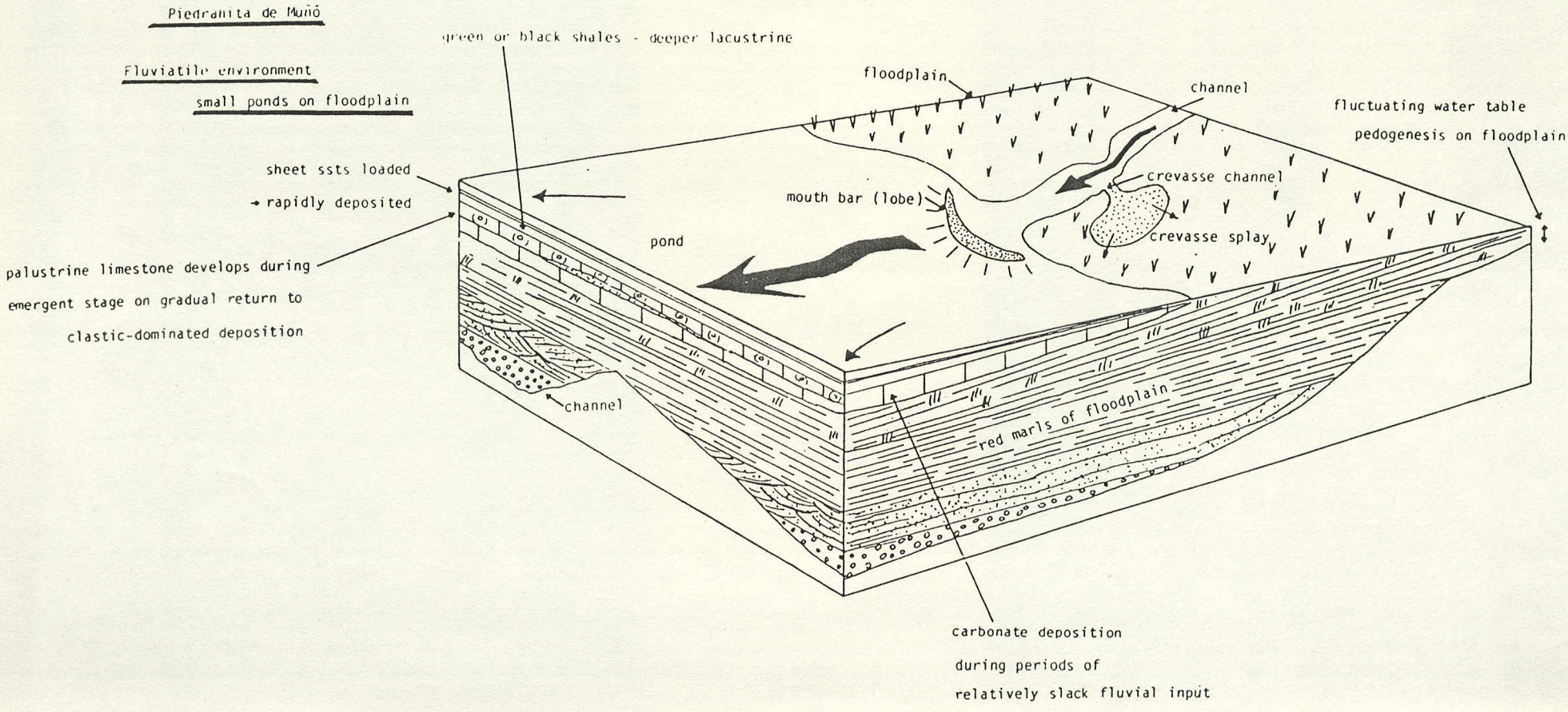
Piedranita de Muñó
Fluviatile environment
small ponds on floodplain
green or black shales - deeper lacustrine
floodplain
channel
fluctuating water table
pedogenesis on floodplain
sheet ssts loaded
→ rapidly deposited
mouth bar (lobe)
crevasse channel
crevasse splay
pond
palustrine limestone develops during
emergent stage on gradual return to
clastic-dominated deposition
channel
red marls of floodplain
carbonate deposition
during periods of
relatively slack fluvial input

Fig 4.22. Thick, generally massive, ?channel fill sand unit from near top of Piedrahita de Muno section of Piedrahita Formation (probably well below the top of the formation itself). Sand is medium grained, massive (right; erosive bases to massive channel units) or locally planar-cross-bedded (left). Sand overlies grey-green mud interpreted as distal floodplain / lacustrine. Looking W/NW. Outcrop is 5m high.

Fig 4.23. Closer view of area shown in right of fig 4.22. Note: very massive nature of sands; erosive base; thin basal pebbly lag and scattered pebbly strings. Suggestion of weak planar cross-bedding?
Interpretation: rapid channel fill, limited internal reworking.

Fig 4.24. Micrograph of sandstone from Piedrahita de Muno Formation (near base). Typical angular to subangular, and often heavily fractured, quartz grains ½ to 1mm in size. K-feldspar also present. Mafic grains 2-5%. Unstained section. Field of view: 9mm. Piedrahita de Muno.

Fig 4.25. Superb example of trough cross-bedding from near top of Piedrahita de Muno section. 2cm sets. Troughs here are viewed in (slightly oblique) transverse section, trough axis approximately perpendicular to outcrop, hence the apparently opposed dip of sets. Sands are micaceous. Fine conglomerate at base (concealed under bracken). Piedrahita de Muno Formation.
Interpretation: migration of lunate current dunes on floor of minor channel.

Fig 4.26. Thick sand unit with planar base truncating grey marl which includes thin tabular sand unit at base (minor crevasse splay). Thick sand is massive at base, but shows development of large-scale trough cross-beds towards top. Quartz pebbles or mud rip-up
clasts have eroded out to leave rounded voids immediately above hammer.
Interpretation: initially rapid sedimentation during incursion of clastic material onto flood plain; later migration of large-scale structure (linguoid sand bar / antidune) perhaps as a result of standing waves in fast-flowing flood water.
Piedrahita de Muno Formation, Piedrahita de Muno section.
Large, rounded and imbricated loose blocks from Quaternary Rio Pedroso river gravels derived from Sierra de la Demanda.

Fig 4.27. Thick sand displaying large-scale cross-bedding, (top and just above hammer). Reactivation surface at top of lower sets. Some quartz pebbles. ?Piedrahita de Muno Formation / Salas Group. Local road from Castrillo de la Reina to Moncalvillo.

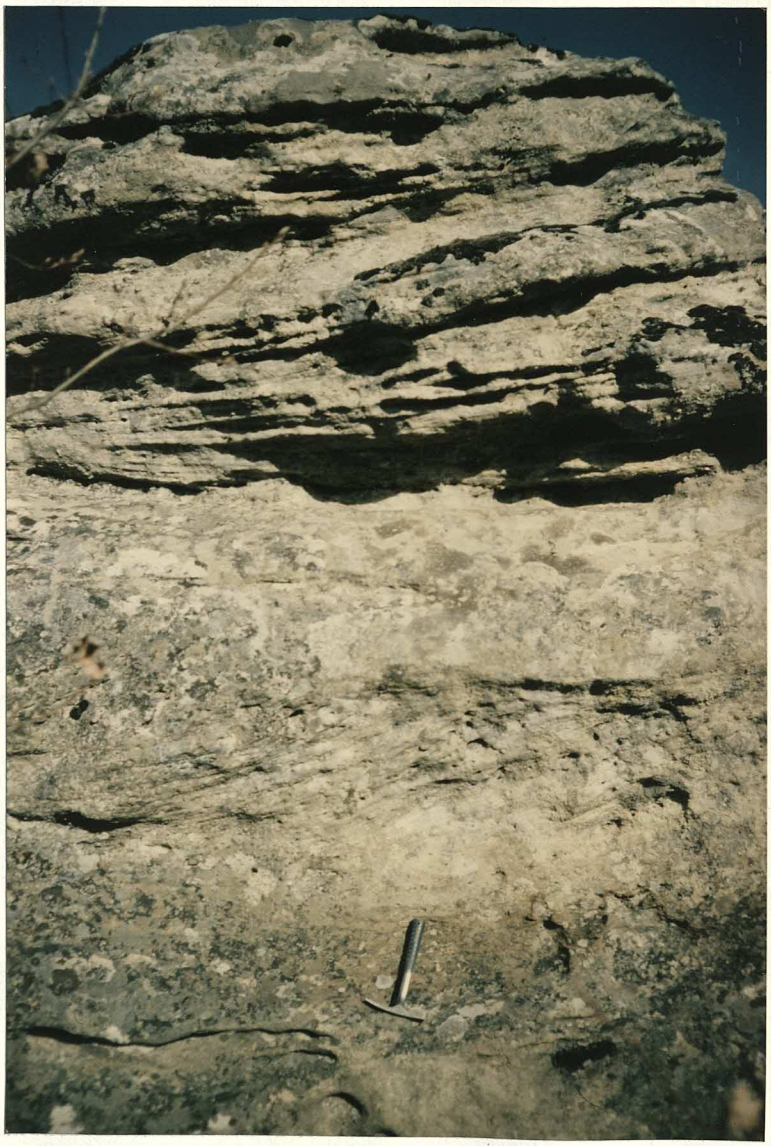

Fig 4.28. Same locality as fig 4.27. Note very large scale of cross-bedding.
Interpretation: Current migration of large-scale structures (eg antidunes?) on channel floor. High energy.

Fig 4.29. Same locality as figs 4.27 & 4.28 - showing internal reactivation surface (just below hammer).

Fig 4.30. Thicker, composite sand unit made up of tabular sand bodies. Trough cross-bedding at top of unit. Some rip-up sand/mud clasts in thin friable sand unit with irregular base (centre). Unit just visible behind gorse bush (top right) is erosive based and cross-bedded conglomerate passing upwards into trough cross-bedded sand. Silts / fine sands and muds above and below composite sand unit (poor outcrop - not visible in photograph) are cracked, deep red, and contain fine green - grey carbonate strings (rootlet action and pedogenesis on floodplain). Piedrahita de Muno Formation. Piedrahita de Muno.

Fig 4.31. Sands from the Piedrahita de Muno Formation on SE side of road from Piedrahita to Vizcainos (approximately 200m NE of church). Small scale cross-bedding picked out by black vegetal débris on sets. Sand units themselves are approximately tabular, although cross-bedded.


Estwing

Fig 4.32. Sharp (?erosive) based sand unit (centre), ?planar cross-bedded. Thinner, more tabular sand units above (right) and stacked tabular sand bodies below (left centre) - these may be proximal crevasse-splay deposits. Change in dip may be a result of tectonic disturbance. An alternative explanation might invoke bank collapse. Piedrahita de Muno Formation. Piedrahita de Muno.

Fig 4.33. Thick, very massive coarse sand unit; weak bedding developed at top. Charophyte biomicrite (fig 4.52) 3m below; nodular limestone with strong prismatic fabric above.
Interpretation: rapidly deposited sand in shallow lacustrine setting - ?mouth bar. Piedrahita de Muno Formation. Piedrahita de Muno.

Fig 4.34. Dominantly muddy sequence with intercalated thin tabular sand units and larger, lensoid sand bodies.
Interpretation: Crevasse splay units and minor crevasse channels on muddy floodplain. ?Piedrahita de Muno Formation.
Laguna Larga, N of Neila. Thick snow, April 1984.

Fig 4.35. Mud-dominated sequence with red, green and yellow-brown muds. Massive sand bodies have convex bases (and, locally, convex tops). Variable dip of sand units and convex tops probably the result of strong differential compaction of lithologically heterogeneous and laterally variable sequence.
Interpretation: Crevasse channels incising flooodplain sequence, relatively near to major channel.
2km N of Salas de los Infantes.

Fig 4.36. Stacked tabular sand units, sharp, mildly erosive bases, no internal structure. Interbedded dark brown marls. Interpretation: Crevasse splay units, background silt/marl deposition in floodplain environment. Dirty brown colour of sands interpreted as the result of mixing with muds - some included as suspended load and some introduced as a result of subsequent bioturbation. Piedrahita de Muno Formation. Piedrahita de Muno.

Fig 4.37. Top of sand unit exhibiting polygonal cracking (probably enhanced by subsequent jointing. Carbonate underneath sand with smaller-scale polygonal cracks just visible. Piedrahita de Muno Formation. 1km N of Piedrahita de Muno.

Fig 4.38. Three-toed footprint on surface of sand overlain by mud. Note morphology in strong contrast to footprints figs 3.120-3.122. Smaller surface area reflects firmer substrate. Piedrahita de Muno Formation. Near Salas de los Infantes.

Fig 4.39. Second print preserved in positive relief. Same locality as fig 4.38. Beds not inverted. Positive, rounded relief suggests the following interpretation for their formation and preservation:

1) deposition of sand
2) deposition of mud
3) imprint into mud
4) print filled by sand of overlying bed
5) erosion of beds 4) & 2) leaves sand fill of print resting on earlier sand bed 1).

Fig 4.40. Trail of prints (6 visible) from same locality as figs 4.38 & 4.39. Bipedal gait, stride 1.7m. Elongate rille on bedding plane behind sedimentologist may be gutter cast (or ??tail track). Sand bed is tabular and laterally extensive - probably a crevasse splay unit deposited onto floodplain muds.

Fig 4.41. Mottled marls (bottom) overlain by sharp-based massive sand with lobate internal geometry.
Interpretation: rapid sedimentation of sand over mud development of load balls. Piedrahita de Muno Formation. Piedrahita de Muno.

Fig 4.42. Mottled marl from Piedrahita de Muno Formation. Complex network of sheet cracks and desiccation cracks. Marls contain tubular 1cm diameter irregular carbonate cylinders up to 3cm in length.
Interpretation: Burrowing in interdistributary floodplain environment. Piedrahita de Muno Formation. Piedrahita de Muno.

Fig 4.43. Sequence younging to right including pedogenic carbonate shown in fig 4.45 (left) and slightly lenticular, erosive-based sand (right; ?sheet-flood). Floodplain marls above (centre) show mottling, a few carbonate nodules and complex pattern of carbonate-filled fine cracks - root network? Piedrahita de Muno Formation, near base. Piedrahita de Muno.

Fig 4.44. Closer view of floodplain marl shown in figs 4.45 & 4.43. Interpretation: Complex network of root hairs and larger roots, some additional desiccation brecciation. Piedrahita de Muno Formation. Piedrahita de Muno.

Fig 4.45. Typical sequence from lower part of Piedrahita de Muno Formation. Younging to right.

a) thick sand unit (left) with mildly erosive base and rare cross-bedding
b) muds, with interbedded
c) tabular sand bodies (eg centre)
d) nodular carbonate profile (by hammer) with mottling, increasing carbonate content and more nodular fabric to top.

Interpretations:

a) rapid clastic sedimentation on floodplain - terminal alluvial fan?
b) floodplain overbank / interchannel muds
c) crevasse splay units
d) pedogenic carbonate nodules ("cornstones"; cf fig 3.64) forming calcimorph nodular carbonate soil. Piedrahita de Muno.

Fig 4.46. Closer view of carbonate profile shown in fig 4.45. Large nodules of impure carbonate developed on bioturbated, red floodplain silt. Increasing carbonate content towards top (right); weak prismatic fabric in mottled marls (left). Carbonate concentration was facilitated by rapid flood- and desiccation-induced vertical fluctuations of the water table, allowing alternations between phreatic, vadose and dry conditions. Piedrahita de Muno Formation. Piedrahita de Muno.

Fig 4.47. Another carbonate profile from Piedrahita de Muno Formation, Piedrahita de Muno section. Very nodular aspect of carbonates; some brecciation at top suggests minor reworking. Younging to right.

Fig 4.48. Marls displaying strong vertical mottling overlain by impure white carbonate with strong prismatic fabric.
Interpretation: Strong pedogenic modification of floodplain marls associated with root penetration, followed by carbonate production in lacustrine interlude. Subsequent emergence and strong pedogenic modification of carbonate; some brecciation at top.
Piedrahita de Muno Formation. 1km NE of Vizcainos.

Fig 4.49. Closer view of mottled carbonate exhibiting strong vertical mottling and minor carbonate nodule development. Impure carbonate above displaying very nodular fabric.
Interpretation: Pedogenic modification of floodplain marl associated with root penetration. Piedrahita de Muno Formation. 1km NE of Vizcainos.

Fig 4.50. Micrographs of nodular carbonate shown in fig 4.47. Note: glaebule; circumgranular cracks; much included quartz as fine detrital grains (white blobs in matrix). Similar fabric to that shown by pedogenically-modified lacustrine carbonates (see figs 3.53 - 3.56; 3.71; 3.87 etc), but much higher detrital content.
Interpretation: Development of carbonate by growth of replacive calcite.
Piedrahita de Muno Formation. Piedrahita de Muno.

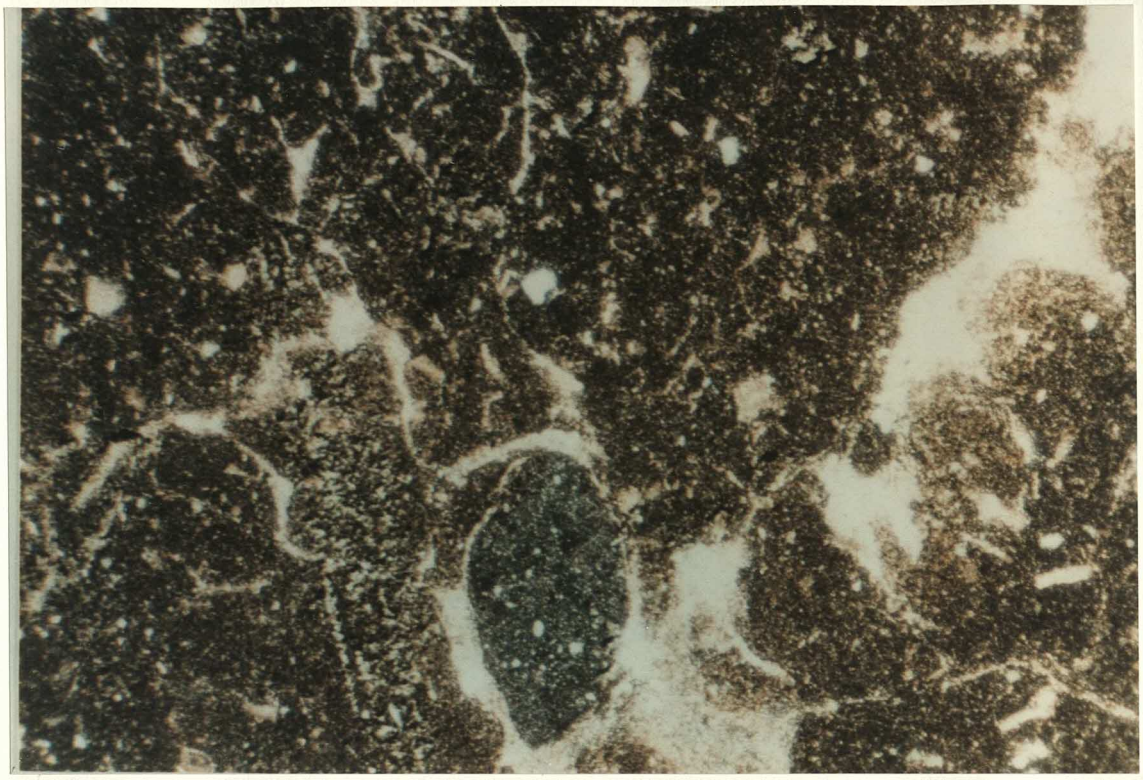

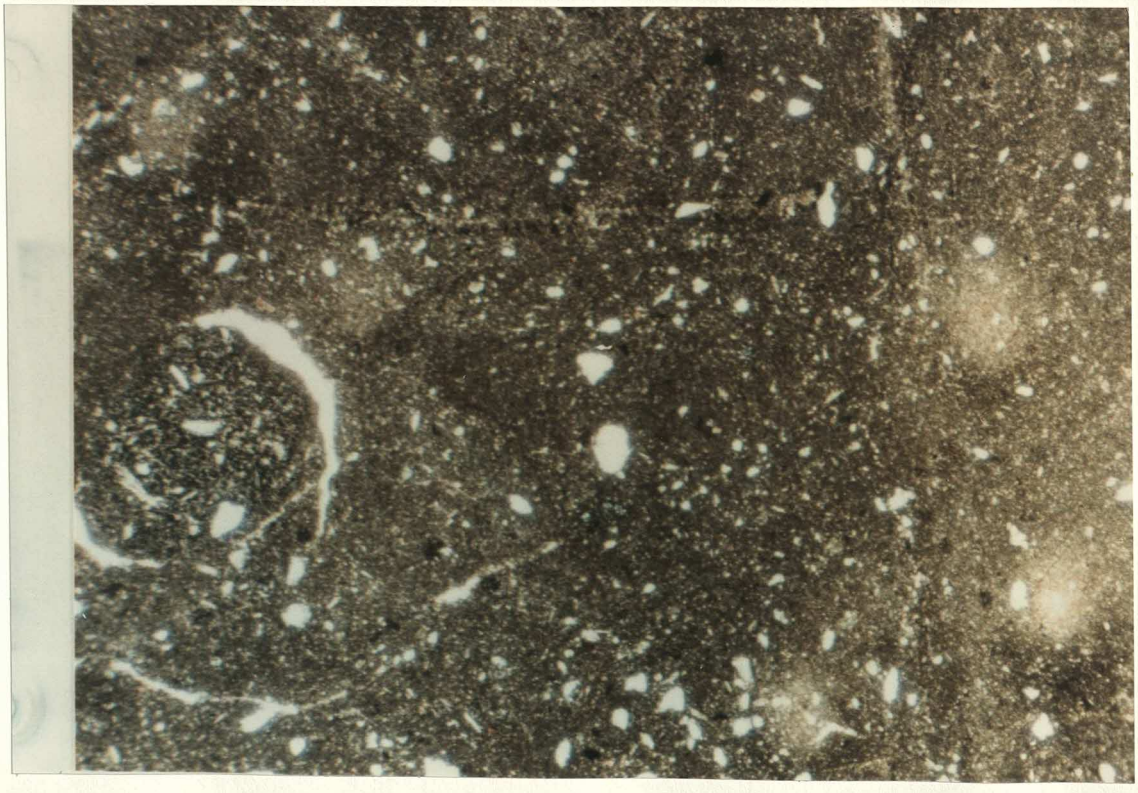

Fig 4.51. Formation of perched water tables as a result of temporary floods - a mechanism for the production of pedogenic carbonates in semi-arid environments.

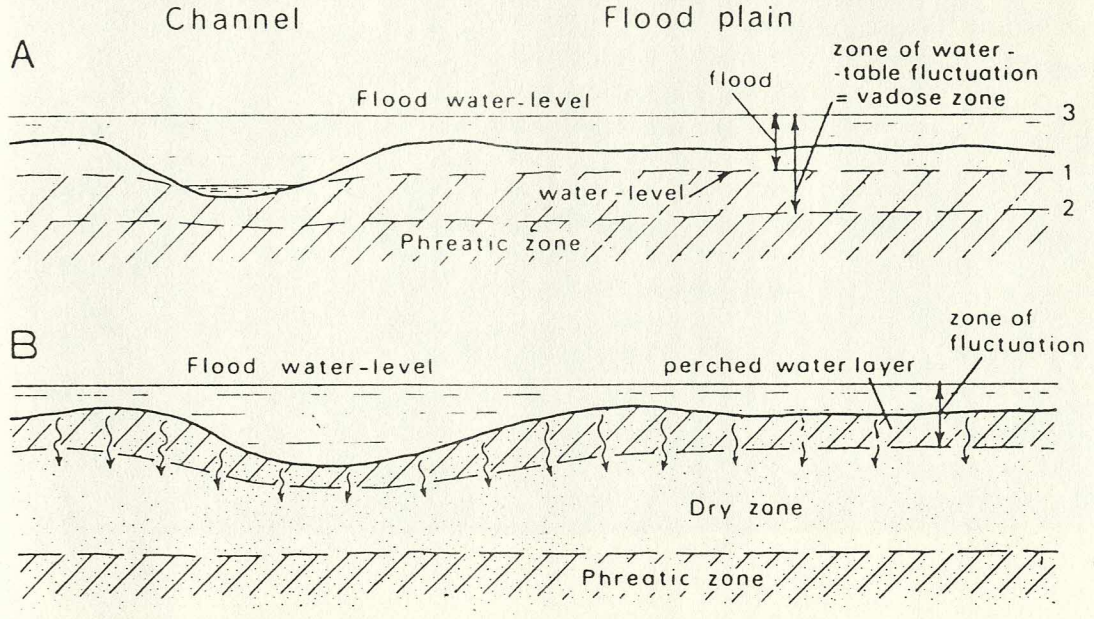

Possible relationships between flood-plain soil formation and water-table fluctuation.

A. The phreatic water-table is of variable depth, being in equilibrium with the free water of the adjacent channel during low-water stage (line 1), or with subterranean waters when the channel is dry (line 2). Highest phreatic level occurs only during floods (3) when the water-table rises above soil level. This is the classical mechanism leading to reoxidized gley soils (see Fig. 34).

B. Alternative hypothesis: the phreatic water-table is very deep and is separated from the soil by a dry zone. When flood-waters inundate the flood-plain these waters impregnate the uppermost mudstones, forming a perched water-table, and disappear progressively by evapo-transpiration, or by infiltration downwards to the deeper phreatic water. In this example, evolution of the soil is not complete there being no permanently saturated near-surface zone, and therefore no gley horizon. This is the mechanism of pseudo-gley formation, both in soils affecting Paris Basin loesses (Duchaufour 1964) and fluvial plains such as Mesopotamia (Purser et al. 1982).

Freytet & Plaziat (1982)

Fig 4.52. Biomicrite with charophyte stems in transverse and oblique sections. Stems preserve central tube. Attached (and abundant disarticulated) cortical cells. Also oogonium, showing cellular furrows and internal cavity. Thin and thicker shell fragments (ostracods and gastropods) also present. Interpretation: Quiet open lacustrine deposition. Stained section. Field of view: 9mm. Piedrahita de Muno Formation. Piedrahita de Muno (just to left, ie below or to SW of section shown in fig 4.33).

Fig 4.53. Carbonate unit shown in right of fig 4.33. Note: apparently gradational base above green - grey marl; strong prismatic fabric.
Interpretation: Strong pedogenetic modification of slightly impure marginal lacustrine carbonate. Green silt / marl may be a clastic lacustrine deposit. Piedrahita de Muno Formation. Piedrahita de Muno.

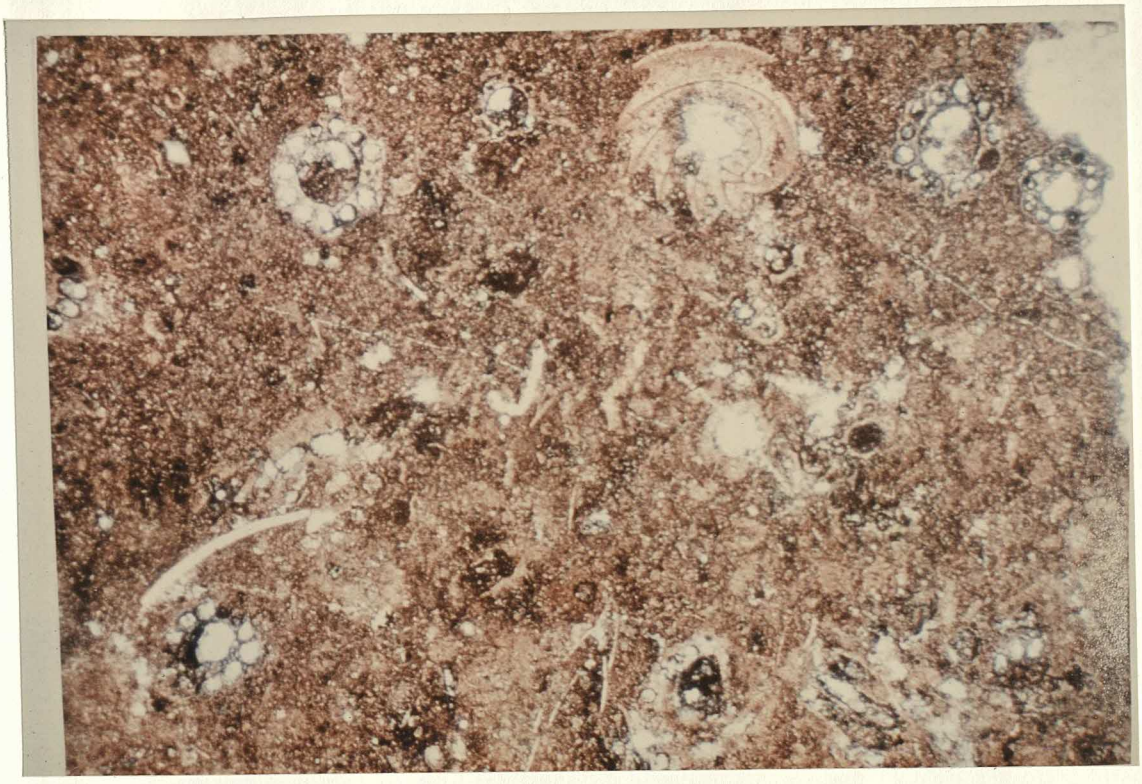

Fig 4.54. Pedroso Group: facies associations.

PEDROSO GROUP: FACIES ASSOCIATIONS.

FACIES ASSOCIATION	INTERPRETATION
HORTIGUELA FORMATION	
San Martin Member	
1) red & green mottled marls-thin tabular sands	distal alluvial deposition, some crevasse splays
Zurramujeres Member	
2) green marls-yellowish micaceous ssts-nodular mottled lsts	alluvial plain, pedogenic carbonates developed on long emergence
3) lsts, micritic at base, oncoids larger to top, some x-bedding	high energy lake flat, shoaling-upward sequence
PIEDRAHITA DE MUNO FORMATION	
4) stacked tabular sand bodies (some x-beds)-clay partings	sheet flood sedimentation (initially from bed load, later out of suspension from waning flow)
5) thick sand bodies, local x-bedding & reactivation surfaces	sand channel fill
6) tabular sands-bioturbated mudstones-nodular carbonates	distal alluvial sedimentation, crevasse splays, pedogenesis
7) lacustrine limestones-massive sands-lsts + prismatic fabric	shallow-water biogenic lacustrine sedimentation, sediment dumping in littoral zone at clastic mouthbar
8) green silts-tabular sand bodies	clastic lacustrine sedimentation, high rates of clastic supply cf interdistributary bay environment

PLATT N (1986)

Fig 5.1. Criteria for the field distinction between the Salas Group and the Utrillas Formation.

CRITERIA FOR THE FIELD DISTINCTION OF THE SALAS GROUP AND THE UTRILLAS FORMATION.

FACIES / PROPERTY	SALAS GROUP	UTRILLAS FORMATION
1) conglomerates	qzite clasts characteristically brown, yellow, often cracked	qzite clasts white, grey, pink
	clasts include: limestone a) ochre - marine Jurassic b) red/grey - Rupelo/Hortigüela Fm	no calcarous clasts
	relatively immature	mature
	not channelled	often strongly channelled
	poorly-sorted	generally better sorting
2) sands	sands characteristically dark brick red	sands white, locally mottled deep pink
3) weathered sands/muds ie soil colour	rich brown to dark red	white / grey to pale pink
4) limestones	calcarenites and calcrudite beds - reworked oncoids	no limestones
5) muds	significant thicknesses of dark brown-red muds between coarser beds	little or no mud
6) muds+pedogenesis	mottled marls carbonate nodules in marls nodular carbonates	pink-purple to green mottled slightly more mud-rich horizons

PLATT N (1986)

Fig 5.2. Panoramic view looking N from Las Mamblas (approximately 1 km W of Mambrillas de Lara; see fig 1.7). Palaeozoic forming rounded mountains, far right distance; Upper Cretaceous limestone forming scarp/ridge running from left horizon. Anticline cored by marine Jurassic limestones forming grassy ridge, left centre. Prominent dip surface (with scrubby bushes on right) consists of Rupelo Formation limestone. Hortigüela Formation (Zurramujeres Member) limestones forming weak and discontinuous features on ridge with pylons (just visible beyond dirt road). Salas Group clastics lying under cornfields with red soil, occasional calcarenites forming discontinuous ridges with scrubby vegetation. Utrillas Formation sands above with characteristic thick heather cover and white sand outcrops. Road in foreground is N-234.

Fig 5.3. Integrated facies model for the Salas Group.

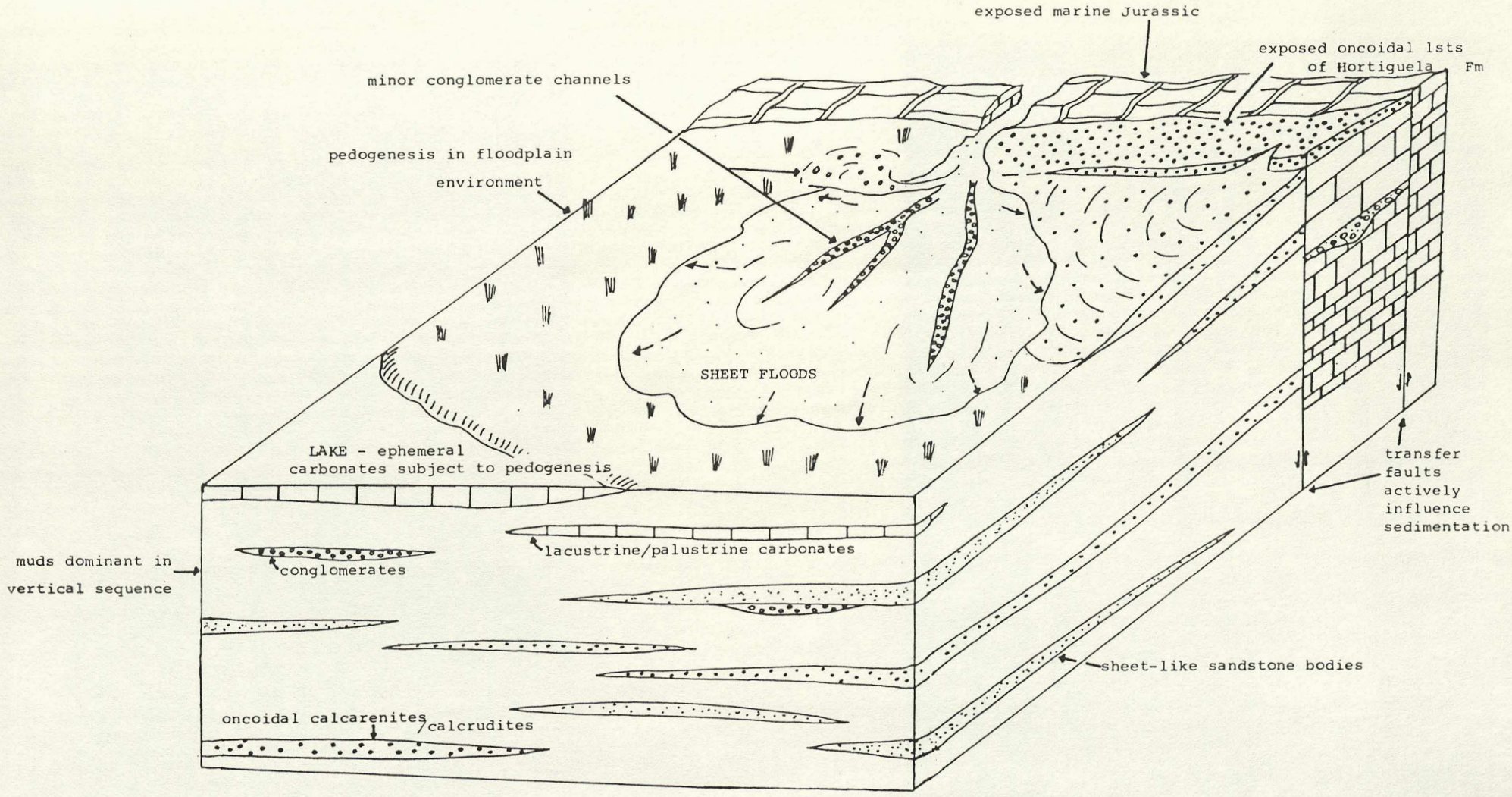

SALAS GROUP:
INTEGRATED FACIES MODEL.

Fig 5.4. Approximately parallel bedded, poorly sorted and relatively immature clast-supported conglomerate. Abundant subrounded to subangular (cracked) quartzite pebbles. Brownish yellow quartzite pebbles especially common - characteristic of the Salas Group. The ochre coloured clasts consist of weathered marine Jurassic limestone (eg ?Lower Callovian) - probably derived fairly locally. Red clasts of sandstone from underlying Pedroso Group or Senora de Brezales Formation and of highly-weathered micritic limestone (marine Jurassic or charophyte-bearing Rupelo Formation). Matrix of sand and grit-sized clasts.

Fig 5.5. Closer view of soil profile shown in fig 5.0. Sheet-like lower carbonate unit shows internal horizontal fabric, brecciated towards top. Vertical carbonate nodules - some bifurcate downwards (eg 1m to right of hammer) - some may be root replacements. Mottled marl/silt host. Nodules coalescing above hammer to give sheet-like unit with weak horizontal structure. Scattered vertical nodules above; upper part of profile clearly truncated by sandstone. Compare figs 3.19, 3.39, 3.44, 3.70.
Interpretation: formation of carbonate soil by growth of carbonate nodules in fine alluvial substrate.


TAMRON

Fig 5.6. Brown - green weathering calcarenite containing limestone clasts from the marine Jurassic (?Lower Callovian) in addition to weathered and commonly fragmented reworked 0.5-3cm oncoids from Hortigüela Formation (Zurramujeres Member). Sandstone is cross-bedded on a 30cm scale. Approximately 800m E of Quintanilla de las Vinas on new road to Lara de los Infantes.

Fig 5.7. Outcrop photograph of Salas Group sediments. Younging to left. Tabular sand and brown-quartz-pebbly conglomerate units interbedded with green marls (right). Heavily mottled red-brown silt/mud with carbonate nodules overlain by limestone bed and nodular powdery limestone (centre). Red silts/muds above. Behind loose blocks to left are erosive-based conglomerate units consisting of numerous reworked and fragmented oncoids (see figs 5.8 & 5.9. Upper Cretaceous carbonates forming scarp in left distance. 500m W of Cubillo del César, looking E.

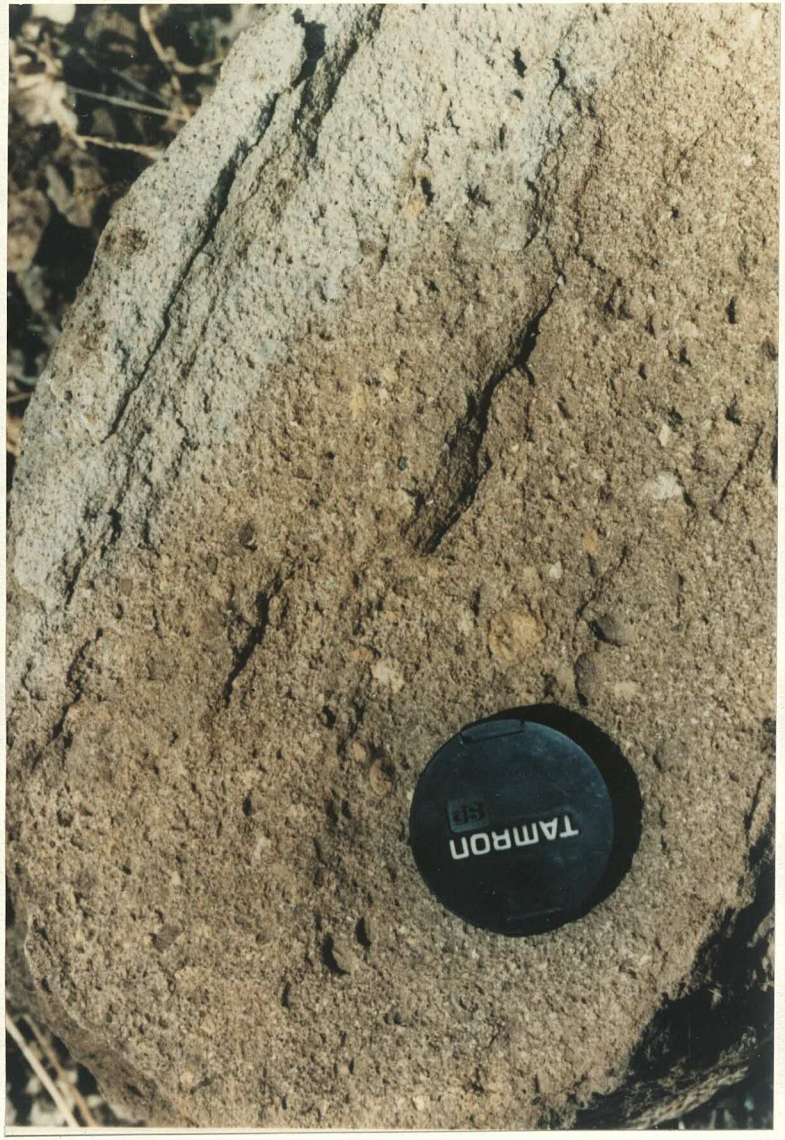
TAMRON

Fig 5.8. Closer view of central part of outcrop shown in fig 5.7.
a) Mottled silt/mud with some carbonate nodules overlain by
b) nodular limestone.
c) Massive, sharp-based limestone above has numerous 1-3cm oncoids visible weathering out (left of vertical root).
d) Green nodular marly limestone above (just to right of hammer).
e) Sequence of variably nodular and brecciated limestones above, local purple and green mottling.

Interpretation:
a) overbank mud, pedogenic modification on poorly-drained floodplain.
b) pedogenetically modified lacustrine limestone.
c) littoral lacustrine, high energy.
d) reworking and pedogenesis acting on c).
e) thick carbonate soil profile developed on limestone and floodplain marls. Some clastic input from floodplain (red silt) and some subaqueous clastic input periodically within lake (green silt/marl).

Fig 5.9. Closer view of reworked-oncoid conglomerate shown at extreme left of fig 5.8. Loose block, youinging to top of photograph. Erosive-based and cross-stratified fining-up unit of reworked and occasionally abraded or fragmented 0.5 to 3cm oncoids interbedded with brick red medium-grained fluvial sandstones. Some larger and more angular limestone clasts (base).
Interpretation: Fluviatile erosional reworking of oncoidal limestone of Hortigüela Formation.

Fig 5.10. Hand specimen of oncoidal calcarenite from locality shown in figs 5.7-5.9. (Unit c, fig 5.8). Note: abraded and irregular oncoids and fragments; numerous fragments in coarse calcarous matrix. ?Weak grading. One oncoid (left) has green marl nucleus. Scale bar in centimetres.

Fig 5.11. Micrograph of oncoidal calcarenite from locality shown in figs 5.7-5.9. (Unit c, fig 5.8). Note: concentric structure 1consisting of alternating layers of dense and more porous, spongy carbonate; rare radial filaments; irregular margins; interstitial quartz grains, rarely forming oncoid nuclei. Compare with fig 4.7: similarity in oncoid morphology suggests derivation from the Hortigüela Formation.

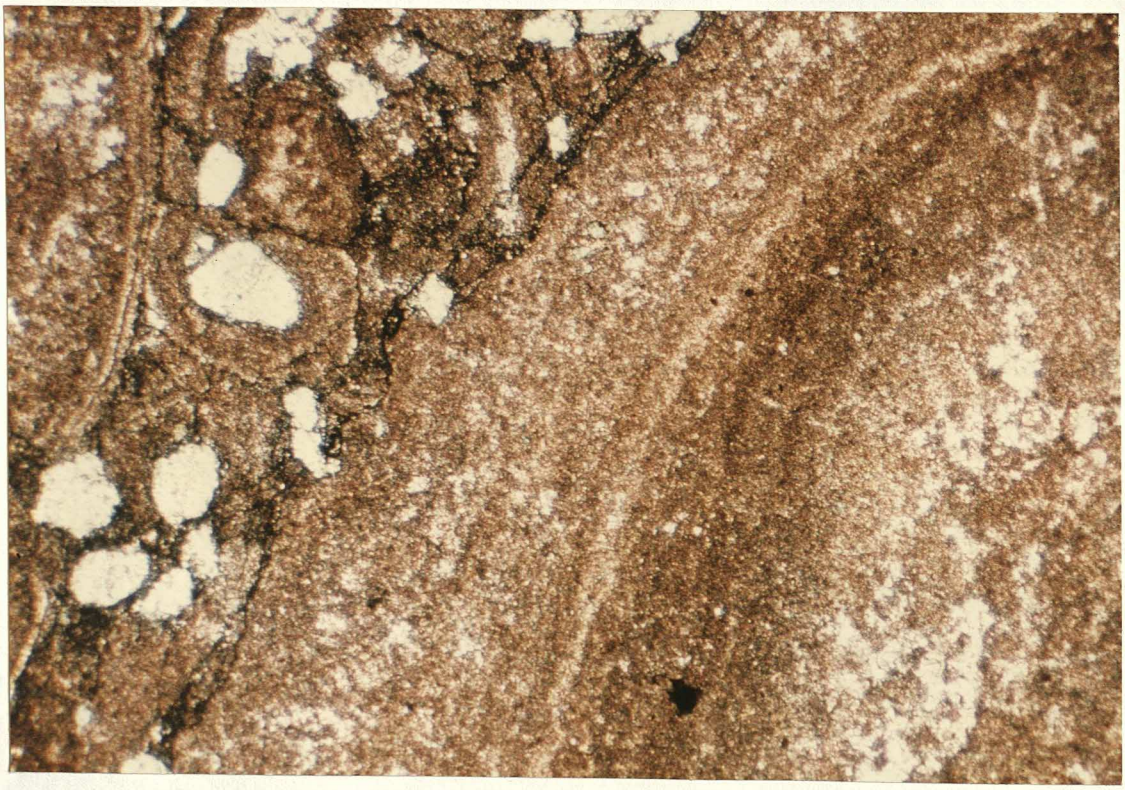

Fig 6.1. Linear range of low hills marking outcrop of Utrillas Formation, younging to left. Heather cover approximately marking base. Utrillas Formation also underlies cornfields, left, as indicated by pale white to pinkish sandy soils and outcrop of white to pink sands beneath poplars, centre. Salas Group and Pedroso Group clastics generally not outcropping in cornfields to right, brown soil. Thin limestones outcropping in patchy scrub, centre right. Utrillas Formation is exploited economically (chiefly for road ballast) at several localities along strike (where heather absent). Marls of Santa Maria de las Hoyas Formation forming grey-brown soil, centre foreground (top of Utrillas Formation just below, beneath "oyster bed"); Picofrentes Formation marl forming pale grey to white soil, left centre.

Fig 6.2. Integrated facies model for the Utrillas Formation.
Note: many, laterally-mobile channels on braidplain;
laterally migrating gravel bars; strong internal reworking;
subaerially exposed islands, pedogenesis mottled
palaeosols.

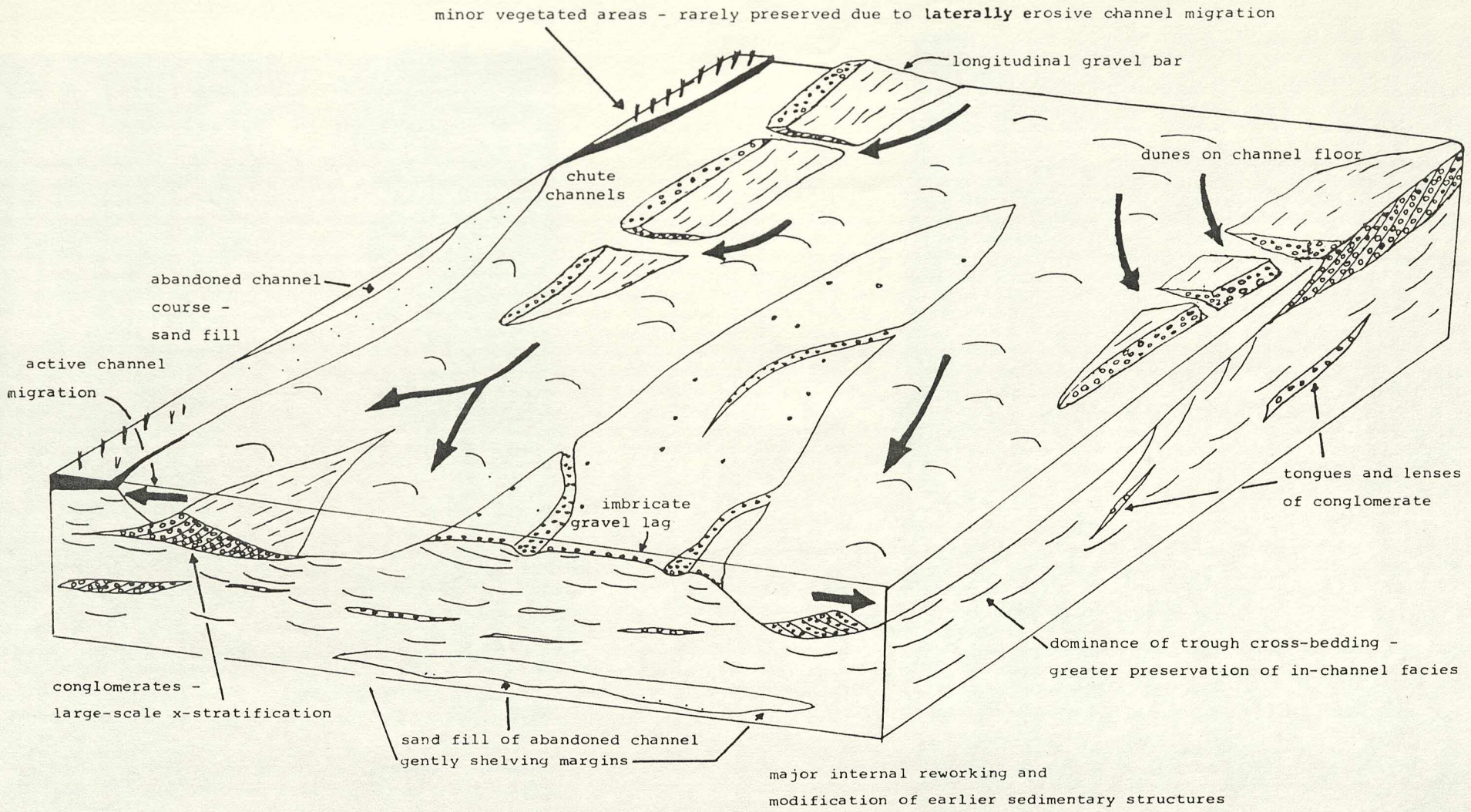

UTRILLAS FORMATION:

INTEGRATED FACIES MODEL.

Fig 6.3. Channel outcropping in Utrillas Formation. Note: conglomerate fill of deeply-incised channel; steeper channel margins than those evident in fig 6.13; stratification dipping towards right channel margin suggesting large-scale lateral accretion of longitudinal gravel bar. 2km S of Navaleno, looking NW.

Fig 6.4. Closer view of area near hammer in fig 6.3. Note sharply erosive base, coarse, rounded, quartzite clasts at base. Sorting generally increasing upwards. Several phases of fill. Fining upward especially in small-scale finer-grained sequences (eg just below lens cap).

Fig 6.5. Lenticularly-bedded conglomerates (each unit 30cm thick and 2-3m in lateral extent) separated by sand-rich layers. Pebbles have their long axis aligned parallel to bedding. Sand occasionally forms lenticular cross-beds of similar dimensions (eg right). Small quarry 100m W of Mambrillas de Lara - Campolara road.

Fig 6.6. Closer view of prominent sand lens shown in right of fig 6.5. Note sharp margins to sand lens and cross-bedding. Lower conglomerate unit displays weak imbrication and shows thin sand layer which indicates dip of cross-stratification. Consistent current indicators. Pebbles discoid. Small quarry 100m W of Mambrillas de Lara - Campolara road.

Fig 6.7. Pebbly sands and thin intercalated sand lenses in Utrillas Formation showing large-scale cross-stratification dipping to left. Difficult to identify individual depositional units. Note penetration by modern root is 2m. Geologist is 1.95m tall. Small quarry 100m W of Mambrillas de Lara - Campolara road.

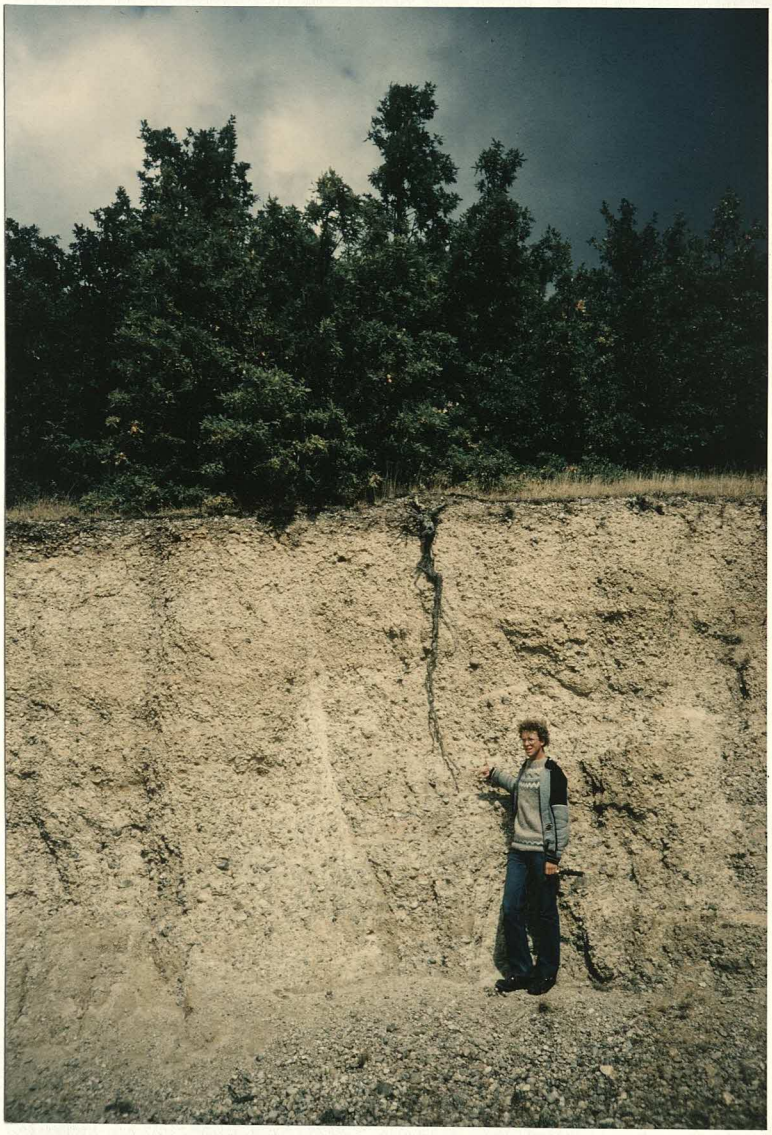

Fig 6.8. Tongues and lenses of sandstone (eg below hammer) in matrix-supported conglomerates/pebbly sandstones. Exposure in road cut 1km S of La Yecla. Looking N.

Fig 6.9. Closer view of outcrop near La Yecla showing coarse conglomerates of quartzite pebbles. Dips of large quartzite pebbles above hammer indicate large-scale accretion surfaces? Some pebbles show opposite sense of dip (?imbrication). Near La Yecla. Looking S.


60

Fig 6.10. Pebbly sandstones in lenticular beds; intercalated thin sand units. Looking N. Sediment geometry is clearly complex with multiple reactivation surfaces. Above hammer, cross-stratification is apparently weakly to left. Small quarry 100m W of Mambrillas de Lara - Campolara road.

Fig 6.11. Conglomerates (showing fining-upwards) and sands showing well-developed trough cross-bedding in oblique section. Several reactivation surfaces (eg: A - just above white line on photograph above hammer, gentle dip to left with a few pebbles on surface;

B - truncating trough cross-bedded sands above A. Cross-stratification above B dipping gently to right. 3km SSE of Mamolar. Looking NE. This outcrop is mapped as "Oxfordian" on the forthcoming IGME 1:50 000 geological sheet "Santo Domingo de Silos".

Fig 6.12. Trough cross-bedded sands showing multiple reactivation surfaces. Sedimentary structures in sands truncated by sharp erosive base of overlying channelised conglomerates. Same locality as fig 6.11.

Fig 6.13. Channel in Utrillas Formation sands. Note: sand fill of shallow channel; gentle slope of channel margins; undulating, broad channel floor; weak mottling in sands below erosive base. Cubiejo. Looking SE.

Fig 6.14. Stacked channel sequence in Utrillas Formation pebbly sandstones and conglomerates. Photograph courtesy of Owen Vaughan (1986).

Fig 6.15. Petrified fragments of tree bark preserved in ferruginous fine sandstone collected from near base of Utrillas Formation between Mamolar and Pinilla de los Barruecos. Scale bar in centimetres. Morphology, especially ridged nature, of bark analogous to modern conifers - cf those currently colonising modern sandy soils developed on poorly consolidated Utrillas Formation (eg figs 6.3 & 6.7).

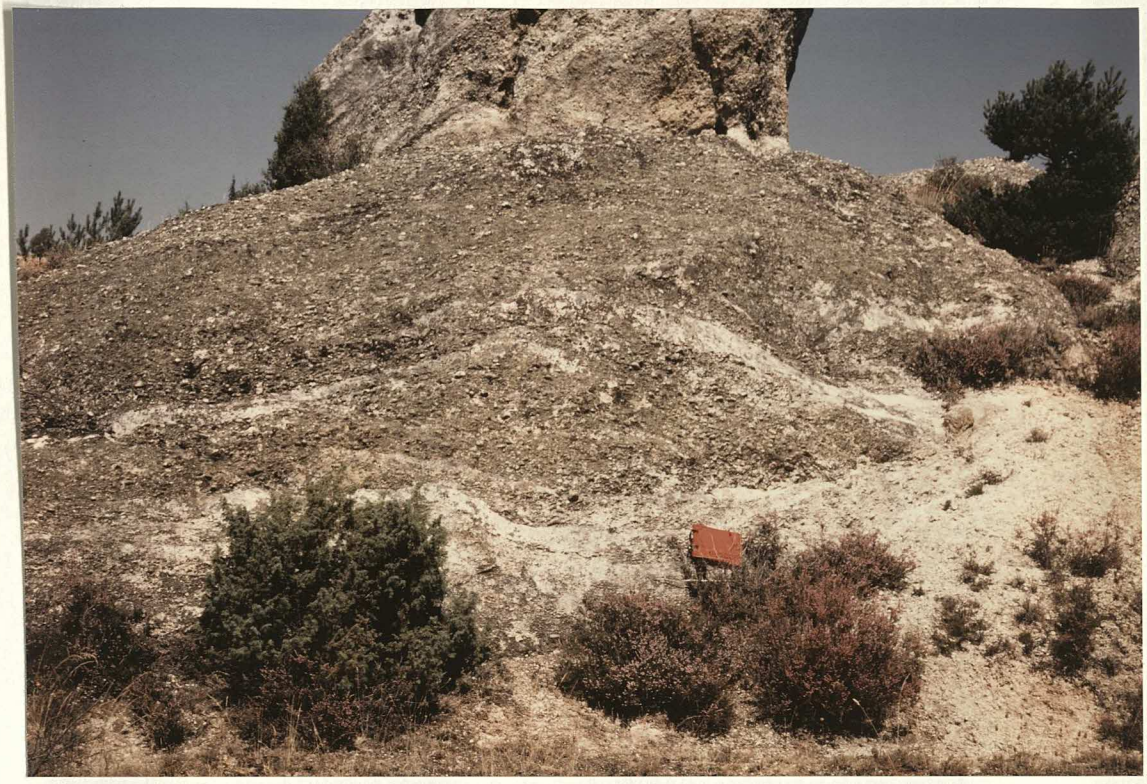

Fig 6.16. Large fossil tree trunk - one of several set up in the village of Hacinas, 4km S of Salas de los Infantes. Note similarity of bark to that shown in fig 6.15 and substantial girth of tree trunk.

Fig 6.17. A. Complex sedimentary structures in road cut through Utrillas Formation sands. Coarse sands and grits at base incised by channels with basal conglomerates. Imbricate pebbles draped above mark major undulating reactivation surface. Trough cross-bedded sands above, right, again truncated by reactivation surface marked by imbricate pebbles. N-234, Burgos - Sagunto road, near Quintanilla de las Vinas turn off. Looking NE.
B. Interpretation.
Photograph courtesy of, and interpretation modified after, Tom Faulkner (1985).

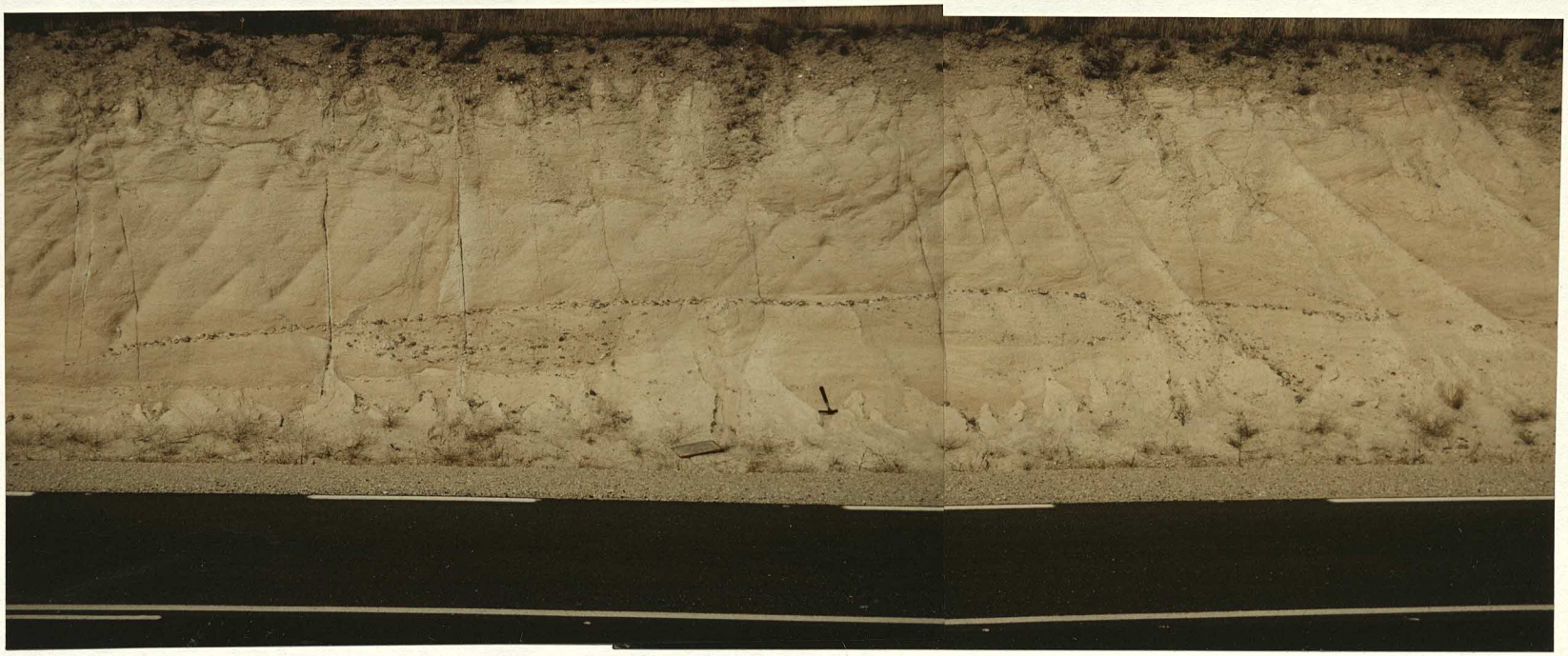

Fig 6.17. A. Complex sedimentary structures in road cut through Utrillas Formation sands. Coarse sands and grits at base incised by channels with basal conglomerates. Imbricate pebbles draped above mark major undulating reactivation surface. Trough cross-bedded sands above, right, again truncated by reactivation surface marked by imbricate pebbles. N-234, Burgos - Sagunto road, near Quintanilla de las Vinas turn off. Looking NE.
B. Interpretation.
Photograph courtesy of, and interpretation modified after, Tom Faulkner (1985).

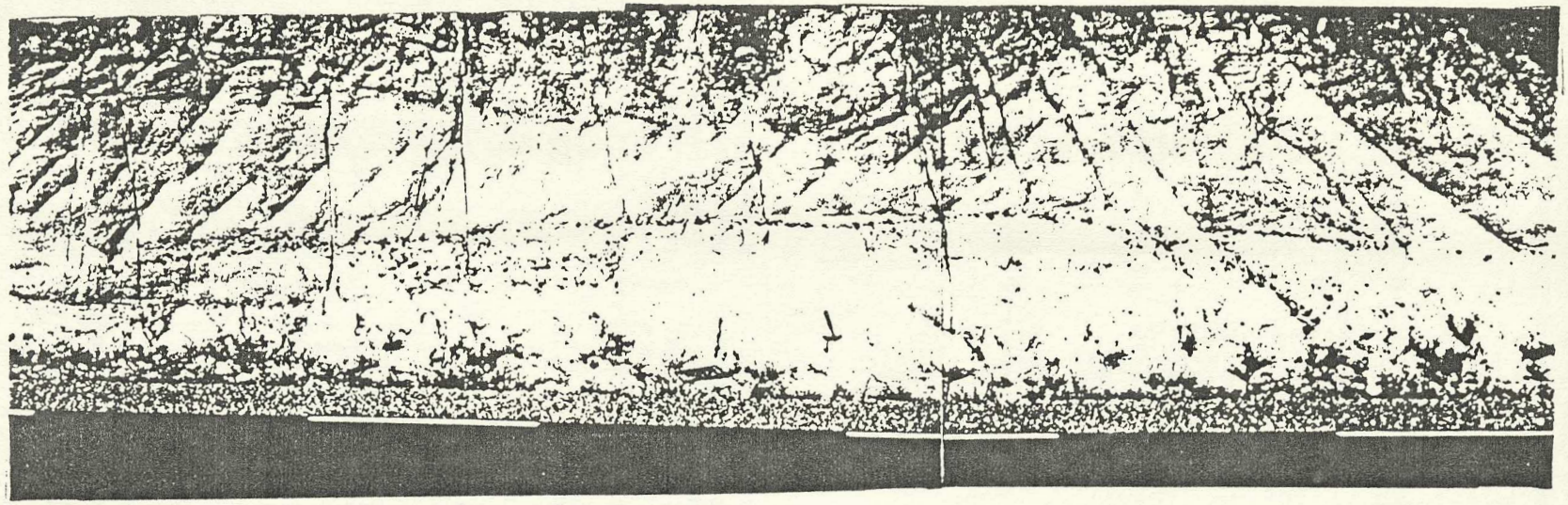

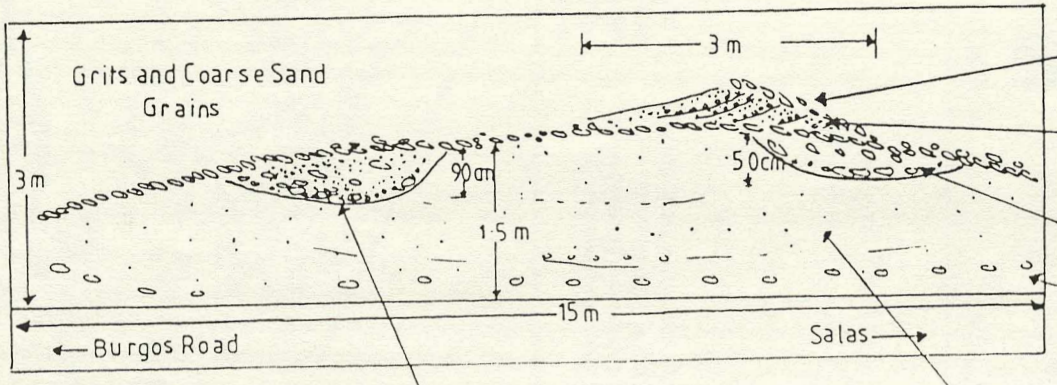

Imbricate pebbles

Reactivation surface truncating the dune.

Cross bedded dune with fining upward sets.

Channelling

Basal conglomerate.

Channel with basal conglomerate. Long axis of pebbles is parallel to the base of channel.

Dominantly coarse sands and grits (poorly cemented).

Fig 6.18. Facies model for the South Saskatchewan River - after Cant & Walker (1978) as given in Walker (1984), and predicted sequences of sedimentary structures.

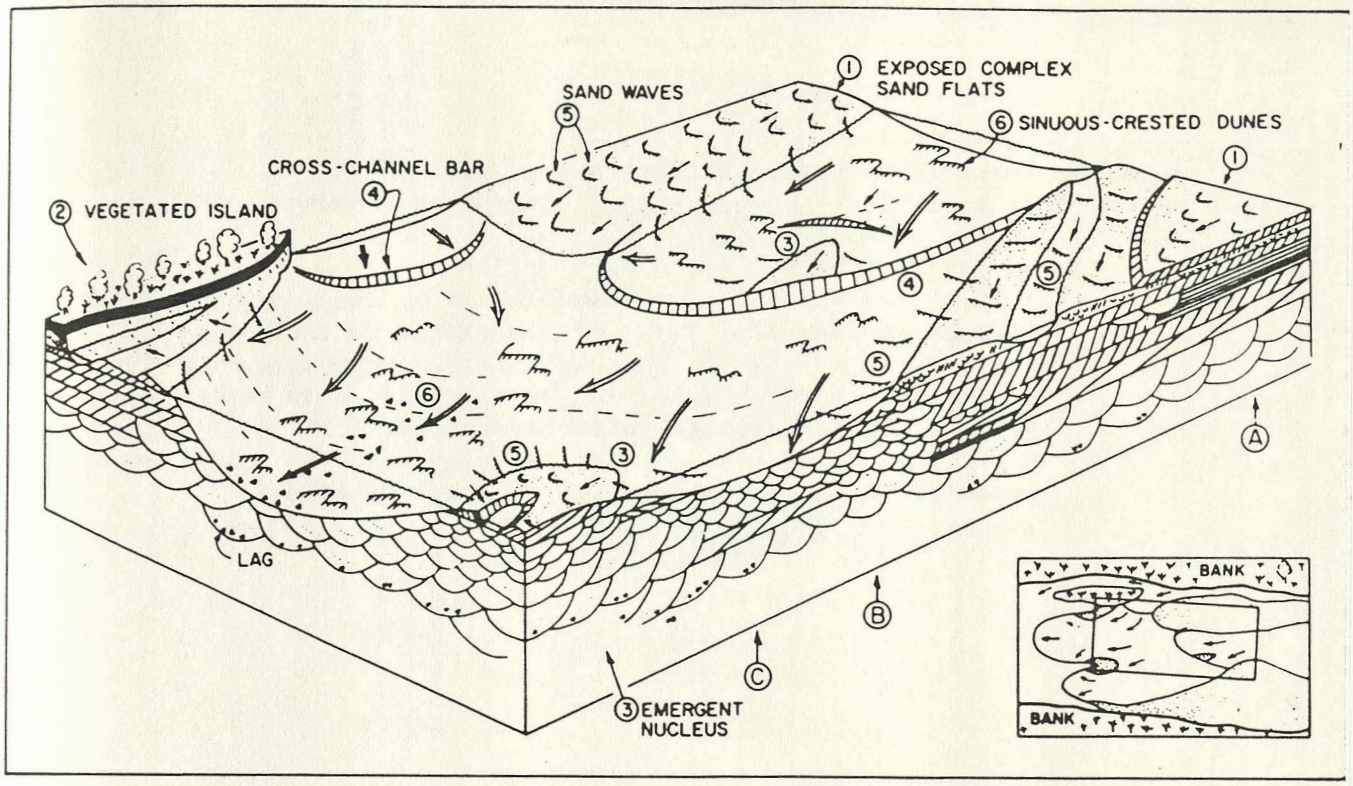

Block diagram showing elements (numbered) of a braided sandy river, based on the South Saskatchewan. Stippled areas exposed, all other areas underwater. Bar in left corner is being driven laterally against a vegetated island, but is separated form the island by a slough in which mud is being deposited. Large sandflats (e.g., right-hand corner) may develop by growth from an emergent nucleus on a major cross-channel bar (see Figs. 15 and 16). Vertical fining-upward sequences A, B and C are shown in Figure 17 and include in-channel and bar top deposits. See text for details.*

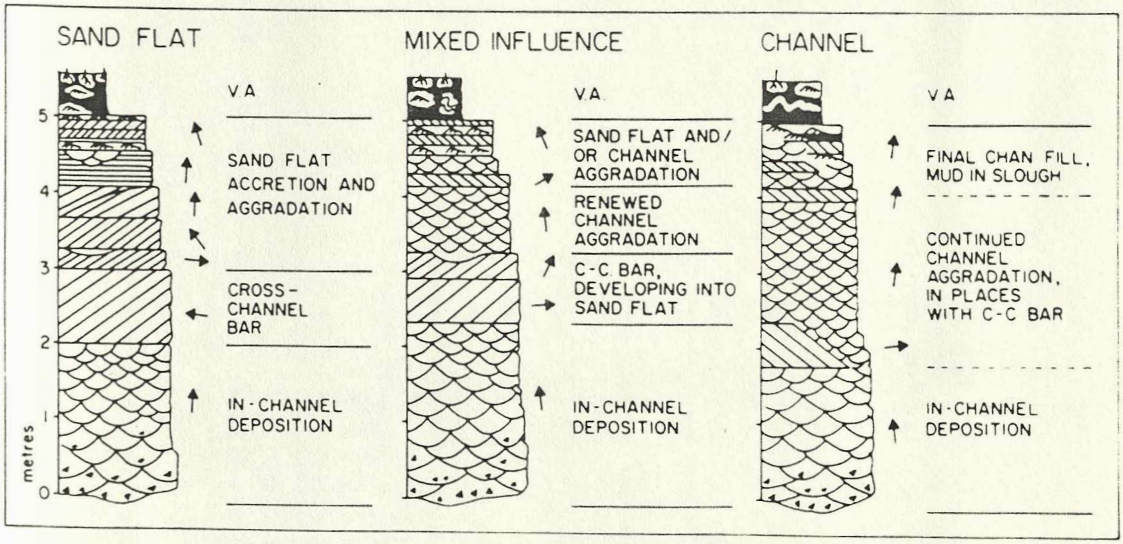

Three proposed sequences of sedimentary structures based on the South Saskatchewan. "Sand flat" corresponds to A (Fig. 14), "channel" to C, and "mixed influence" to B. Arrows indicate generalized paleoflow directions, and sequences are explained in the text.

Fig 6.19. Braided-river depositional sequences:
1) South Saskatchewan River, (from Cant & Walker, 1978, in Walker, 1984);
2) Donjek River, (from Miall, 1977);
3) Utrillas Formation, as exemplified by small quarry 100m W of road between Campolara and Mambrillas de Lara (modified after Faulkner, 1985). The Utrillas Formation sequence is comparable to the channel sequence of the South Saskatchewan River - although mud is effectively absent in the Utrillas Formation. There are some similarities with the Donjek River sequence (eg in the proportion of conglomerates).

Types of braided-river depositional profile: Donjek type. Named to suggest a broad similarity with the deposits of the Donjek River, Yukon Territory (Williams and Rust, 1969; Rust, 1972). This type of profile, characterized by cyclic sedimentation, is the most variable of the four. Gravel content varies widely (it is much more abundant in the Donjek than shown here) and cycle thickness may range from less than 1 m to more than 20 m.

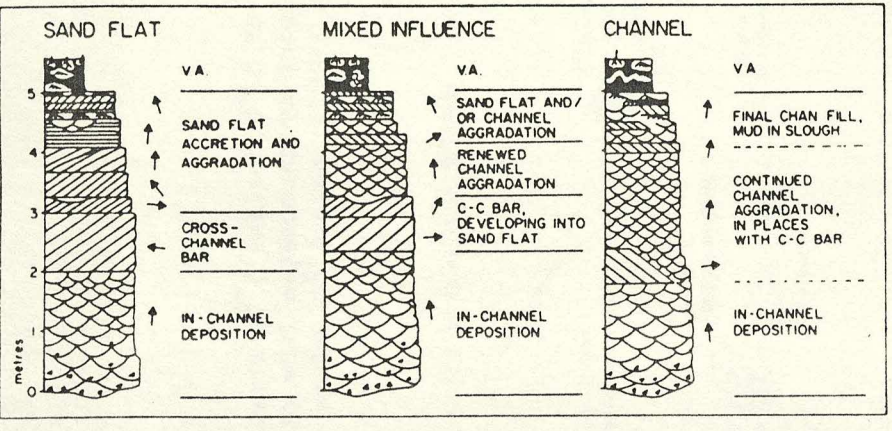

Three proposed sequences of sedimentary structures based on the South Saskatchewan. "Sand flat" corresponds to A "channel" to C, and "mixed influence" to B. Arrows indicate generalized paleoflow directions, and sequences are explained in the text.

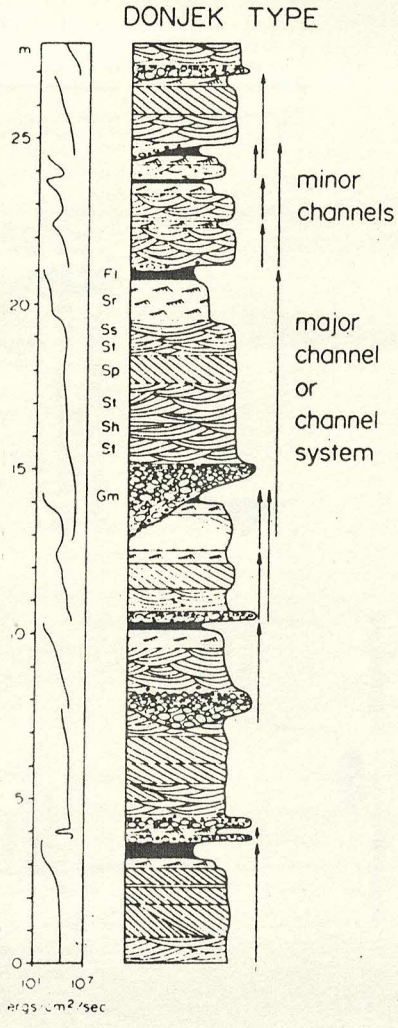

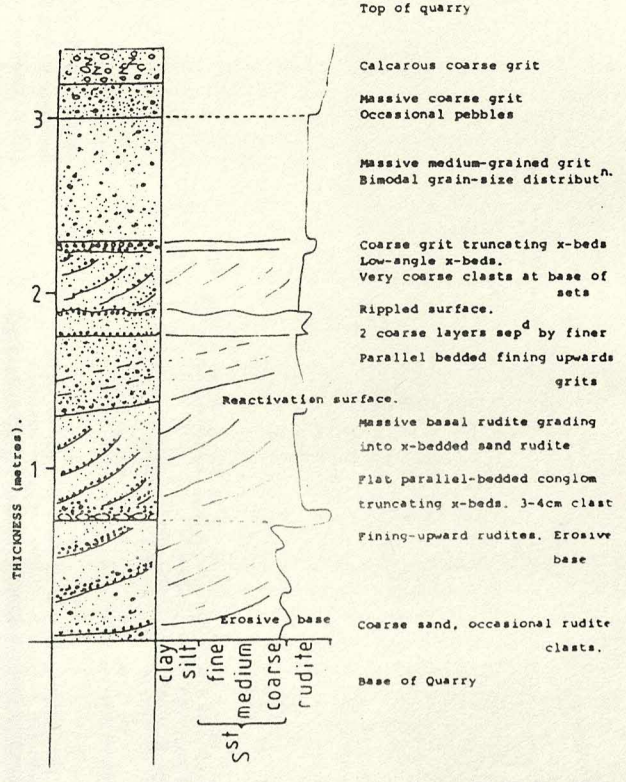

Fig 7.1. Cross-plot of $\delta^{18}O$ against $\delta^{13}C$ showing the characteristic fields occupied by carbonates from different environments. From Hudson (1977). Note $\delta^{18}O$ values should be in PDB, not SMOW.

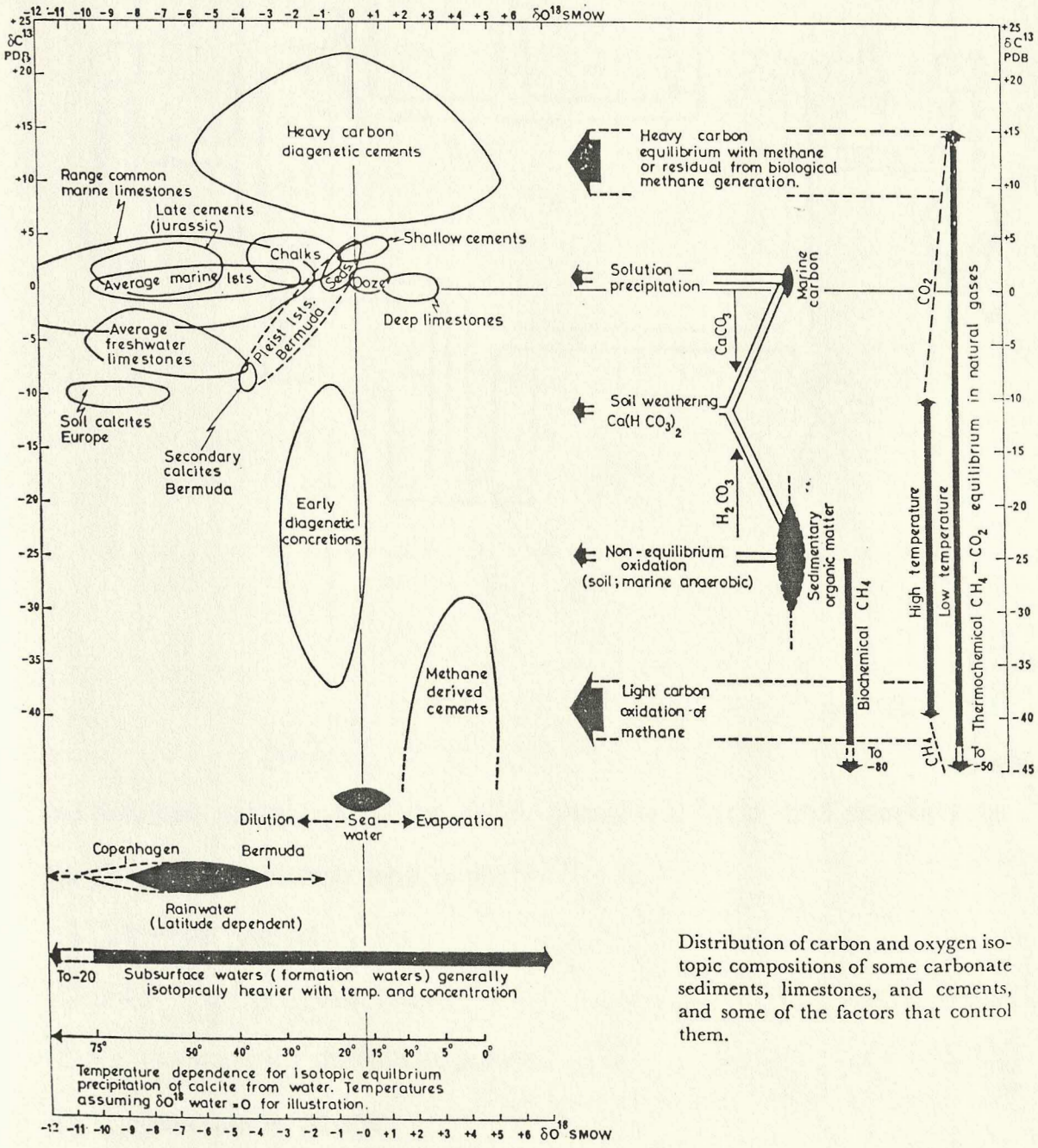

Distribution of carbon and oxygen isotopic compositions of some carbonate sediments, limestones, and cements, and some of the factors that control them.

Fig 7.2. Schematic diagram showing "carbonate line" - the apparatus used to extract CO_2 from carbonate samples for ^{13}C and ^{18}O isotope analysis.

CO_2 EXTRACTION LINE.

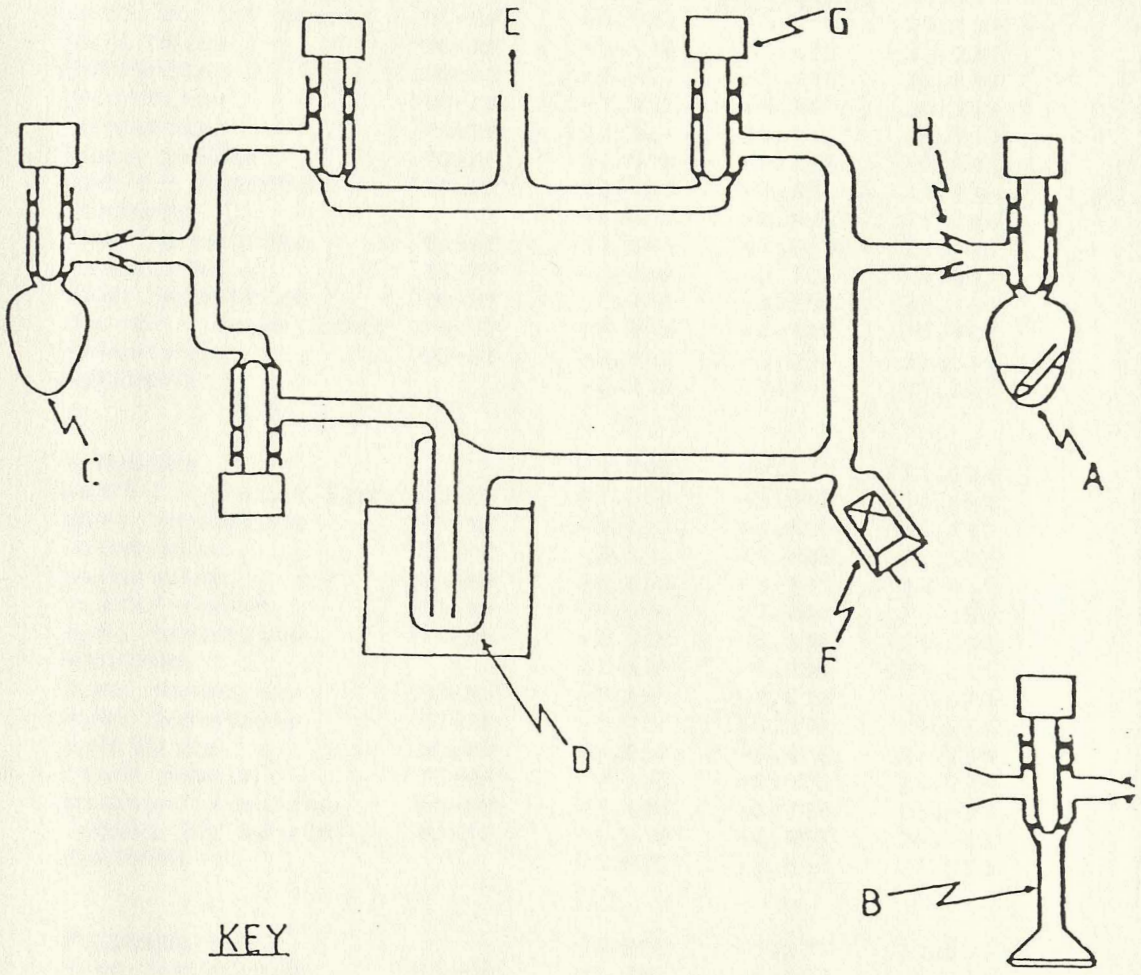

KEY

A) Reaction vessel containing 100% phosphoric acid and sample tube.

B) 'T' tube containing lead acetate.

C) Collection vessel.

D) Solid CO_2 / acetone trap.

E) To rotary and diffusion pumps.

F) Thermocouple gauge.

G) High vacuum stopcock in closed position.

H) B14 joint fitted with Viton 'o' ring ('T' tube inserted for H_2S separation)

Fig 7.3. Table of stable isotope results obtained from carbonate samples from the Rupelo, Hortigüela and Piedrahita de Muno Formations.

STABLE ISOTOPE RESULTS.

	SAMPLE	DESCRIPTION	HORIZON	Del ^{13}C	Del ^{18}O PDB	Del ^{18} SMOW
	RUN 1:					
	MCS-8	STANDARD		-0.757	-9.439	21.130
	343A/1	palustrine - roots	TG-RF	-9.209	-7.236	23.401
	350C/1	oncoidal lst matrix	PG-HF	-6.983	-5.550	25.139
	316B/1	palustrine	TG-RF	-8.518	-5.470	25.221
	341B/1	palustrine	TG-RF	-8.061	-5.144	25.558
	V35A/1	palustrine	TG-RF	-7.966	-4.341	26.385
*	346/1	palustrine	TG-RF	-13.381	-10.817	19.709
*	NP77A/1	black pebble	TG-RF	-11.919	-8.535	22.062
*	49X/1	nodular limestone	PG-PF	-13.753	-9.431	21.138
	MCS-8	STANDARD		-0.625	-8.939	21.645
*	V114/1	open lacustrine	TG-RF	-11.160	-7.649	22.975
	344/1	palustrine	TG-RF	-9.429	-5.702	24.982
	560A/1	open lacustrine	TG-RF	-7.108	-4.359	26.366
	NM4A/B/1 NA	oncoid - dense layer	PG-HF	-9.203	-6.480	24.180
	339B/1	palustrine	TG-RF	-8.157	-5.090	25.613
	MCS-8	STANDARD		-0.718	-9.153	21.425
	RUN 2:					
	MCS-8	STANDARD		-0.799	-9.212	21.364
	NM3A/2 A	oncoid - porous layer	PG-HF	-7.869	-5.992	24.683
	V39/3	open lacustrine	TG-RF	-7.726	-4.603	26.115
	V35/2	palustrine	TG-RF	-8.180	-5.488	25.203
	341A/1	palustrine	TG-RF	-8.463	-5.771	24.911
	V91/1	vadose cement	TG-RF	-10.906	-7.441	23.190
	V39/2	open lacustrine	TG-RF	-7.949	-5.316	25.380
	MCS-8	STANDARD		-0.675	-9.258	21.316
	560B/1	open lacustrine	TG-RF	-7.366	-4.638	26.079
	V39/1	open lacustrine	TG-RF	-7.777	-4.468	26.254
	339A/1	palustrine	TG-RF	-8.652	-6.406	24.256
	B341C/B341B/1	black pebble	TG-RF	-9.193	-6.678	23.976
	49XA/1	nodular limestone	PG-PF	-7.106	-3.748	26.997
	462A/1	oncoid lst matrix	PG-HF	-6.978	-4.967	25.740
	MCS-8	STANDARD		-0.625	-9.061	21.520
	RUN 3:					
	MCS-8	STANDARD		-0.805	-9.279	21.295
	V114/2	open lacustrine	TG-RF	-8.498	-4.567	26.153
	V30/1	open lacustrine	TG-RF	-7.521	-3.442	27.312
	344/2	palustrine	TG-RF	-8.097	-4.748	25.966
	350B/1	oncoid lst matrix	PG-HF	-8.304	-7.335	23.299
	NM3B/1 A	oncoid - porous layer	PG-HF	-7.283	-5.067	25.637
	MCS-8	STANDARD		-0.713	-9.263	21.311
	MCS-8	STANDARD		-0.655	-9.312	21.260
	49YB/1	nodular limestone	PG-PF	-8.388	-4.711	26.003
	49YA/1	nodular limestone	PG-PF	-9.048	-6.911	23.675
	462/1	oncoid lst matrix	PG-HF	-6.794	-4.248	26.481
	V82A/B/1	vadose cement	TG-RF	-10.225	-8.042	22.569
	NP77A/B/1	dark intraclast	TG-RF	-9.034	-7.106	23.535
	MCS-8	SAMPLE		-0.627	-8.854	21.733

TG - Tierra de Lara Group
RF - Rupelo Formation
PG - Pedroso Group
HF - Hortigüela Formation
PF - Piedrahita de Muno Formation
MCS-8 - Del 13 = -0.700; Del 18 = -9.177.
* - discarded data point

PLATT N (1986).
from data obtained at the British Geological Survey, March 1985.

Fig 7.4. Cross-plot of ^{13}C and ^{18}O data from fig 7.3. All results. Note: All results lie in negative $\delta^{13}C$, negative ^{18}O quadrant - typical of fresh-water limestones (see Keith & Weber, 1964; Hudson, 1977); strong correlation of $\delta^{13}C$ and $\delta^{18}O$ values.

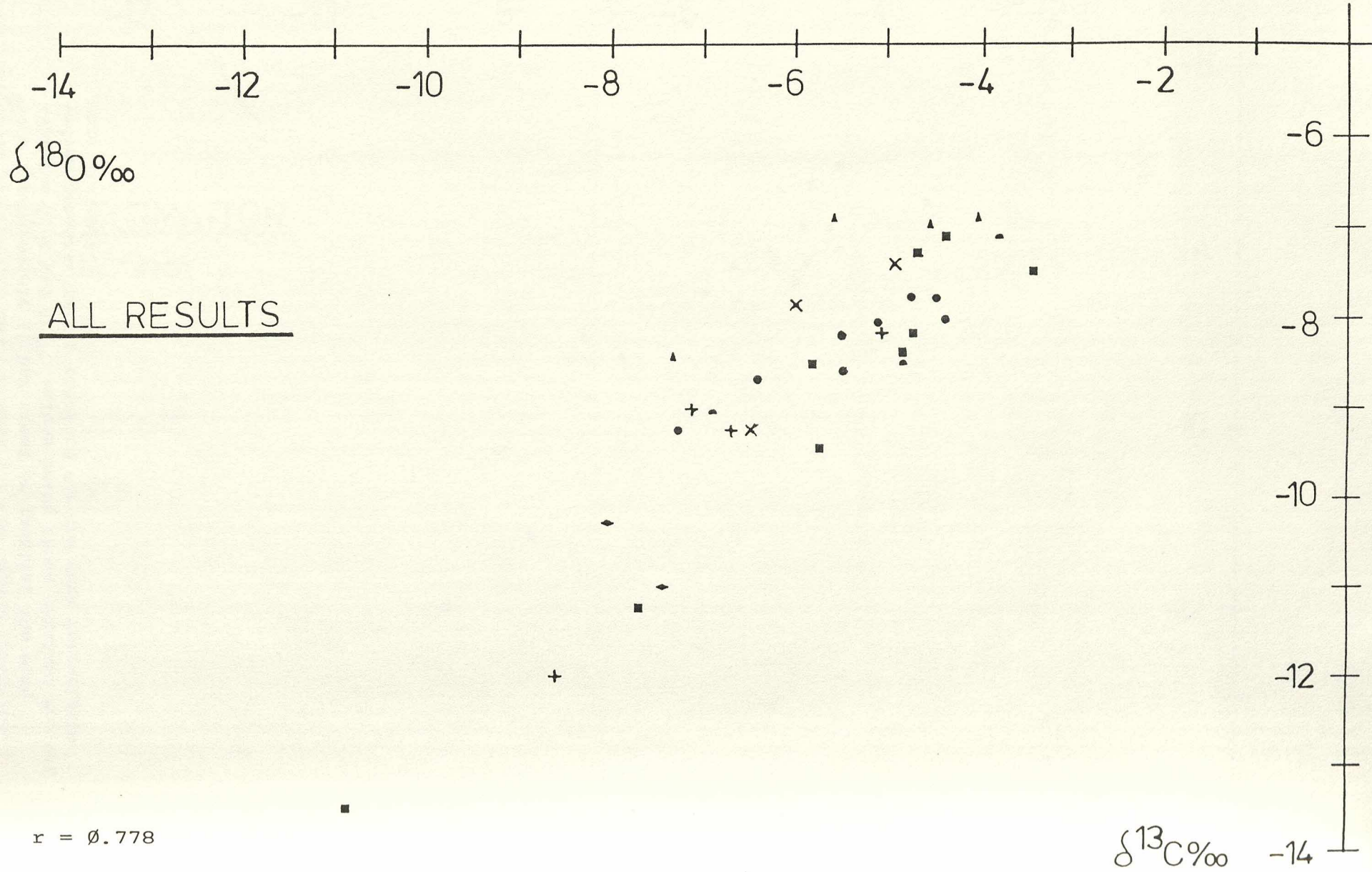
-14
-12
-10
-8
-6
-4
-2
δ18O‰
-6
-8
-10
-12
-14
δ13C‰
ALL RESULTS
r = Ø.778

Fig 7.5. Cross-plot of ^{13}C and ^{18}O data for the Rupelo Formation. Note approximately linear trend of results, the most negative $\delta\,^{13}C$ and $\delta\,^{18}O$ values being those obtained for the vadose cements. Values obtained for the dark intraclasts were variable.

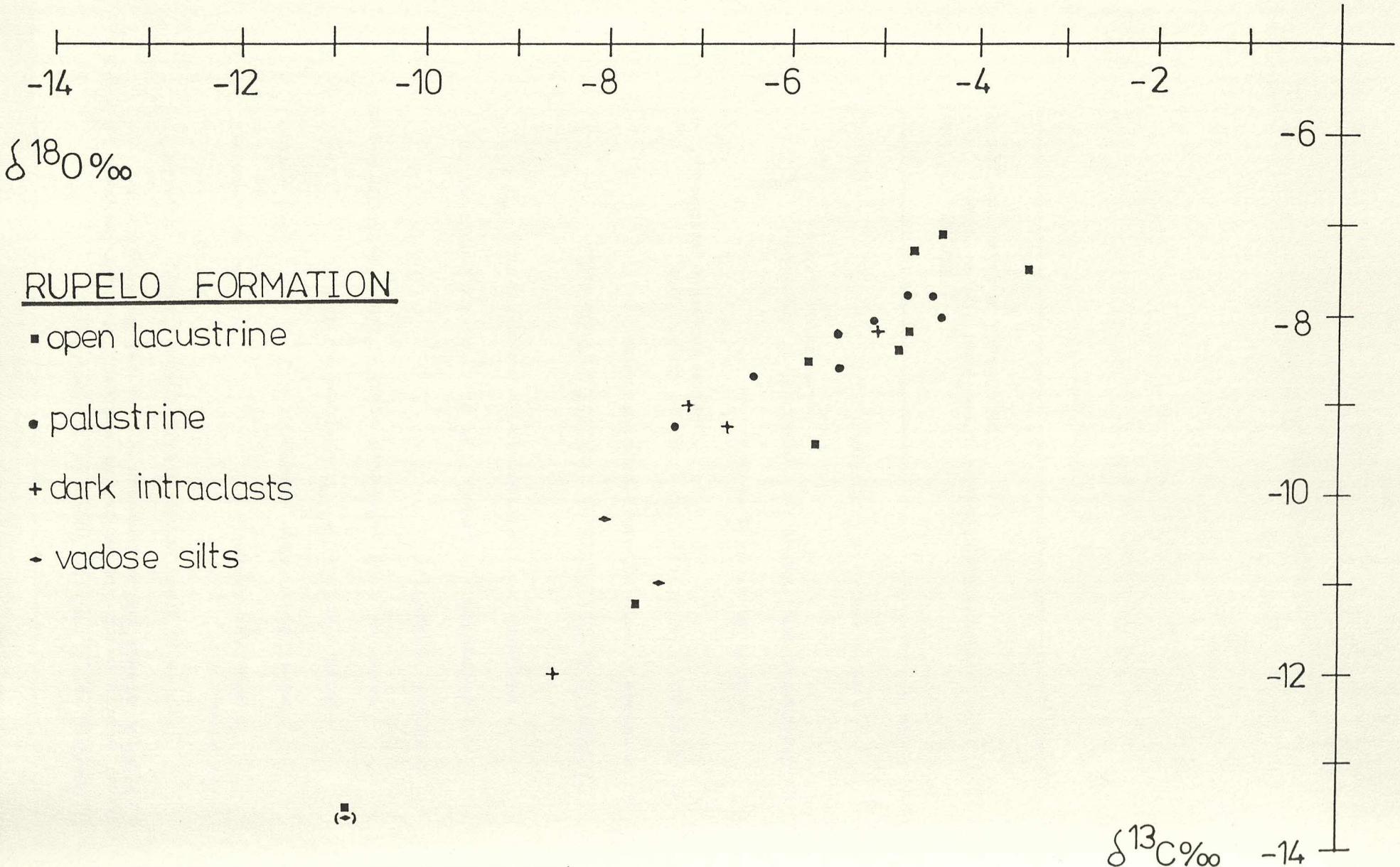

r = Ø.871 (discounting dark intraclasts)
r = Ø.9ØØ (+ black pebbles)

Fig 7.6. Summary chart of possible variables affecting stable isotope compositions of lacustrine carbonates (eg Rupelo Formation).

VARIABLES AFFECTING STABLE ISOTOPE VALUES IN RUPELO FORMATION.

---

1) primary variations in isotopic composition.

- a) open lacustrine

→ more organic productivity → more "light" organic C

- but also:

→ photosynthesis) → ^{13}C enrichment of lake waters

→ equilibrium with atmospheric CO_2)

→ heavy rainfall → ^{18}O enrichment, and

→ sheet wash of vegetated areas → light soil CO_2 input

- b) marginal lacustrine

→ pedogenesis → production of light soil-derived CO_2

→ evaporative fractionation → concentrating ^{18}O & ^{13}C.

2) diagenetic modification of isotopic composition.

- a) possible mineralogical transformations

- b) diagenetic equilibration - vadose conditions below exposure surfaces.

→ more negative δ values

- c) diagenetic equilibration - freshwater phreatic below water table.

→ more positive δ values

PLATT, N (1986)

with acknowledgement to: Bond (pers. comm., 1985)
Oberhänsli & Allen (in press)

Fig 7.7. $\delta^{13}C$ values of soil-derived CO_2 and dependence on the proportion of C_4 and C_3 grass species.

Fig 7.8. Cross-plot of $\delta^{18}O$ against $\delta^{13}C$ showing linear trends interpreted as the products of progressive diagenetic modification. The values reported in this study (figs 7.3 - 7.5) lie approximately on trend (11): Pleistocene limestones and secondary calcites, Bermuda (Gross, 1964). From Hudson (1977).

Relation between the estimated fraction of C_4 grass species relative to all grass species and reported values of ^{13}C of soil CO_2

Fraction C_4 grass	^{13}C of soil CO_2
Low (less than 30%)	−27 to −19‰
Medium (30 to 70%)	−23 to −14‰
High (more than 70%)	−18 to −7‰

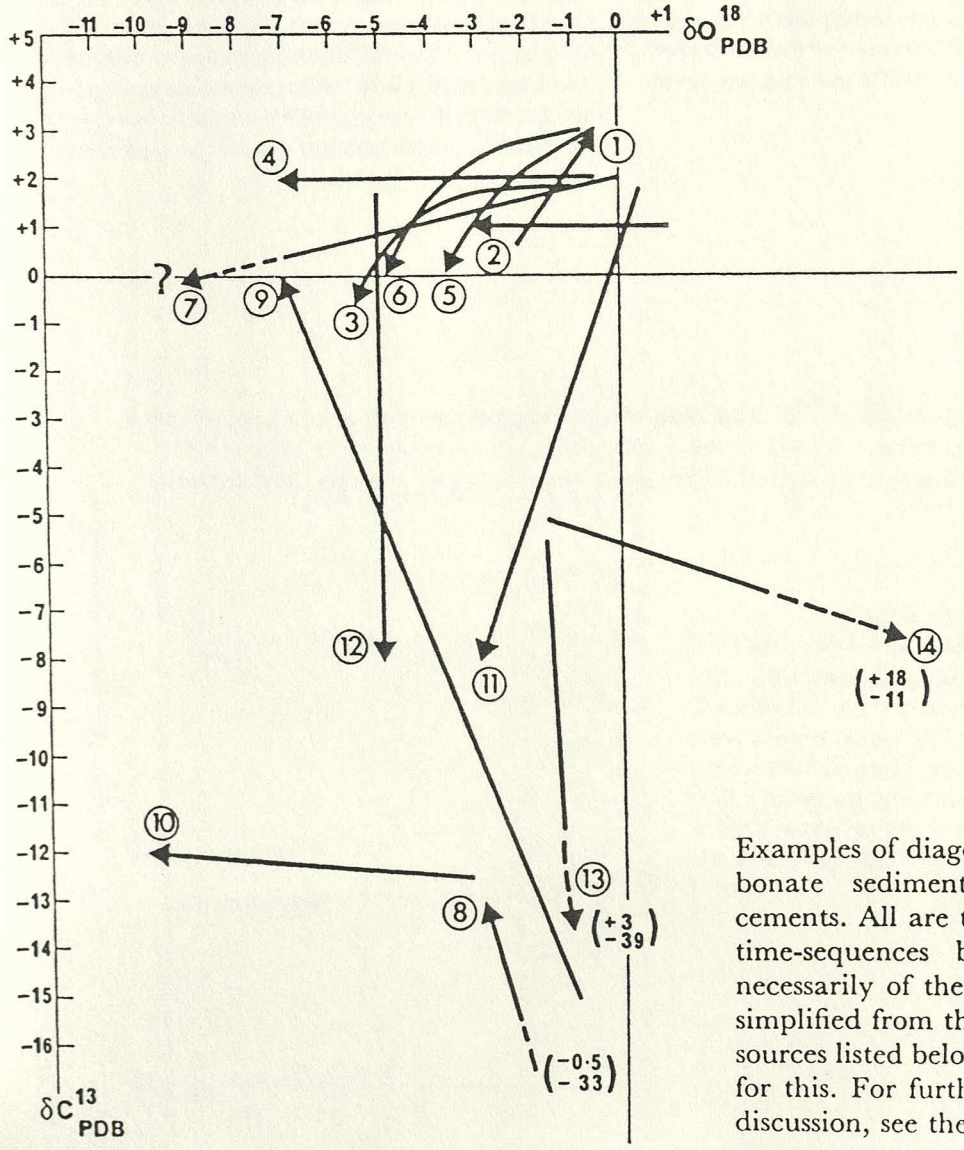

Examples of diagenetic trends in carbonate sediments, limestones and cements. All are thought to represent time-sequences but these are not necessarily of the same kind. All are simplified from the original data; the sources listed below must be consulted for this. For further explanation and discussion, see the text.

Fig 7.9. Plots of $\delta^{13}C$ values showing the difference between recent marine carbonates (positive values) and diagenetically-modified Pleistocene limestones (more negative values). In the case of the Rupelo Formation carbonates, the primary values were probably negative ("freshwater values") and subsequent vadose diagenesis resulted in further depletion of ^{13}C and ^{18}O. Allan & Matthews (1977).

Fig 7.10. Plot of $\delta^{13}C$ against depth below a subaerial exposure surface, showing the effects of vadose and phreatic diagenesis on stable isotope values. Allan & Matthews (1977).

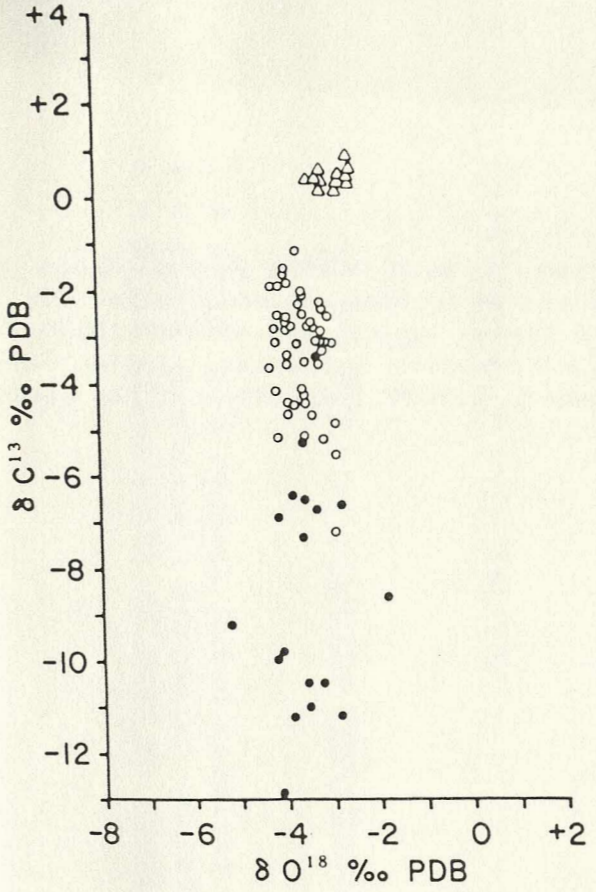

Carbon and oxygen isotopic composition of Barbados Pleistocene diagenetic limestones and Holocene marine sediments. Closed circles represent surface limestone samples; open circles, borehole limestone samples; triangles, marine sediment samples. All surface limestone samples and 39 of 49 borehole limestone samples are 100% calcite. Remaining 10 borehole samples are greater than 70% calcite.

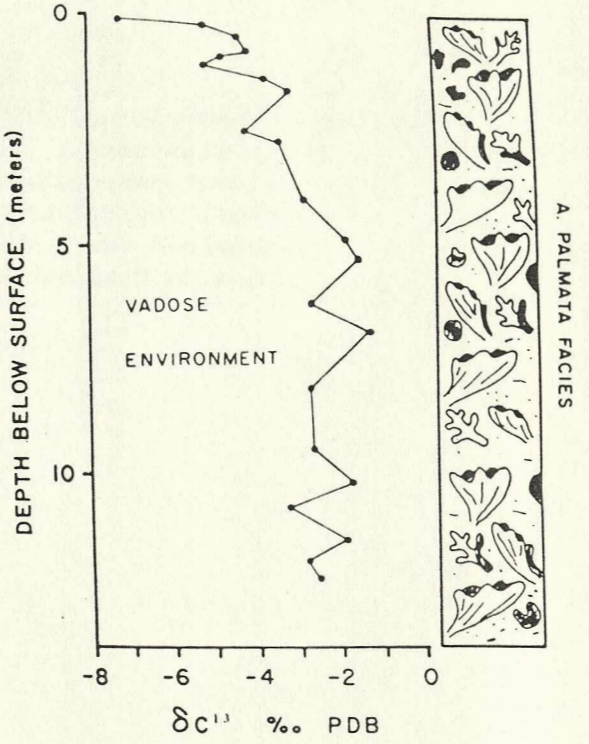

Graph showing δC^{13} versus depth for borehole 16 limestone samples. All samples are whole-rock intercoral matrix from *Acropora palmata* reef-crest facies. Top 32 m of borehole 16 is in vadose environment. First 10 samples below surface are greater than 70% calcite. All other samples are 100% calcite.

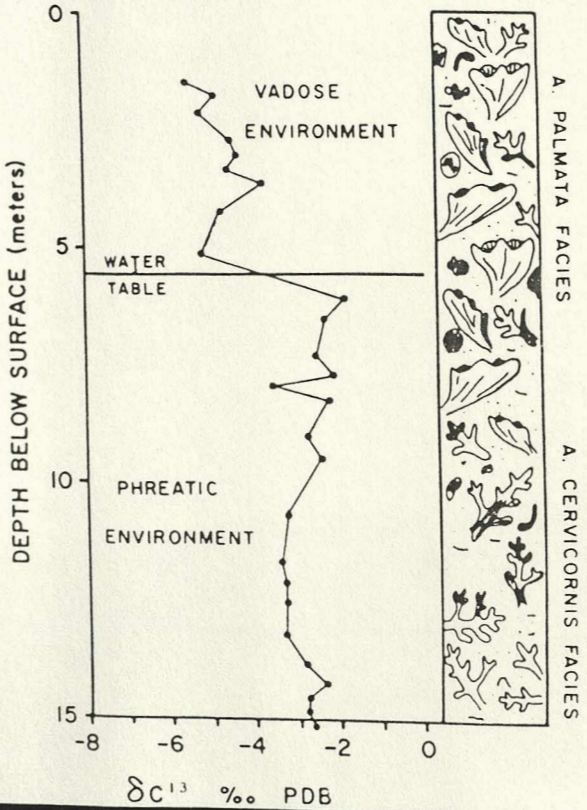

Graph showing δC^{13} versus depth for borehole 17 limestone samples. All samples are whole-rock intercoral matrix. Above 9.5 m samples come from the *Acropora palmata* reef-crest facies; below 9.5 m, from *Acropora cervicornis* reef-slope facies. Interval from 0 to 5.5 m is in vadose environment; from 5.5 to 15.3 m, in freshwater phreatic environment. All samples are 100% calcite.

Fig 7.11. Cross-plot of ^{13}C and ^{18}O data for the Pedroso Group. Note: no significant difference between values obtained for limestones, oncoids (dense layers) and oncoids (bushy, ie algal layers) of the Hortigüela Formation. Similar results obtained for pedogenic, nodular carbonates of the Piedrahita de Muno Formation.

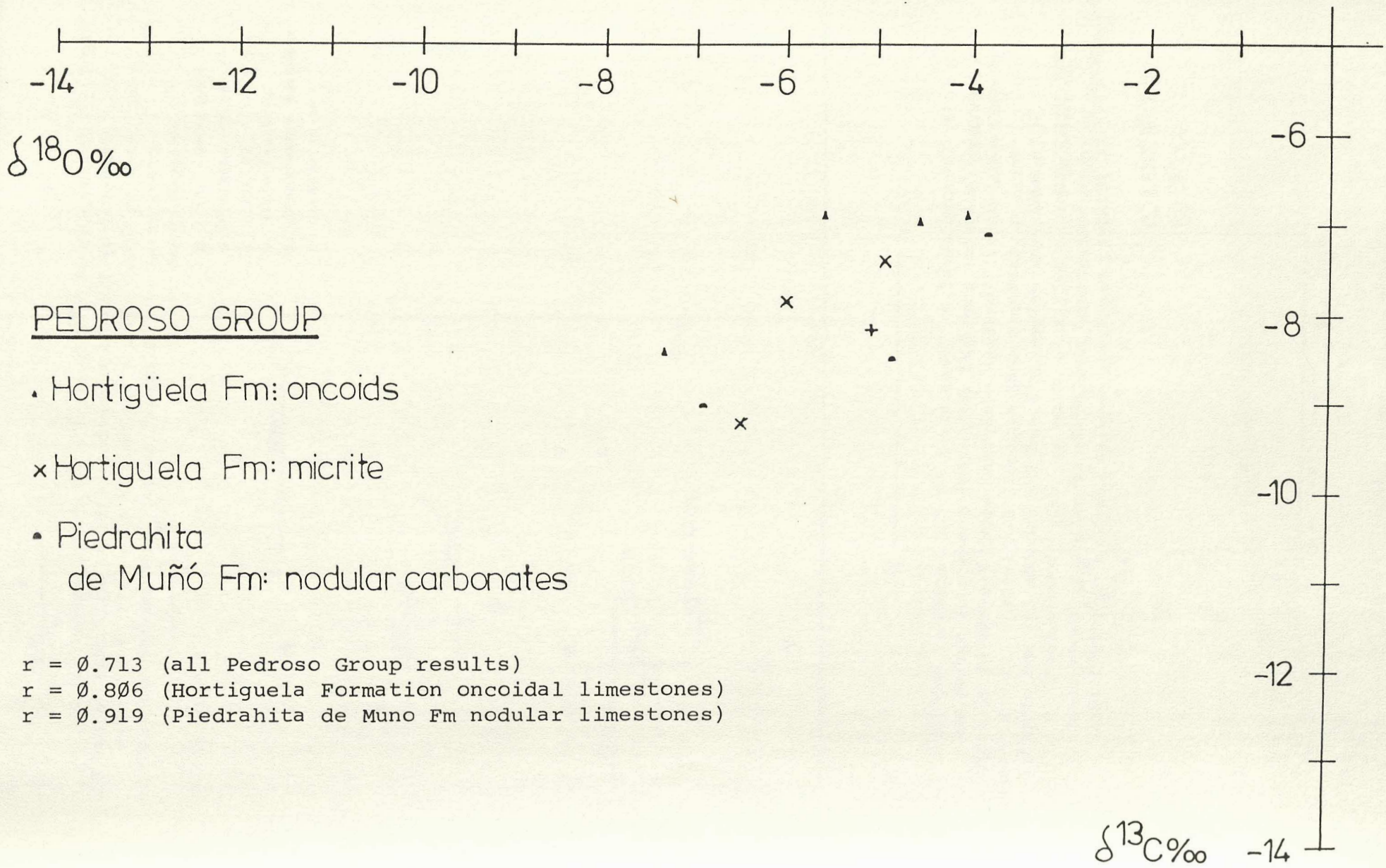

PEDROSO GROUP

▲ Hortigüela Fm: oncoids

× Hortiguela Fm: micrite

● Piedrahita
de Muñó Fm: nodular carbonates

r = Ø.713 (all Pedroso Group results)
r = Ø.8Ø6 (Hortiguela Formation oncoidal limestones)
r = Ø.919 (Piedrahita de Muno Fm nodular limestones)

Fig 7.12. Cross-plot of $\delta^{18}O$ against $\delta^{13}C$ of "calcrete" values, compiled by Talma & Netterberg (1983). Note that values for Pedroso Group nodular carbonates (fig 7.11) lie within normal range of "calcrete" values, but towards the negative part of that range.

Fig 7.13. Cross-plot of $\delta^{18}O$ against $\delta^{13}C$ for Garumnian oncoidal carbonates, compared with other Cretaceous marine and freshwater limestone analyses, after Freeman et al (1982). Note: no isotopic compositional distinction between oncoids and matrix; values obtained for oncoids (O) and oncoidal limestone matrix (L) show strongly "freshwater" characteristics; similarity of values to those obtained for Hortigüela Formation oncoidal carbonates (fig 7.12).

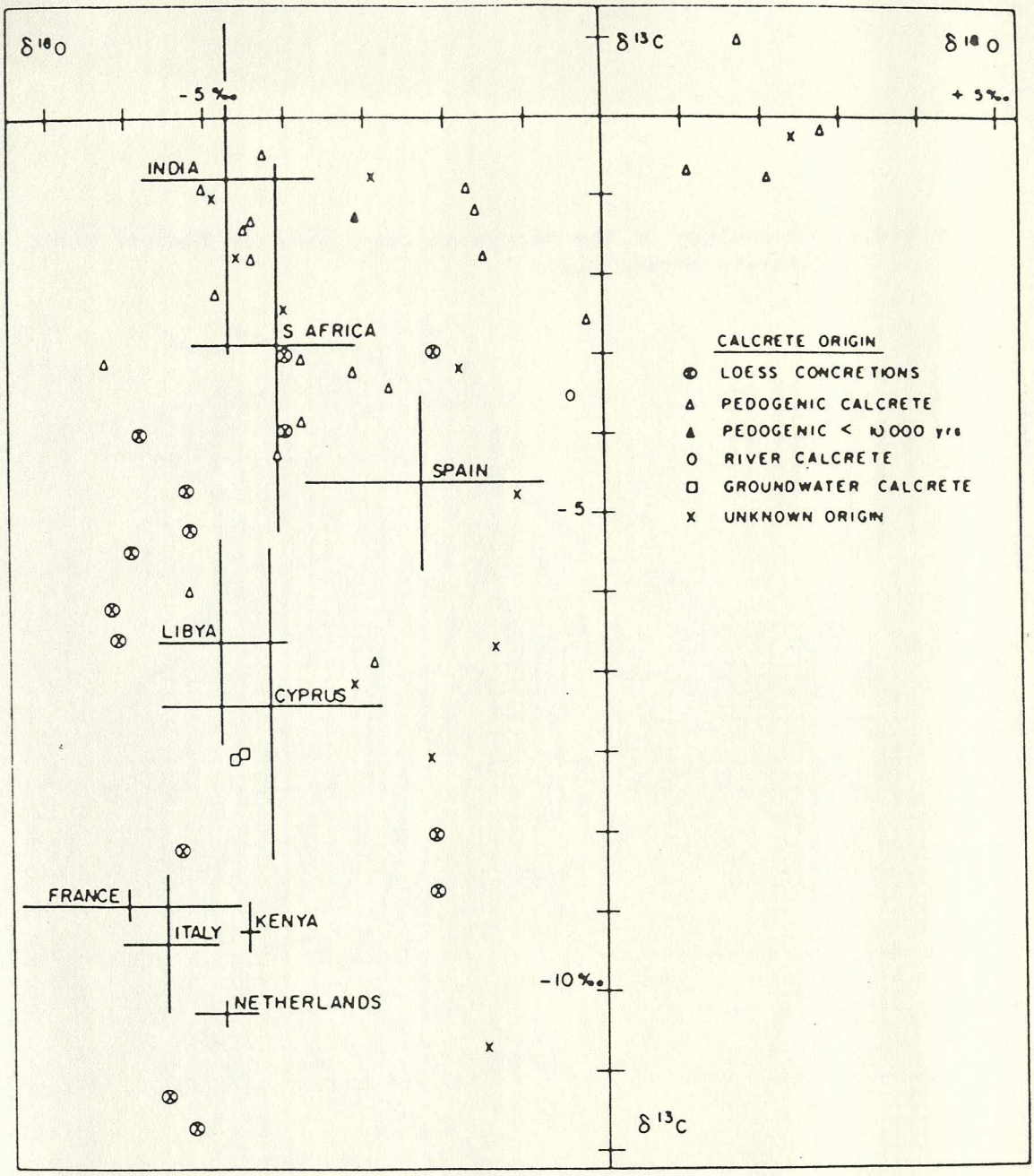

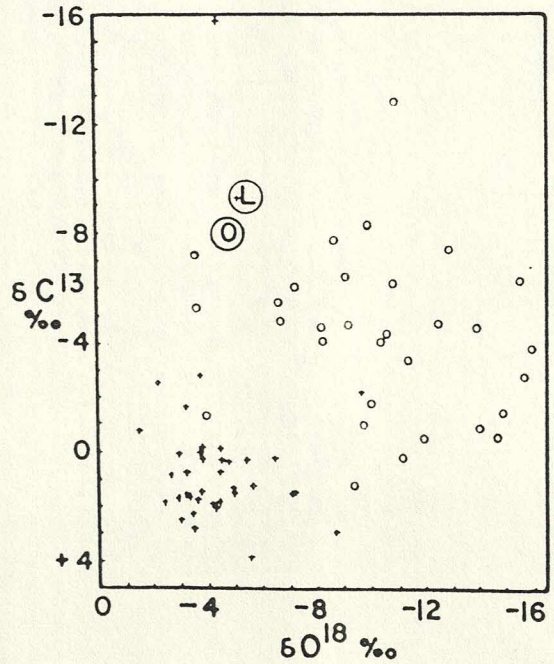

Cretaceous Limestones

- MARINE
- FRESHWATER

(Keith & Weber, 1964)

Ⓛ LIMESTONE
Ⓞ ONCOLITE

Isotopic compositions of limestone and oncolite plotted with numerous isotopic analyses of Cretaceous limestones provided by Keith & Weber (1964).

Fig 8.1. Morphology of the Hercynian Cordillera in Europe. Note: arcuate morphology.

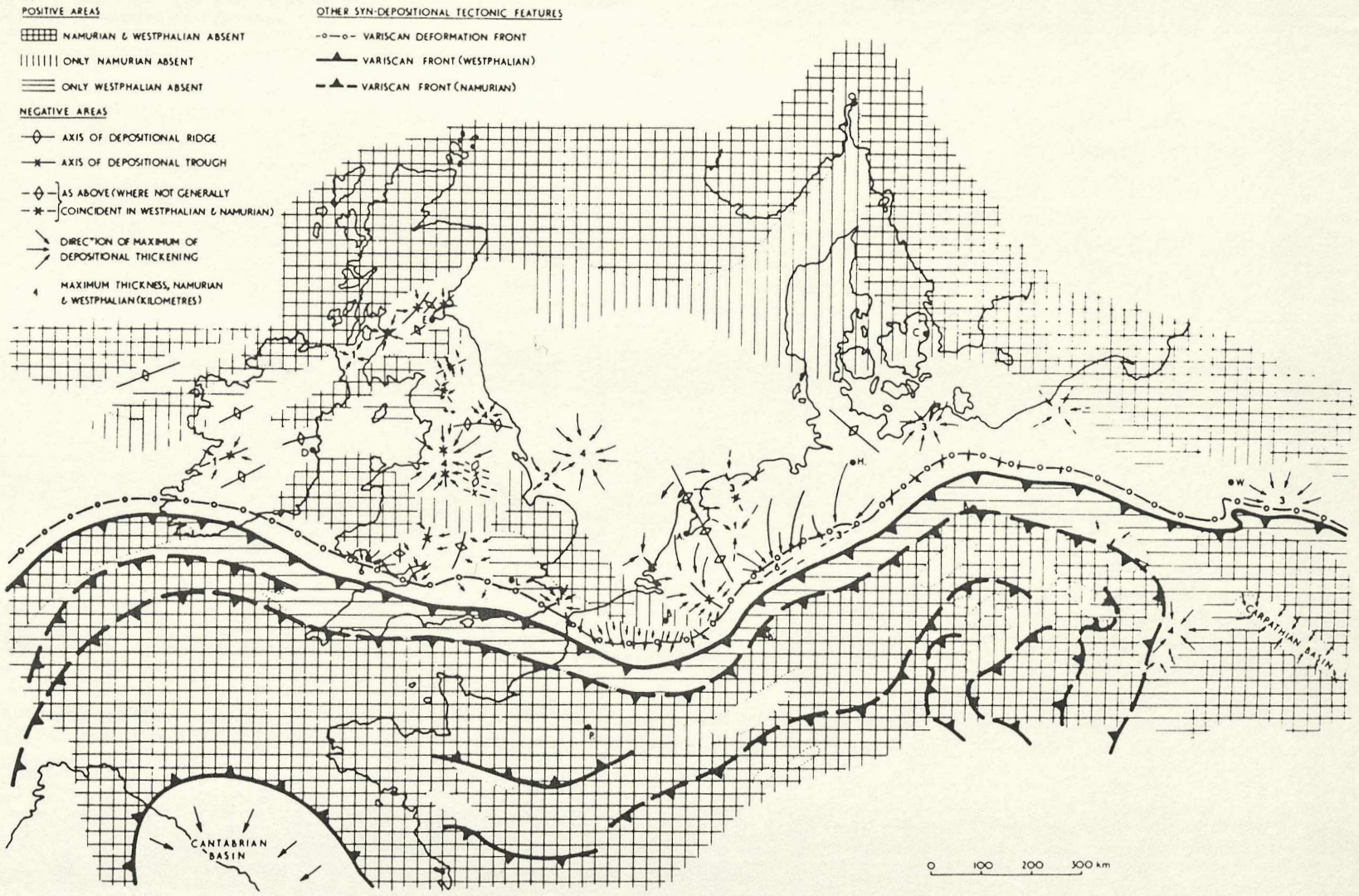

The Carboniferous basins of Europe, based on Ziegler's (1978) figs 5 and 6. D = Dublin, E = Edinburgh, L = London, P = Paris, B = Brussels, etc. Sets of isogonal dip lines have been added around the major basins, and the positions of the more minor depositional basins: those between four short Caledonoid trending 'humps' in Central Ireland, added from Ramsbottom *et al.* (1978); the five minor, but comparatively steep-sided, elongate basins of the Midland Valley of Scotland, added from Francis, in Craig (1965); the Campine–Brabant and the remaining six, shallower, mid to eastern European basins identified, along with most of the others, added from Bless *et al.* (1977).

Fig 8.2. Middle Cretaceous palaeogeography showing the position of the Iberian peninsula.

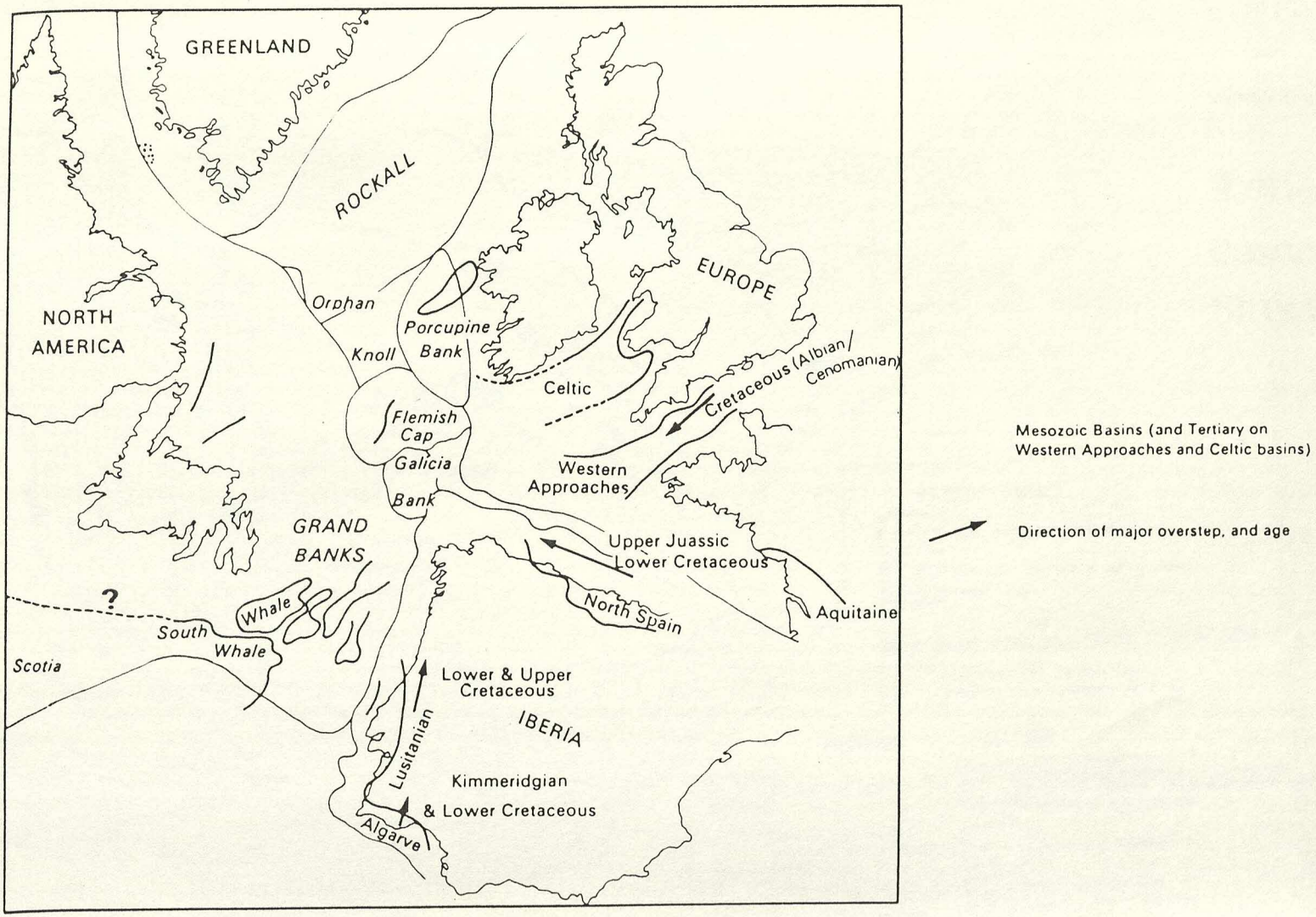

Sketch map showing probable Mesozoic basins formerly adjacent to Iberia. The "microplates" (Galicia Bank, Flemish Cap, Orphan Knoll, Porcupine Bank, Rockall Bank) are assembled into the available space in the correct north–south order

Fig 8.3. Hercynian structural units of the Iberian peninsula.

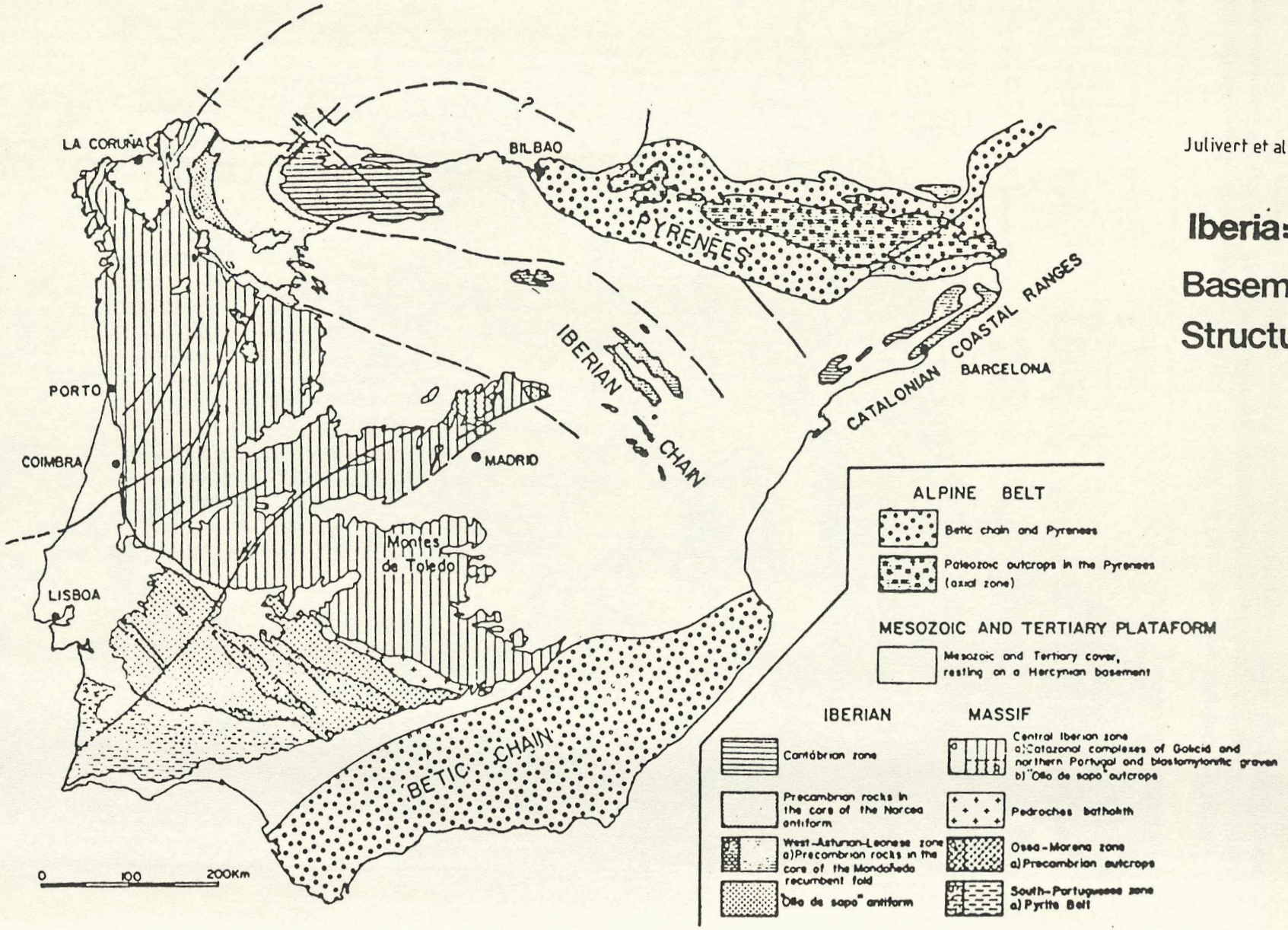

Structural units of the Iberian Peninsula and zonation of the Iberian massif [after Julivert, Fontbote, Ribeiro and Conde, 1972; based on Lotze's zonation (1945b)].

Fig 8.4. Morphology of the Hercynian Cordillera in the N Atlantic region.

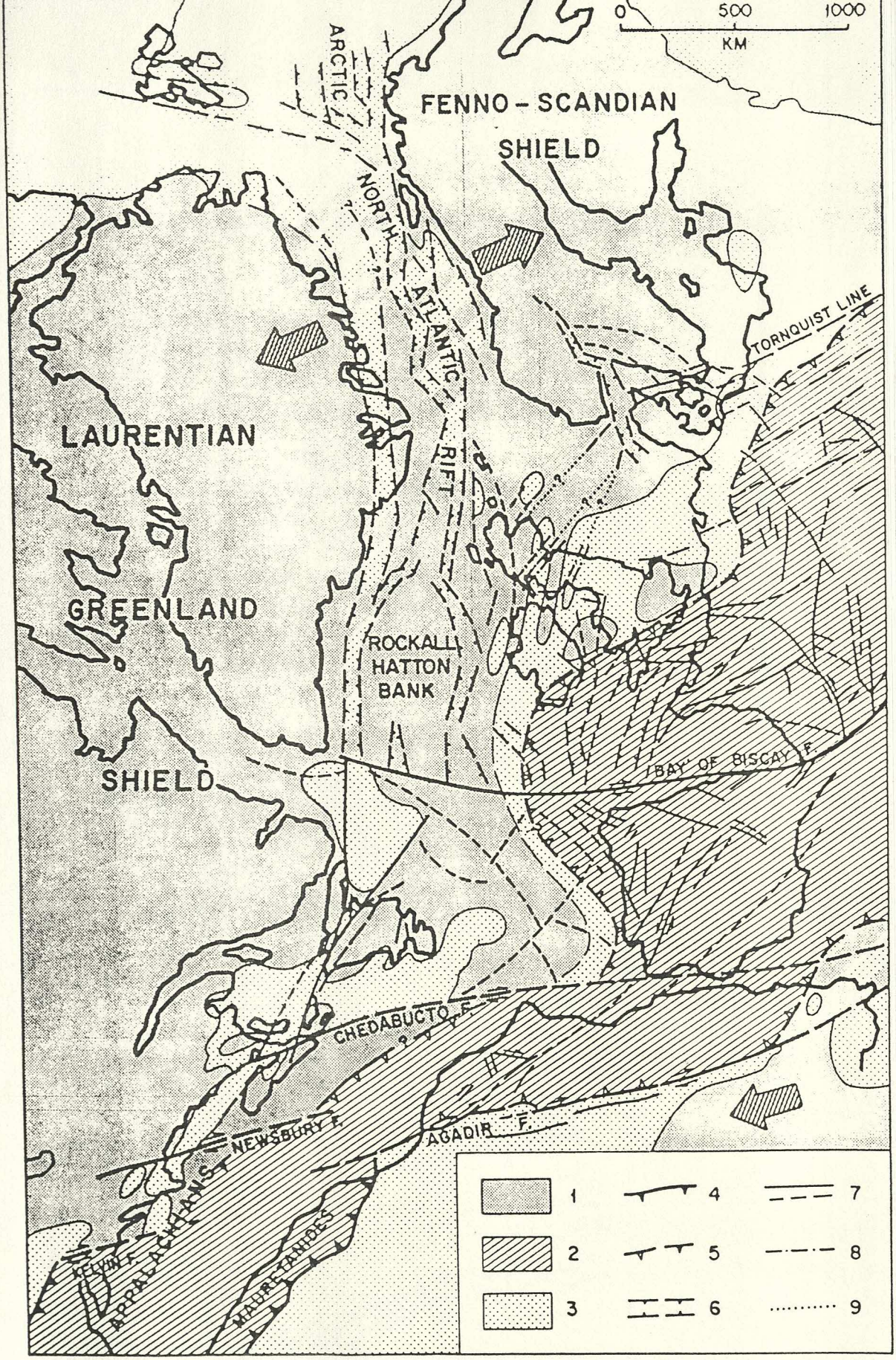

1. Contential cratons and intrabasinal highs; 2. Hercynian fold belts; 3. Carboniferous basins in Hercynian foreland; 4. Alleghenian deformation front; 5. Asturian deformation front; 6. Grabens, rifts; 7. Wrench faults; 8. Dyke swarms; 9. Alignements.

MORPHOLOGY OF THE HERCYNIAN OROGEN IN THE N ATLANTIC REGION

Ziegler, 1982

Fig 8.5. Late-Hercynian wrench faults in Europe (Arthaud & Matte, 1977).

LATE HERCYNIAN WRENCH FAULTS (Arthaud+Matte, 1977).

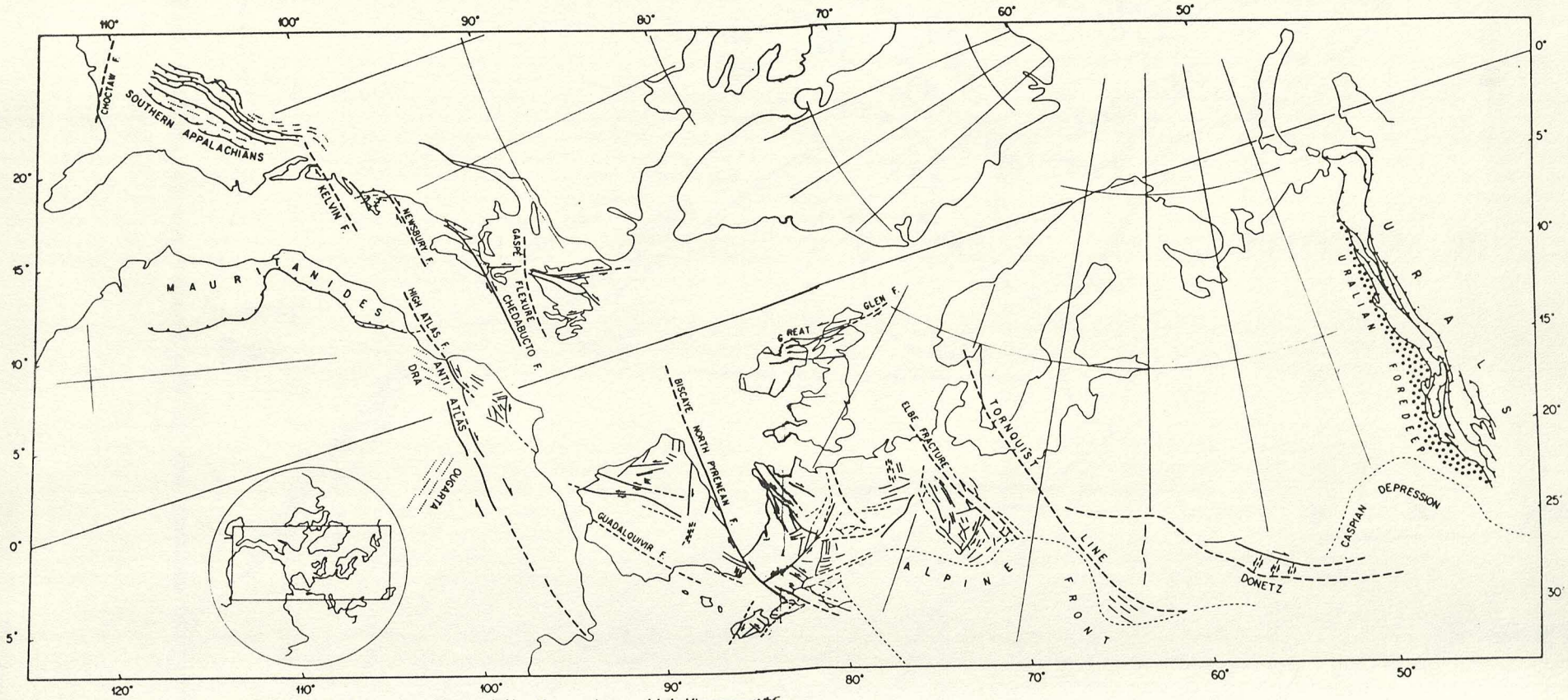

Structural map of the late Variscan structures, from the Urals to the southern Appalachians. Heavy continuous and dashed lines represent the observed and inferred main fractures. Chevron lines are overthrusts; fine dotted lines are folds. Fit of the continents after Le Pichon and others (1977). Oblique Mercator projection with pole at lat 18°S, long 49°E; Europe is in its present position.

Fig 8.6. Highly simplified structural map of the Iberian peninsula.

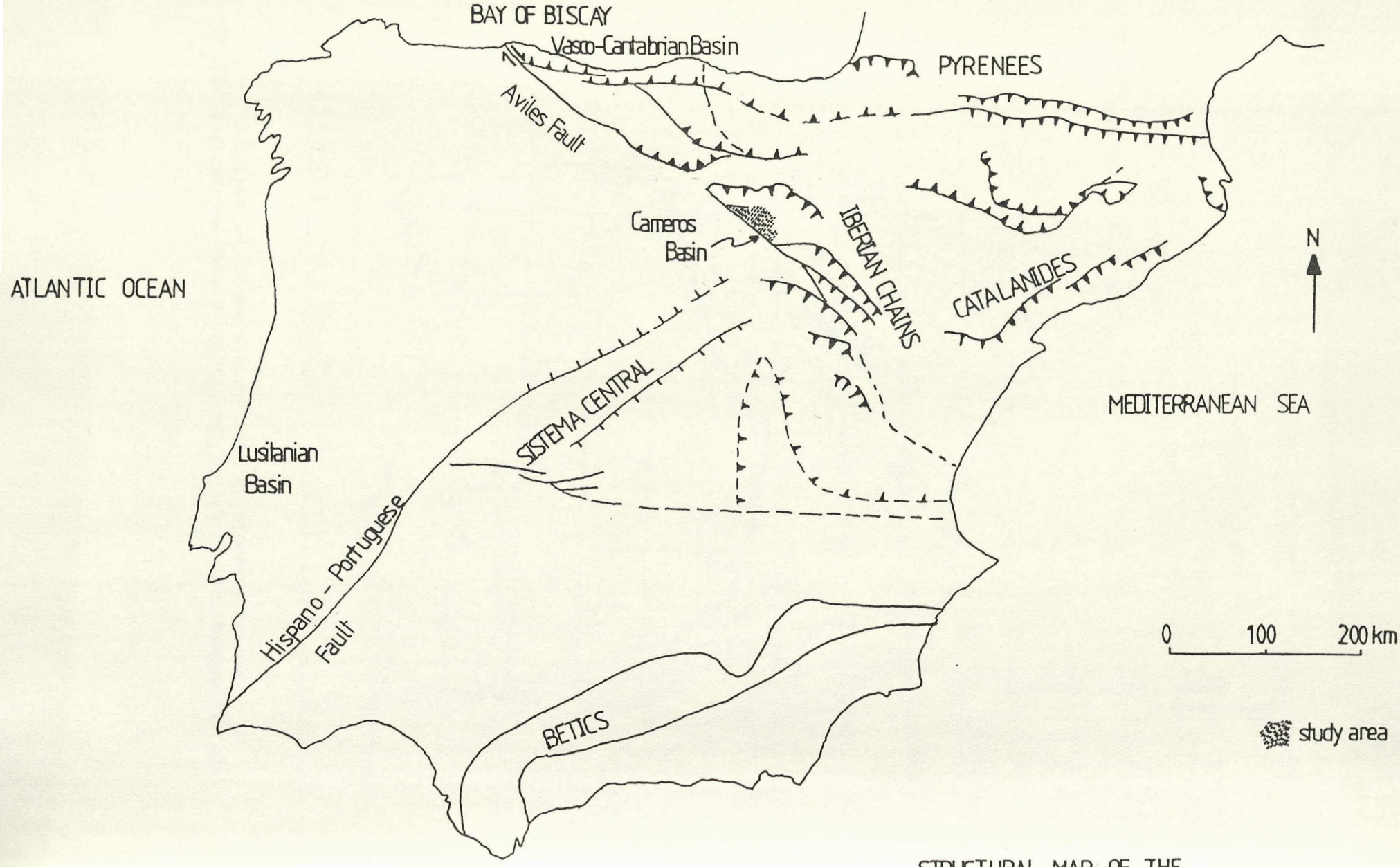

STRUCTURAL MAP OF THE IBERIAN PENINSULA

Fig 8.7. Buntsandstein isopach map of the Iberian peninsula. Note: Iberian Chains already form an elongate trough.


M A R C A N T A B R I C O
F R A N C I A
Madrid
— formación detrítica inferior —
(f. Buntsandstein)
Afloramientos de Paleozoico s str
Límite de existencia mínimo o actual.
Linea isópaca, con indicación de la potencia en centenares de metros.
Trazado cartográfico de la superficie de corrimiento de mantos o de cabalgamientos.
MAPA DE ISOPACAS

Fig 8.8. Triassic isopach map of NW Europe, From Ziegler (1982).

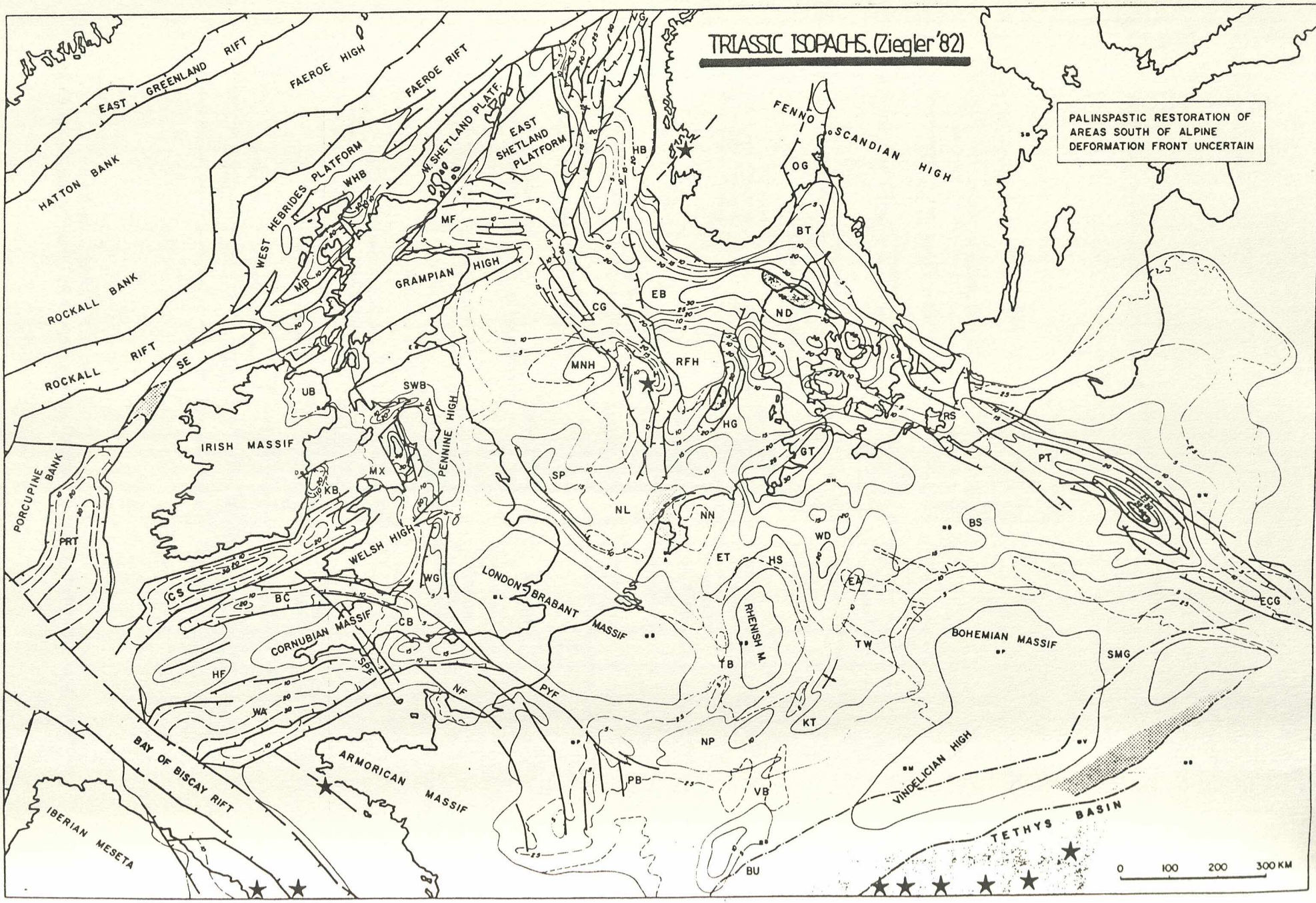
TRIASSIC ISOPACHS. (Ziegler '82)
PALINSPASTIC RESTORATION OF AREAS SOUTH OF ALPINE DEFORMATION FRONT UNCERTAIN
EAST GREENLAND RIFT
FAEROE HIGH
FAEROE RIFT
HATTON BANK
ROCKALL BANK
ROCKALL RIFT
SE
WEST HEBRIDES PLATFORM
WHB
MF
SHETLAND PLATF.
EAST SHETLAND PLATFORM
GRAMPIAN HIGH
MB
UB
SWB
PENNINE HIGH
IRISH MASSIF
PORCUPINE BANK
PRT
KB
MX
WELSH HIGH
WG
CS
BC
CB
CORNUBIAN MASSIF
SDF
HF
WA
NF
PYF
BAY OF BISCAY RIFT
IBERIAN MESETA
ARMORICAN MASSIF
PB
BU
VB
NP
KT
TB
RHENISH M.
LONDON BRABANT MASSIF
NL
SP
MNH
CG
HB
NG
FENNO SCANDIAN HIGH
OG
BT
EB
ND
RFH
HG
GT
RS
PT
NN
ET
HS
WD
BS
EN
TW
BOHEMIAN MASSIF
SMG
ECG
VINDELICIAN HIGH
TETHYS BASIN
0 100 200 300 KM

Fig 8.9. Detailed Jurassic stratigraphy of the Aguilar del Campoo region. Sbeta (1976).

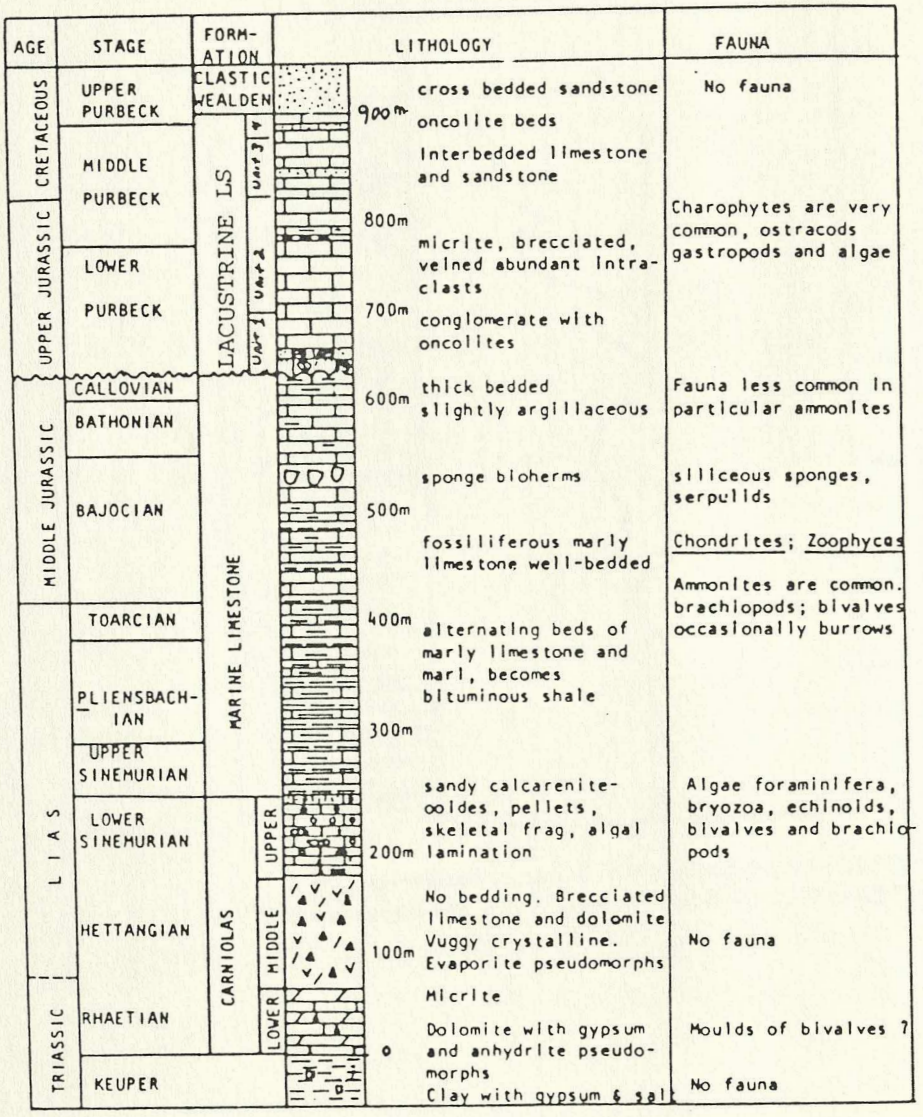

Generalized stratigraphic section of the Jurassic of the Aguilar de Campoo Region (North of Spain)

Fig 8.10 Exxon Global Coastal Onlap curve. From Whittaker (1985).

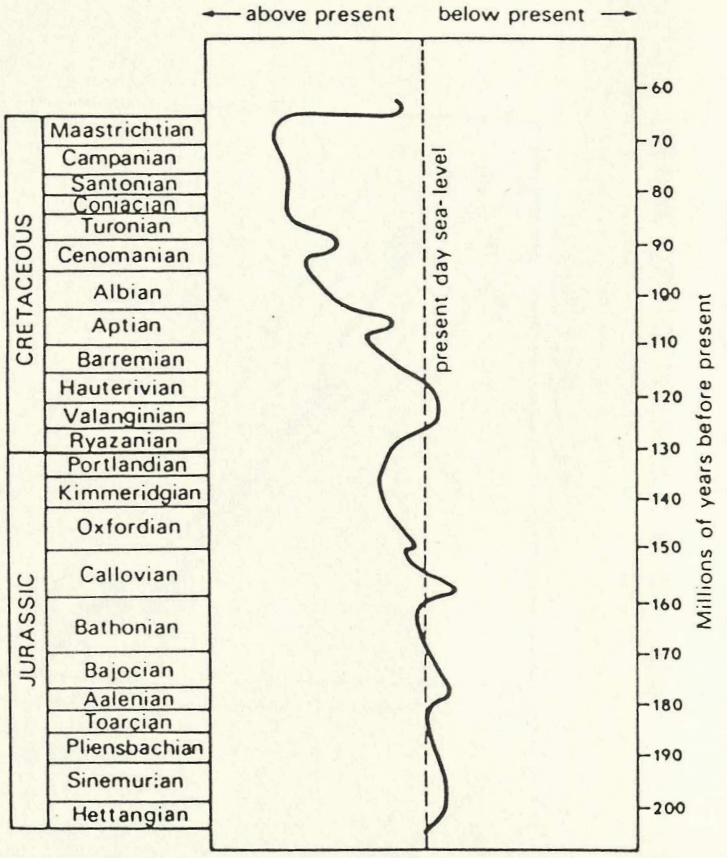

Generalized variation in global sea-level for the Jurassic and Cretaceous periods. Modified after Vail *et al.* (1977) and Hallam (1984).

Fig 8.11. Isopach map for the Liassic of the W Cameros Basin. After Valladares (1976).

VALLADARES (1976). ISOPACHS FOR MARINE JURASSIC

Tectonic control on NE-facing shelf: especially evident in Middle Jurassic

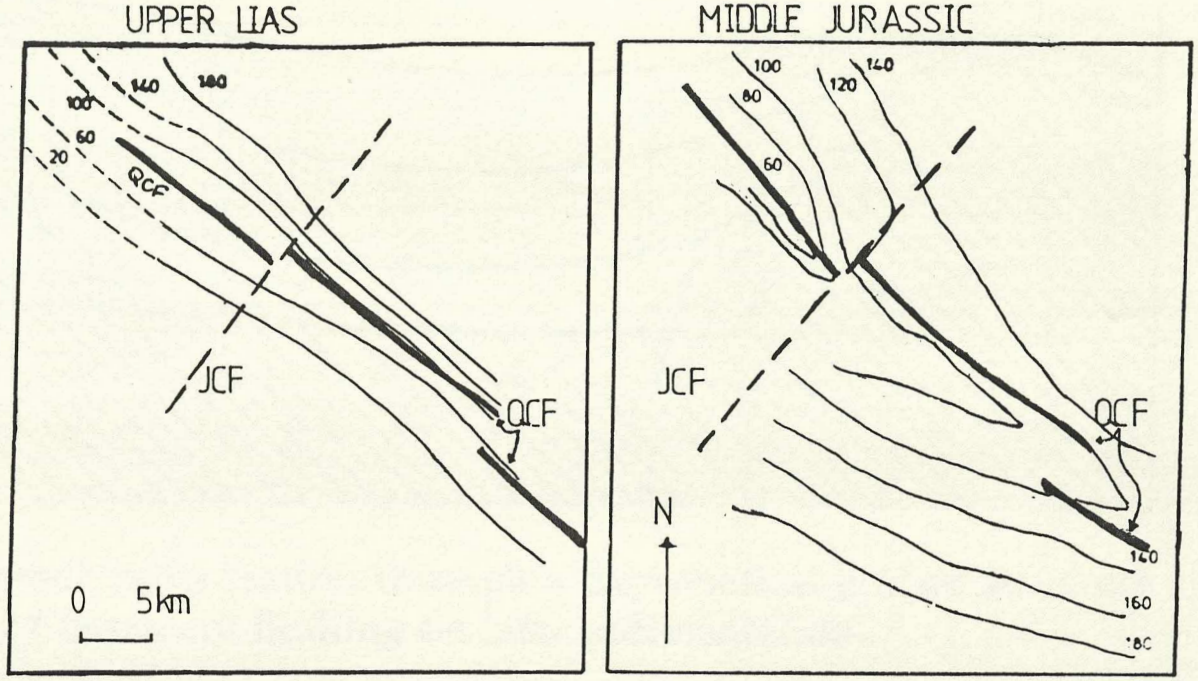

JCF — Jaramillo Covarrubias Fault

QCF — Quintanilla Castrovido Fault

Fig 8.12. Simplified model for the production of basins and swells by basement faulting. Whittaker (1975).

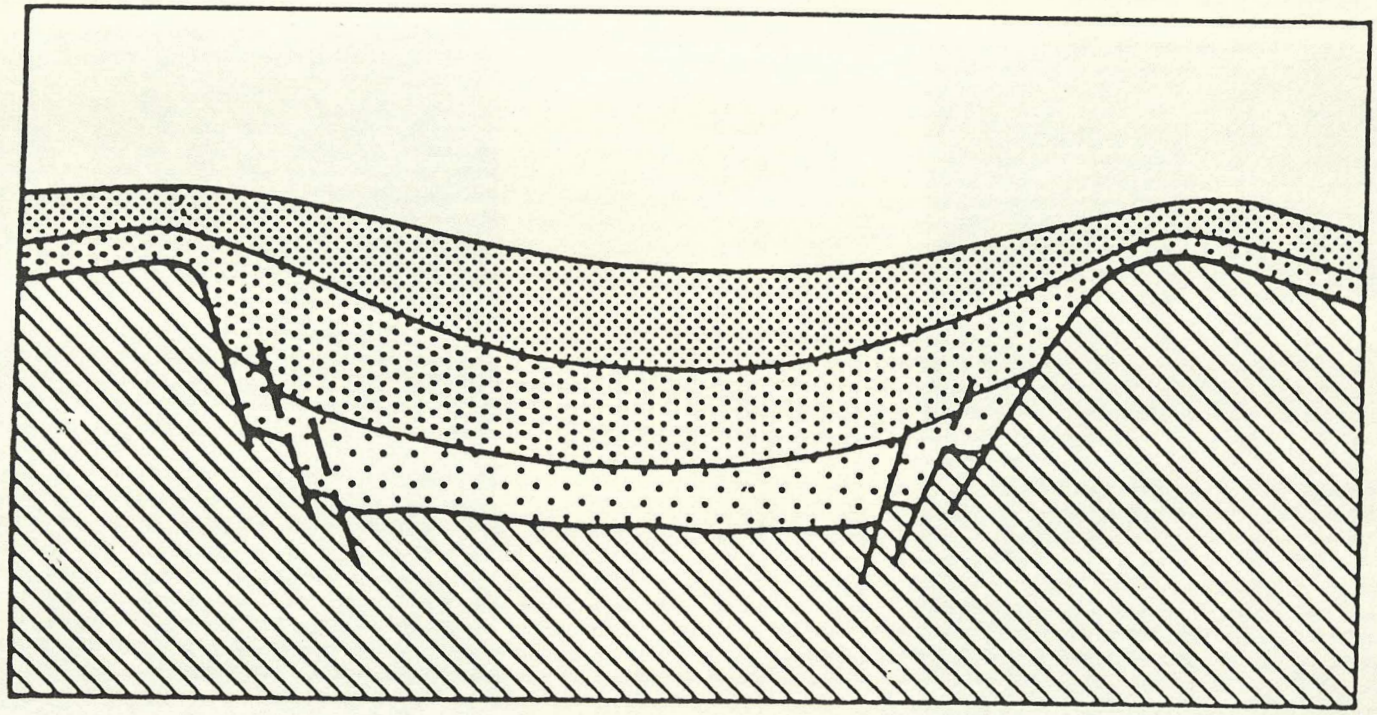

Diagrammatic cross-section through a hypothetical graben structure showing the possible effects of basement faulting on later sedimentation.

Fig 8.13. Middle Jurassic discordance between ?folded, massive sponge limestones of Aalenian and well-bedded unfossiliferous calcarenites of Upper Bajocian. See also fig 2.14 and compare with evolution diagram from Gomez (1979; fig 8.16). Quintanilla de las Vinas. Looking S.

Fig 8.14. Massive limestones of Bathonian (see also fig 2.15) showing presence of black (?algal clasts). Mambrillas de Lara.

Fig 8.15. Sedimentary evolution of the Late Toarcian - Early Bajocian (Ureta & Kalin, 1985) in the Cameros Basin and Sierra de la Demanda.

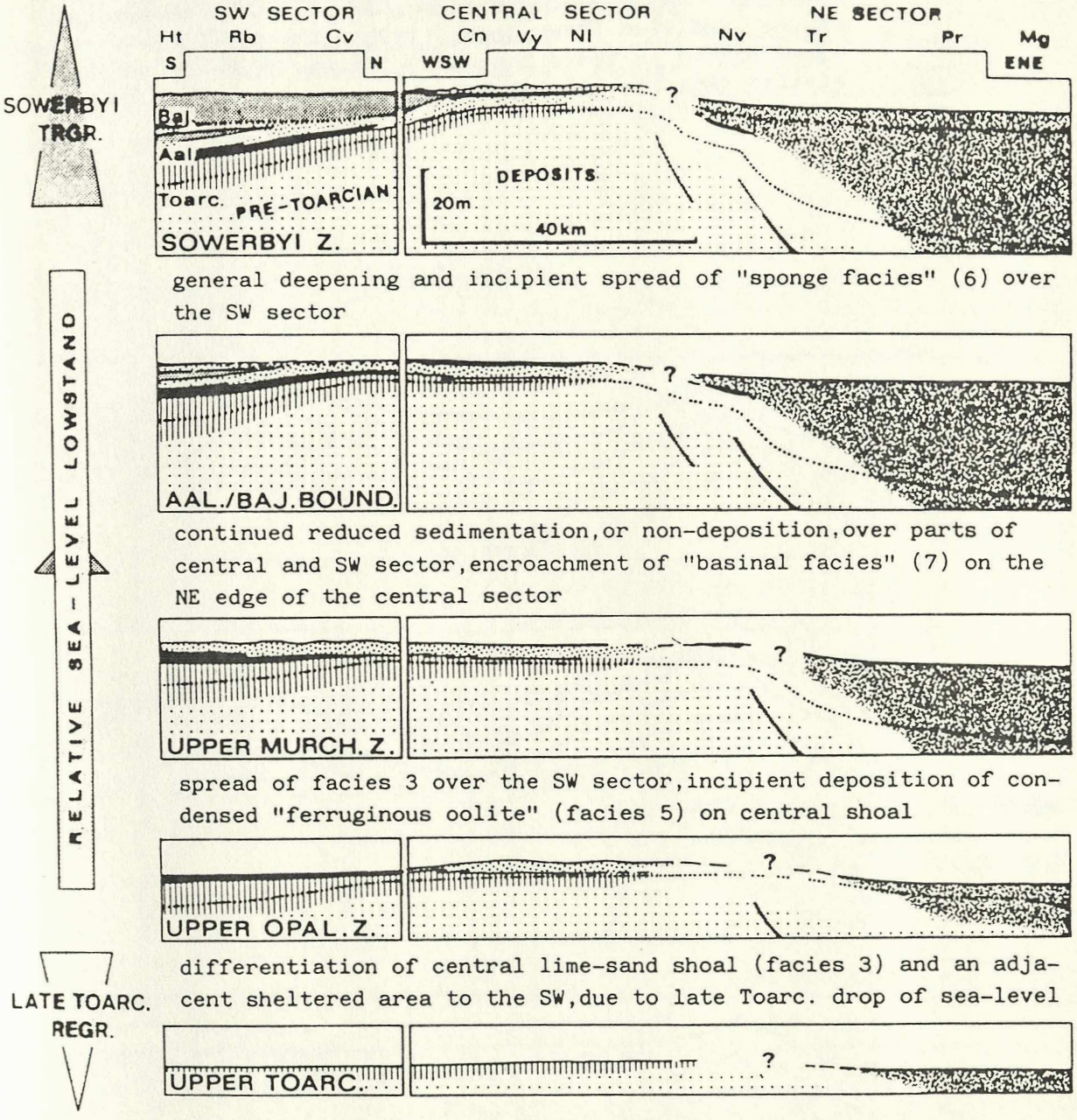

INFERRED LATE TOARCIAN TO EARLY BAJOCIAN SEDIMENTARY EVOLUTION OF THE NW CELTIBERIAN DOMAIN (for legend cf. fig.3); bathymetry and suggested sea-floor morphology not to scale

Fig 8.16. Evolution diagram showing the development of the Late Toarcian - Early Bajocian unconformity in the SE Iberian Chains. Modified after Gomez (1979). The development of this unconformity in the W Cameros Basin was probably very similar (see figs 2.14 & 8.13).

LOWER-MIDDLE JURASSIC UNCONFORMITY OF THE SE IBERIAN CHAINS.

after Gomez (1979). Modification to indicate role of tectonics

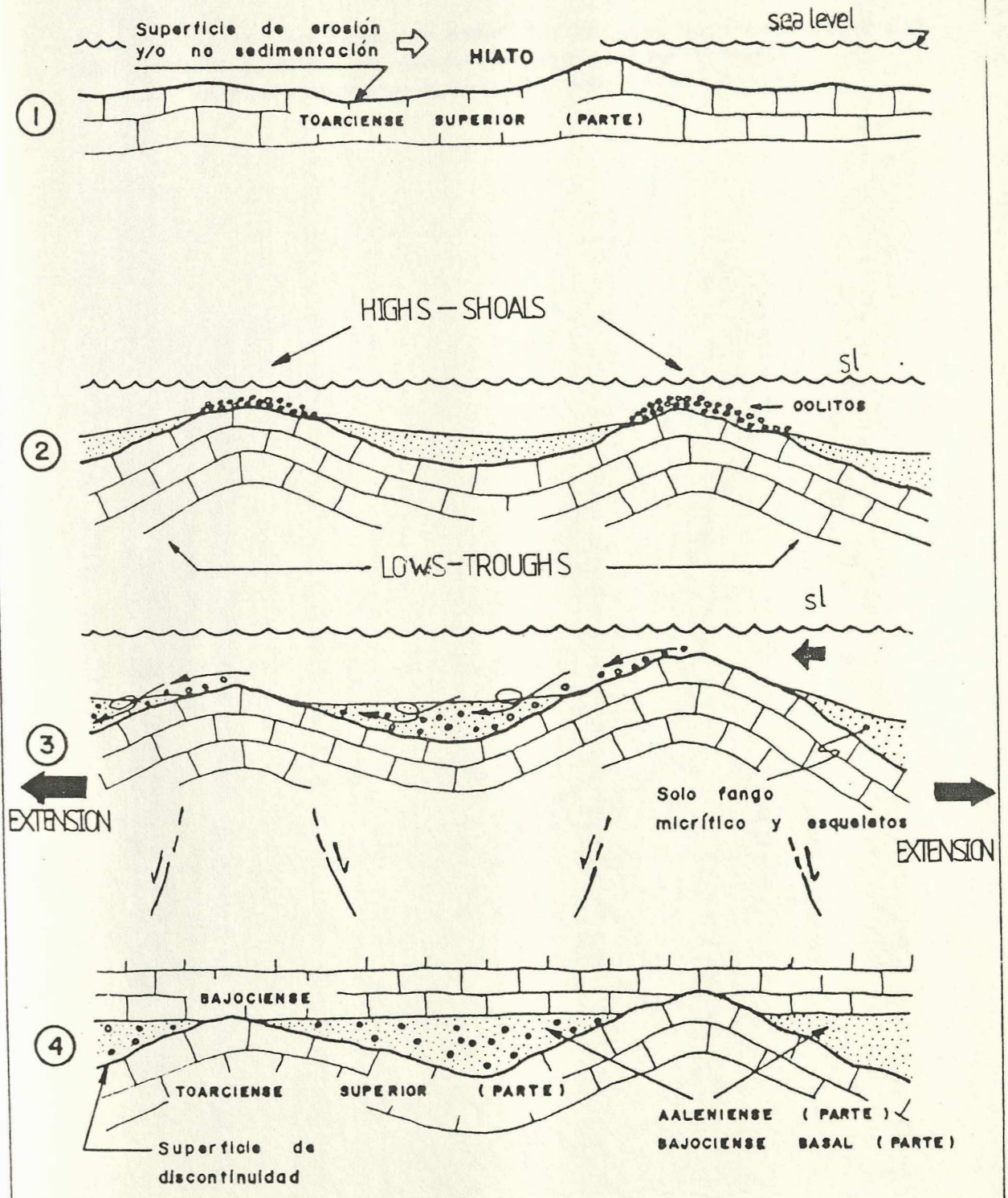

Representación gráfica por secuencias de una de las hipótesis expuestas en el texto sobre el origen de la capa de oolitos ferruginosos y/o fosfáticos de la parte inferior del Jurásico medio. 2 y 3 pueden ser repetitivas, dando como resultado final el estado 4. Figura sin escala.

Fig 8.17. Classical view of the "Late Jurassic retreat of the seas". Supposed gradual E-ward regression. Salomon (1982), after Bulard (1972). See critical discussion in text.

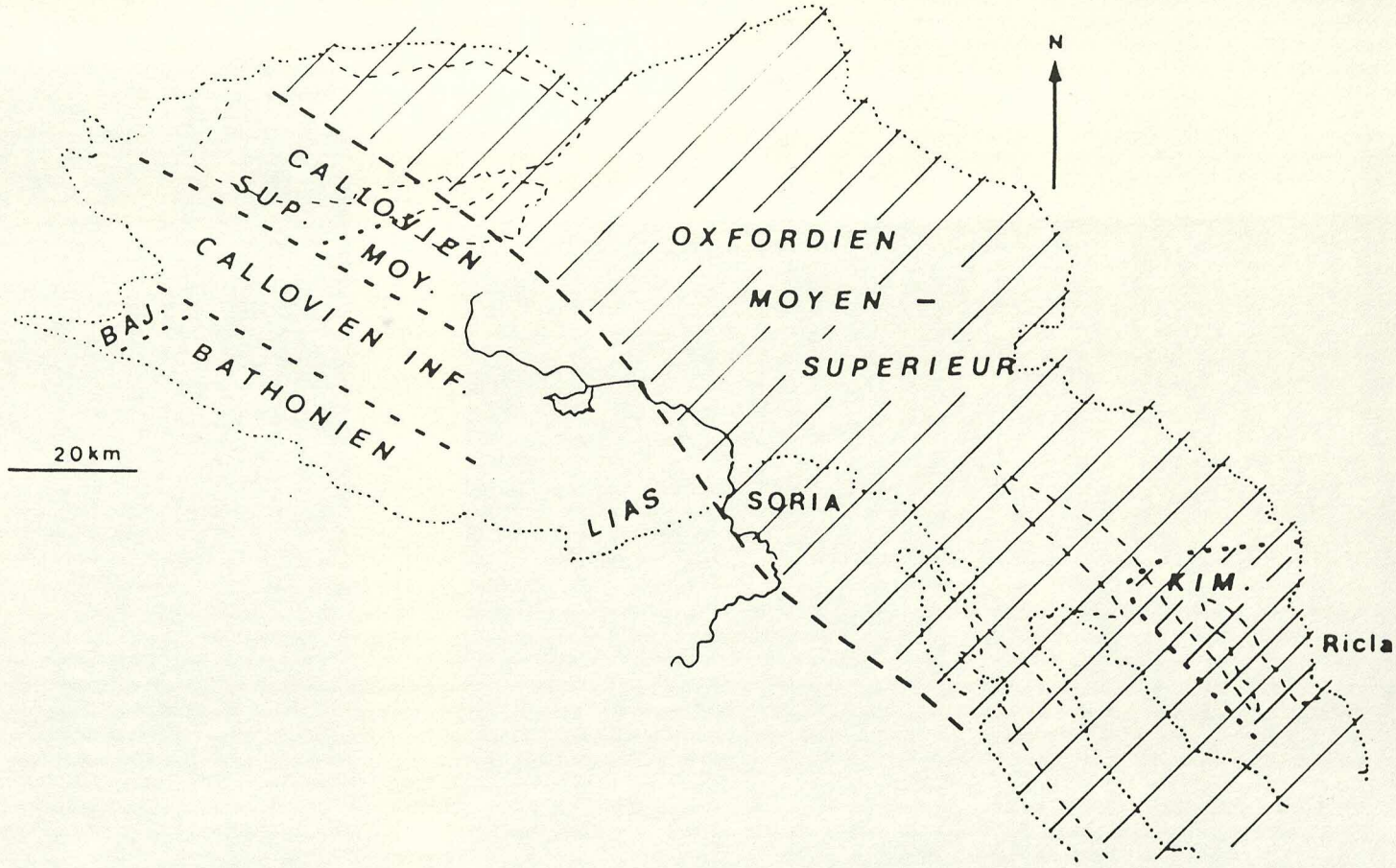

Le NW des Chaînes ibériques après la régression du Kimmeridgien.
Aspect du substratum ante - fossé.

Published view of main Cimmerian unconformity (Salomon, 1983): progressive retreat of sea to NE.

1 map omits U Oxfordian Lr Kimmeridgian Talveila Formation.

2 organic rich M/U Callovian probably deposited over whole area during time of elevated sea level.

Fig 8.18. Red-mottled and nodular limestones lying above Bathonian carbonates.
Interpretation: Subaerial exposure and pedogenetic modification.
Contact with base of the (Upper Oxfordian) Talveila Formation. Hortezuelos. W Cameros Basin and correlation with S England.

Fig 8.19. Coarse cross-bedded gritty yellow sands showing numerous reactivation surfaces and synsedimentary extensional normal faults. Clear differences in thickness of coarser gritty sand units discernible across fault (passing lower centre to upper left, to left of hammer). Lower Talveila Formation. Hortezuelos. Looking NE.

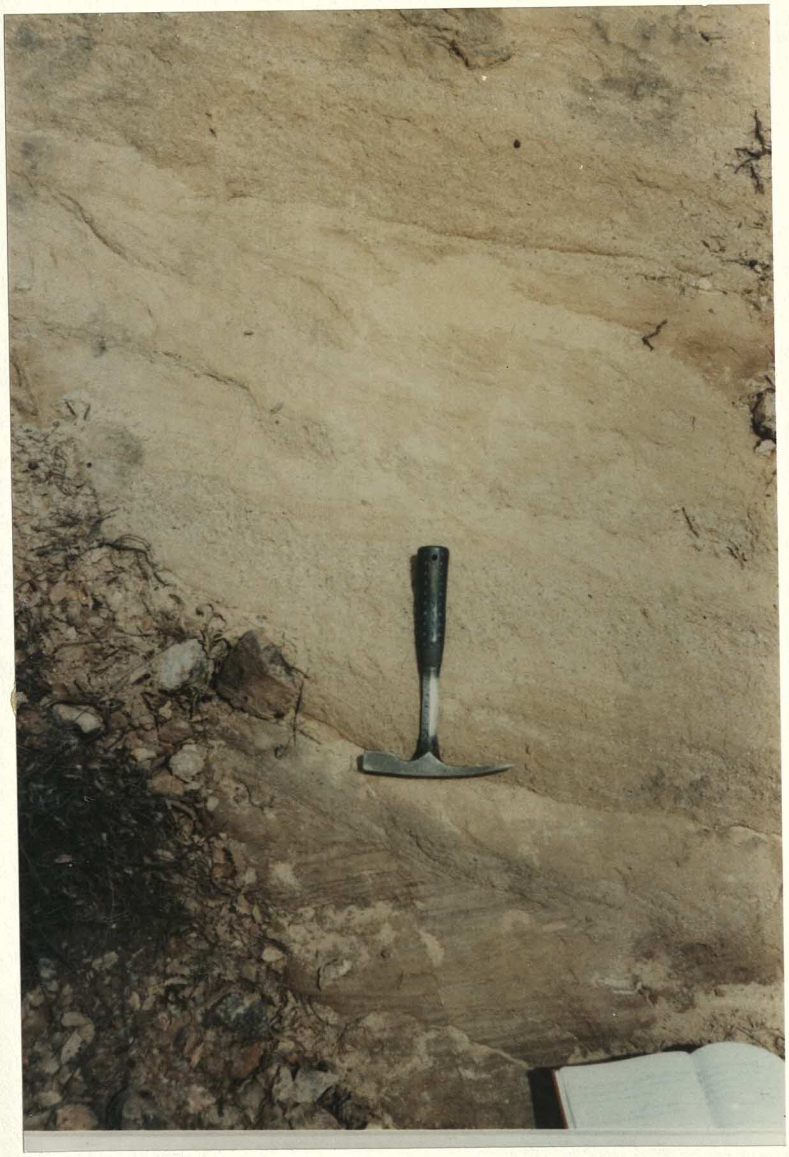

Fig 8.20. Yellow gritty sandstones, calclithites and red silts exhibiting synsedimentary extensional normal faults. Note thickness differences across faults (most clearly visible for red horizons), small-scale "horst and graben" structure, undermining of red silt above hammer. Near base of Talveila Formation. Hortezuelos (1km W of village). The presence of thin and graded clastic laminae in a fine-grained background indicates quiet, possibly deep water sedimentation.

Fig 8.21. Interbedded cross-bedded arenites and quartz-pebbly sands showing synsedimentary extensional normal faults. Note clear thickness variation across fault. Possible development of anticlinal "rollover" structure (upper right). Fining upward of conglomerate sand sequences visible. Lower Talveila Formation. Hortezuelos.

Fig 8.22. Vertical arrangement of Talveila Formation facies. From Diaz-Molina et al (1983).

Regressive cycles

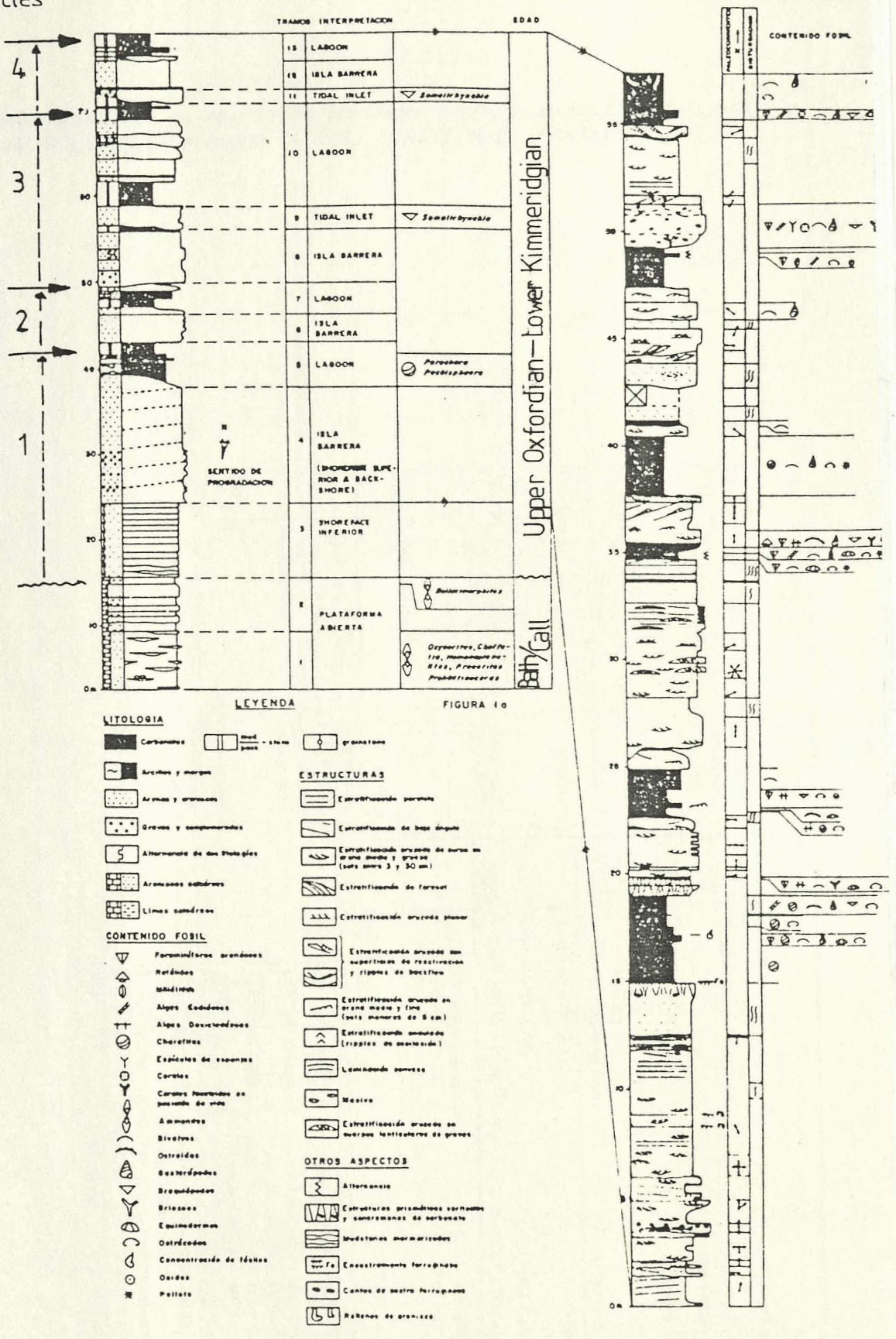

TALVEILA FORMATION - regressive cycles

(modified after Diaz et al, 1983).

Fig 8.23. Diagram showing sequence of facies in the Corallian of S England. From Talbot (1973). Compare with fig 8.22.

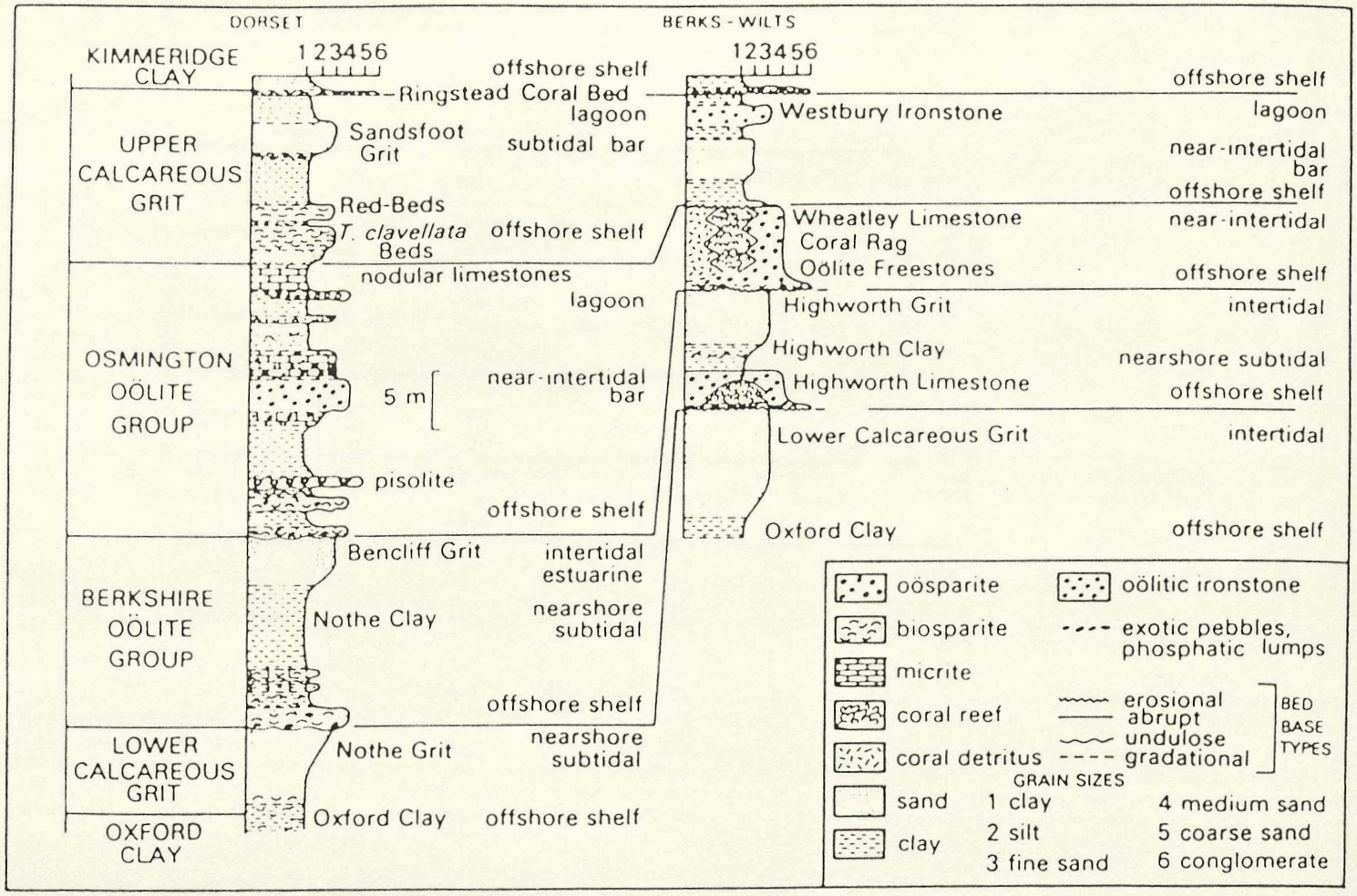

Cyclic sequences and interpretation of depositional environments of the Corallian (upper Oxfordian) in S. England (after Talbot 1973).

Fig 8.24. Detailed stratigraphy of the Corallian of S England. From Wright (1986) and Talbot (1973).

Stratigraphic subdivisions of south Dorset

Kimmeridge Clay

	Formation		Thickness (m)	
CORALLIAN GROUP	Ringstead	Ringstead Coral Bed Osmington Mills Ironstone Ringstead Clay	0.15–0.2 3.5–5.0	UPPER OXFORDIAN
	Sandsfoot	Sandsfoot Grit Sandsfoot Clay	7.2–11.3 5.0–15.5	
	Trigonia clavellata	Red Beds Clay Band Chief Shell Beds Sandy Block	2.32 0.6 1.35–2.12 1.52–2.27	
	Osmington Oolite	Nodular Rubble Shortlake Upton	1.6–3.9 5.9–7.7 7.9–13.2	MIDDLE OXFORDIAN
	Redcliff	Bencliff Grit Nothe Clay Preston Grit	6.7 10.0–13.5 1.8	
	Nothe Grit	Not subdivided	9.3	LOWER OXFORDIAN (PART)

Oxford Clay

Thick horizontal lines represent marine transgressions

Fig 8.25. Depositional model for the Corallian of S England. From Talbot (1973).

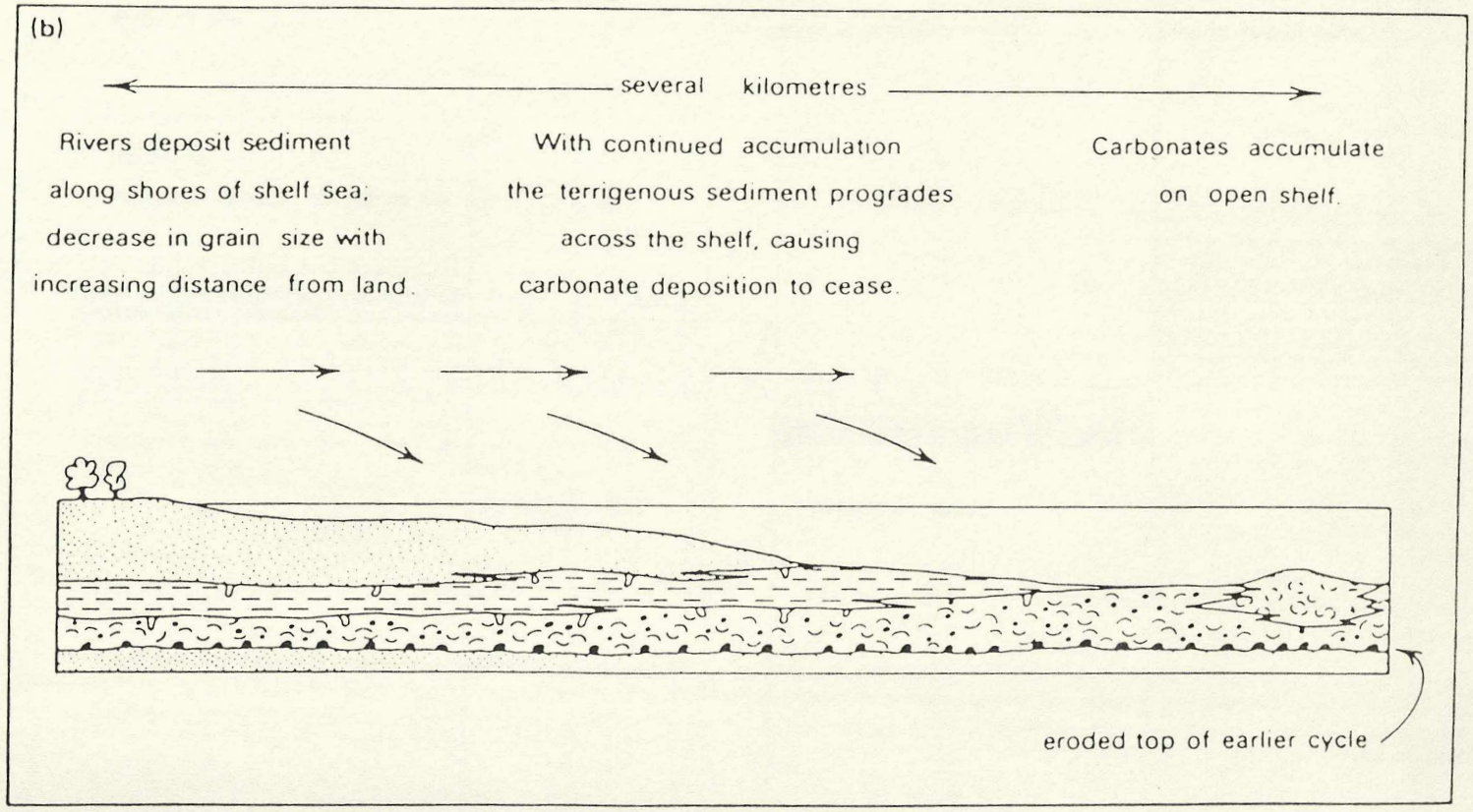

Depositional model for the origin of the limestone–clay–sand cycle in the Corallian of S. England (after Talbot 1973).

Fig 8.26. Sketch map / section of the Talveila sections showing the rôle of NE-SW faults in controlling the variable preservation of the upper Talveila Formation limestones beneath the sub-Senora de Brezales Formation unconformity.

SKETCH SECTIONS AROUND TALVEILA — (N OF SAN LEONARDO FAULT).

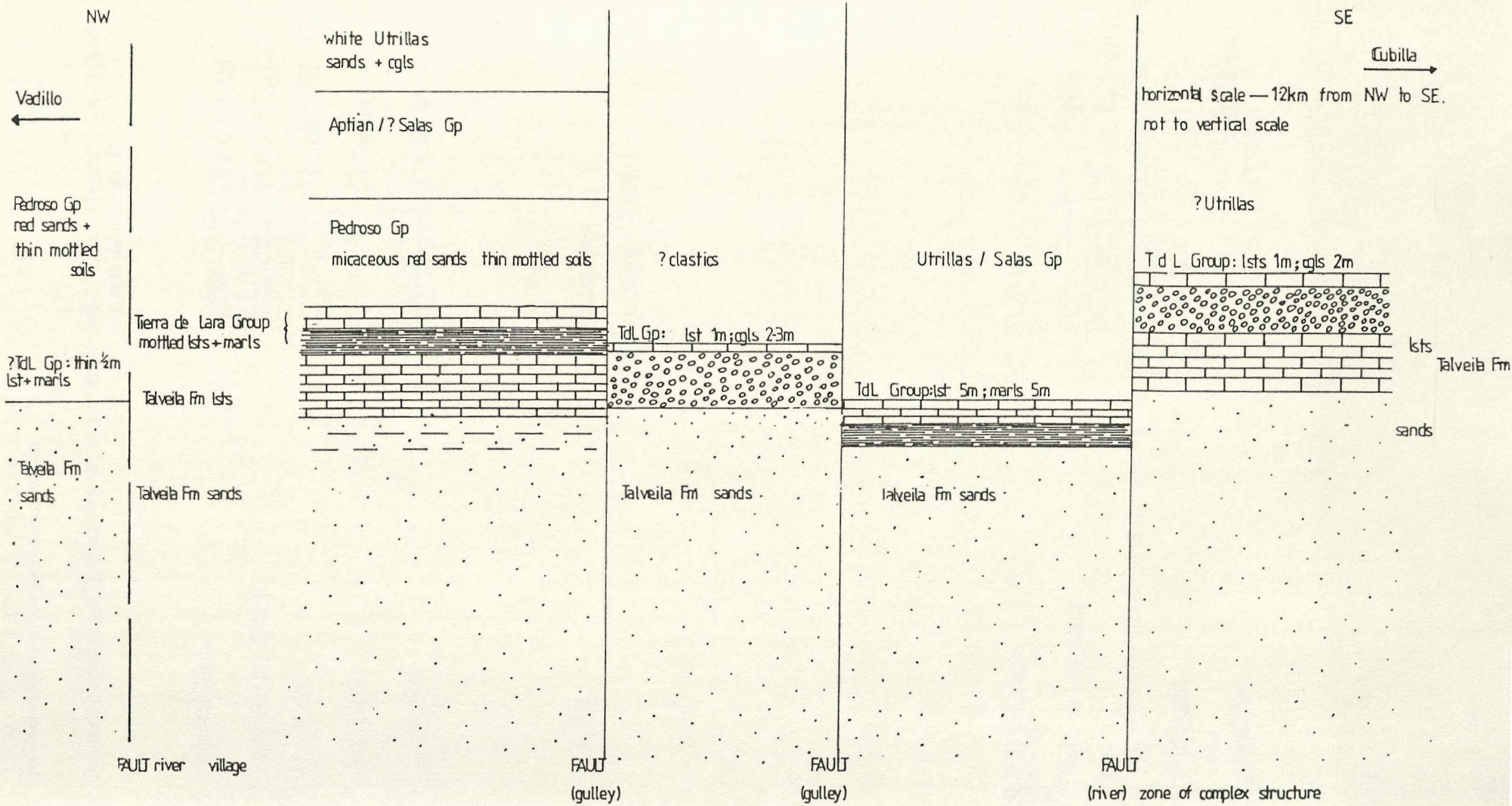

NOTE facies, thickness changes across faults
local preservation of Talveila Fm lsts on some fault blocks only
faults must have multiphase reactivation

Fig 8.27. Middle and Upper Jurassic sequences from four sectors of the W Cameros Basin.

MIDDLE/UPPER JURASSIC SEQUENCES FROM FOUR SECTORS OF THE W CAMEROS BASIN

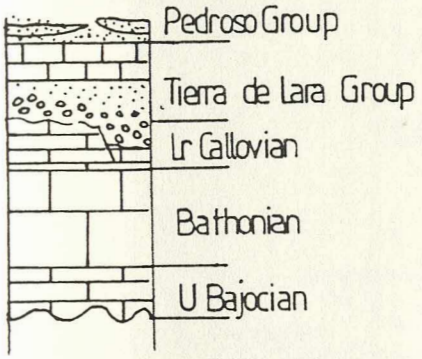

NW

(Quintanilla de las Viñas)

(TdL Group)

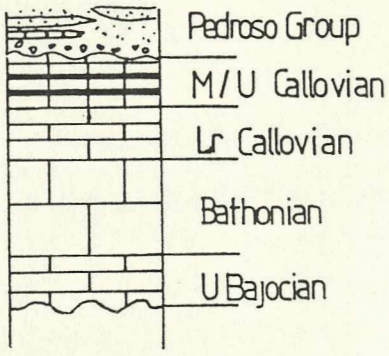

NE

(Villavelayo)

(Barbadillo del Pez: left)

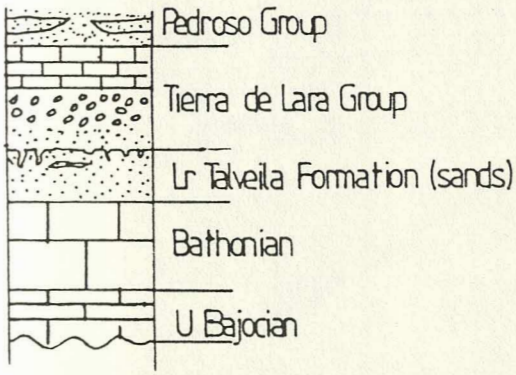

SW

(Hortezuelos)

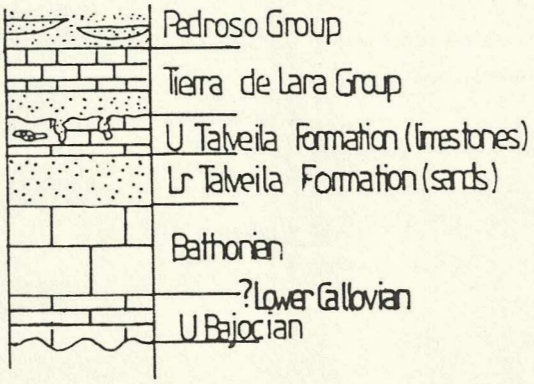

SE

(Talveila)

Fig 8.28. Simplified model for the geometry of Late Jurassic unconformities (not accounting for the rôle of faulting).

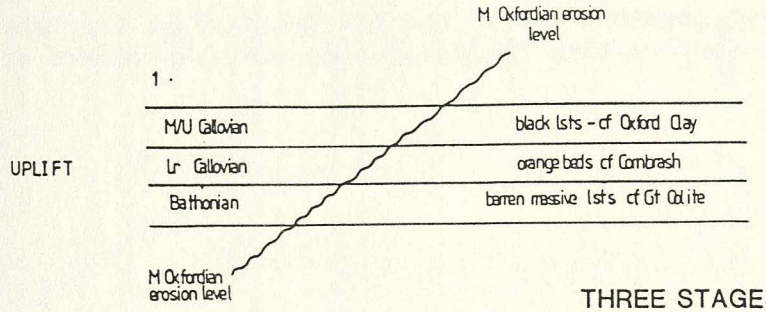

THREE STAGES IN THE DEVELOPMENT OF THE LATE CIMMERIAN UNCONFORMITY

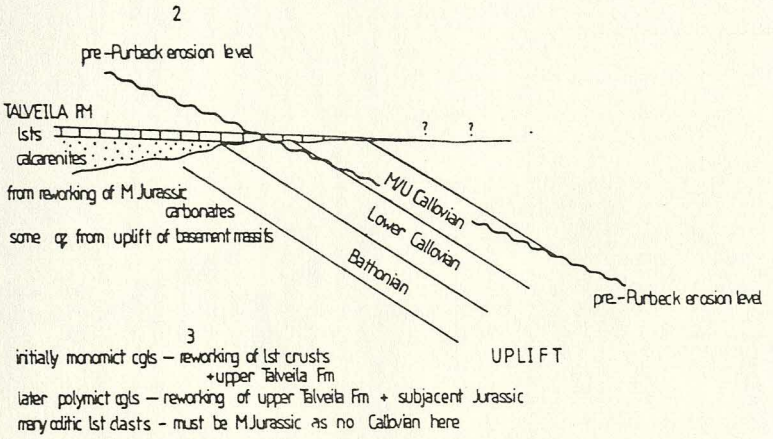

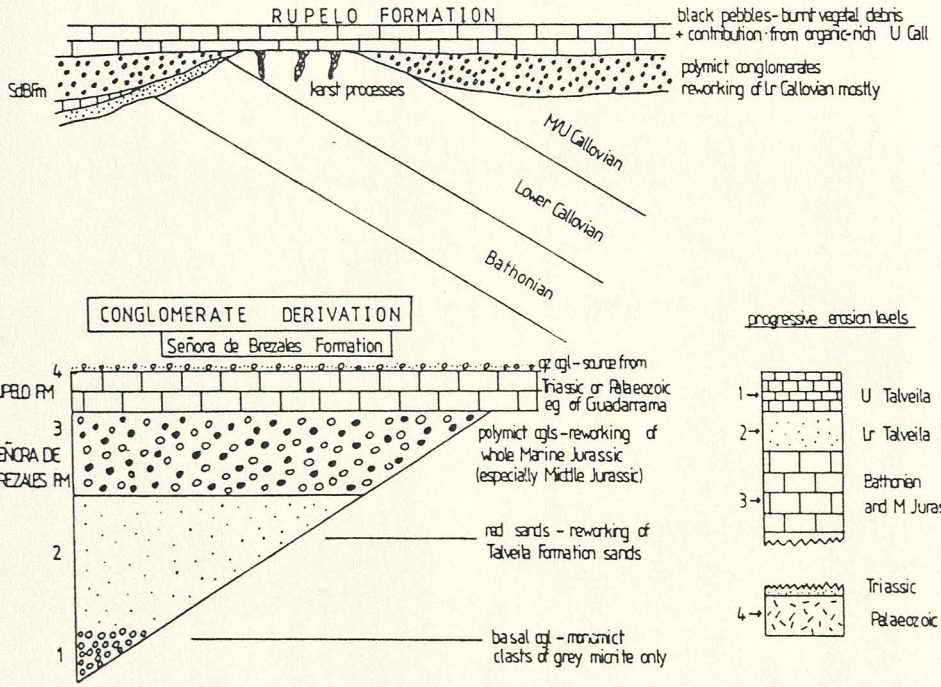

Fig 8.29. Two possible models for the geometry of the Late Jurassic unconformities taking into account the effect of faulting.

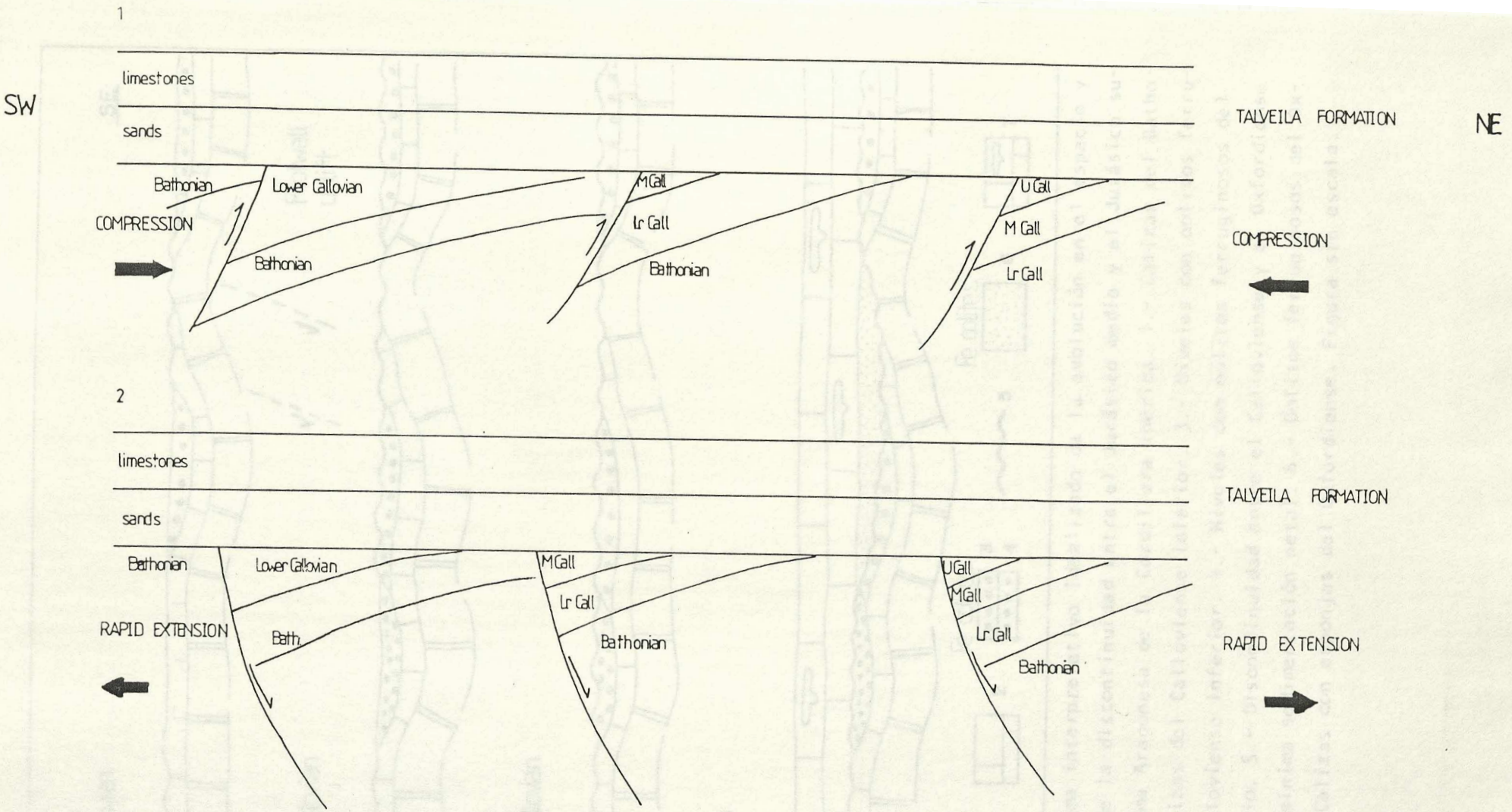

Two models for the pre- Upper Oxfordian unconformity in the W Cameros.

1) Compression - inversion and truncation (maximum truncation in areas of previously maximum subsidence)
2) Extension & sea level fall - footwall uplift, erosion at crestal axes of rotated fault blocks

"Marine Jurassic" horizons generally thicken to NE
- Jurassic fault geometry more likely to have been as in 2).

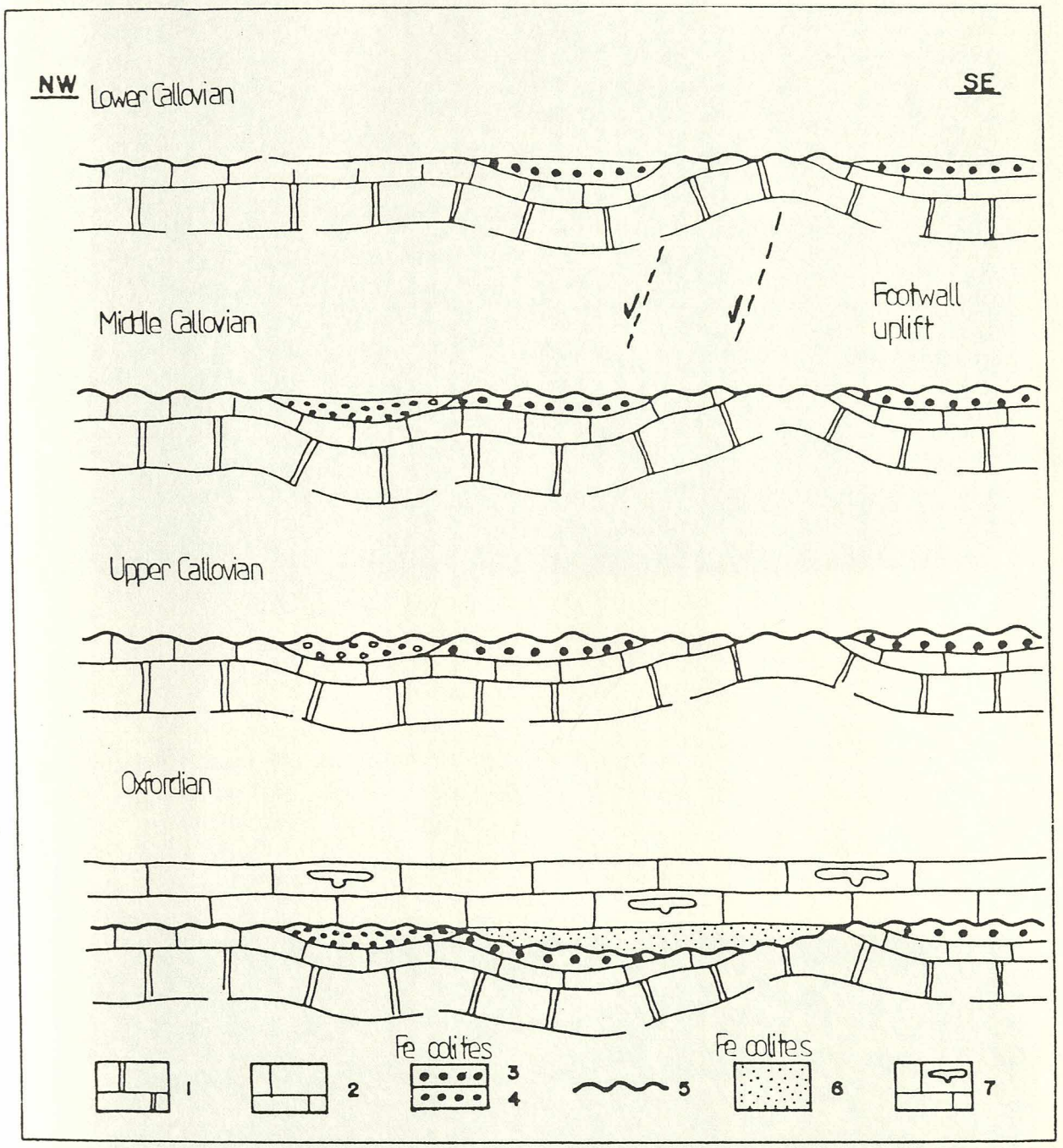

Esquema interpretativo idealizado de la evolución en el espacio y en el tiempo, de la discontinuidad entre el Jurásico medio y el Jurásico superior en la Rama Aragonesa de la Cordillera Ibérica. 1.- Calizas del Bathoniense. 2.- Calizas del Calloviense inferior. 3.- Niveles con oolitos ferruginosos del Calloviense inferior. 4.- Niveles con oolitos ferruginosos del Calloviense medio. 5.- Discontinuidad entre el Calloviense y el Oxfordiense (superficie de mínima sedimentación neta). 6.- Oolitos ferruginosos del Oxfordiense. 7.- Calizas con esponjas del Oxfordiense. Figura sin escala.

Fig 8.30. Pocket of conglomerate just below top contact of upper Talveila Formation limestones. Red sand matrix, angular, locally derived limestone clasts. Red sand also following joints.
Interpretation: Karst pot-hole / doline developed in Talveila Formation carbonates during exposure at onset of Senora de Brezales Formation deposition. Conglomerate fill of cavity derived by partial roof-collapse; sand also exploiting joints. Exposure of carbonates impressive karst. Talveila.

Fig 8.31. Upper Talveila Formation limestones showing piping of red Senora de Brezales Formation sands along cracks and joints.
Interpretation: Karst processes modifying Talveila Formation carbonates at onset of Senora de Brezales Formation deposition. Limestones relatively resistant to erosion karst erosion; cf sands easily reworked.
1km SE of Pinilla de los Barruecos.

Fig 8.32. Red Senora de Brezales Formation sands resting on brecciated upper Talveila Formation limestones. Pinilla de los Barruecos.

Fig 8.33. Red sands apparently filling cavity below Senora de Brezales Formation conglomerates. 1km SE of La Gallega, beside forest track to Huerta del Rey.

Fig 8.34. Bedding plane of upper Talveila Formation limestones showing karst penetration of red Senora de Brezales Formation sandstones. Pinilla de los Barruecos.

Fig 8.35. Thick red sands (lithology cf Senora de Brezales Formation) occurring below upper Talveila Formation carbonates.
Possible interpretations:
a) interdigitation of Talveila and Senora de Brezales Formations;
b) karst, piping red sands into cavities along fissures outside the plane of this outcrop.
In view of the evidence from figs 2.30 & 2.31 of karstic processes and of a clear erosive break between the two formations, interpretation b) seems most reasonable.
Rio Helechal, Hortezuelos.

Fig 8.36. Heavily disturbed karst surface of upper Talveila Formation limestones. Red sands and conglomerates of Senora de Brezales Formation above. Especially coarse breccia to right of fault (behind hammer). Fault does not appear to offset overlying Senora de Brezales Formation above horizon of breccia - movement approximately dated at onset of continental deposition. Looking E. Hortezuelos.

Fig 8.37. Red sands present below upper contact of lower Talveila Formation arenites. Red sands fill 10-30cm depressions and penetrate yellow arenites only 10cm.
Interpretation: Limestones of upper Talveila Formation removed (or absent) at this locality. Subaerial exposure of sands minor karst, easy erosion. Circular depressions might be karst hollows or tree/bush roots.
Hortezuelos.

Fig 8.38. NW sector: contact between marine Jurassic pediment (here of Lower Callovian age) and base of continental sequence, showing piping of red sand of Senora de Brezales Formation along cracks/joints in subjacent limestone. Irregular top surface of limestone. 1km NE of Pinilla de los Barruecos (10m SE of road to Piedrahita de Muno, just before first sharp curve).

Fig 8.39. NW sector: contact between marine Jurassic pediment (bottom of photograph) and Tierra de Lara Group above. Pediment (here of Lower Callovian age) is strongly discoloured and brecciated below hammer - this reflecting pedogenetic modification as a result of subaerial exposure prior to deposition of basal Rupelo Formation carbonate crust (just above hammer) - ?Senora de Brezales Formation equivalent. Mambrillas de Lara.

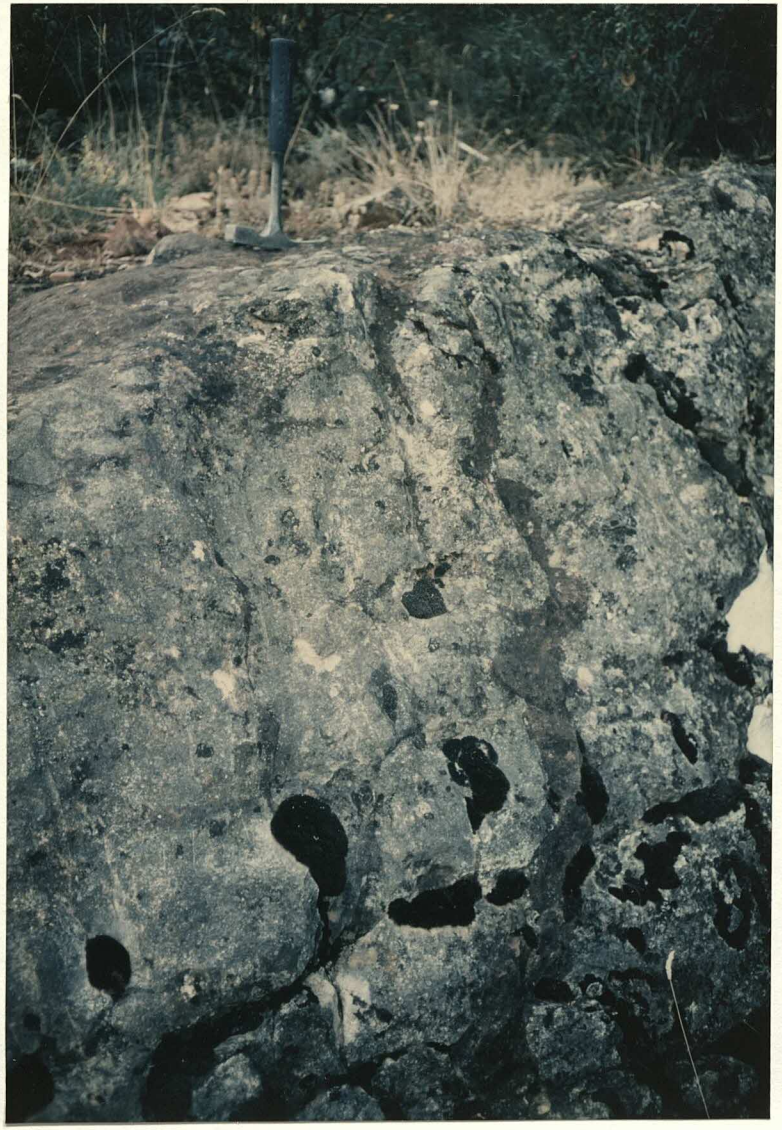

Fig 8.40. NE sector: contact between marine Jurassic pediment and Tierra de Lara Group above. Pediment here of Lower (-Middle?) Callovian age, strongly discoloured. Overlain by matrix-supported conglomerate of 0.5-1cm rounded clasts. Interpretation: Palaeosoil development - pedogenetic modification of marine Jurassic pediment in interchannel areas. Senora de Brezales Formation. Castrovido.

Figs 8.41 - 8.43. Yellow Lower Callovian limestones incised by Senora de Brezales Formation channelised polymict conglomerates. Laminated limestone lying above conglomerates at edge of field, which lies on Las Vinas Member red marls. Mountain of Upper Cretaceous limestone (Penalara) in background. See interpretative sketch map showing morphology of unconformity and fault control on some of the conglomerate channels (fig 8.44). 1km SW of Quintanilla de las Vinas.

Figs 8.41 - 8.43. Yellow Lower Callovian limestones incised by Senora de Brezales Formation channelised polymict conglomerates. Laminated limestone lying above conglomerates at edge of field, which lies on Las Vinas Member red marls. Mountain of Upper Cretaceous limestone (Penalara) in background. See interpretative sketch map showing morphology of unconformity and fault control on some of the conglomerate channels (fig 8.44). 1km SW of Quintanilla de las Vinas.

Fig 8.44. Sketch map of area 1km SW of Quintanilla de las Vinas shown in figs 8.41-8.43 showing the nature of the Lower Callovian - Tierra de Lara Group unconformity. Map is oriented to give appreciation of a sectional view through the unconformity.

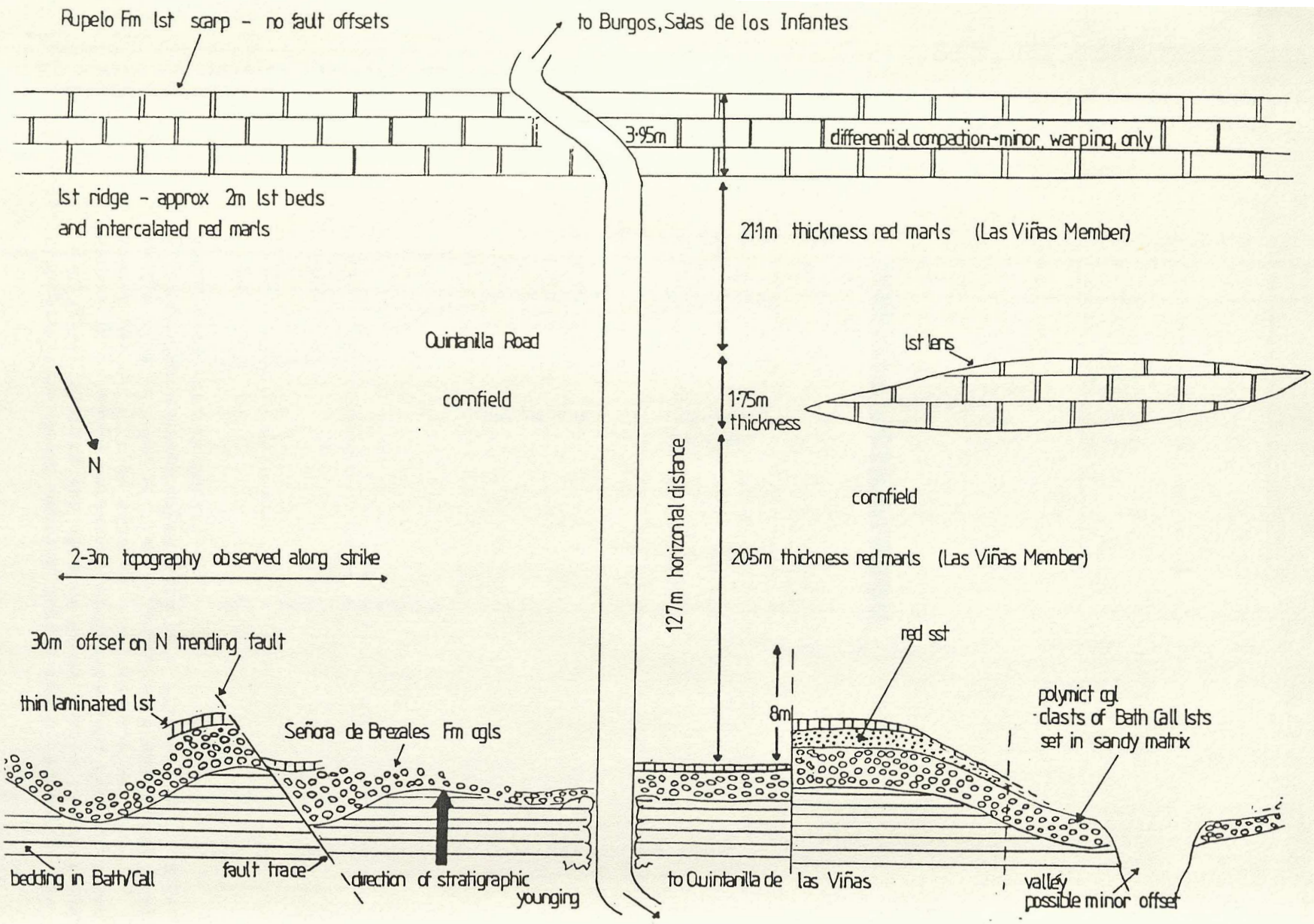
Rupelo Fm lst scarp - no fault offsets
to Burgos, Salas de los Infantes
3·95m
differential compaction-minor, warping, only
lst ridge - approx 2m lst beds
and intercalated red marls
21·1m thickness red marls (Las Viñas Member)
Quintanilla Road
cornfield
lst lens
1·75m
thickness
N
cornfield
2-3m topography observed along strike
127m horizontal distance
20·5m thickness red marls (Las Viñas Member)
30m offset on N trending fault
red sst
8m
polymict cgl
clasts of Bath Gall lsts
set in sandy matrix
thin laminated lst
Señora de Brezales Fm cgls
bedding in Bath/Gall
fault trace
direction of stratigraphic
younging
to Quintanilla de las Viñas
valley
possible minor offset

Fig 8.45. Interpretative NW-SE section across the N sectors of the study area, showing the rôle of NE-SW faults in controlling Senora de Brezales Formation sedimentation. Some of these faults may in fact be related - intuitively we would expect some of them to link at depth - in which case they might be the surface expression of a "flower" type suite of small-scale wrench faults.

Schematic cross-section of NW sector south of Quintanilla de las Vinas - Castrovido showing fault control of Senora de Brezales Formation conglomerates and sands.
Jaramillo - Covarrubias Fault is a major transfer fault - others are more minor parallel faults which often do not cut overlying strata.

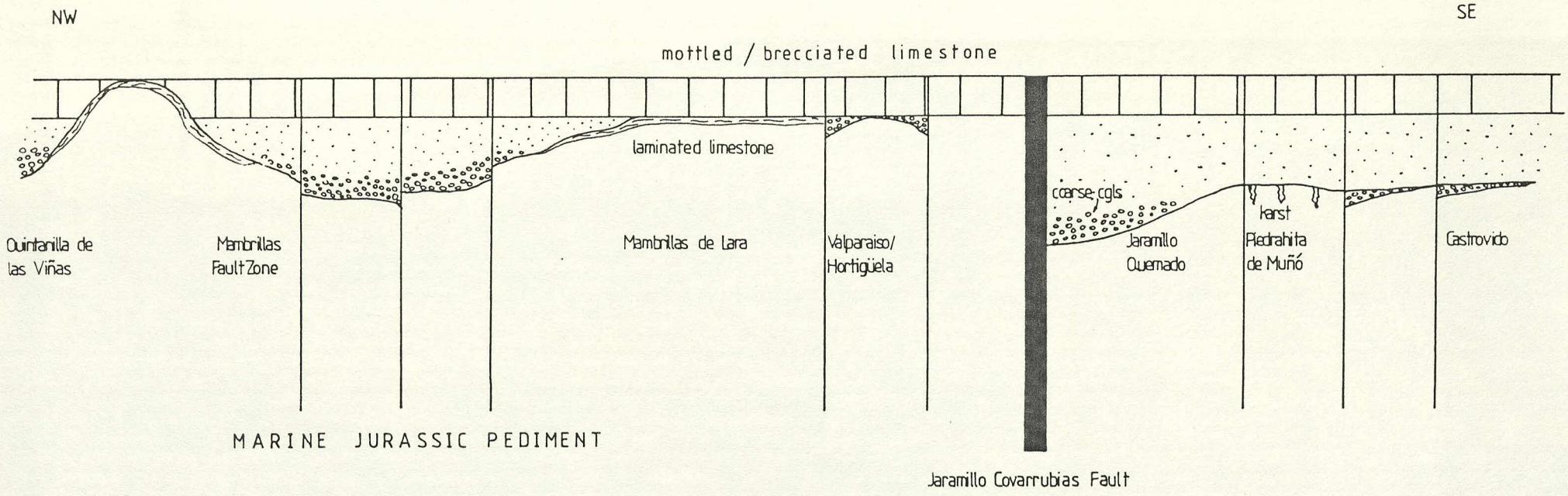

Fig 8.46. Panorama looking N across Mambrillas Fault Zone (approximately 2km NW of Mambrillas de Lara), with field sketch for interpretation: Note jointed channel floor; location of channel adjacent to NE-SW fault; channel now located on upthrown block - reversal of fault throw.

MAMBRILLAS FAULT ZONE - PANORAMA LOOKING NORTH-EAST

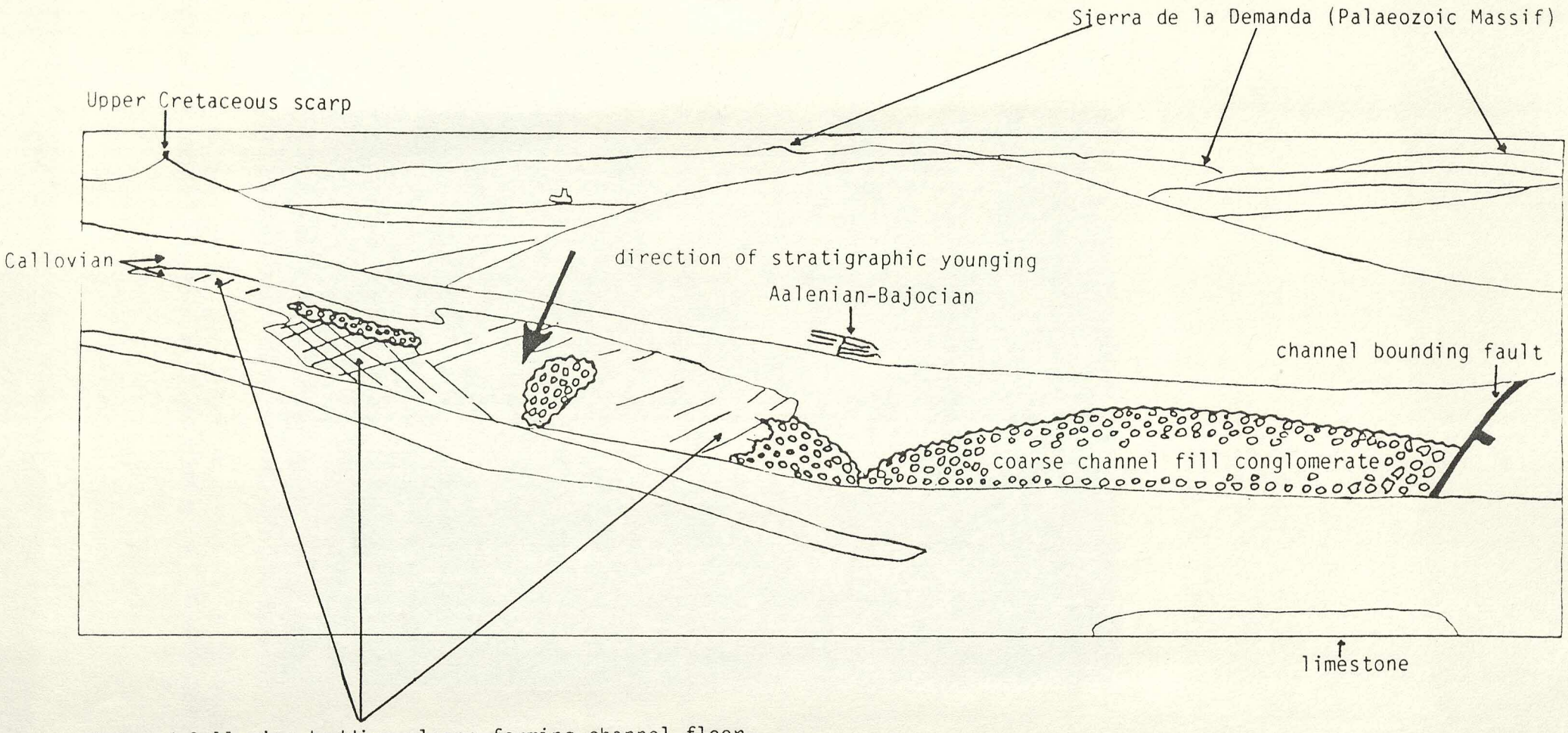

Fig 8.47. Jointed pavement of Lower Callovian limestone forming channel floor, Mambrillas Fault Zone (see fig 8.46).

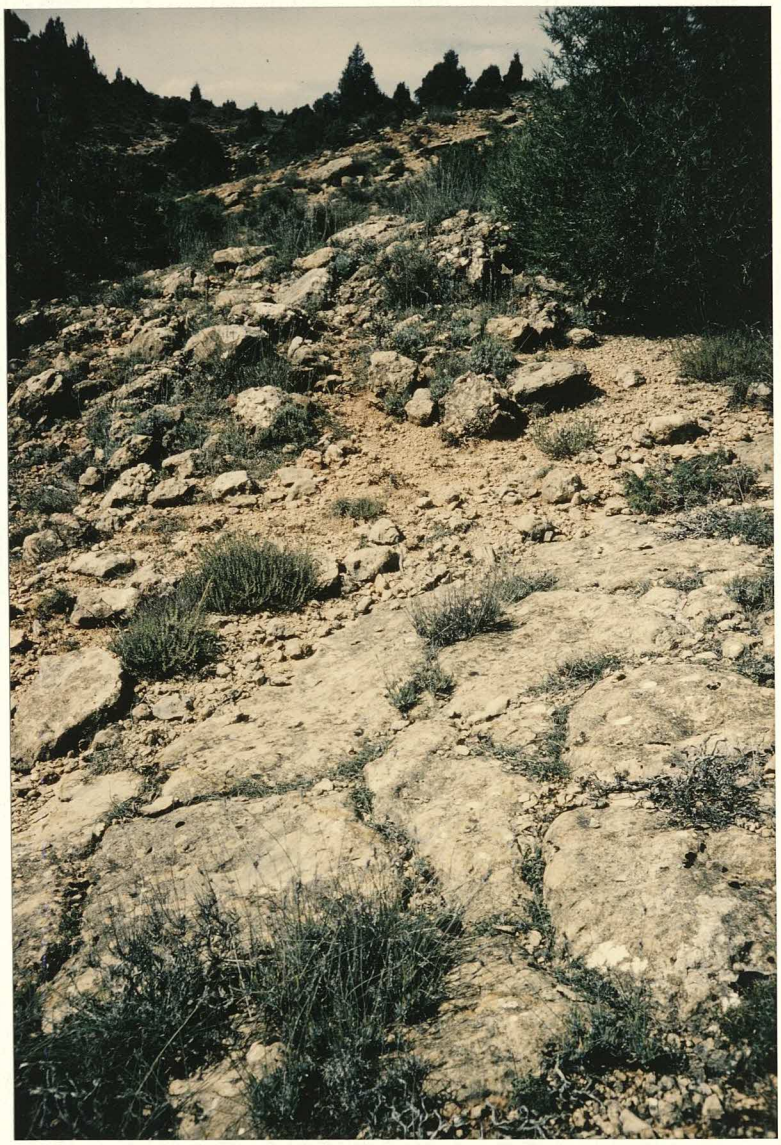

Fig 8.48. Interpretative sections drawn across Mambrillas Fault Zone. See figs 8.46 & 8.47.

Note: 1) channel now lies on uplifted fault block, ie fault throw has subsequently been reversed. In the model presented here this reversal is dated before the deposition of the Rupelo Formation limestones

2) limestone conglomerate adjacent to fault (see fig 8.60) - interpreted as the product of this fault reversal.

MAMBRILLAS FAULT ZONE : POSTULATED SEDIMENTARY HISTORY OF TIERRA DE LARA GROUP

SE NW

Stage 1: undeformed

"orange beds"

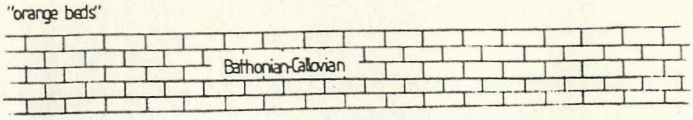

Stage 2: extensional faulting of palaeosurface

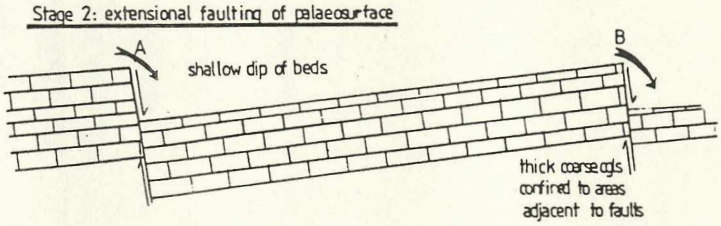

Stage 3: deposition of fluvial facies in fault-bounded channel

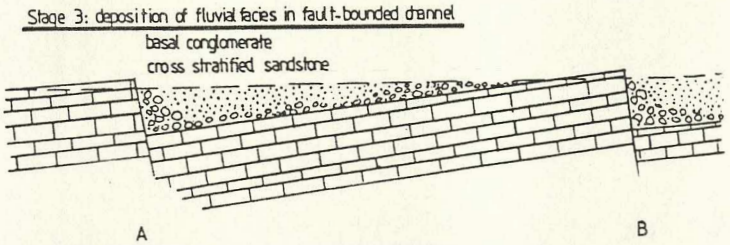

Stage 4 lst deposition pedogenetically-modified lst

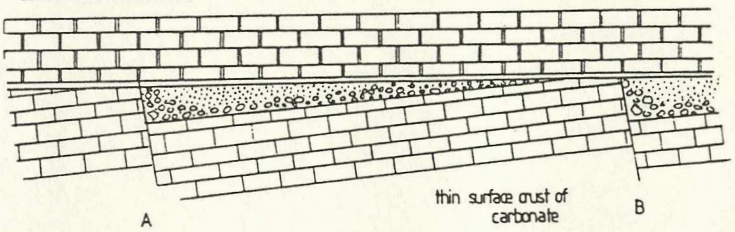

Stage 5: fault reactivation in inverse sense

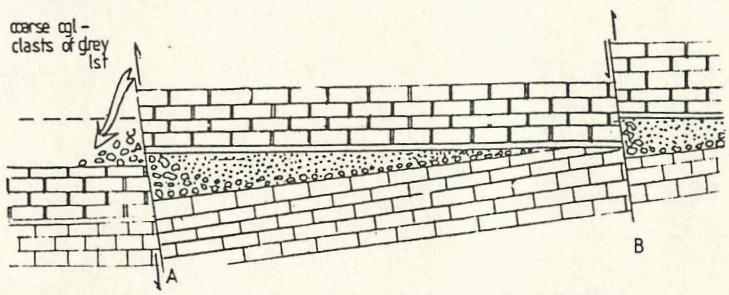

Stage 6: deposition of red marls (Las Viñas Member) and lsts of Rupelo Formation

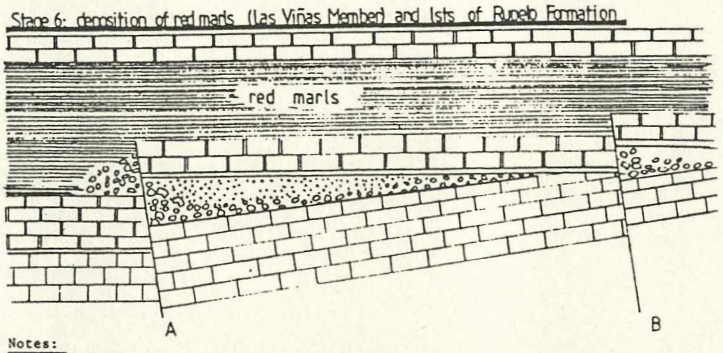

Notes:

1. Downthrown side of Fault A is now on SE.

2. Consideration of conglomerate and sandstone thicknesses indicates that NW side was downthrown during deposition.

3. Limestones above Las Vinas Member not cut by faults A or B.
?sense of movement on faults reversed before deposition of Ladera Member.

Fig 8.49. Thickness distribution map for the W Cameros Basin: Senora de Brezales Formation.

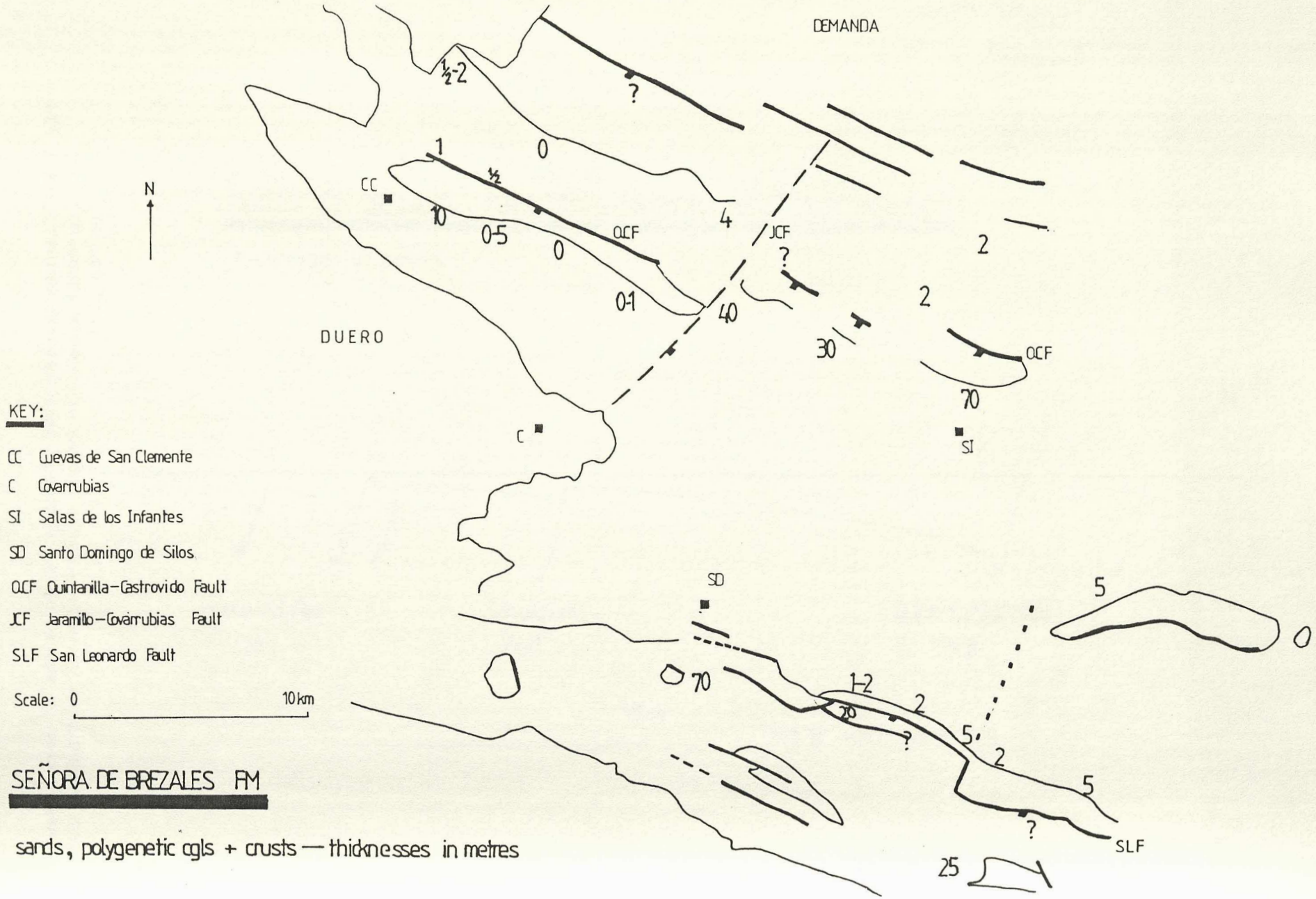

SEÑORA DE BREZALES FM

sands, polygenetic cgls + crusts — thicknesses in metres

Fig 8.50. Diagram illustrating possible "down to the S" normal fault movement suggested by the distribution of thicknesses shown in fig 8.49.

SEÑORA DE BREZALES FORMATION — "down to the S" fault movement?

thicknesses in metres

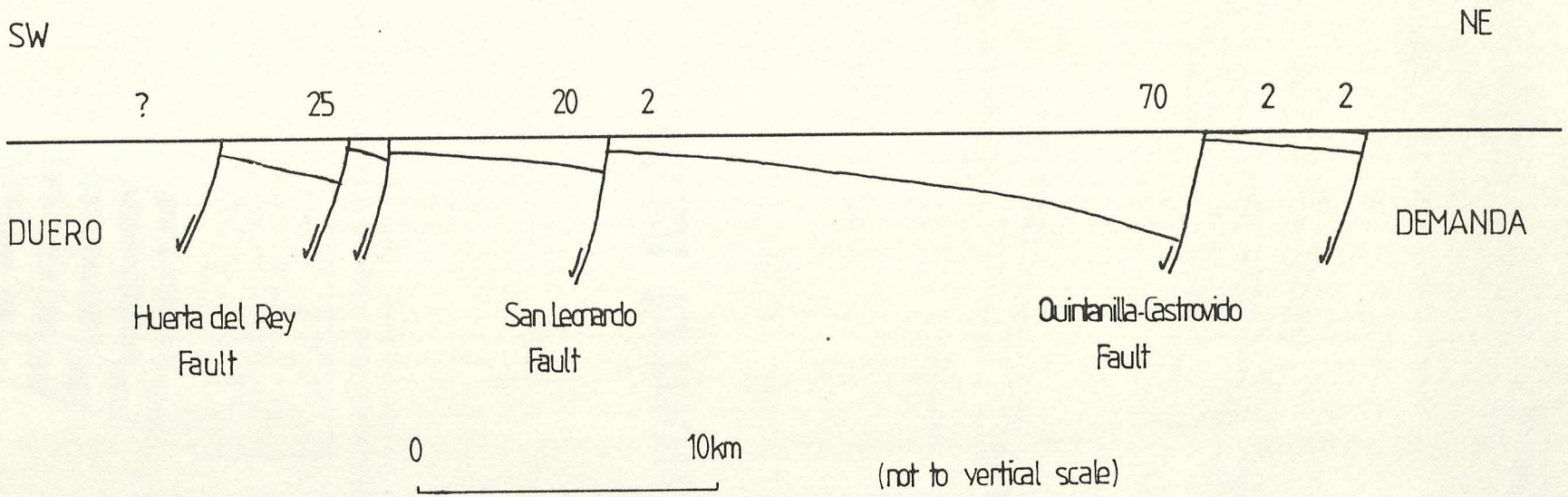

Fig 8.51. Diagram of hypothetical graben system showing the importance of antithetic normal faulting at all scales of normal fault movement.

Chadwick (1985)

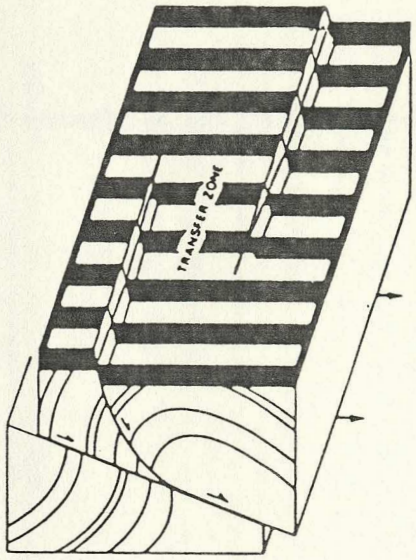

Schematic block diagram of normal faults, offset by a transfer zone and lying above a reactivated thrust.

normal faults

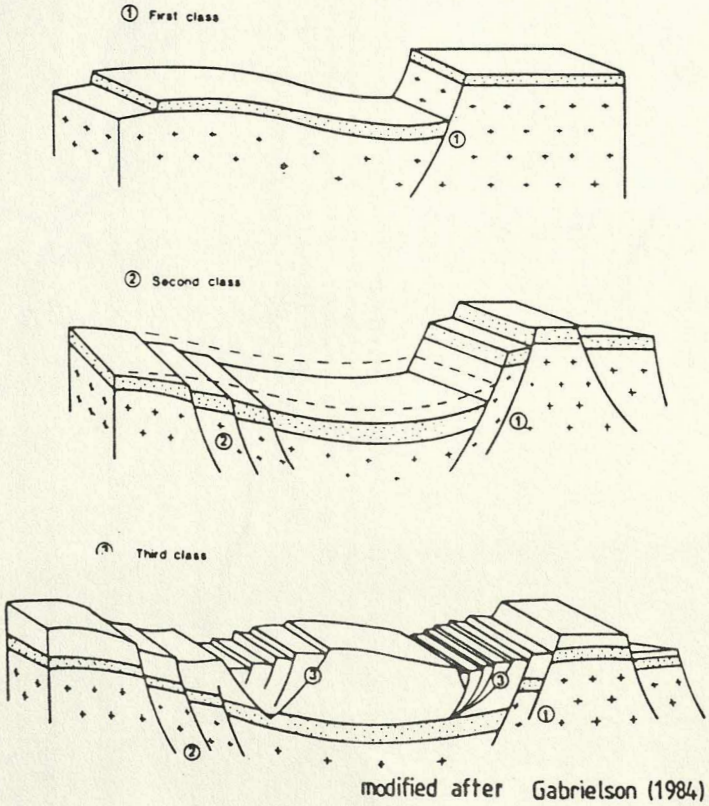

modified after Gabrielson (1984)

Fig 8.52. Thickness distribution map for the W Cameros Basin: Ladera Member of the Rupelo Formation.

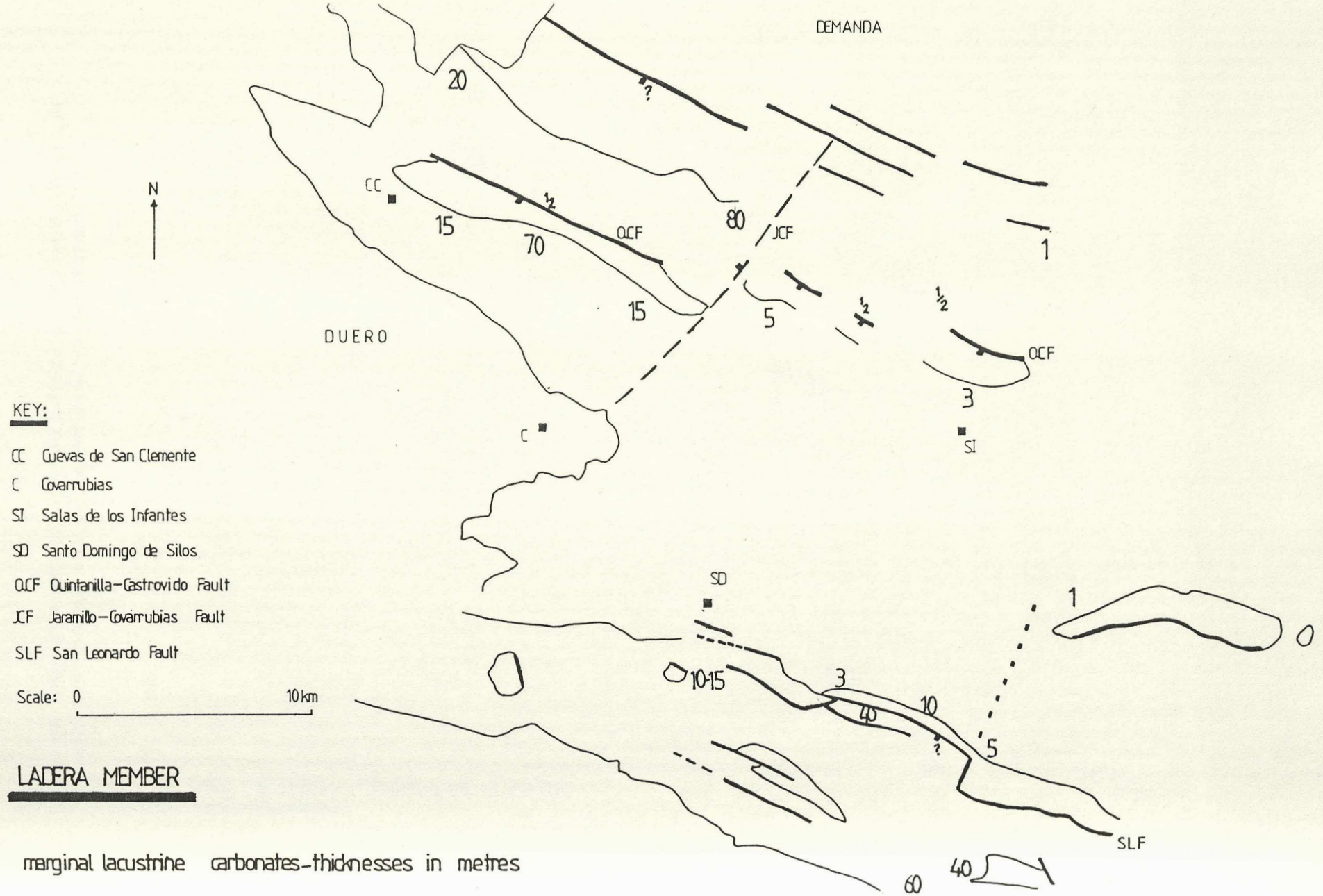

KEY:

CC Cuevas de San Clemente

C Covarrubias

SI Salas de los Infantes

SD Santo Domingo de Silos

QCF Quintanilla–Castrovido Fault

JCF Jaramillo–Covarrubias Fault

SLF San Leonardo Fault

Scale: 0 10 km

LADERA MEMBER

marginal lacustrine carbonates–thicknesses in metres

Fig 8.53. Thickness distribution map for the W Cameros Basin: Mambrillas de Lara Member of the Rupelo Formation.

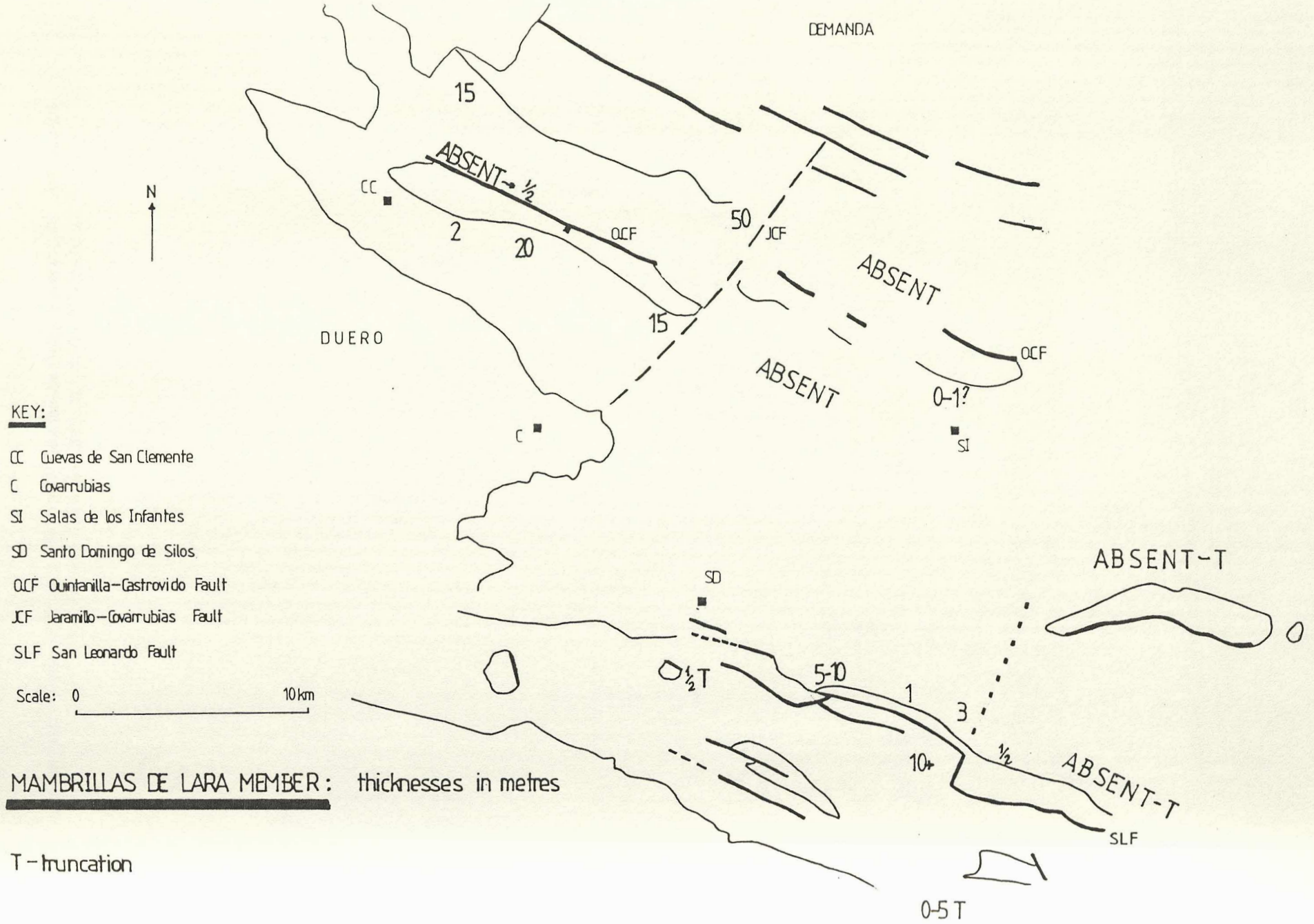

MAMBRILLAS DE LARA MEMBER: thicknesses in metres

T - truncation

Fig 8.54. Thickness distribution map for the W Cameros Basin. Rio Cabrera Member of the Rupelo Formation.

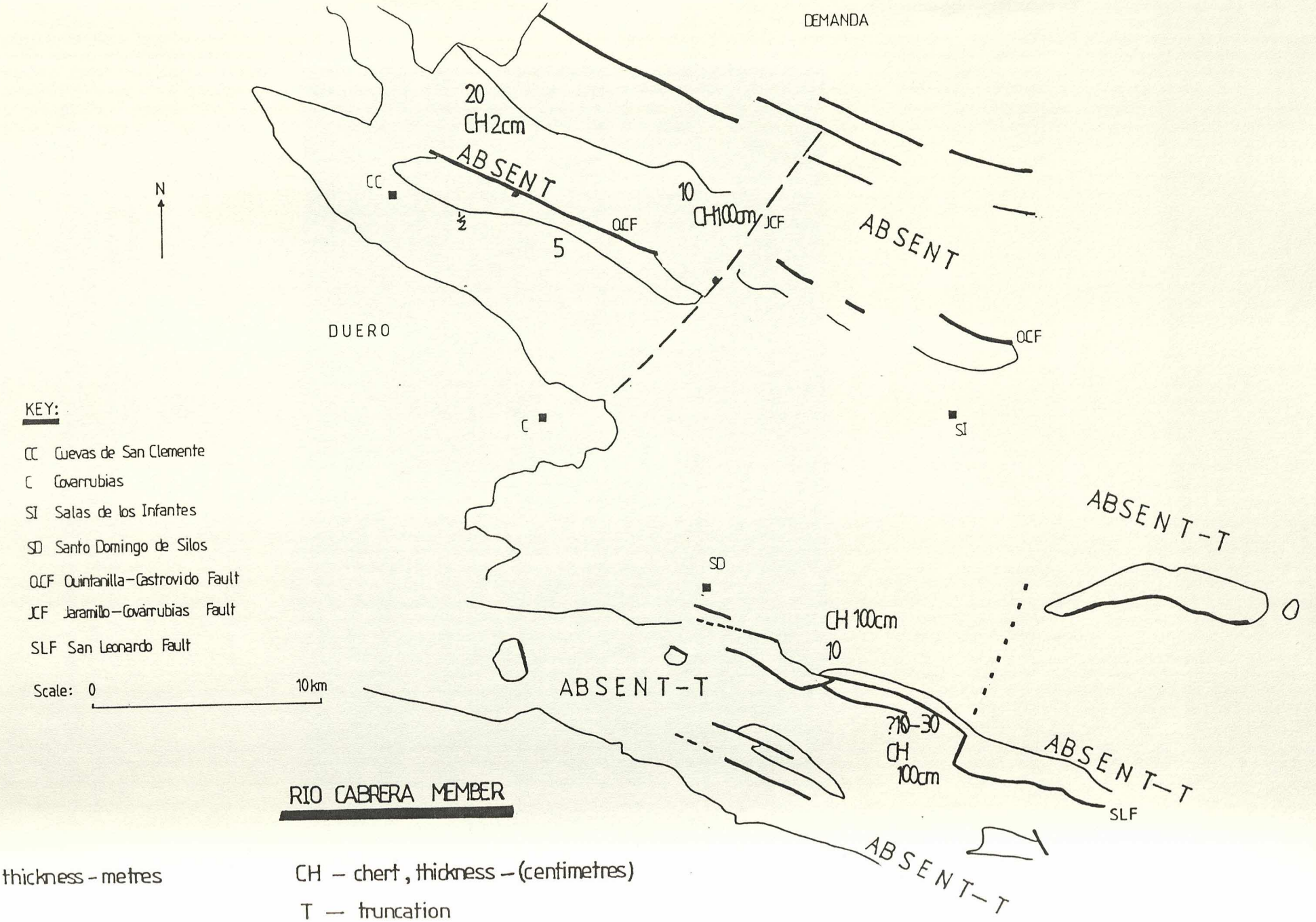
DEMANDA
20
CH 2cm
ABSENT
CC
10
CH 100cm
JCF
ABSENT
N
QCF
½
5
DUERO
QCF
C
SI
KEY:
CC Cuevas de San Clemente
C Covarrubias
SI Salas de los Infantes
SD Santo Domingo de Silos
QCF Quintanilla–Castrovido Fault
JCF Jaramillo–Covarrubias Fault
SLF San Leonardo Fault
Scale: 0 10km
ABSENT-T
SD
CH 100cm
10
ABSENT-T
?10-30
CH
100cm
ABSENT-T
SLF
RIO CABRERA MEMBER
ABSENT-T
thickness - metres
CH – chert, thickness – (centimetres)
T – truncation

Fig 8.55. Coarse, locally derived limestone conglomerate shown in fig 8.48 adjacent to fault scarp. This limestone conglomerate persists for only 10-20m laterally away from the fault. Mambrillas Fault Zone.

Fig 8.56. Aguilar Formation at its type locality in SW Cantabria. The Aguilar Formation is thicker than the Ruopelo Formation (up to 900m according to Sbeta, 1976) but the lithological, sedimentological and stratigraphic similarity with the Rupelo Formation of the W Cameros is such as to suggest at least intermittent communication between the two areas. Dr Victoriano Pujalte provides scale. Aguilar Inferior Member. Quarry 800m N of Aguilar del Campoo.

Fig 8.57. Facies distribution map for the W Cameros Basin - Pedroso Group.

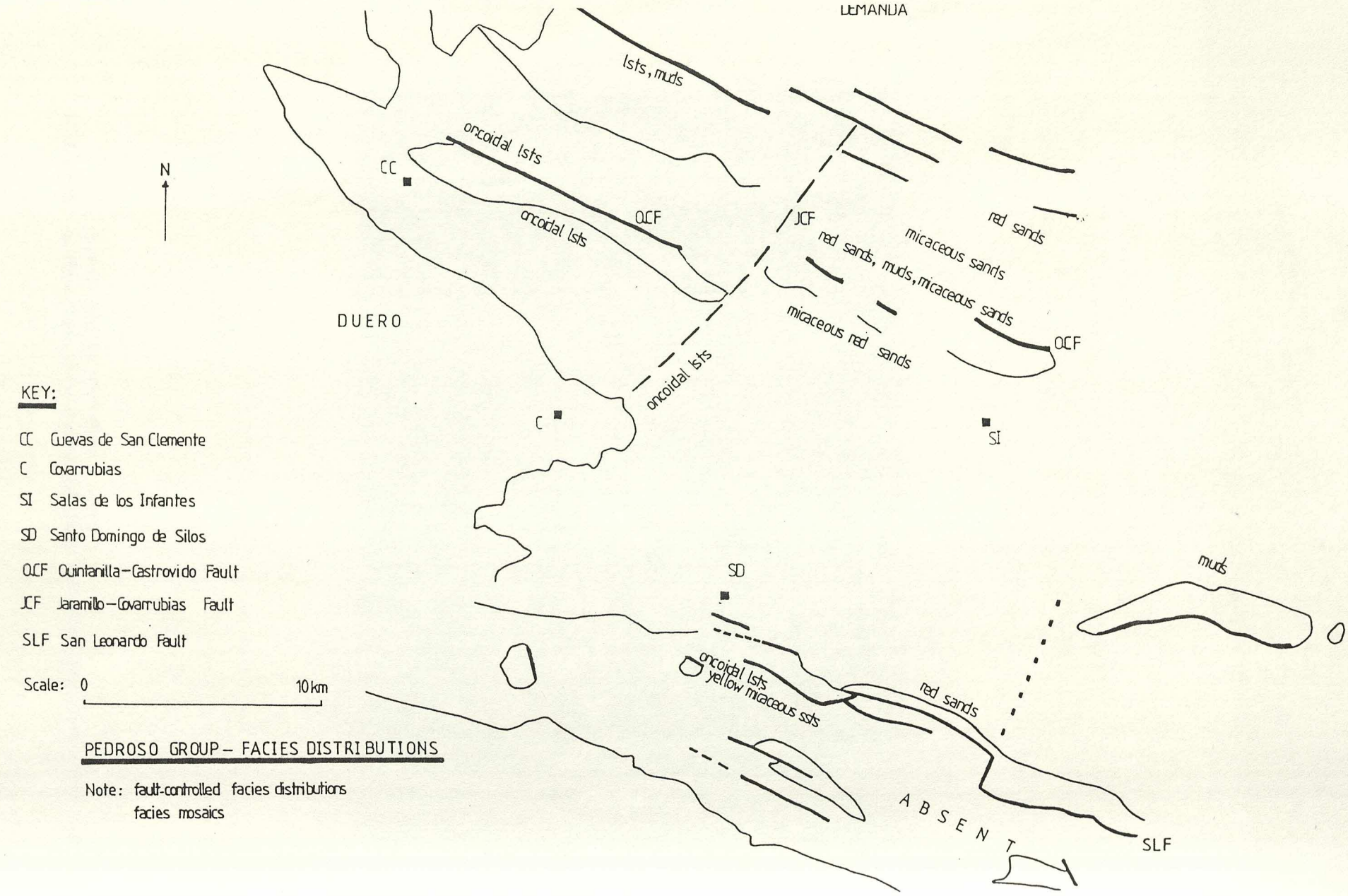
LEMANJA
lsts, muds
oncoidal lsts
CC
QCF
oncoidal lsts
JCF
red sands
micaceous sands
red sands, muds, micaceous sands
micaceous red sands
QCF
N
DUERO
oncoidal lsts
C
SI
KEY:
CC Cuevas de San Clemente
C Covarrubias
SI Salas de los Infantes
SD Santo Domingo de Silos
QCF Quintanilla–Castrovido Fault
JCF Jaramillo–Covarrubias Fault
SLF San Leonardo Fault
Scale: 0 10km
SD
muds
oncoidal lsts
yellow micaceous ssts
red sands
ABSENT
SLF
PEDROSO GROUP – FACIES DISTRIBUTIONS
Note: fault-controlled facies distributions
facies mosaics

Fig 8.58. Evaporites from the E Cameros Basin. "Chicken wire" texture. Group III of Salomon (1982).

Fig 8.59. Highly schematic cross-section through the SE Iberian Chains indicating Early Cretaceous rifting, from Vilas et al (1982).

IBERIAN CHAINS — SEDIMENTATION AND TECTONICS.

simplified model (Vilas et al, 1982).

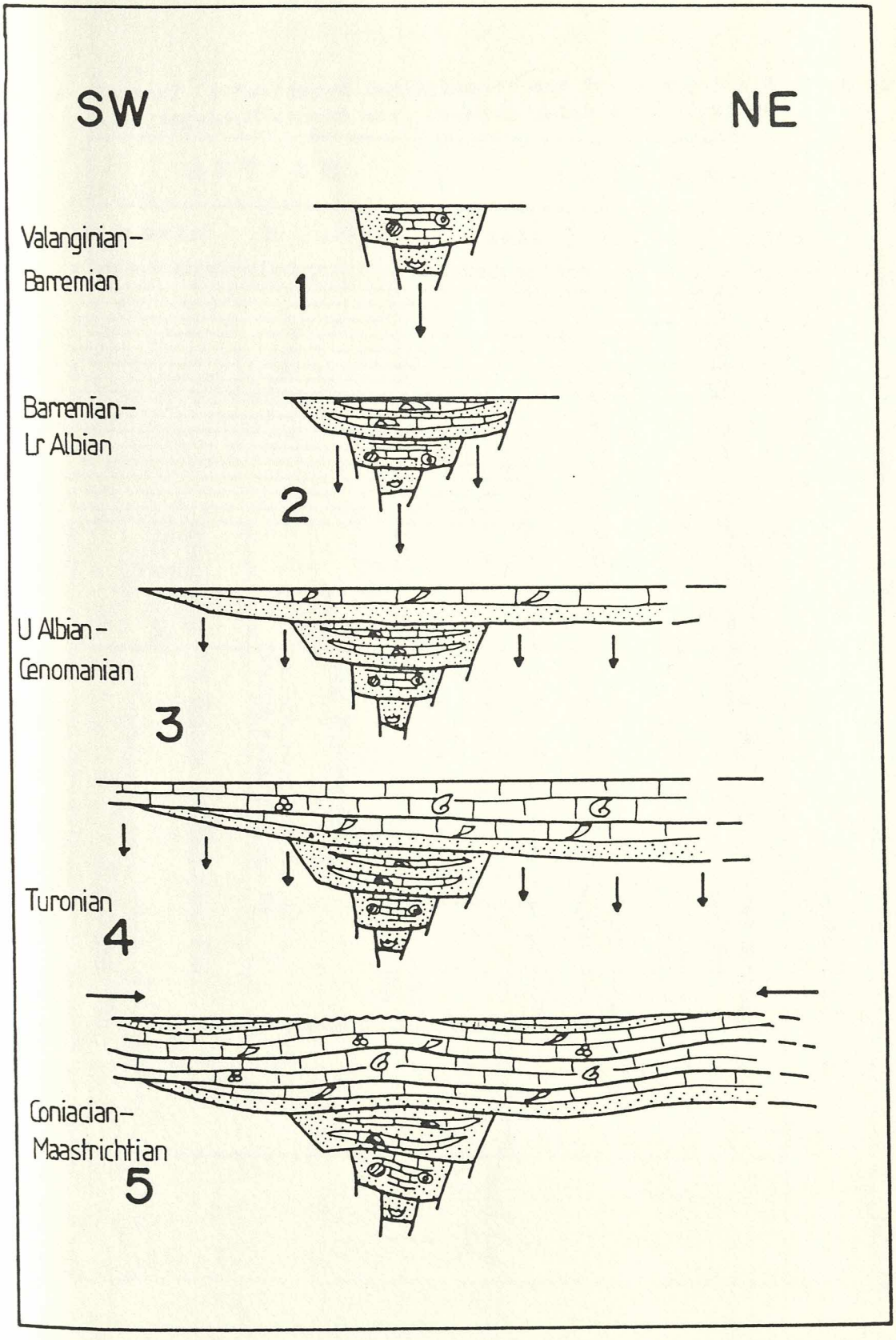

Fig 8.60. Stratigraphy of the "Continental Urgonian" (lateral equivalent of Salas Group), from Garcia-Mondejar et al (1985).

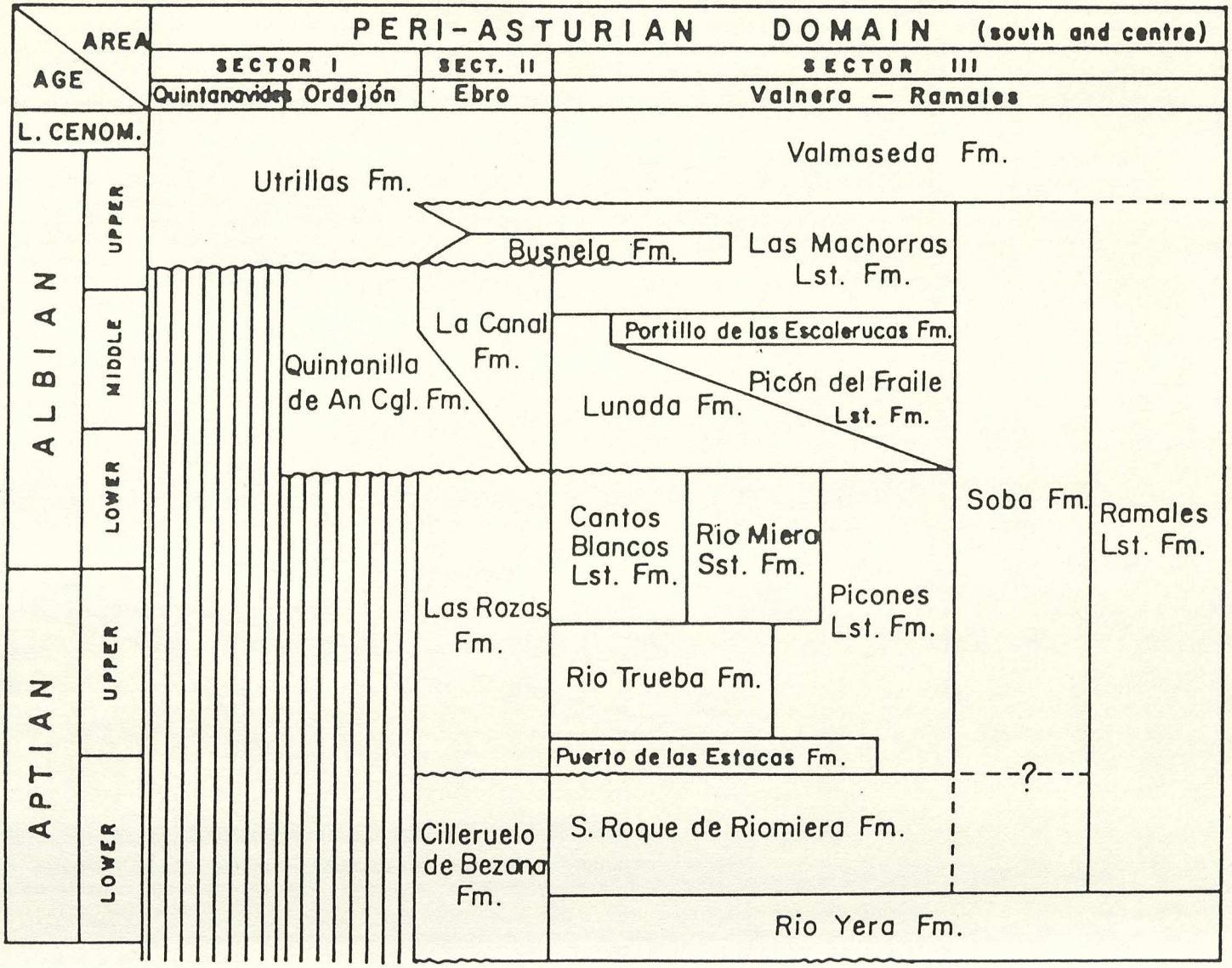

Lithostratigraphic scheme of the Aptian-Albian of the Peri-Asturian Domain (southern and central).

Garcia-Mondejar et al (1985)

Fig 8.61. Models for the formation of the pre - Upper Albian unconformity in the W Cameros Basin.

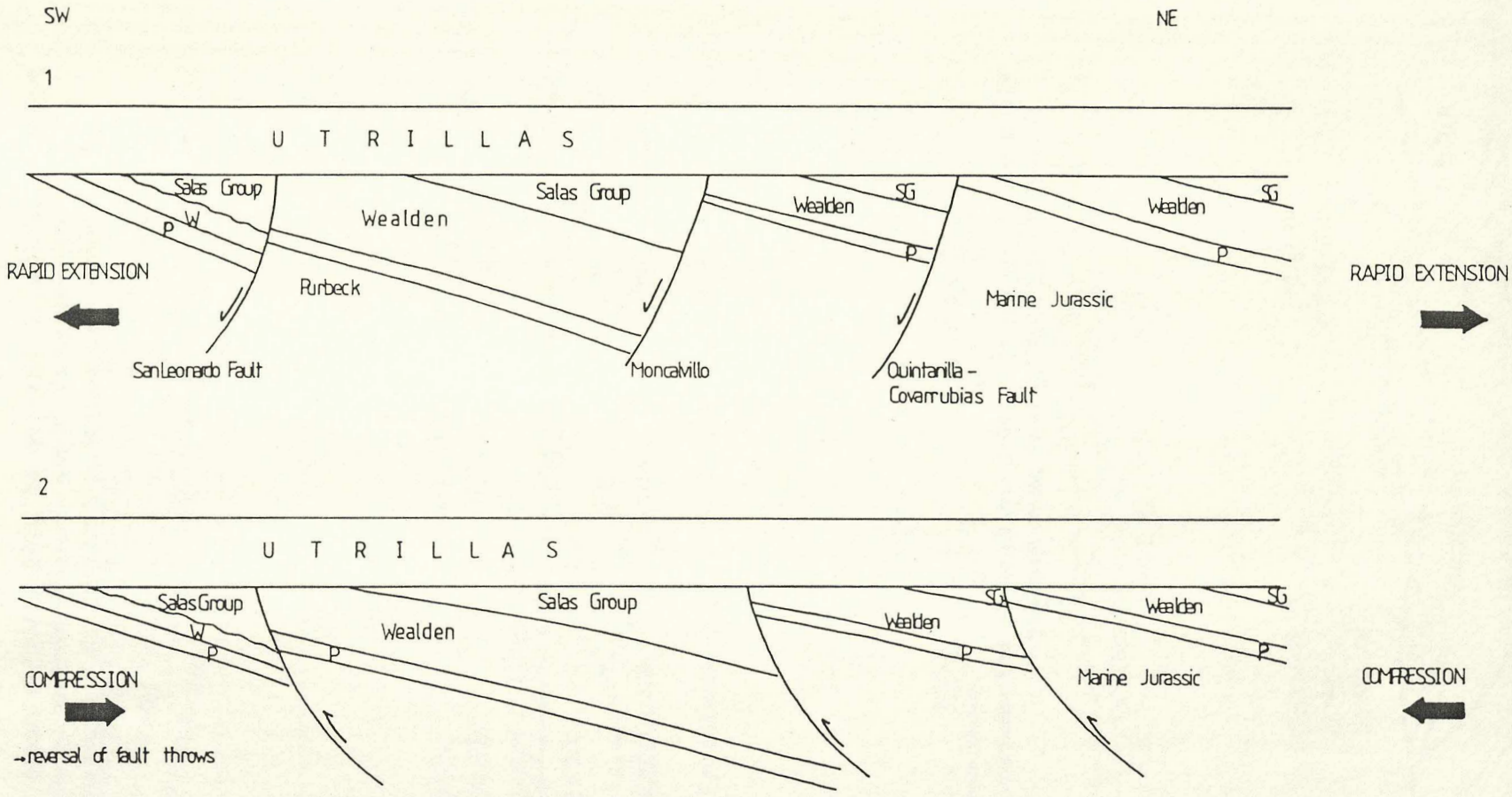

TWO MODELS FOR THE DEVELOPMENT OF THE MIDDLE CRETACEOUS UNCONFORMITY.

1) Extension, footwall uplift and erosion on crestal axes of rotated fault blocks.
2) Compression, inversion of faults, resulting in truncation (often most severe in areas of previously maximum subsidence).

Seismic sections across central Cantabria (Hossack, pers. comm., 1986) would favour interpretation 2).
- However, general thickening of continental sequence on S sides of faults would favour fault geometry as in 1). This might also be partially the result of truncation on N sides of faults during successive extensional episodes.
Reversal of fault throws might also be achieved as a result of antithetic fault movements; faults dipping to SW not shown in this figure.

Fig 8.63. Westward overstep of Middle Albian Gault Clay over progressively older strata. Further evidence of Middle Cretaceous tectonic activity in S England.

Fig 8.62. Examples of Middle Cretaceous deformation ("Ringstead" or "Austrian" phase) in S England.

The westward overstep of Albian–Cenomanian sediments in S. England and their associated facies changes.

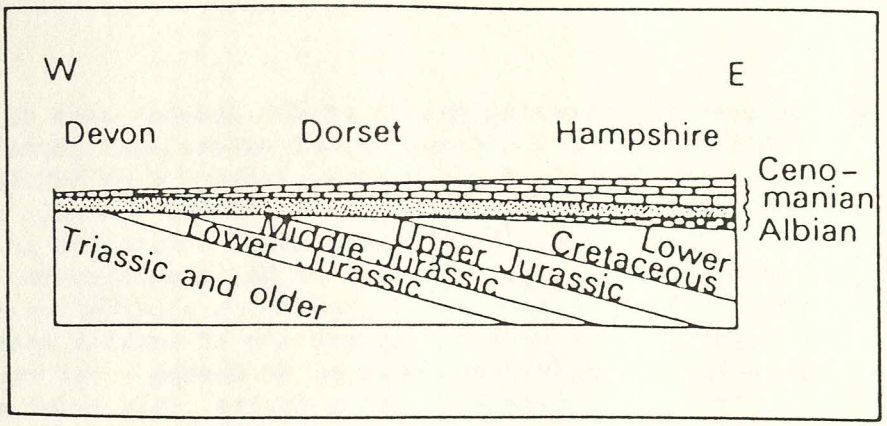

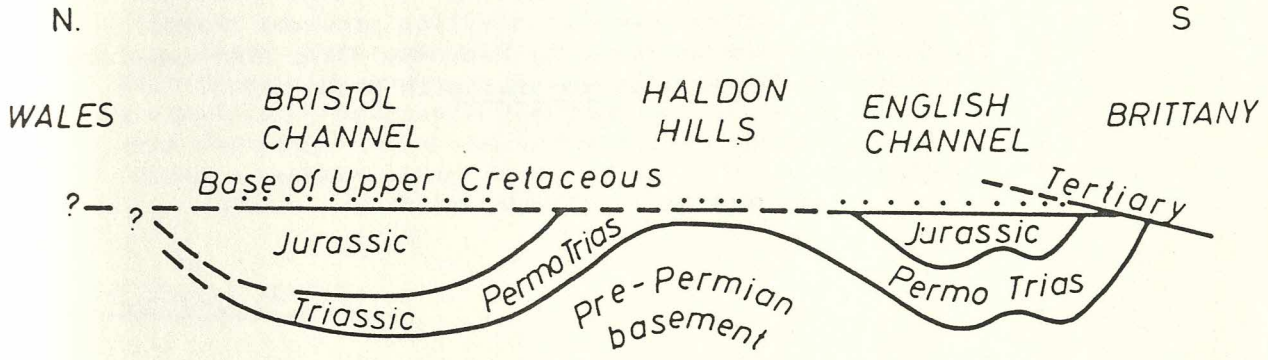

Upper Cretaceous overstep in South and South-West England.

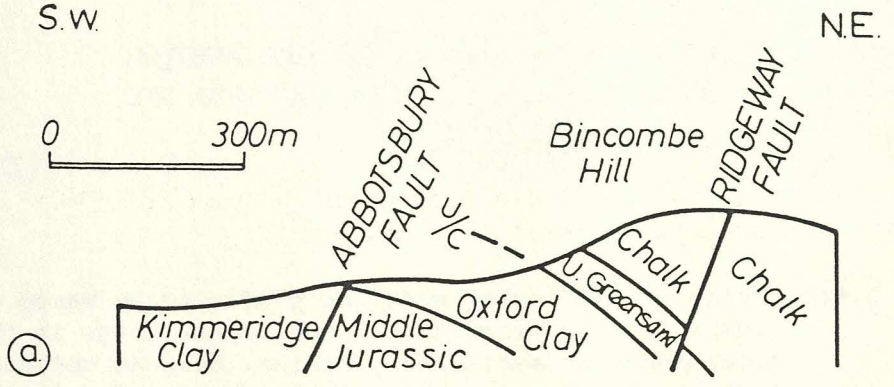

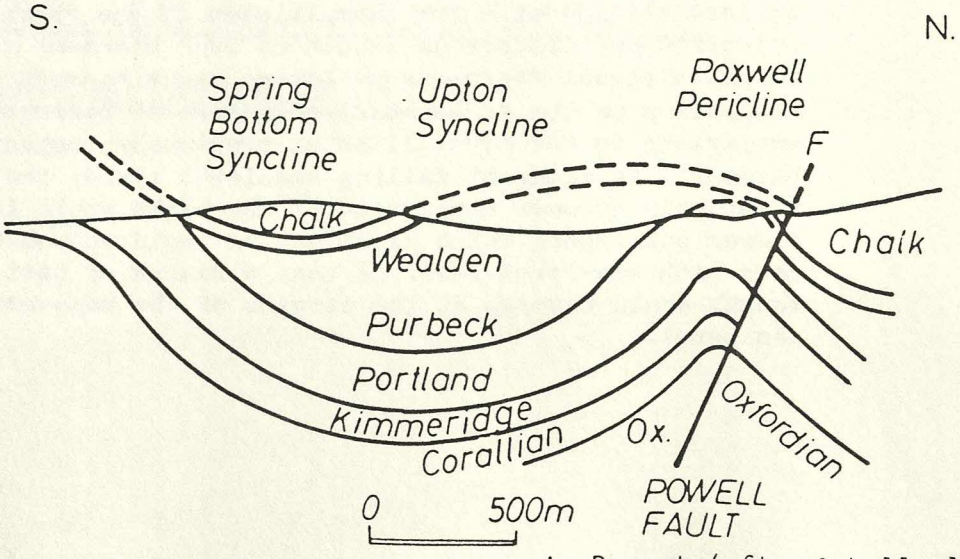

Mid-Cretaceous structures in Dorset (after Arkell, 1946).

Fig 8.65. Diagram illustrating uplift of the crestal axes of footwall fault blocks as a consequence of extensional normal faulting utilising listric fault planes. Jackson & Mc Kenzie (1983) estimated that the relative magnitude of footwall uplift could reach up to 10% of hangingwall subsidence in comparison with the magnitude of basin subsidence. "Footwall uplift" of this type could provide an alternative model to account for the variable truncation of earlier strata beneath the Upper Cretaceous of NW Europe - the truncation is strongest adjacent to major faults. This model envisages the fault movements as extensional. See fig 8.61, which gives an alternative model showing the fault movements at this time as contractional, inverting previous normal displacements (as favoured by Hossack, 1985, who postulated major Middle Cretaceous shortening in N Iberia).

Fig 8.64. "Steer's head" onlap model as predicted by Watts et al (1982) for the late thermal subsidence stage in the development of sedimentary basins. Diagram modified to indicate the local stratigraphic development in the W Cameros Basin. There are several possible reservations against this model - for example part of the reason for thinner Upper Cretaceous sequences over basement highs than in depositional basins in NW Europe might be much greater compaction of the sedimentary sequences of basins in comparison to the crystalline or previously compacted basement. In times of falling sea-level stand, the relatively reduced compaction of the highs would lead to slower subsidence which might not be rapid enough to keep pace with sea-level fall, so that a hiatus of variable length would develop at the margins of the basement massifs (as here).

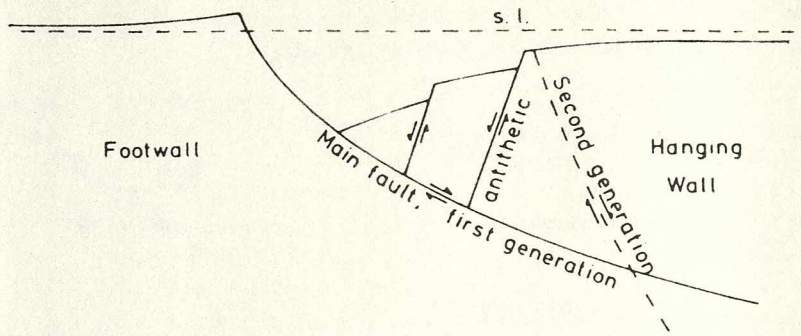

Sketch of a normal fault system to show uplift of the footwall and to define the terminology used. Although the main fault is shown as a gentle curve, the arguments presented in the text suggest that, in areas where major crustal extension occurs as a result of normal faulting, a significant change in dip is likely at the brittle-ductile transition, near the base of the largest antithetic faults.

FOOTWALL UPLIFT

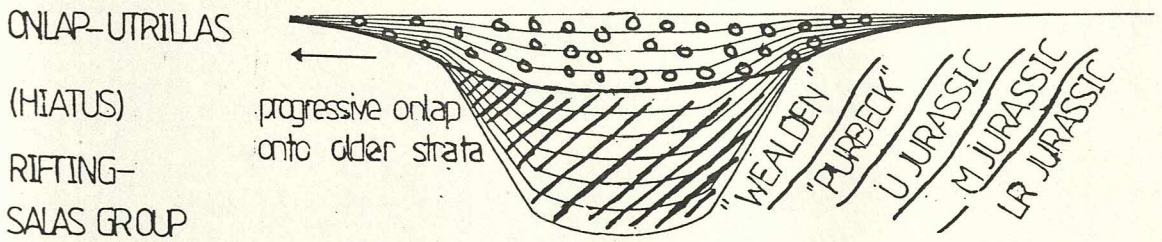

"STEER'S HEAD" ONLAP-EXPLANATION FOR THE SUB UTRILLAS UNCONFORMITY?

Fig 8.66. Upper Cretaceous lithostratigraphy of the W Cameros Basin (from Floquet, 1982) with additional notes on the timing and scale of eustatic and tectonic events.

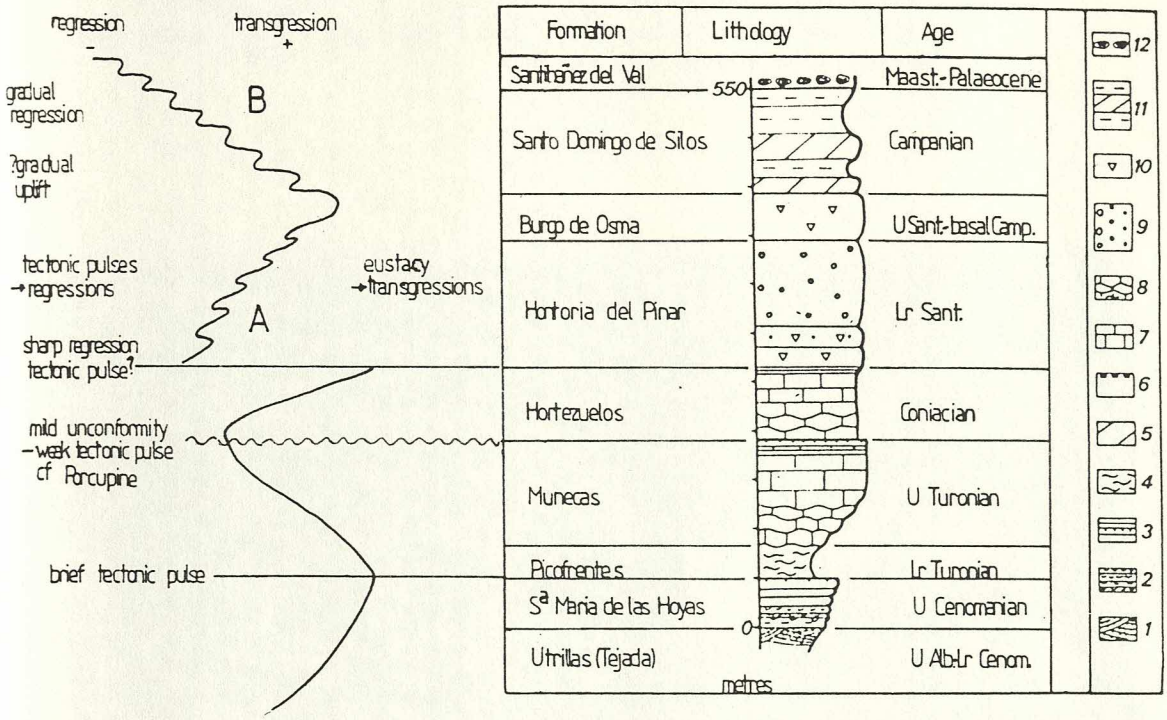

Upper Cretaceous lithostratigraphy and the relative roles of eustacy and tectonics as influences upon vertical facies evolution.

Section figured schematically is for the area of Santo Domingo de Silos. (after Floquet, 1982; additional information from Alonso et al, 1982).

Key:

1) cross-bedded continental sandstones and unconsolidated sands
2) sandy mudstones/marls and limestones with oysters
3) well-bedded limestones; hardground
4) muds and marls with ammonites
5) massive dolomitic limestones
6) laminated limestones and black-pebble breccias
7) variably-bedded limestones
8) micritic limestones; nodular limestones with rare ammonites
9) calcarenites with Lacazina towards the top
10) limestones with rudists
11) mixed facies - dolomitic limestones, sandy limestones
12) "Garumnian" facies: lacustrine limestones, red sandy mudstones etc..

A - effect of eustacy > effect of tectonics

B - effect of tectonics > effect of eustacy

Fig 8.67. Clear evidence for tectonic activity around the Turonian-Coniacian boundary - angular unconformity between Turonian (interbedded limestones and marls) and Coniacian (massive limestones) at the edge of the meseta, approximately 100km N of the study area. Drs Vilas and Pascal for scale.

Fig 8.68. Upper Cretaceous isopachs in the Vasco Cantabrian Basin, from Amiot et al (1982). Note: much greater thicknesses than in the W Cameros.

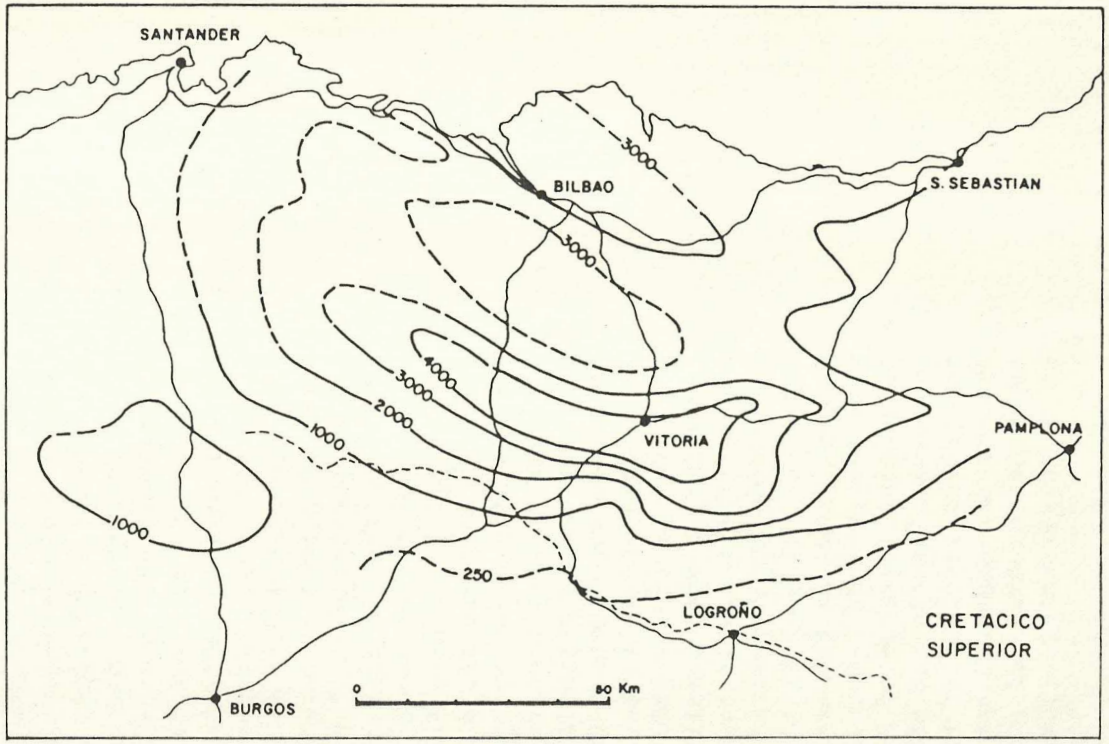
SANTANDER
BILBAO
S. SEBASTIAN
VITORIA
PAMPLONA
LOGROÑO
BURGOS
3000
3000
4000
3000
2000
1000
1000
250
0
50 Km
CRETACICO
SUPERIOR

Fig 8.69. Correlation chart for the Upper Cretaceous of the study area indicating relationship of previously defined units with chronostratigraphy, and showing probable correlation with the Upper Cretaceous sequence of S Britain (as given in Anderton et al, 1979). See also fig 2.50.

Note: 1) diachronous parallelism of facies between S Britain (listed first) and the W Cameros and S Britain (eg Gault, Middle Albian Santa Maria de las Hoyas or Picofrentes Formations, Upper Cenomanian Lower Turonian; Lower Chalk, Cenomanian Munecas Formation, Upper Turonian; etc.),

2) presence of approximate facies equivalents in the W Cameros and basement-fringing areas of Britain (eg Grey Chalk, Glauconitic Marl, Glauconitic Sandstone, White Limestone, Plenus Marl: all find approximate analogues in W Cameros).

3) Presence of important hiatuses / unconformities at similar stratigraphic horizons in the W Cameros and S England. These indicate the effects of contemporaneous tectonic or eustatic events.

4) Variable preservation of the latest Upper Cretaceous horizons in S Britain according to locality. This is analogous to the situation in the W Cameros. The extent of truncation depends on the intensity of tectonic inversion - for example in strongly inverted areas (eg Sole Pit Trough, Yorkshire) much of the Upper Cretaceous is removed; in areas of little or no inversion (eg N North Sea) there is complete preservation even of the Maastrichtian - Danian Chalks. The preservation of Palaeocene strata in the Santo Domingo de Silos Basin may partially reflect weaker tectonic inversion at that locality, which is close to the line of the La Yecla backthrust. This inversion post-dated the deposition of the Palaeocene sequence, which might thus originally have been present (even if thinner) over much wider areas than its current preservation would suggest. The Palaeocene sequence of S England is also only preserved locally and often close to major structures (eg Isle of Wight, Hampshire; close to Purbeck and Weymouth anticlines lying above basement thrusts) and similar problems exist there as to the extent of Palaeocene sedimentation.

UPPER CRETACEOUS STRATIGRAPHY - CORRELATION CHART OF PREVIOUS WORKS.

FLOQUET et al (1982) ALONSO et al (in press)	FAULKNER (1985)	VAUGHAN (1986)	S ENGLAND EQUIVALENT (ANDERTON et al, 1979)	AGE
Santibanez del Val		Santibanez del Val Fm	Maastrichtian - ~~ Danian Chalks ~~	Palaeocene Maastrichtian
Santo Domingo de Silos		Santo Domingo de Silos Fm		Campanian
Burgo de Osma			Upper Chalk	
Hontoria del Pinar Hortezuelos	massive mudst lst bedded mudst lsts	Yecla Group		Campanian - Coniacian
Munecas	oolitic lsts bioclastic lsts lst	Munecas Fm	Chalk Rock	Coniacian - Turonian
Picofrentes		Picofrentes Fm	Middle Chalk	Lower Turonian
Sa Cruz del Tozo	glauconitic sst		Melbourn Rock	
Sa Maria de las Hoyas	marls	Santa Maria de las Hoyas Fm	Lower Chalk - Plenus Marls - Grey Chalk & - Chalk Marl	Upper Cenomanian
Tejada	sands	Tejada Fm	Glauconitic Marl	Lower Cenomanian
			U Greensand	Upper Albian

hardground ------- non sequence / unconformity.

PLATT N (1986)

Fig 8.70. Palaeogeographies of the Iberian peninsula in the Upper Cretaceous, indicating the location of basement faults exerting control on facies distributions and thicknesses.

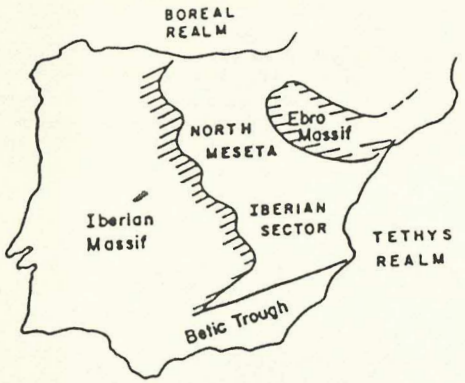

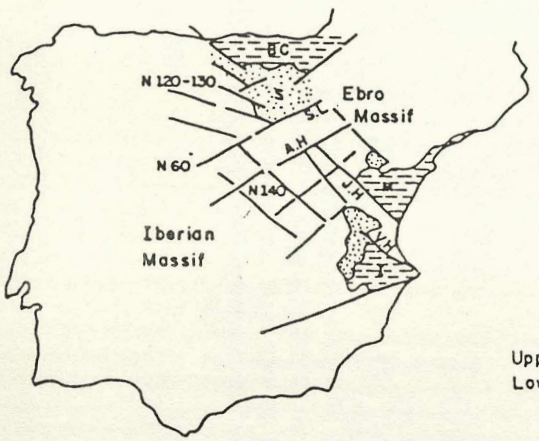

Upper Albian – Lower Cenomanian

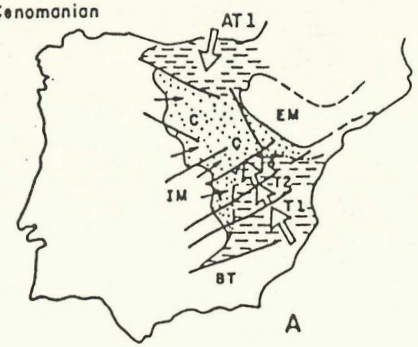

A

Upper Cenomanian

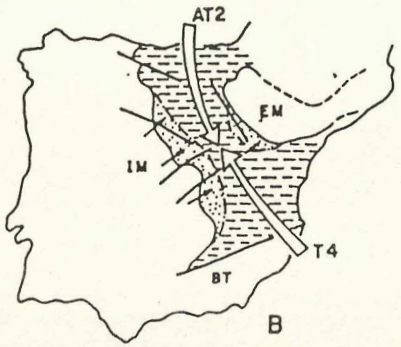

B

Upper Cenomanian Lower Turonian

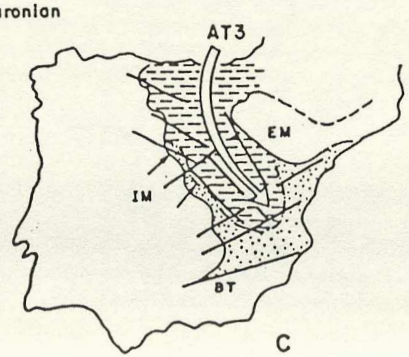

C

Upper - Coniacian boundary

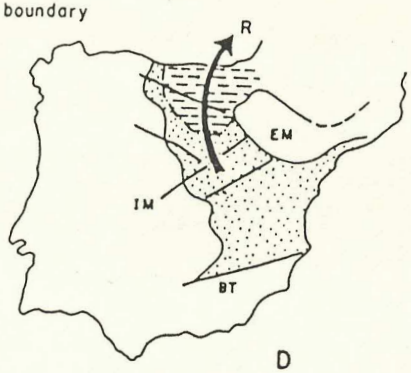

D

Coniacian

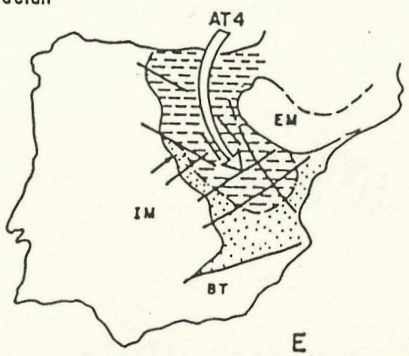

E

Lower - Middle Santonian

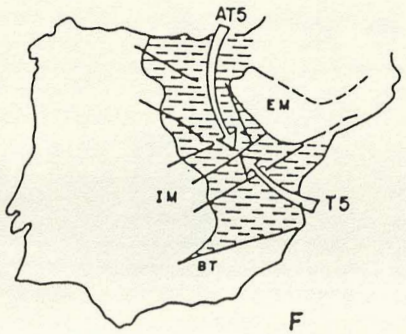

F

Upper Campanian

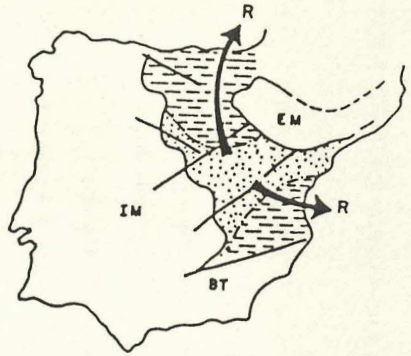

G

Maastrichtian

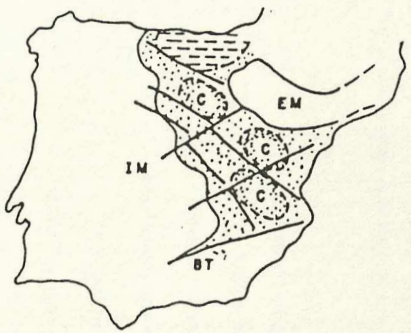

H

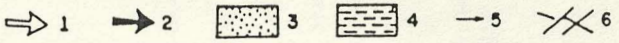

KEY:

1 transgression
2 regression
3 continental
4 marine
5 clastic supply
6 faults

UPPER CRETACEOUS—

SEDIMENTATION AND TECTONICS

(Alonso et al, in prep).

fault directions of graben-bounding and transfer structures of U Jurassic + Lr Cretaceous

Fig 8.71. Integrated facies models and facies geometries for the Maastrichtian - Palaeocene of the Santo Domingo de Silos region, in the W of the study area. From Floquet et al (1985). Note: inferred minor folding and faulting by the onset of the Palaeocene. See discussion in text.

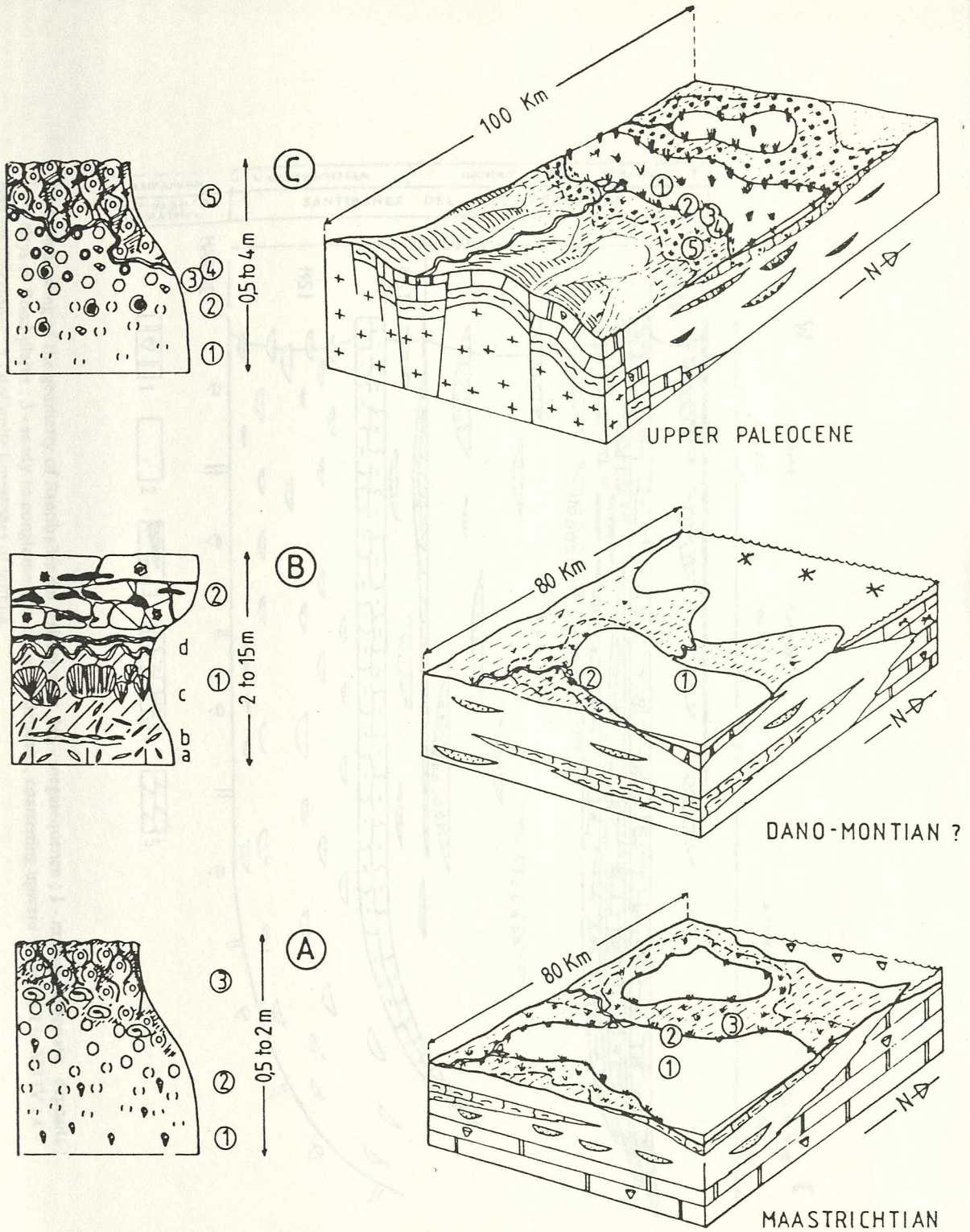

Carbonate sequences and environmental evolution of the continental basin of Santo Domingo de Silos from Maastrichtian (A), to upper Paleocene (C).

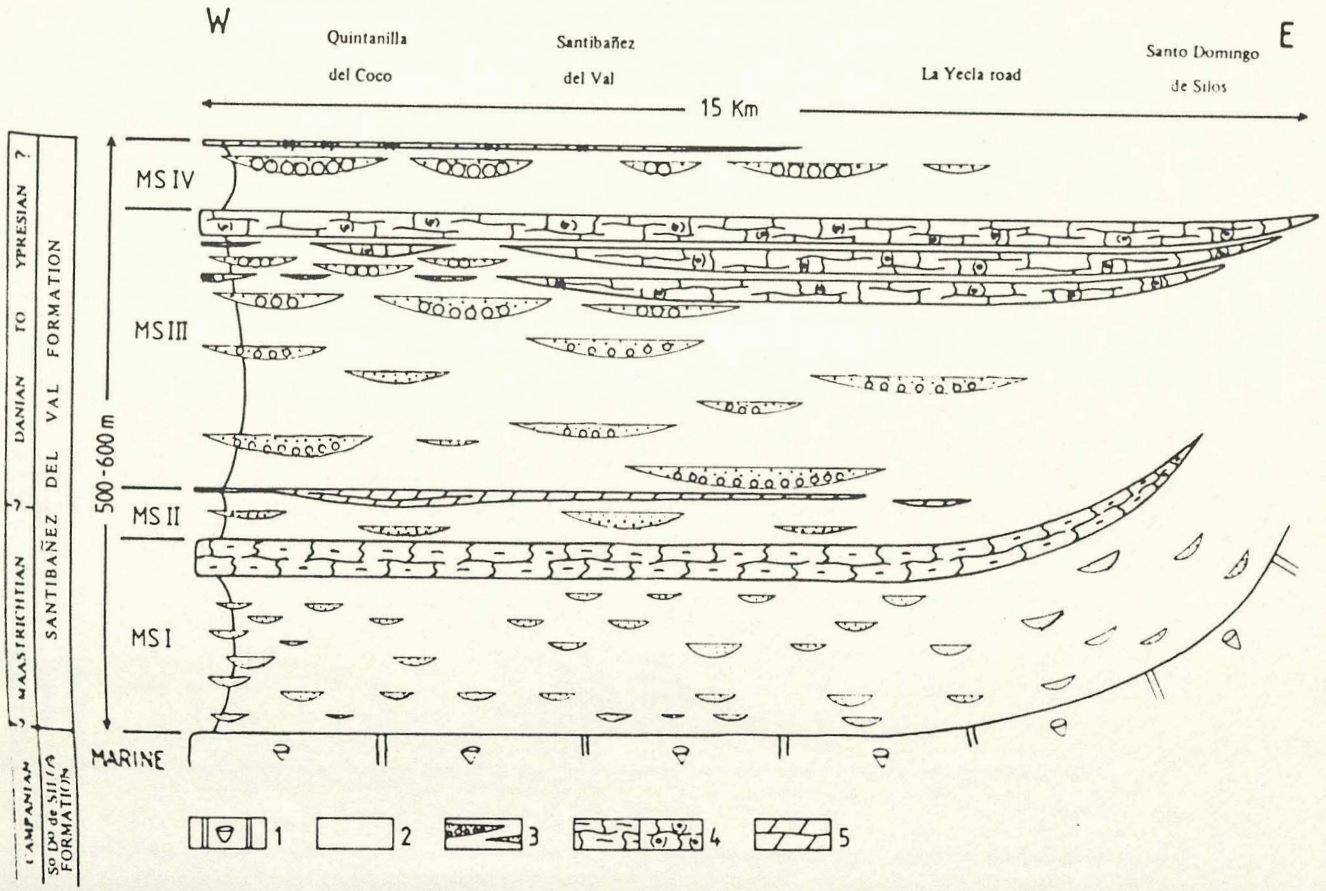

Schematic drawing of the geometry of Santibañez del Val deposits. MS - megasequence ; 1 - marine carbonate deposits ; 2 - red clays of flood-plains ; 3 - sandy to conglomeratic channel deposits, coarsening upward from MS I to MS IV ; 4 - lacustrine limestones ; 5 - dolomite limestones of sebkha.

Fig 8.73. Extremely coarse monomict conglomerate with locally-derived, rounded to subangular, clasts of Upper Cretaceous limestone up to 1m in size. Looking N. Hortigüela - Covarrubias road. OligoMiocene.

Fig 8.74. Extremely coarse monomict conglomerates with many rounded clasts of Upper Cretaceous limestone 50-100cm across. Rio Arlanza Gorge behind. Looking W. Hortigüela - Covarrubias road. OligoMiocene.

Fig 8.75. Coarse monomict conglomerates similar to those in figs 8.73 & 8.74. Clasts angular and irregular - short transport distance. Strong carbonate cementation. Looking NE. Hortigüela - Covarrubias road. Oligomiocene.

Fig 8.76. Monomict conglomerates, clasts of Upper Cretaceous limestone probably locally derived from anticline developed over blind /ramping Las Mamblas thrust front. Note: coarse clast size; channelling. Hammer provides scale just below channel base. Looking NE. Hortigüela - Covarrubias road. OligoMiocene.

Fig 8.77. Polymict conglomerate, exposed on Hortigüela - Covarrubias road, channelled into fine conglomerate / pebbly sandstone. Clasts in polymict conglomerate include: purple meta-arenites, white / brown quartzite (Palaeozoic); brown sandstone, grey limestone (Mesozoic).
Interpretation: clasts derived from many different horizons within Phanerozoic sequence - much larger catchment area than the conglomerates shown in figs 8.74 - 8.77. Breaching of Upper Cretaceous ridge of Las Mamblas thrust front along Jaramillo - Covarrubias Fault: a major Mesozoic transfer structure reactivated and exerting control on drainage during Tertiary (see fig 8.80). The modern Rio Arlanza utilises the same course.

Fig 8.78. Large, rounded quartzitic conglomerate clast in polymict conglomerate exposed on Hortigüela - Covarrubias road. Brown sandstone clasts to right.

Fig 8.79. Polymict conglomerate consisting of clasts of Upper Cretaceous limestone, red sandstone, grey limestone. Interpretation: mixed source conglomerate.

Fig 8.80. Interpretative sketches showing rôle of Las Mamblas thrust front and Jaramillo - Covarrubias Fault in Tertiary conglomerate deposition. Note: increased catchment area of fan sourced from along major transfer structure. JCF breaches blind/emergent thrust front which forms anticlinal ridge of Upper Cretaceous limestone and otherwise acts as a barrier to clast transport from more distant sources (eg Palaeozoic of Sierra de la Demanda).

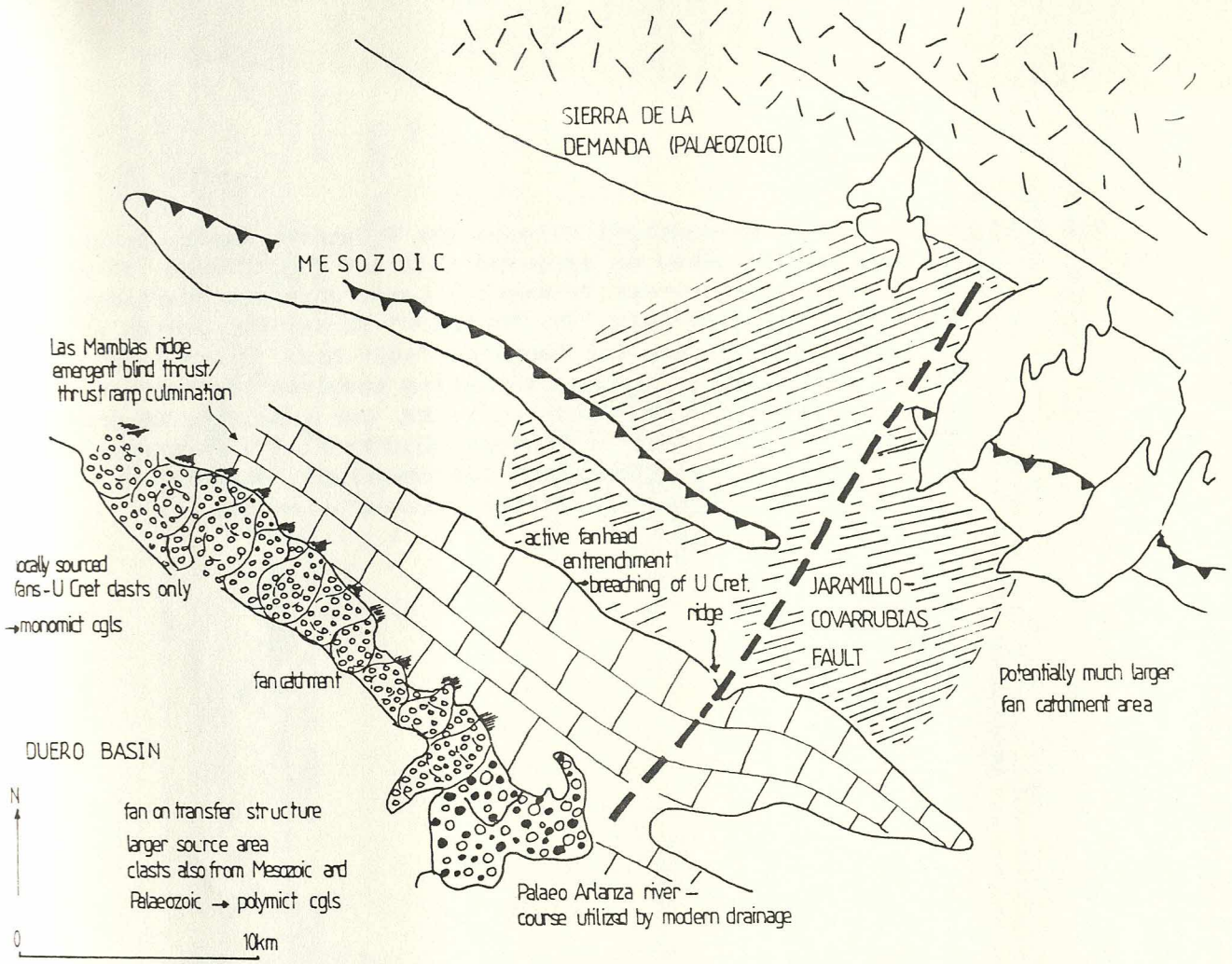
SIERRA DE LA
DEMANDA (PALAEOZOIC)
MESOZOIC
Las Mamblas ridge
emergent blind thrust/
thrust ramp culmination
ocally sourced
fans - U Cret clasts only
→monomict cgls
active fanhead
entrenchment
→breaching of U Cret.
ridge
JARAMILLO -
COVARRUBIAS
FAULT
potentially much larger
fan catchment area
fan catchment
DUERO BASIN
N
fan on transfer structure
larger source area
clasts also from Mesozoic and
Palaeozoic → polymict cgls
0
10km
Palaeo Arlanza river -
course utilized by modern drainage

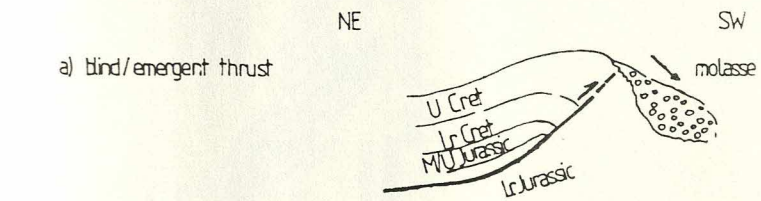
NE
SW
a) blind/emergent thrust
molasse
U Cret
Lr Cret
M/U Jurassic
Lr Jurassic

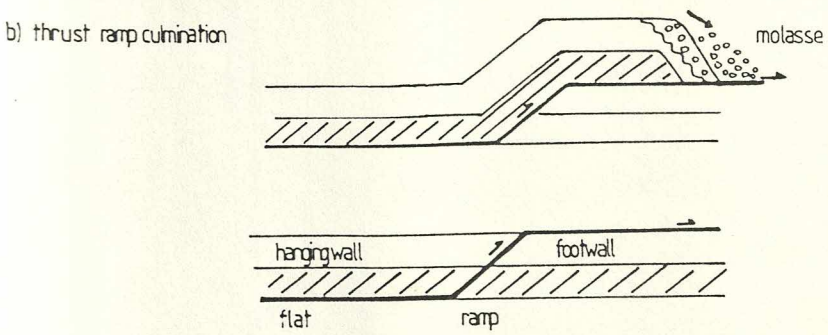
b) thrust ramp culmination
molasse
hanging wall
footwall
flat
ramp

Fig 8.81. Schematic cross-sections through the W Cameros Basin. Lines of section indicated on extended abstract fig 1. Note: décollement is chiefly along Latest Triassic - Lower Jurassic "Carniolas", but with some duplexes using the "Purbeck" facies evaporites of the Rio Cabrera Member in the San Leonardo Fault Zone; blind / emergent thrusts at SW basin margin; thrusting involves basement at Moncalvillo; dominant thrusting to SW, but some N or NE-directed thrusting (eg La Yecla backthrust, Quintanilla - Castrovido Fault). This section is not "balanced" (ie restored). Deformation may include "thin-skinned" or "thick-skinned" elements

W CAMEROS BASIN — SCHEMATIC CROSS-SECTIONS

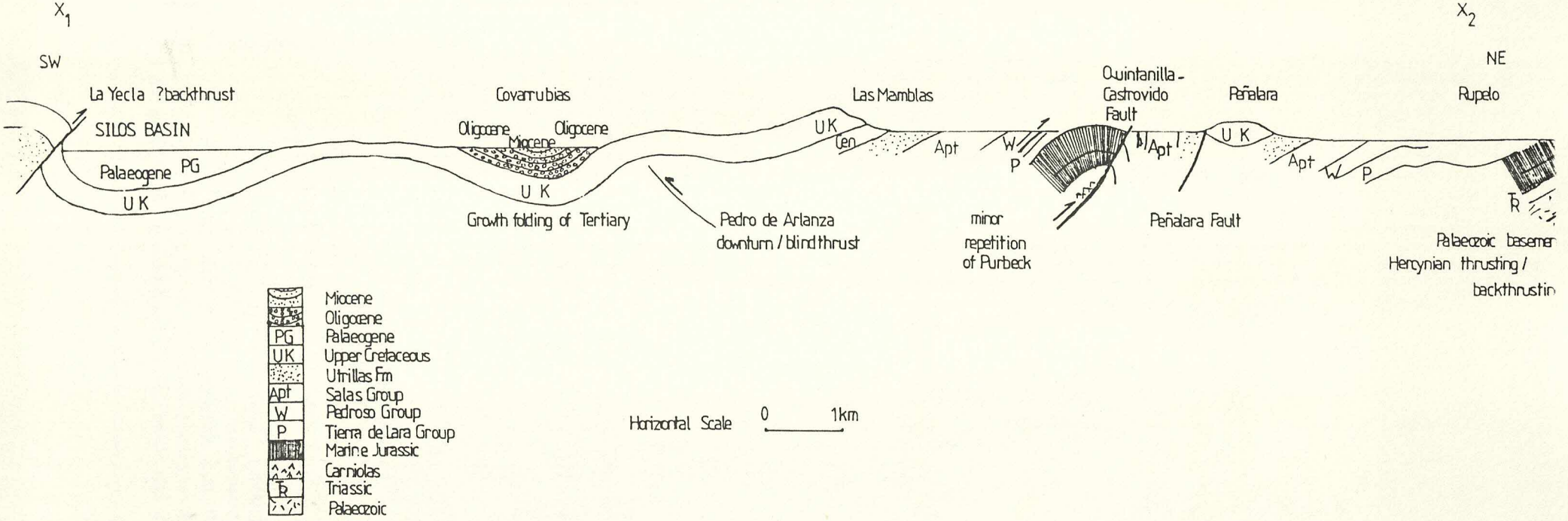

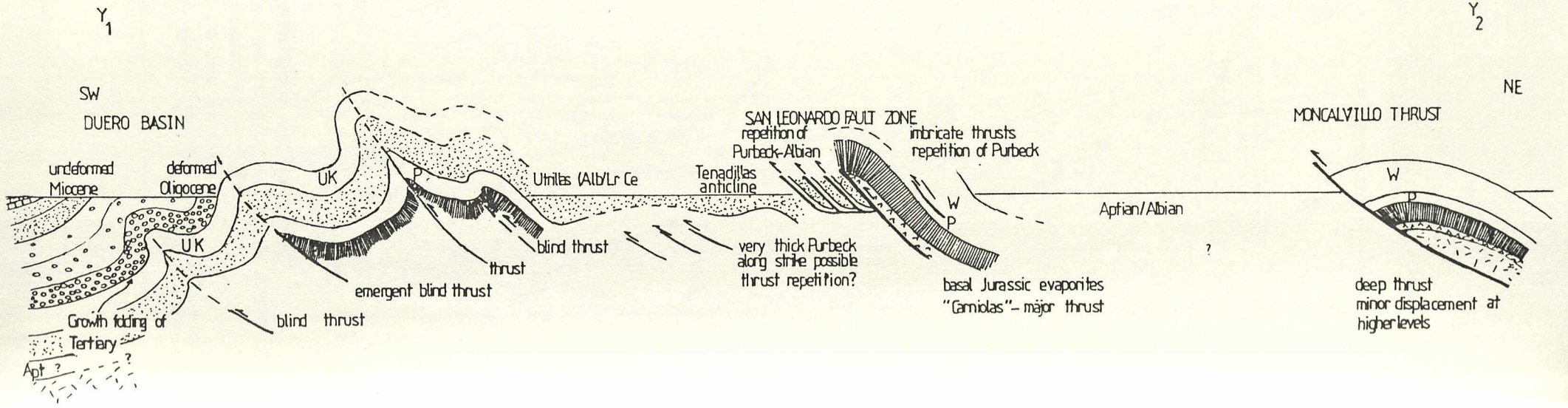

Fig 8.82. Palaeogeography of part of the Swiss Molasse Basin showing the rôle of faults transverse to the basin axis. Cross-faults determine the patterns of alluvial sedimentation under compression by conditioning the sites of fan-head entrenchment. From [illegible] & Allen (1985).

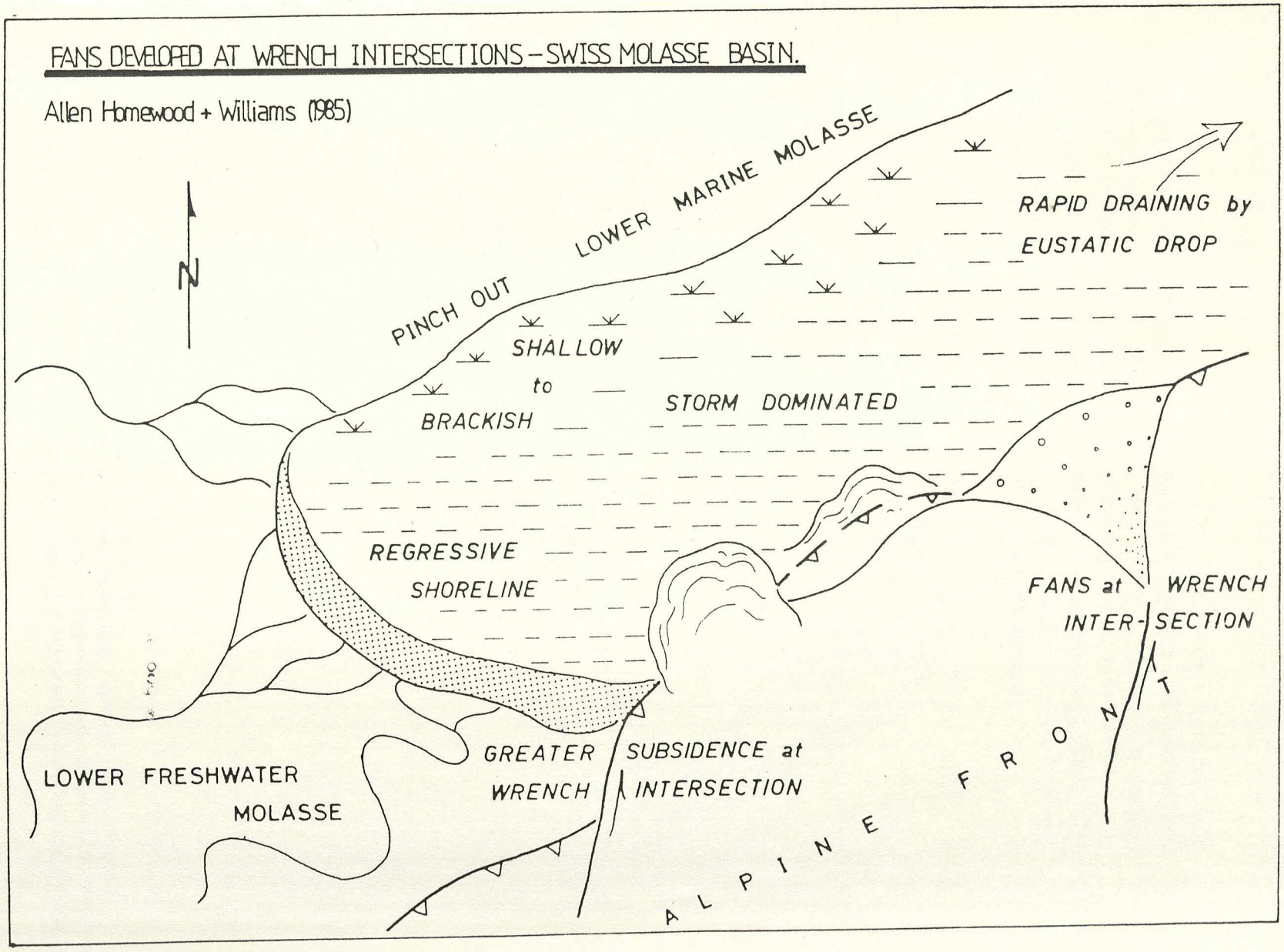
FANS DEVELOPED AT WRENCH INTERSECTIONS – SWISS MOLASSE BASIN.
Allen Homewood + Williams (1985)
N
LOWER MARINE MOLASSE
PINCH OUT
SHALLOW
to
BRACKISH
STORM DOMINATED
RAPID DRAINING by
EUSTATIC DROP
REGRESSIVE
SHORELINE
FANS at WRENCH
INTER-SECTION
LOWER FRESHWATER
MOLASSE
GREATER
WRENCH
SUBSIDENCE at
INTERSECTION
ALPINE FRONT

Fig 8.83. Interpretative sketch showing alluvial sedimentation in the Siwaliks of Pakistan. Note influence of transverse streams which allow breaching of emergent thrust front. After Parkash, Sharma & Roy (1980).

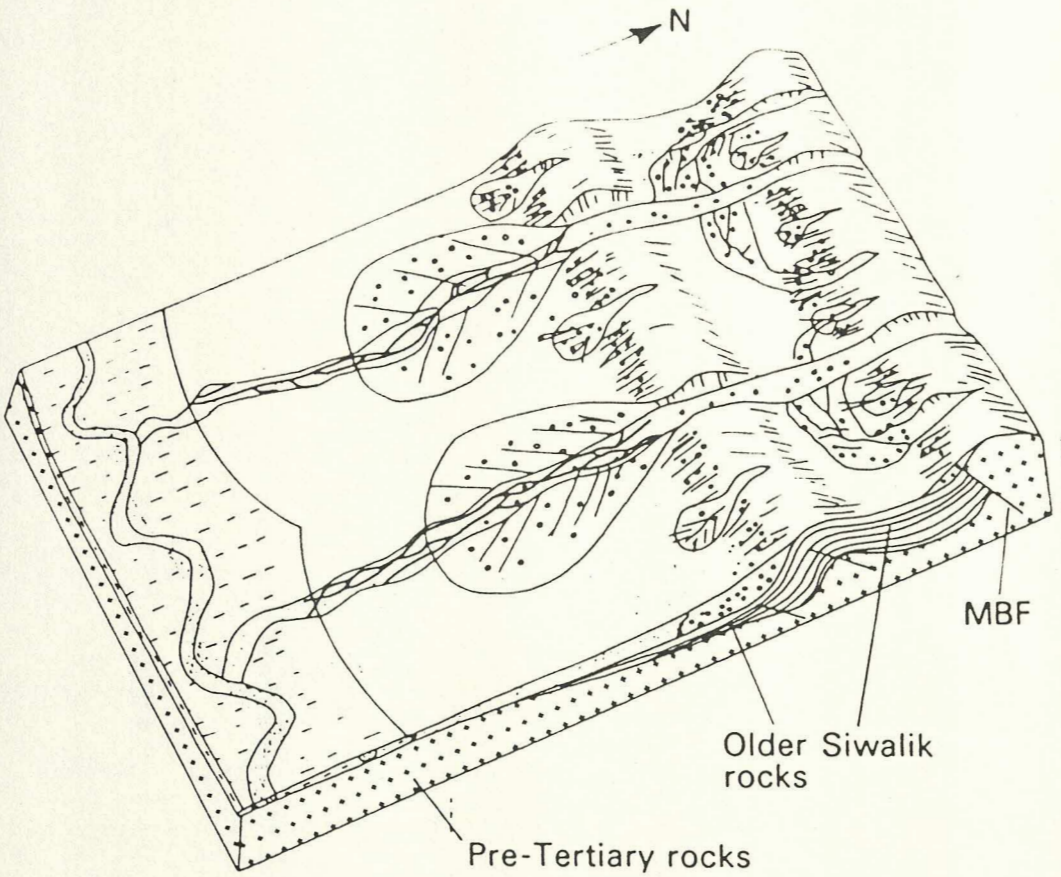

Sedimentation of Siwaliks on southern margin of the Himalayas (after Parkash, Sharma and Roy, 1980). Transverse alluvial fans are of three types; large megacones debouching from major rivers; small fans reworking older Siwaliks and fans and braided rivers forming within fold-thrust related troughs. In the major basins the large megacones pass distally into braided rivers which turn longitudinally into the main alluvial basin.

Fig 8.84. Sketch map of Jaca Basin, S Pyrenees, indicating possible rôle of transverse faults on Tertiary conglomerate deposition. Analogy with the W Cameros would suggest that these transverse faults may be reactivated Mesozoic transfer structures.

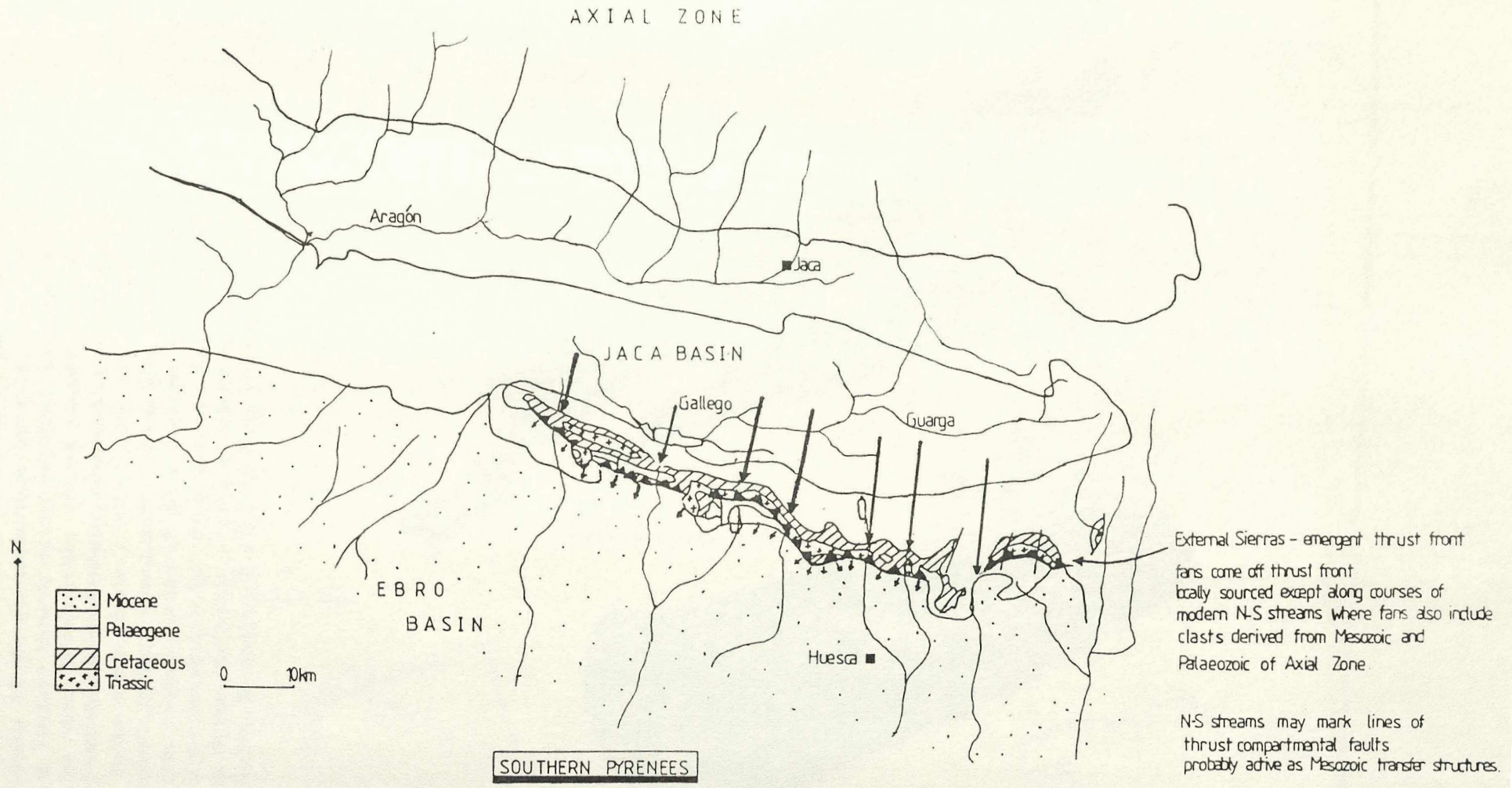

SOUTHERN PYRENEES

Fig 8.85. Tectonic map of SW Britain. Note: faults bounding Mesozoic basins are oriented approximately NE-SW (possible control of Caledonide or late-Hercynian wrench trends) and E-W (Hercynian thrust faults reactivated under extension). Cross-cutting "transfer faults" trend SE-NW; interpretation of Gayer & Underhill (1985) views these as of Oligocene age - movement documented from Bovey Tracey, Petrockstow and Lough Neagh Basins, also from emplacement date of Lundy Granite - but analogy with the W Cameros would suggest faults were probably active under extension as wrench faults compartmenting grabens into a series of offset segments.

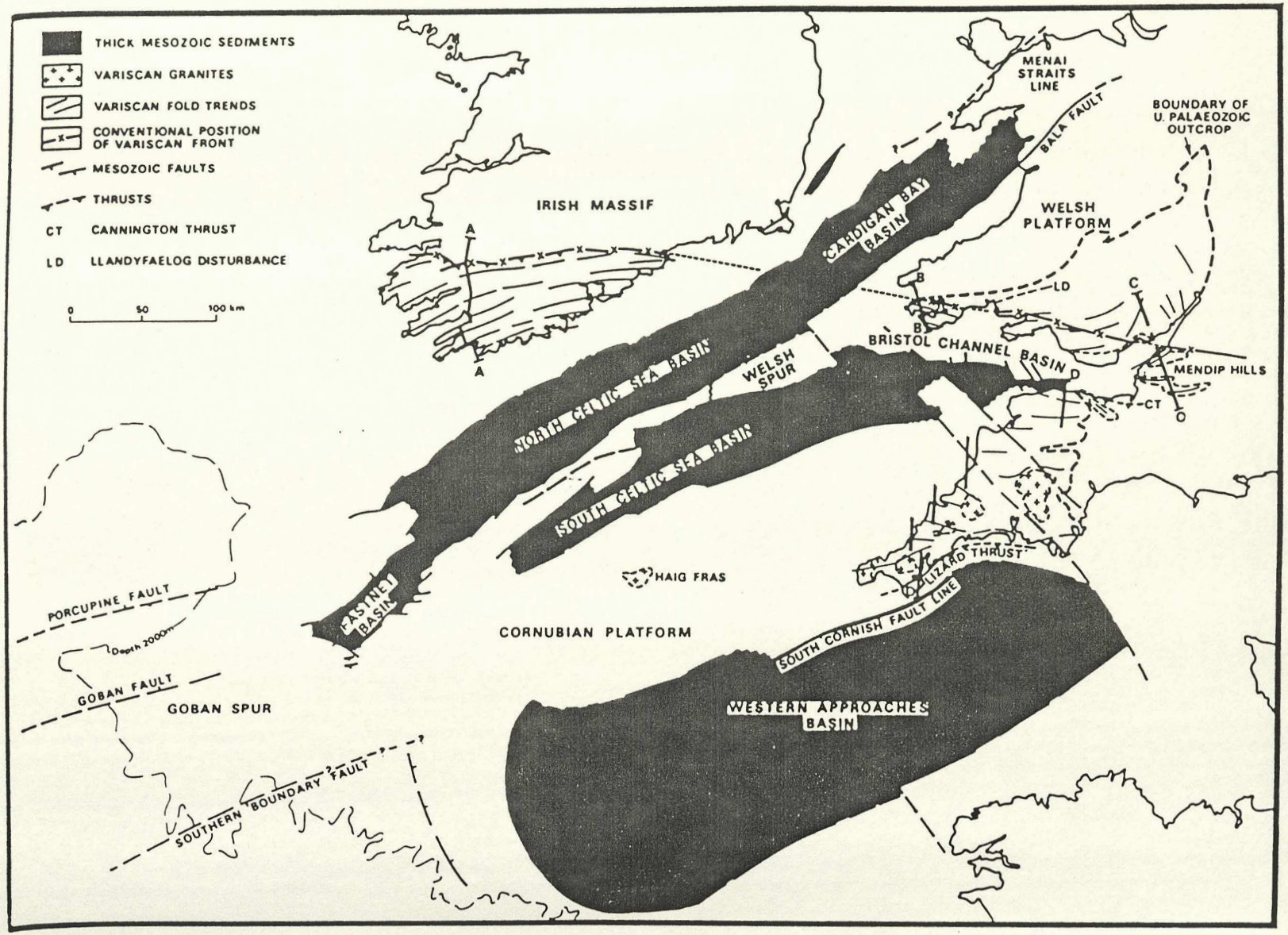

Mesozoic tectonic framework of the Southwestern British Isles and adjacent continental margin. Offshore data from Pegrum & Mountenay (1978), Zeigler (1978), Dingle & Scrutton (1979), Kamerling (1979), Robinson *et al.* (1981) and Fig. 3 of this paper. Onshore structural trends from Dunning (1966) and Max (1979). Black areas show locations of thick Mesozoic sediments. A–A, B–B, C–C, D–D, are the lines of the sections shown in Fig. 4.

Fig 8.86. Table listing some of the contrasts between OligoMiocene sedimentation in the W Cameros and in SW Britain.

COMPARISON OF PALAEOGENE SEQUENCES OF THE W CAMEROS AND S ENGLAND.

W CAMEROS	HANTS./I.o.W.	DIFFERENCES
no marine influence deposition above sea-level	important marine influence deposition near sea- level	a) uplift greater in W Cameros; also b) pre-uplift (Upper Cretaceous) environments shallower in W Cameros - greater influence of basement massif - Meseta
abundant conglomerates	few conglomerates	greater deformation and differential uplift in W Cameros
evaporites present	no evaporites reported	more arid climate in W Cameros - further S and inland
impure lacustrine carbonates (SVF^d & SVF^e) pedogenetic modification impure	pure lacustrine carbonates (Bembridge Lst) pedogenetic modification but relatively pure	a) less clastic input in S England b) erosion in S England virtually restricted to U Cretaceous (chalk) carbonates erosion of other lithologies in W Cameros - lacustrine carbonates restricted to areas away from input of pre - U Cretaceous clasts. c) more humid climate in S England - more stream inflow more chemical weathering - abundant dissolved $CaCO_3$ in river supply.

PLATT N (1986)

Fig 8.87. Polymict conglomerates from the Ranas Formation (Plio-Quaternary) at Piedrahita de Muno. Clast derivation from Mesozoic and Palaeozoic sequences, but apparently no Upper Cretaceous clasts. Note passing lithological similarity with Senora de Brezales Formation conglomerates.

Fig 8.88. Ranas Formation conglomerates (poor outcrop, brick red soil with scrubby bushes and trees, top and right) lying unconformably upon and truncating interbedded tabular sands (crevasse splay units) and marls/muds (overbank deposits) of Piedrahita de Muno Formation. 1km N of Piedrahita de Muno.

Fig 8.89. Sketch map showing the distribution and morphology of Ranas Formation outcrops. Map pattern suggests deposition as a series of lobate alluvial fans with apices at major fault intersections on the S margin of the Sierra de la Demanda. Area of fig 8.90 is marked by box.

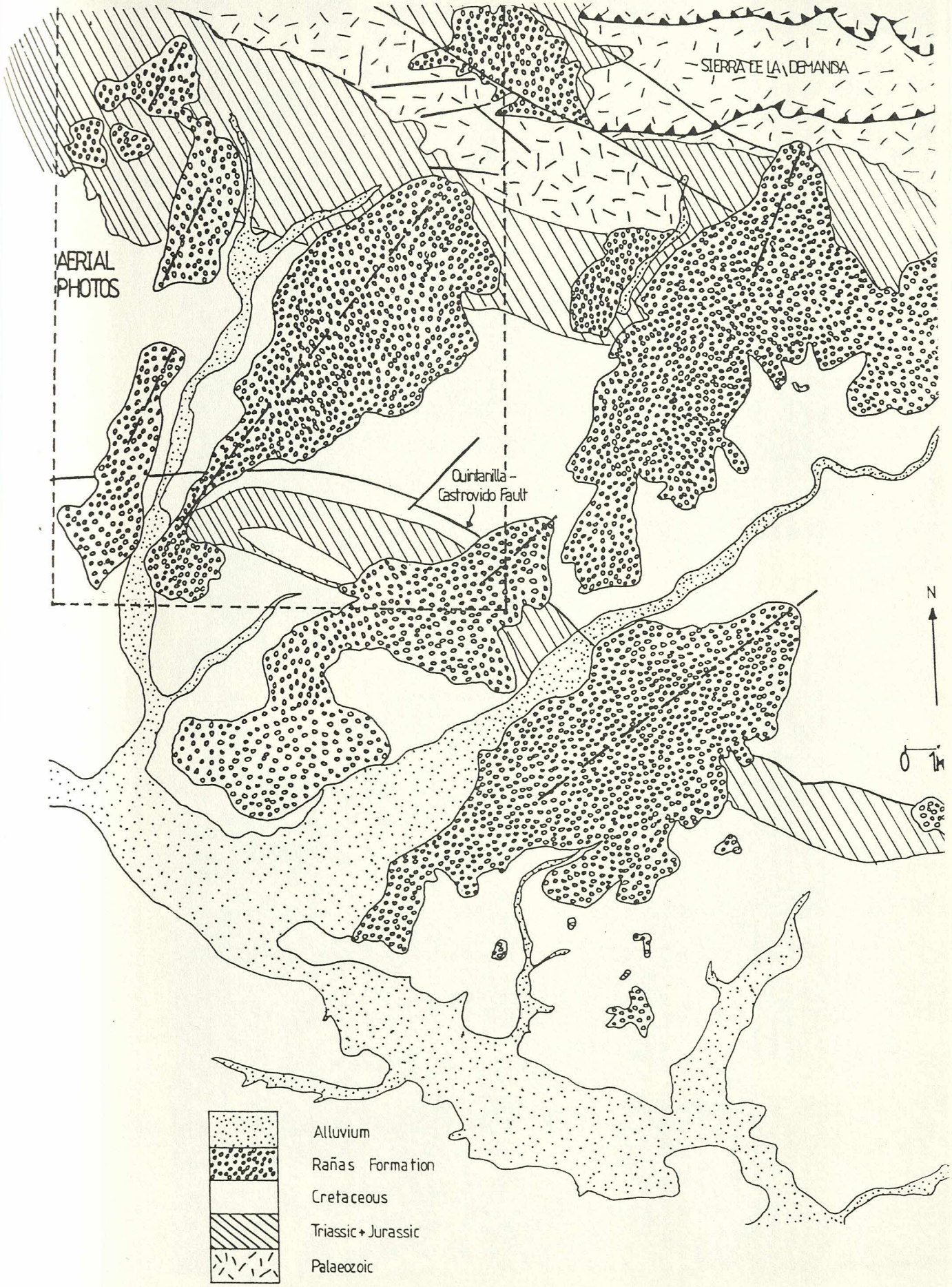

RAÑAS FORMATION: OUTCROP MAP

alluvial fan geometry - fans draining Palaeozoic of Sierra de la Demanda and sourced at intersection of NW-SE + NE-SW faults.

Fig 8.90. Aerial photograph of part of area shown in fig 8.89. The Ranas Formation is easily differentiated in this view by virtue of its dense bushy scrub vegetation cover (dark colour in photograph). Unfortunately, this dense cover makes for very poor outcrop in the field.

N

AERIAL PHOTOGRAPHS SHOWING RAÑAS FORMATION OUTCROPS

Scale — 0 1km

Fig 8.91. Map of Central Interior N Spain showing major basins and structural lineaments and distribution of Quaternary alluvium. Note dominance of NE-SW, E-W and NW-SE trends in Quaternary drainage.

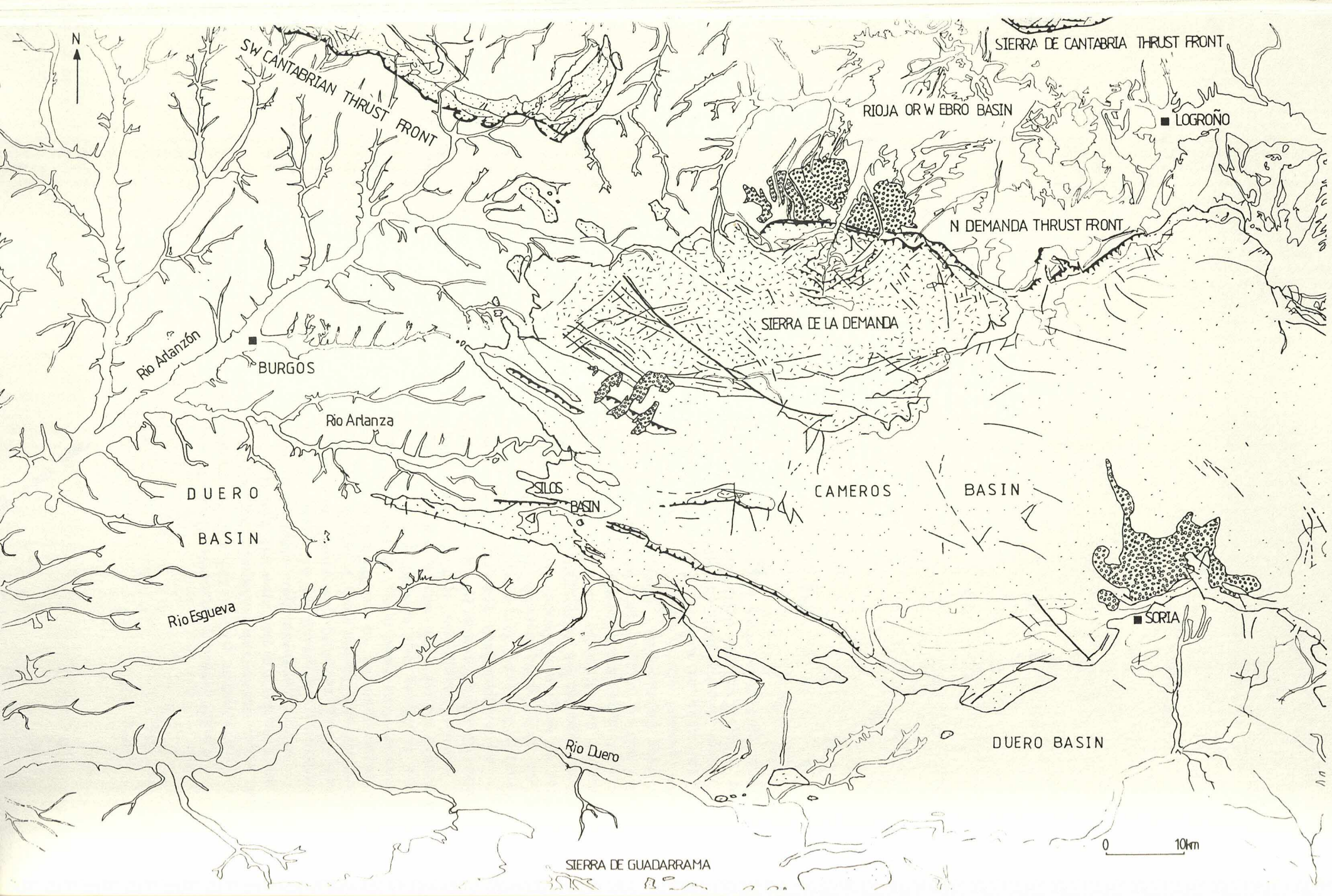
N
SW CANTABRIAN THRUST FRONT
SIERRA DE CANTABRIA THRUST FRONT
RIOJA OR W EBRO BASIN
LOGROÑO
N DEMANDA THRUST FRONT
SIERRA DE LA DEMANDA
Rio Arlanzón
BURGOS
Rio Arlanza
DUERO
BASIN
SILOS
BASIN
CAMEROS
BASIN
Rio Esgueva
SORIA
Rio Duero
DUERO BASIN
SIERRA DE GUADARRAMA
0
10km

Fig 8.92. Map of Central Interior N Spain showing interpreted structure. Note dominance of the following structural trends: NE-SW (including major transfer structure inferred along course of Arlanzon River through Burgos offsetting the W Cameros and SW Cantabria basins, and numerous other subparallel structures recognisable by Quaternary stream couses); NW-SE (including San Leonardo, Quintanilla - Castrovido and Huerta del Rey faults and the W section of the SW Cantabria thrust front); E-W (including E section of SW Cantabrian thrust front - ie N margin of Rioja Basin - and also structures inferred along course of Arlanza and Duero Rivers and parallel streams in the E Duero Basin). The NW-SE and NE-SW structural trends are interpreted as a conjugate set of late Hercynian wrench faults active as basin-bounding normal faults under Mesozoic extension and then locally reactivated under Tertiary compression as contractional faults with minor thrust splays. E-W structures mark the orientation of Hercynian thrust planes (see eg in the N part of the Sierra de la Demanda) which were locally active as extensional faults during the Mesozoic and reactivated as thrusts in the Tertiary, especially where the Mesozoic sequence is thinner and Hercynian structures are closer to the surface (eg: in the Villavelayo syncline, a small faulted sub-basin in the area of the Sierra de la Demanda; at Moncalvillo in the central part of the Cameros Basin; and at the N margin of the Rioja Basin). The capacity of the Quaternary drainage patterns to pick out the deep structure is remarkable, especially in view of the very thick Tertiary sequences in the Duero and Rioja Basins (up to 4km). It seems likely that the same faults were active during Tertiary sedimentation.

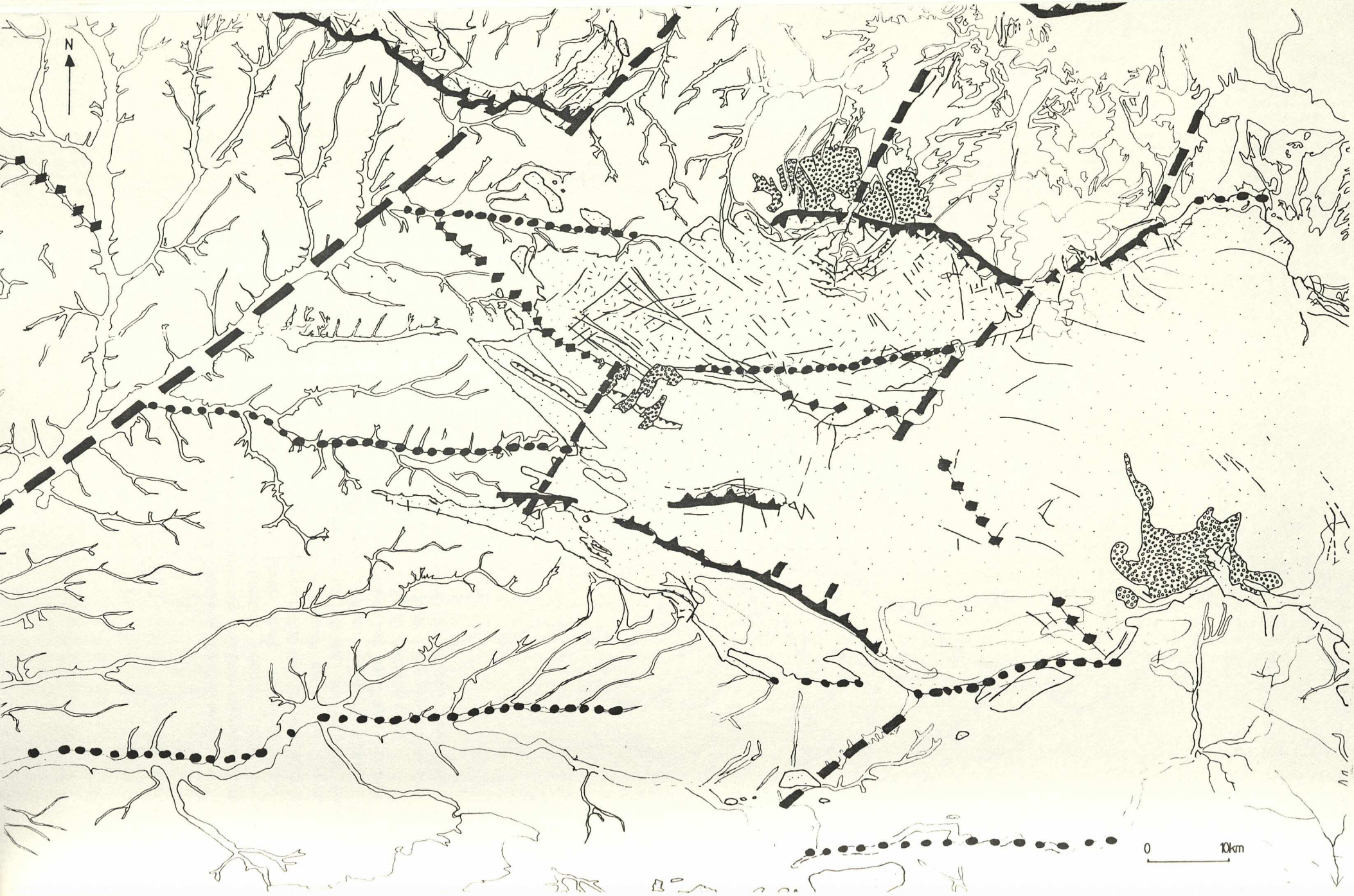
N
0
10km

Figs 8.93 & 8.94. Structural maps of the W Cameros Basin and immediately surrounding areas showing faults mapped during the course of this study and structural trends identifiable from published geological maps. Note that the more minor structures show the same dominance of NE-SW, NW-SE and E-W trends, and that geological features such as major sequence boudaries are made up of a series of NE-SW, NW-SE and E-W segments (eg: S margin of Cameros Basin; base of Upper Cretaceous in S of the basin; Las Mamblas and San Carazo Upper Cretaceous mountains and NW basin margin. Structurally complex areas occur at the intersection of major structures (eg: La Yecla - Mamolar area; Espejon).

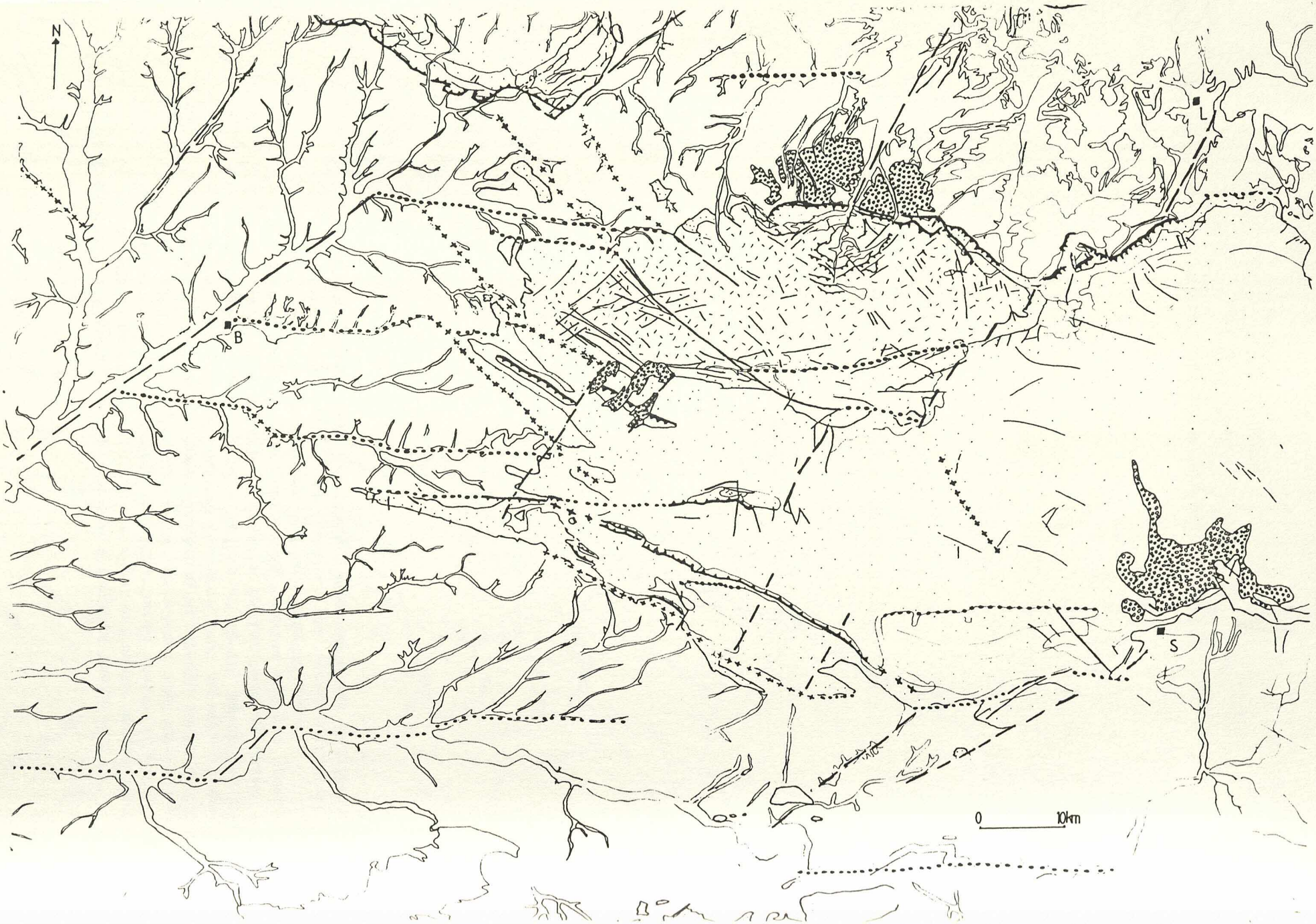
N
B
L
S
0
10km

Figs 8.93 & 8.94. Structural maps of the W Cameros Basin and immediately surrounding areas showing faults mapped during the course of this study and structural trends identifiable from published geological maps. Note that the more minor structures show the same dominance of NE-SW, NW-SE and E-W trends, and that geological features such as major sequence boudaries are made up of a series of NE-SW, NW-SE and E-W segments (eg: S margin of Cameros Basin; base of Upper Cretaceous in S of the basin; Las Mamblas and San Carazo Upper Cretaceous mountains and NW basin margin. Structurally complex areas occur at the intersection of major structures (eg: La Yecla - Mamolar area; Espejon).

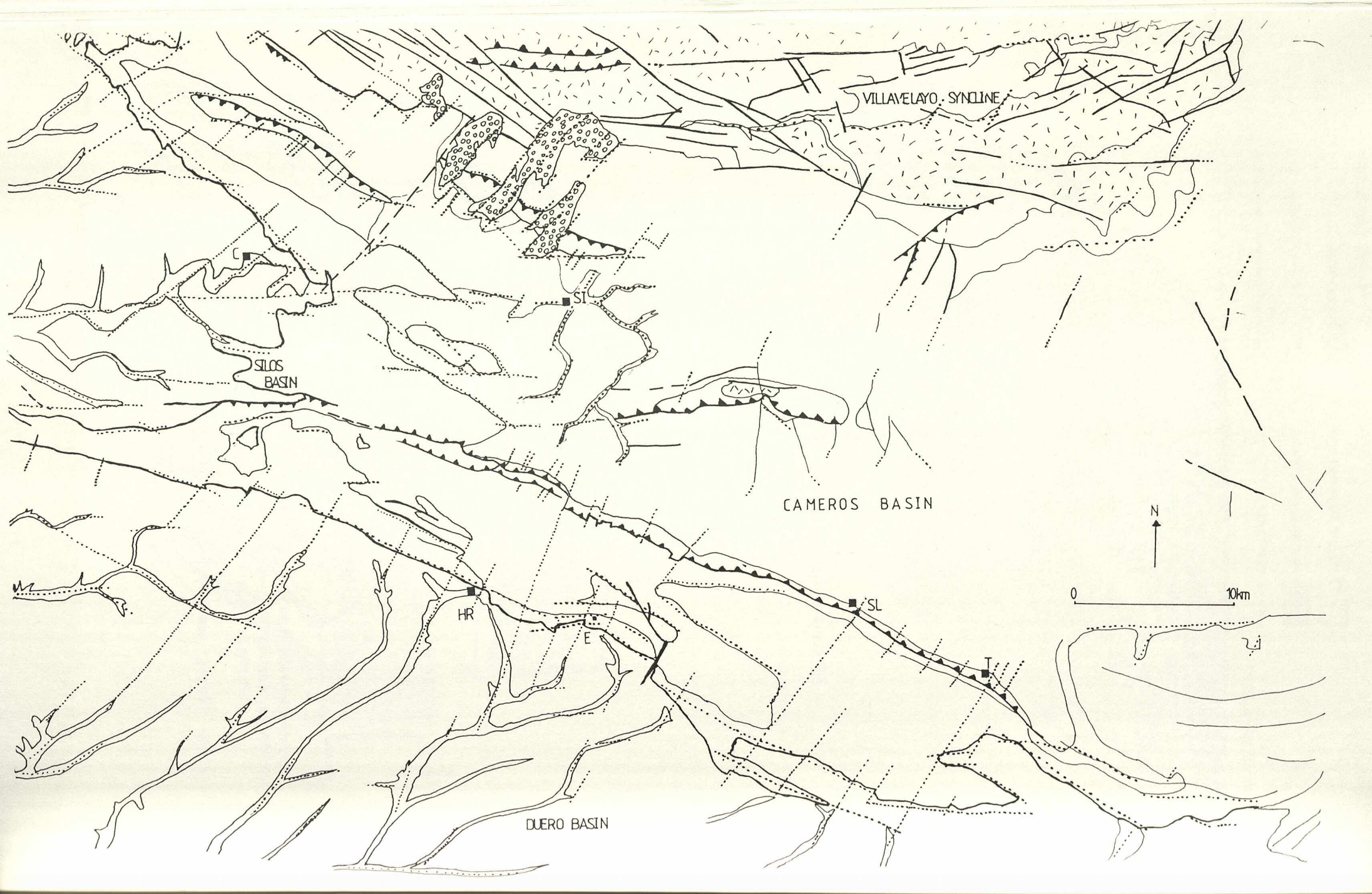
VILLAVELAYO SYNCLINE
C
SI
SILOS
BASIN
CAMEROS BASIN
N
0
10km
HR
E
SL
T
DUERO BASIN

Fig 8.95. Schematic representation of graben system (Bally, 1981) showing:

a) basin-bounding extensional normal faults
b) cross-graben wrench or "transfer" faults segmenting the graben into a series of offset compartments.

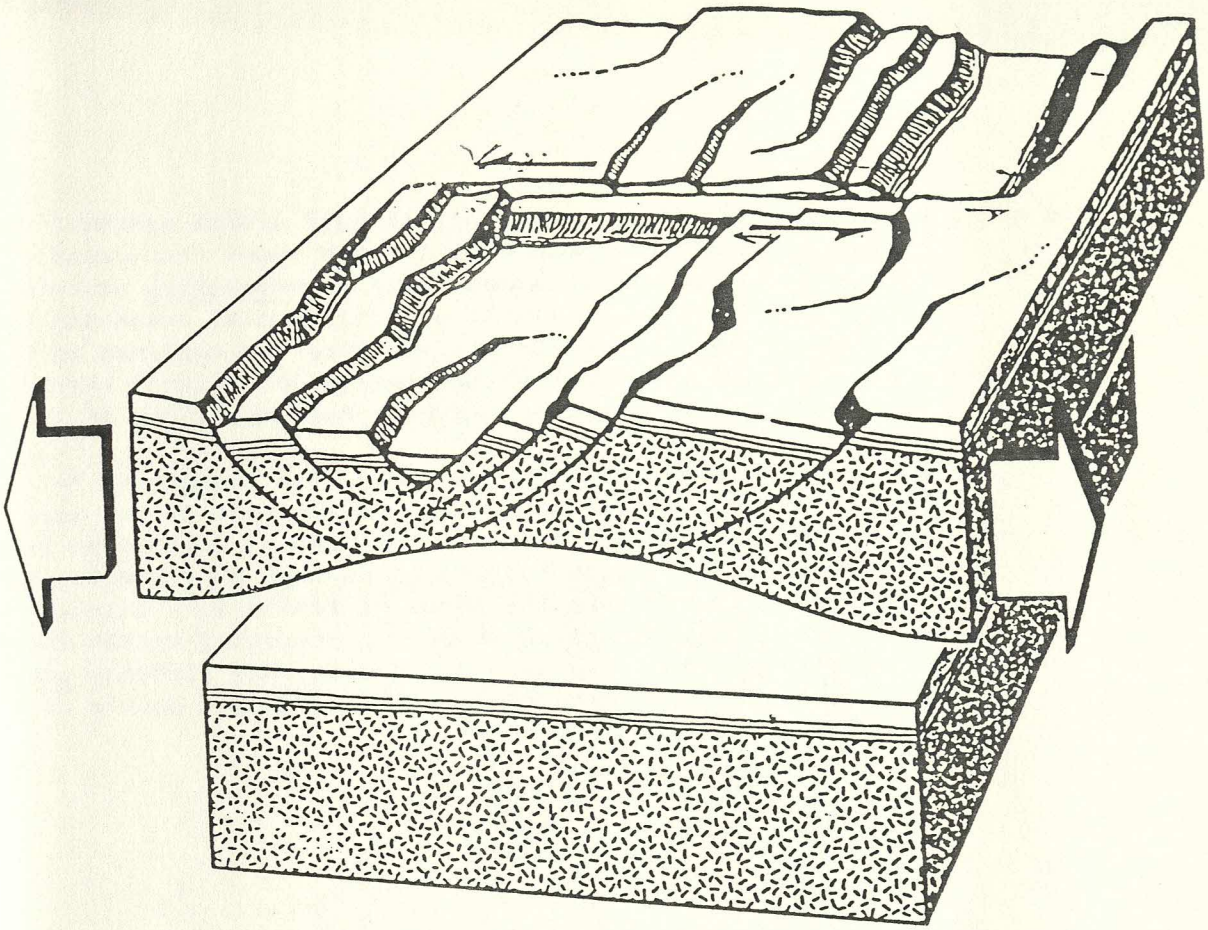

Bally (1981)

TRANSFORM ZONE SEPARATING TWO HALF - GRABEN SEGMENTS

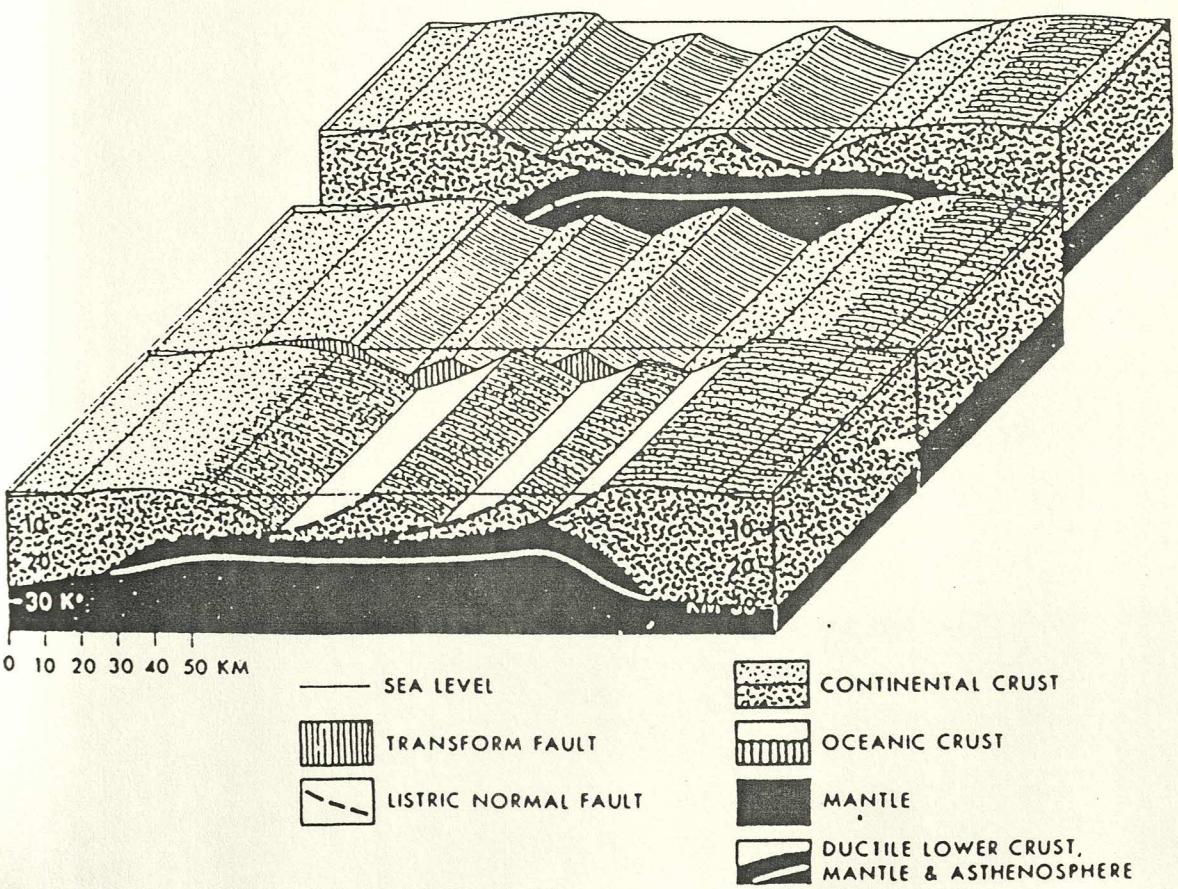

Fig 8.96. Schematic representation of offset half graben system from Lister et al (1986). Note that in this model the transfer faults are envisaged as essentially accommodation structures which were formed as a result of differential extension in the various basin compartments (ie they are confined to the graben system itself and do not generally continue beyond it); the transfer faults would have been initiated at the onset of extension).
In the W Cameros, the transfer faults are thought to be late-Hercynian features, and are thought to continue well beyond the graben system itself (eg Hispano-Portuguese Fault continues as far as the coast near to Cape St Vincent). This evidence indicates that the transfer faults were actually pre-existing structures which were reactivated at the onset of Mesozoic extension. The transfer faults thus probably conditioned the pattern of extension rather than developed merely as local accommodating tear faults.

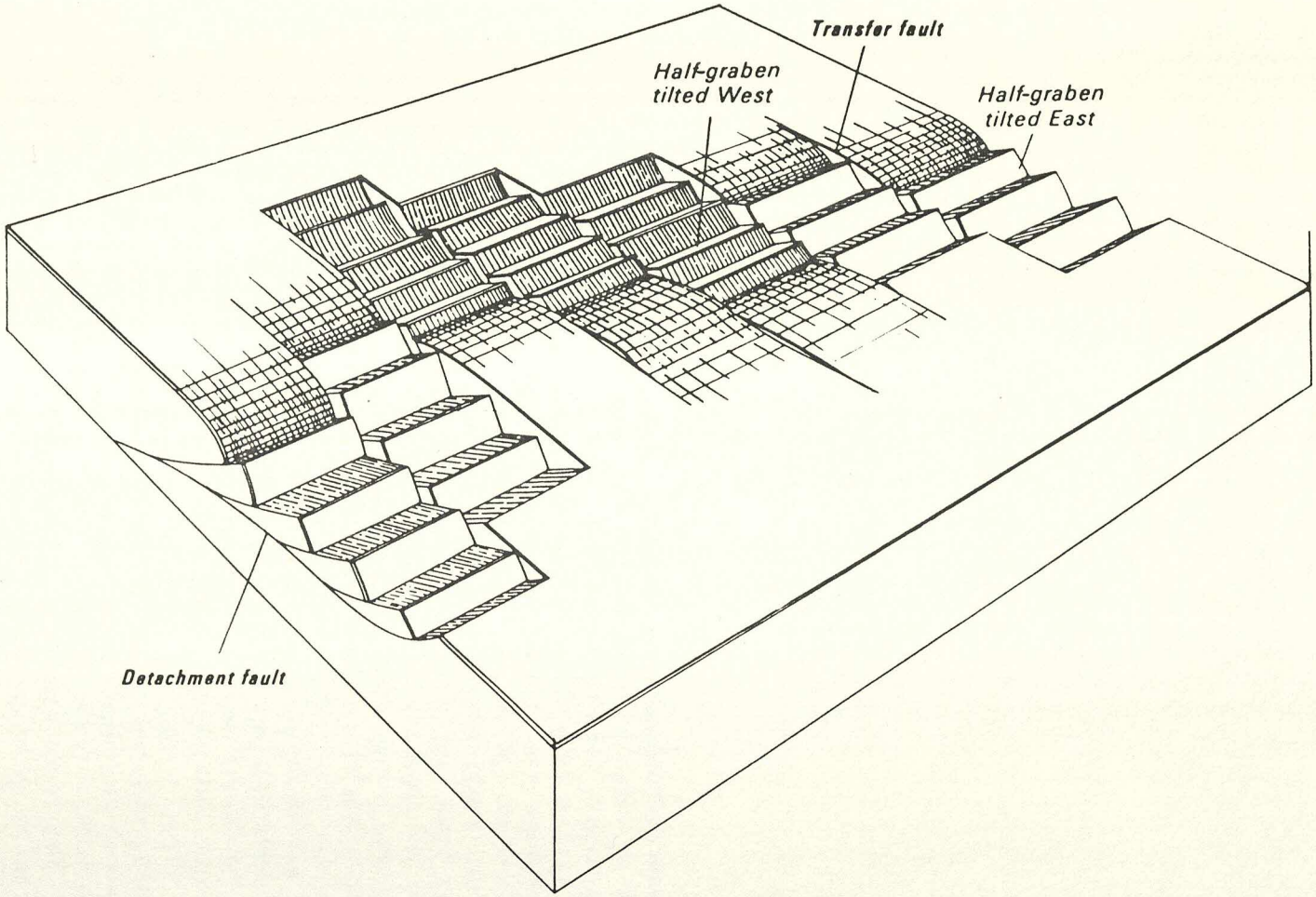
Transfer fault
Half-graben
tilted West
Half-graben
tilted East
Detachment fault

Figs 8.97 & 8.98. Imbricate fans. Documented examples from Boyer & Elliot (1982) and Vann et al (1986). Note similarity of structures to that shown on fig 8.81 for the SW Cameros Basin between San Leonardo Fault Zone and SW basin margin. Note that thrust tectonic interpretations involve the linking of these thrusts in a single basal detachment. Published models for the Canadian Rockies show basal thrust falts up to 80km in length. This model has recently been applied to Alpine regions (eg Swiss Molasse Basin) where Ziegler (1982) and Homewood et al (1985), Allen, Homewood & Williams (in press) invoke basal detachment under the basin on Tertiary evaporites along a single plane or along a very few deep thrust planes. In view of the substantial thickness variations visible in the sedimentary pile of Mesozoic basins (eg Cameros Basin) it seems clear that at the onset of Tertiary compression, early Mesozoic incompetent horizons would have been significantly offset and segmented by normal faults (as a result of later Mesozoic extension). Thus it becomes difficult to envisage simple slip along long unbroken thrust flats. It is also clear that the sequences and stratigraphy of Mesozoic extensional basins (eg Cameros Basin) are extremely variable both along and across structural strike with strong control exerted by basin-bounding and transfer structures so that assumptions of layer-cake or template (uniformly increasing thickness) stratigraphy are not realistic.

IMBRICATE FANS

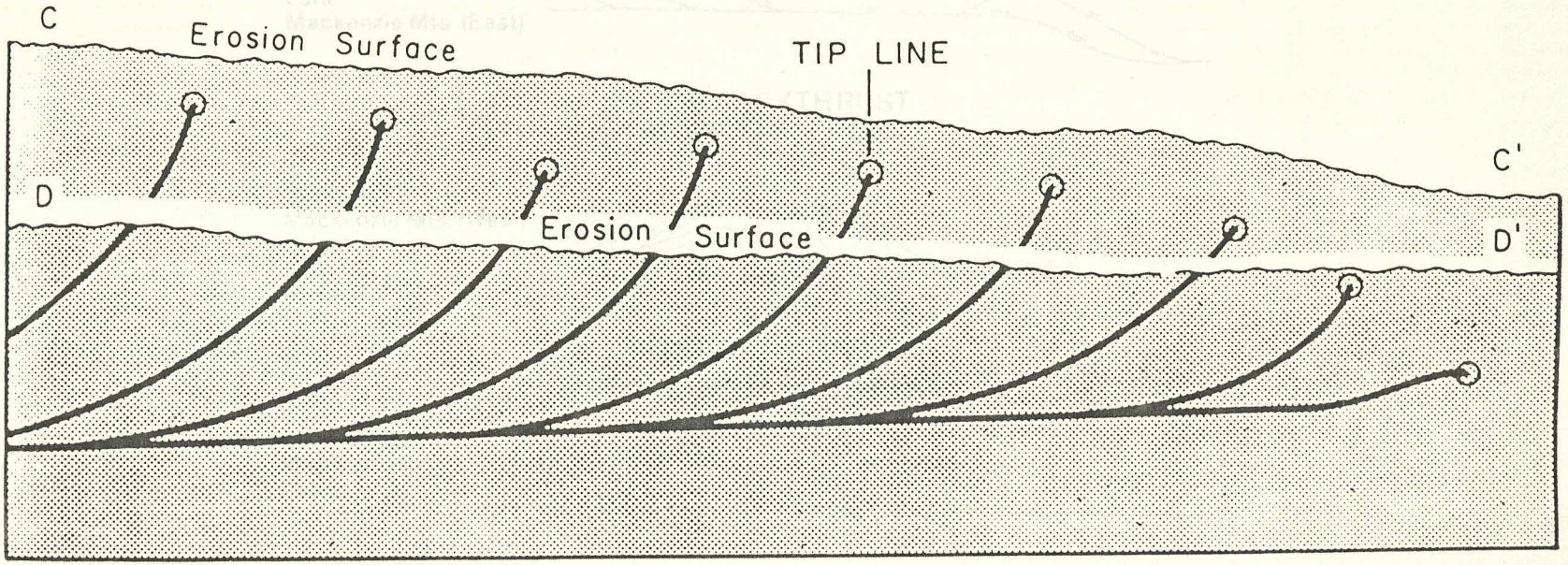

Cross section of imbricate fan at two different levels of erosion. Each thrust sheet is an upward-opening crescentic slice, and all curve asymptotically downward to a common basal sole thrust. If most faults cut synorogenic erosion surface DD′ we have an emergent imbricate fan. Alternatively, it is possible that tip lines do not reach synorogenic erosion surface CC′, producing blind imbricate fan. Note that subsequent erosion (CC′ down to DD′) may obliterate any means of distinguishing two kinds of imbricate fans.

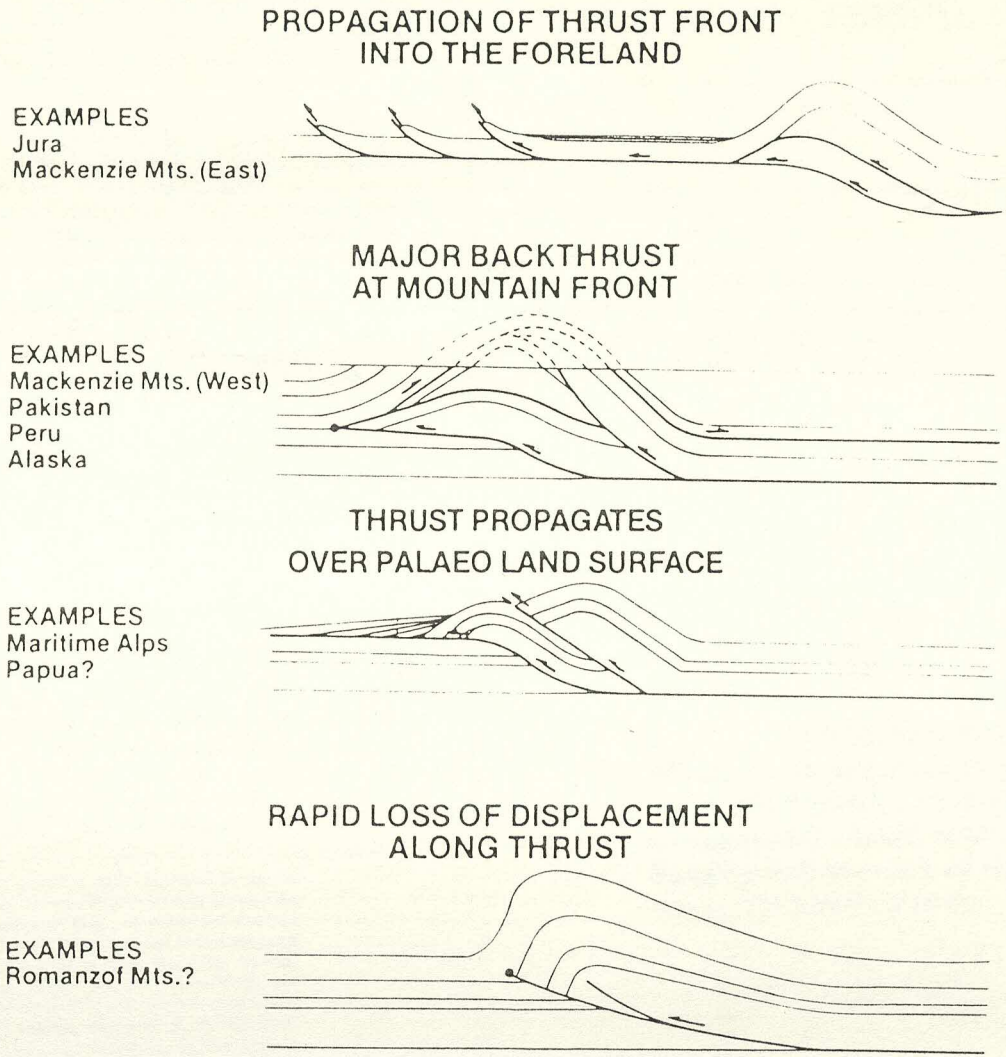

Four possible solutions to the problem posed in Fig. 1. (a) Sub molasse detachment implying transported molasse basin. (b) Major backthrust at the mountain front. (c) Buried emergent thrust. (d) Tip line strain.

Fig 8.99. Passive roof duplex. In this model, the sticking of forward-propogating thrusts results in the development of backthrusts higher in the structural pile. (see Morley, 1986; Banks & Warburton, 1986). This might be thought to be a possible explanation for the occurrence of backthrusts behind the San Leonardo Fault Zone in the La Yecla area.

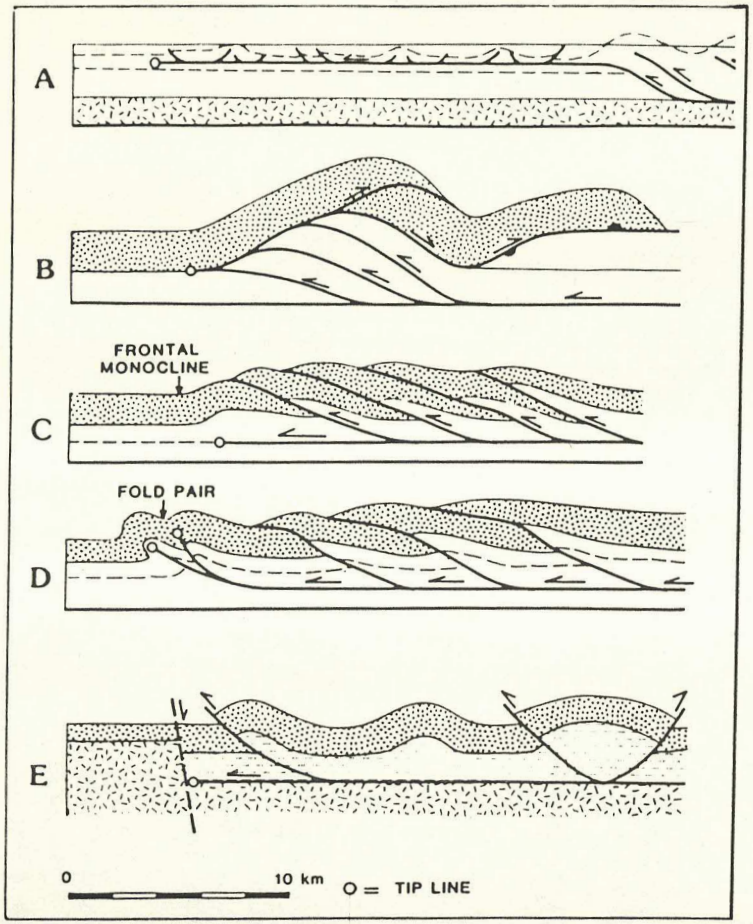

Variations in deformation style displayed by buried thrust fronts. (A) Type 1 (slow stress relaxation) with broad zone of low strain above detachment (e.g., Appalachian Plateau folds, after Root, 1973). Type 2, buried thrust fronts that end abruptly (B-D). (B) Passive roof duplex. Examples include Alberta syncline (Dahlstrom, 1970; Price, 1981; Jones 1982), and Jebel Zalarh area of Moroccan Rif. (C) Frontal monocline. Examples include external Sierras, Pyrenees (J. R. Hossack, 1984, personal communication), and Baronnies, Nyons, western Alps (Flandrin et al, 1975). (D) Complex fold tip line over ramping thrust (e.g., internal Rides, Moroccan Rif). (E) Stratigraphic influence. Examples include Appalachian Plateau folds (Wiltschko and Chapple, 1977) and external Rides, Moroccan Rif.

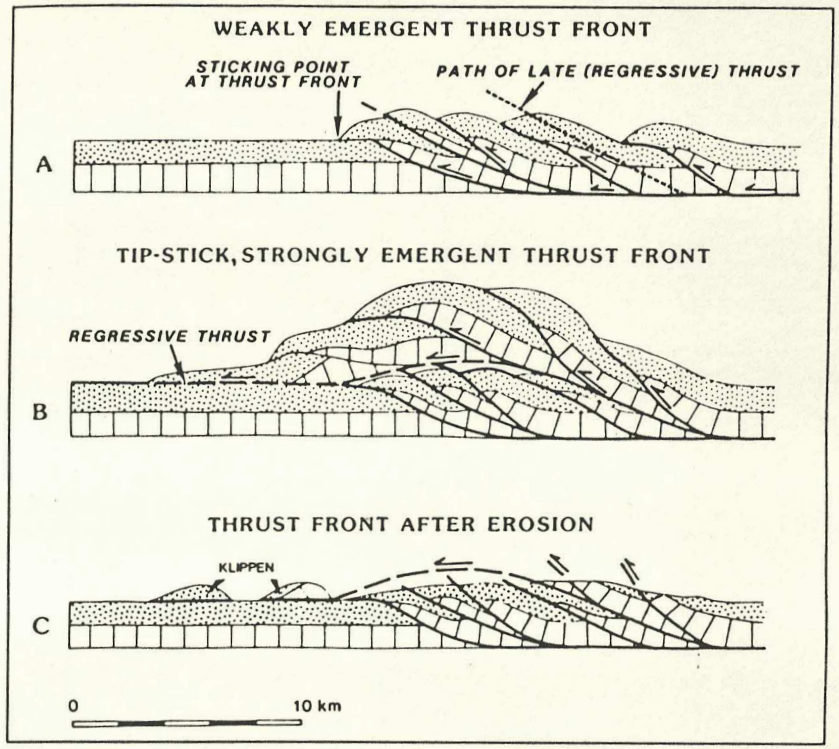

Idealized development of tip-stick thrust front. (A) Model of in-sequence thrusting, showing probable sticking point. (B) Sticking of sole thrust and development of new (out-of-sequence) thrust behind sticking point. (C) Erosion of hanging-wall sequence of regressive thrust, leaving isolated klippen on the foredeep basin.

Fig 8.100. Experimental model showing the development of backthrusts to the rear of a forward propogating thrust wedge. From Davis et al (1983). This might be a good model to account for backward directed thrusting well back from the SW Cameros Basin margin itself (eg Quintanilla - Castrovido Fault).

BACKTHRUSTING

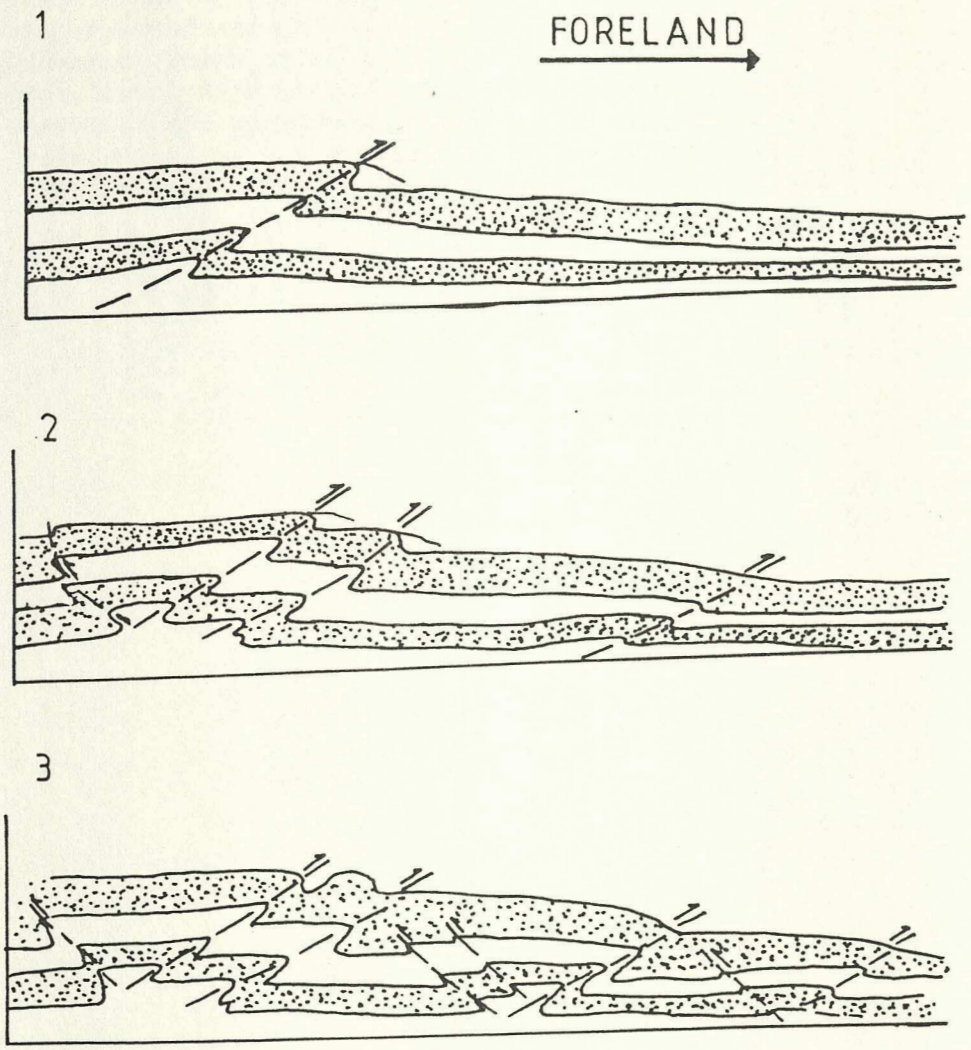

sand box models of orogenic thrust wedge under progressively increasing deformation

note: development of backthrusts towards rear of wedge.

Fig 8.101. Possible mechanisms for the development of backthrusting (Morley, 1986 - passive roof duplex; Butler, 1982; Fischer, 1984). The occurrence of backthrusts in the La Yecla area close to and behind a major lateral ramp in the San Leonardo Fault (Mamolar area) favours Butler's explanation, which suggests that the backthrusts may develop associated with thrust ramps. A more controversial view might suggest that the style and location of both lateral ramping and backthrusting is actually conditioned by the presence of pre-existing transfer structures.

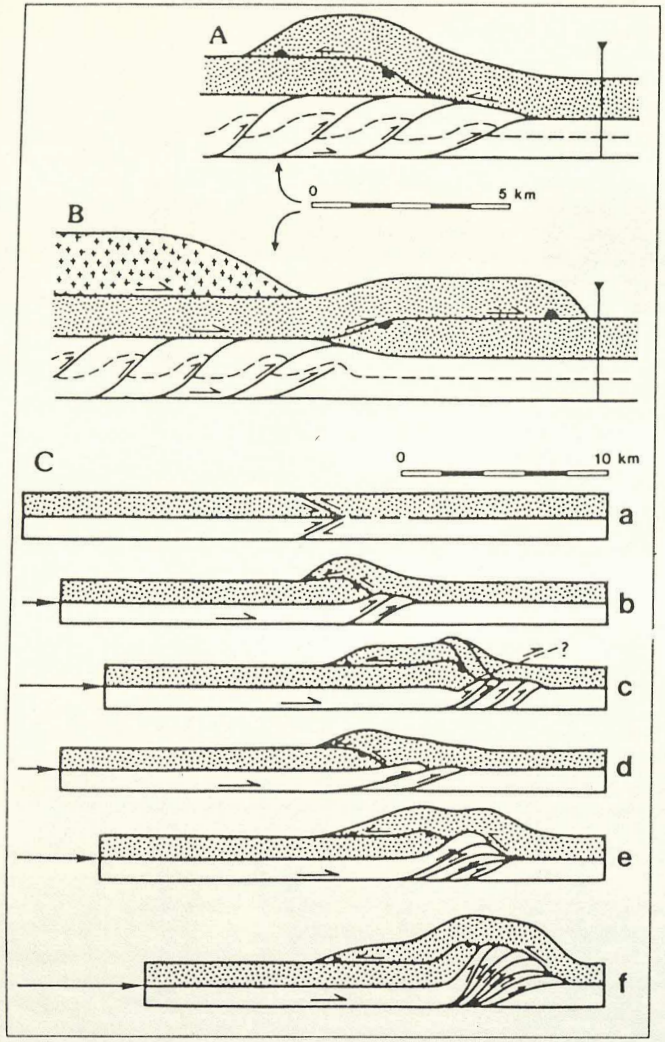

Passive roof duplex. (A) Typical geometry of passive roof duplex with a hinterland-directed roof thrust and foreland-directed floor thrust. (B) Presence of overburden (another thrust sheet) is likely to inhibit the development of a backthrust. (C) Development of passive duplex wedge. (a) Initial stage showing wedge shape before deformation. (b, c) Wedge grows as zone of imbrication. Leading edge of imbricate becomes separated farther from footwall cutoff of the roof thrust as deformation progresses, weakening the wedge shape. (d, e, f) Wedge grows as an antiformal stack, strengthening the wedge shape, but ultimately it creates an unwieldy structure that locks.

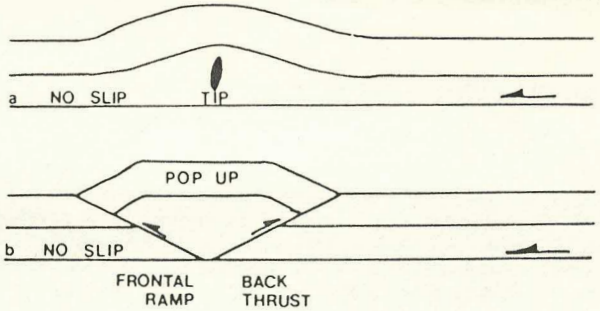

Development of a pop up. (a) Layer-parallel shortening at a tip in front of a propagating thrust. (b) The developed pop up after thrusting.

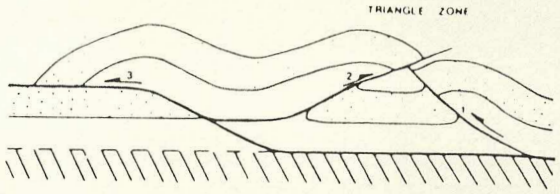

Development of a triangle zone where a pop up back thrust (2) and a forward-directed imbricate thrust (1) converge. The thrusts are numbered in order of their relative displacement and the sequence continues with the development of a frontal ramp (3) at the leading edge of the pop up.

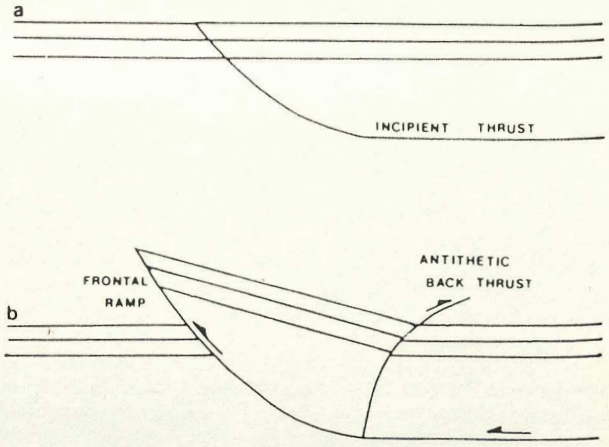

The development of an antithetic back thrust (after Mandl & Crans 1981, fig. 13). (a) Before displacement, (b) After displacement.

BACKTHRUSTING

Fig 8.102. Complex structure in Upper Cretaceous carbonates at the SW margin of the Cameros Basin, 1km S of Espejon (see figs 1.6 & 8.81). Looking SE. Synform showing vergence to right (ie SW), associated with "blind" thrusts. Additional complexities due to intersection (fig 8.94) of NE-SW, NW-SE and E-W faults (for discussion see text).

Fig 8.103. Highly-deformed marine Jurassic (?Middle Jurassic) calcilutites, SW margin of the Cameros Basin. Looking E, 1km N of Espejon. Dominant vergence to right (ie S). Local development of thrusts by failure of anticlinal noses (eg upper right centre).

Fig 8.104. Highly-deformed marine Jurassic calcilutites, locality as fig 8.103. Looking W. Structure cf large-scale "kink bands" (see Boyer, 1986 for discussion).

Fig 8.105. Structural map of the W portion of the San Leonardo Fault Zone. Note: San Leonardo Fault has been previously mapped as a simple reverse fault or thrust - our mapping has shown it to be a stack of up to five imbricate thrusts with additional detachment on Purbeck evaporites; faults cross-cutting the thrust zone (so-called "hanging wall drop faults" or "thrust-compartmental faults") are probably reactivated Mesozoic faults - analysis of the Senora de Brezales Formation sequences shows that the occurrence of basal conglomerates is controlled by these cross-faults, as indeed is the preservation of Talveila Formation sequences (eg near Pinilla de los Barruecos and in Talveila area - fig 8.26).

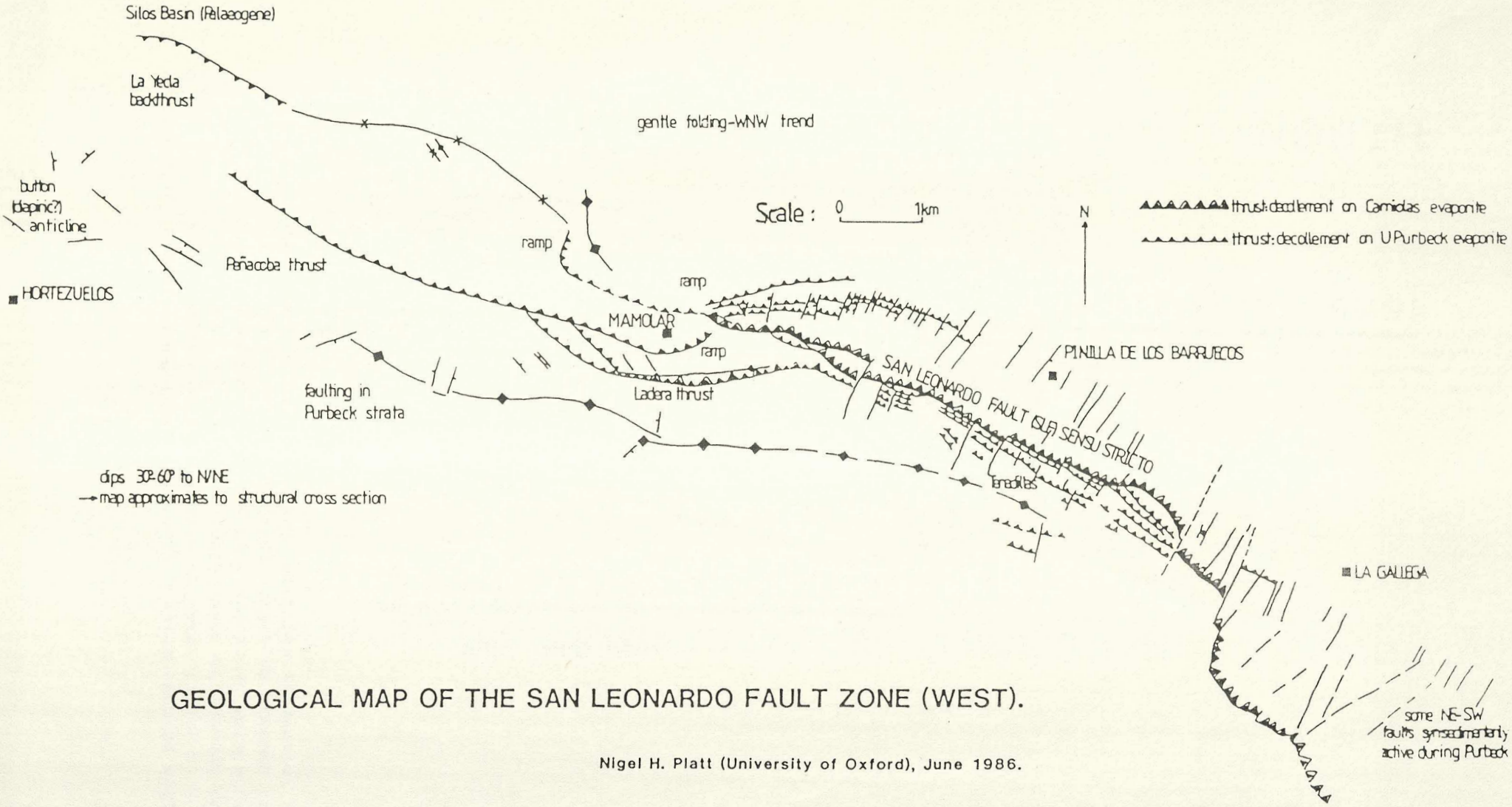

GEOLOGICAL MAP OF THE SAN LEONARDO FAULT ZONE (WEST).

Nigel H. Platt (University of Oxford), June 1986.

Fig 8.106. Diagram showing how initially shallow-dipping structures may be steepened as a result of backrotation as a consequence of the later emplacement of thrusts in a forward-propogating piggy-back sequence. This model was previously proposed by Parish (1984) to account for the occurrence of steep-dipping Hercynian structures in the Pyrenees.

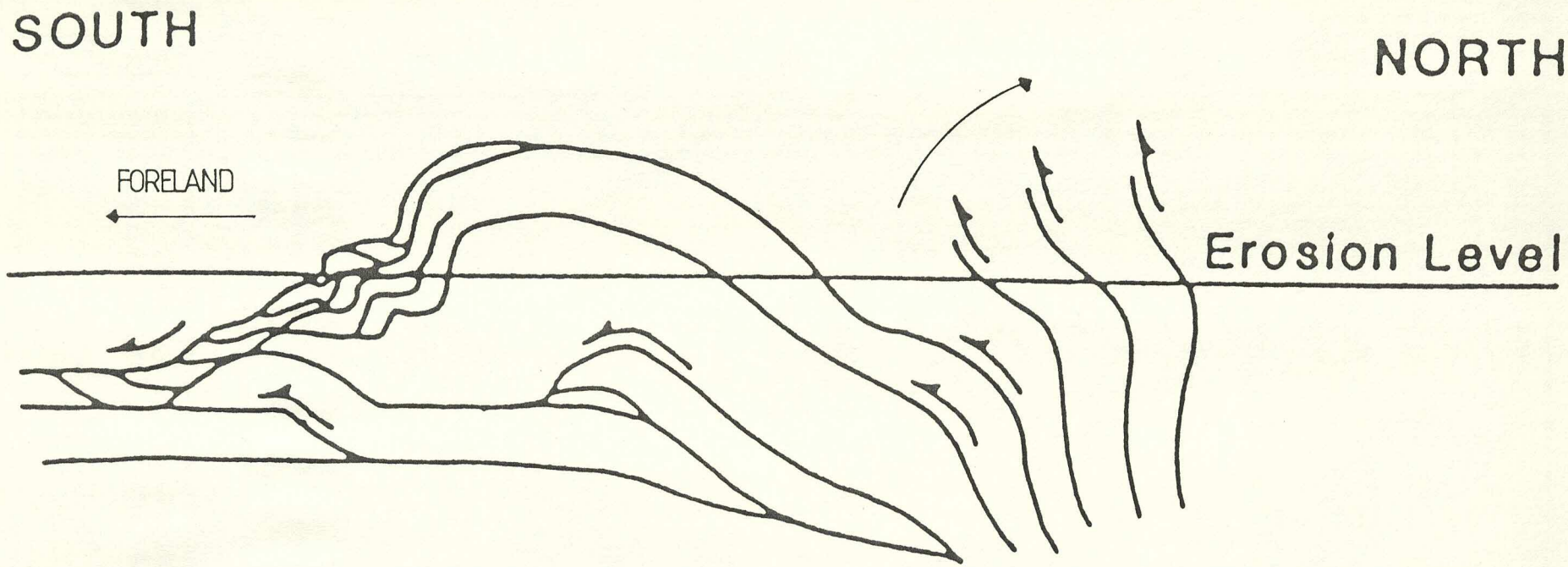

STEEPENING OF THRUSTS BY BACK-ROTATION

(after Parish 1984).

Fig 8.107. Map showing lines of major transverse structural elements in N Iberia ("transfer faults") eg Pamplona line, Toulouse line etc.. According to Hossack (1986 and pers. comm., 1986), these faults bound segments of the N Spanish margin with opposed directions of structural vergence. They may well have been transfer structures delimiting zones with opposed extensional asymmetries during the Mesozoic.

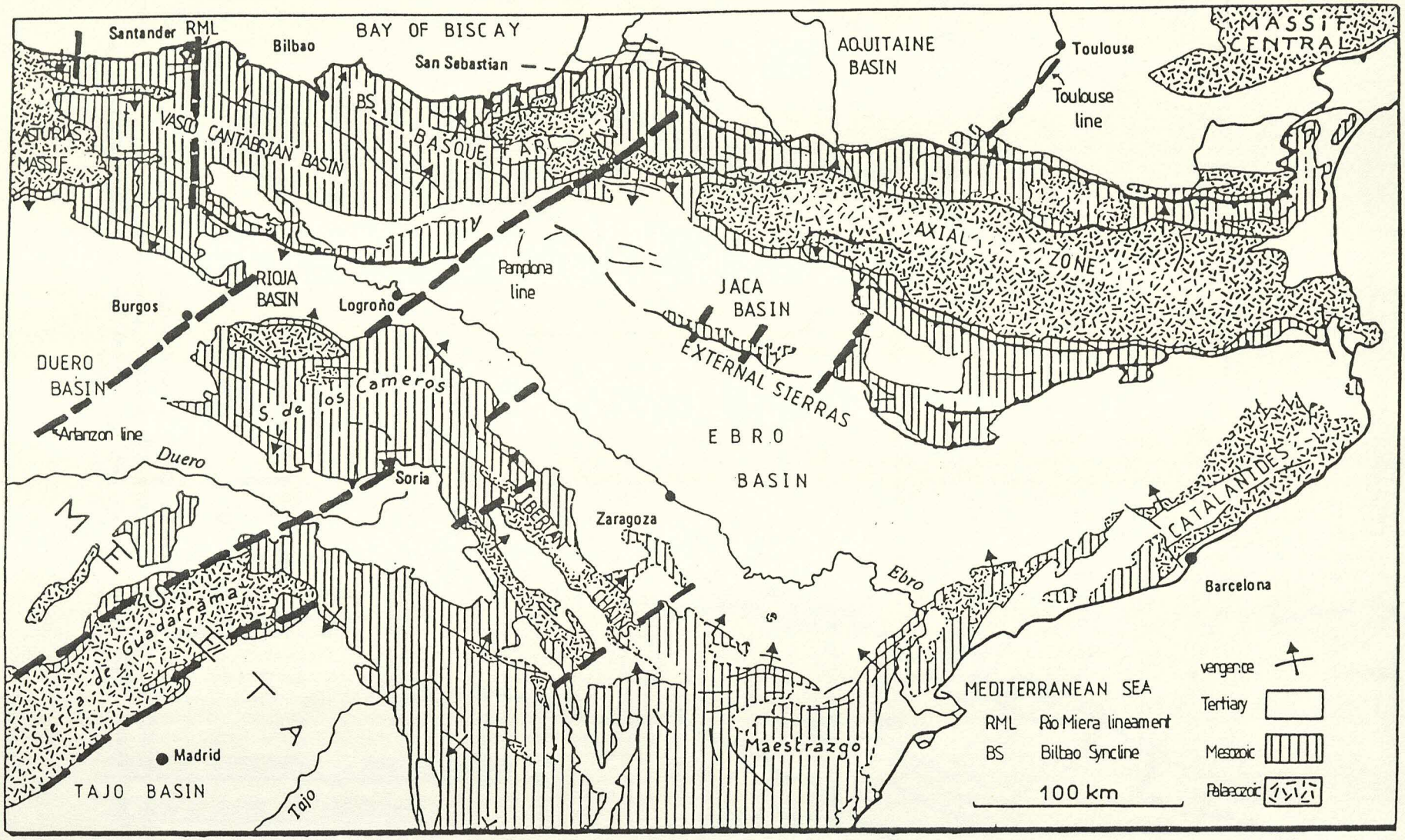

NORTHERN SPAIN—— GEOLOGICAL MAP SHOWING VERGENCE AND TRANSVERSE STRUCTURAL ELEMENTS

modified after Rat (1983)

Fig 8.108. Interpretative sketch map of the W Cameros Basin showing the proposed control of transfer faults on the location of backthrusting and lateral ramping.

TRANSFER STRUCTURES — POSSIBLE CONTROL ON LOCATION OF RAMPS AND BACKTHRUSTS.

Fig 8.109. Laubscher's (1972) map of the Jura Mountains showing the presence of cross-cutting transfer structures which pre-dated the onset of compression (they date from the initiation of the Rhine-Bresse Graben system) but which affect the style of deformation.

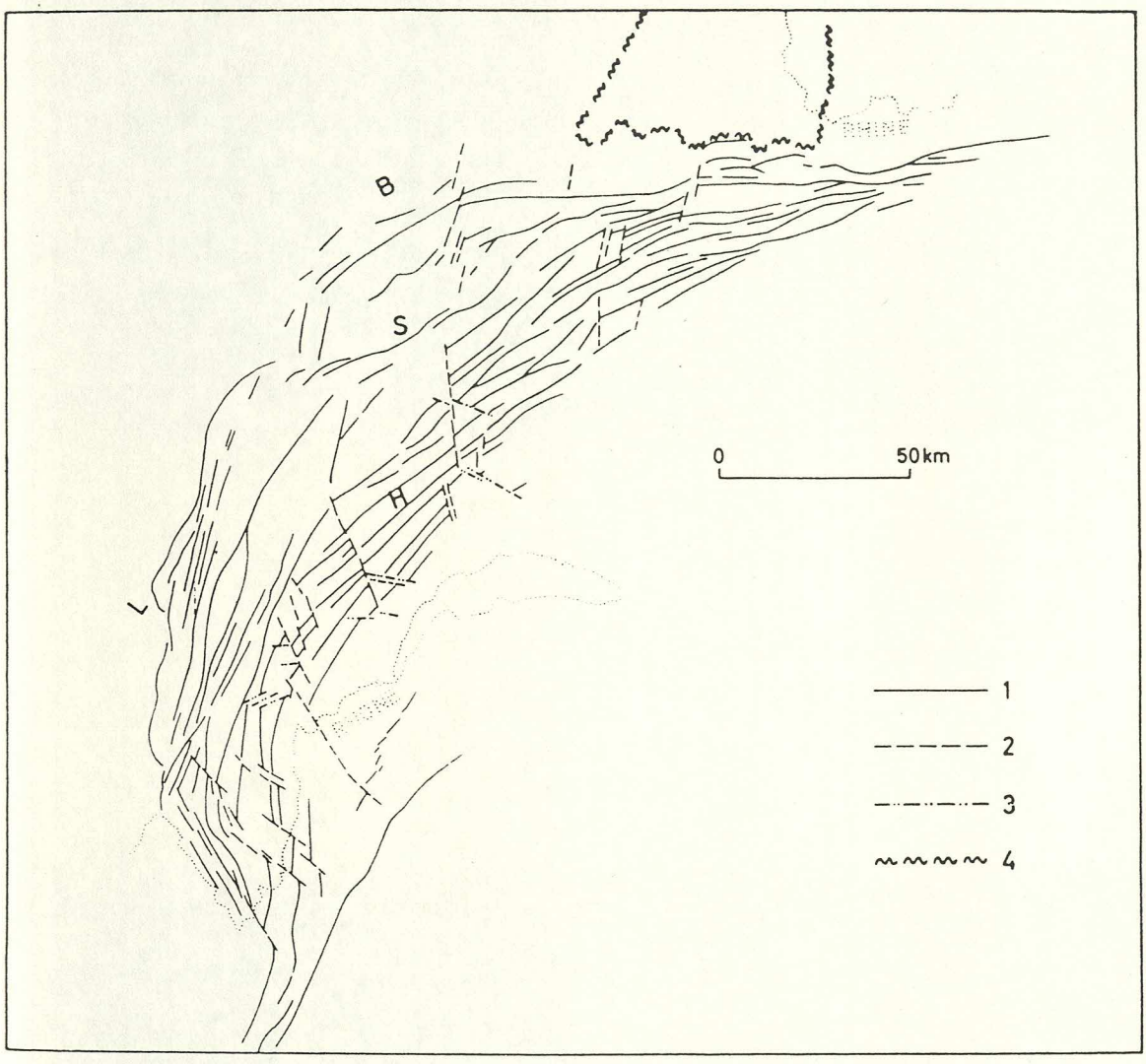

Simplified tectonic map of the Jura. Fold bundles ("faisceaux"): L = Ledonian, B = Bisontine, S = Salins, H = Helvetic. 1 = fold axes, 2 = sinistral wrench faults and inherited normal faults of the Rhine graben system (eastern Jura), 3 = dextral wrench faults, 4 = boundary of the main part of the Rhine graben.

Fig 8.110. Complex structure above thrust tip. Anticline-syncline pair developed in Upper Cretaceous limestones interpreted by Vaughan (1986) as accommodation structure over lateral tip. Looking W. Penacoba. Compare with figs 8.112 & 8.113 which show figures taken from and adapted from Coward & Potts (1983), showing similar structure at thrust tip in Moine Thrust Zone, NW Scotland.

Fig 8.111. Complex structure in Rupelo Formation limestones associated with lateral thrust ramp. Mamolar. Looking E.

Fig 8.112. Interpretation of figs 8.110 & 8.111 (slightly modified from Vaughan, 1986). Proposed mechanism for the development of complex structures at thrust tips involves formation of anticline - syncline pair, these being developed as accommodation structures over lateral ramp.

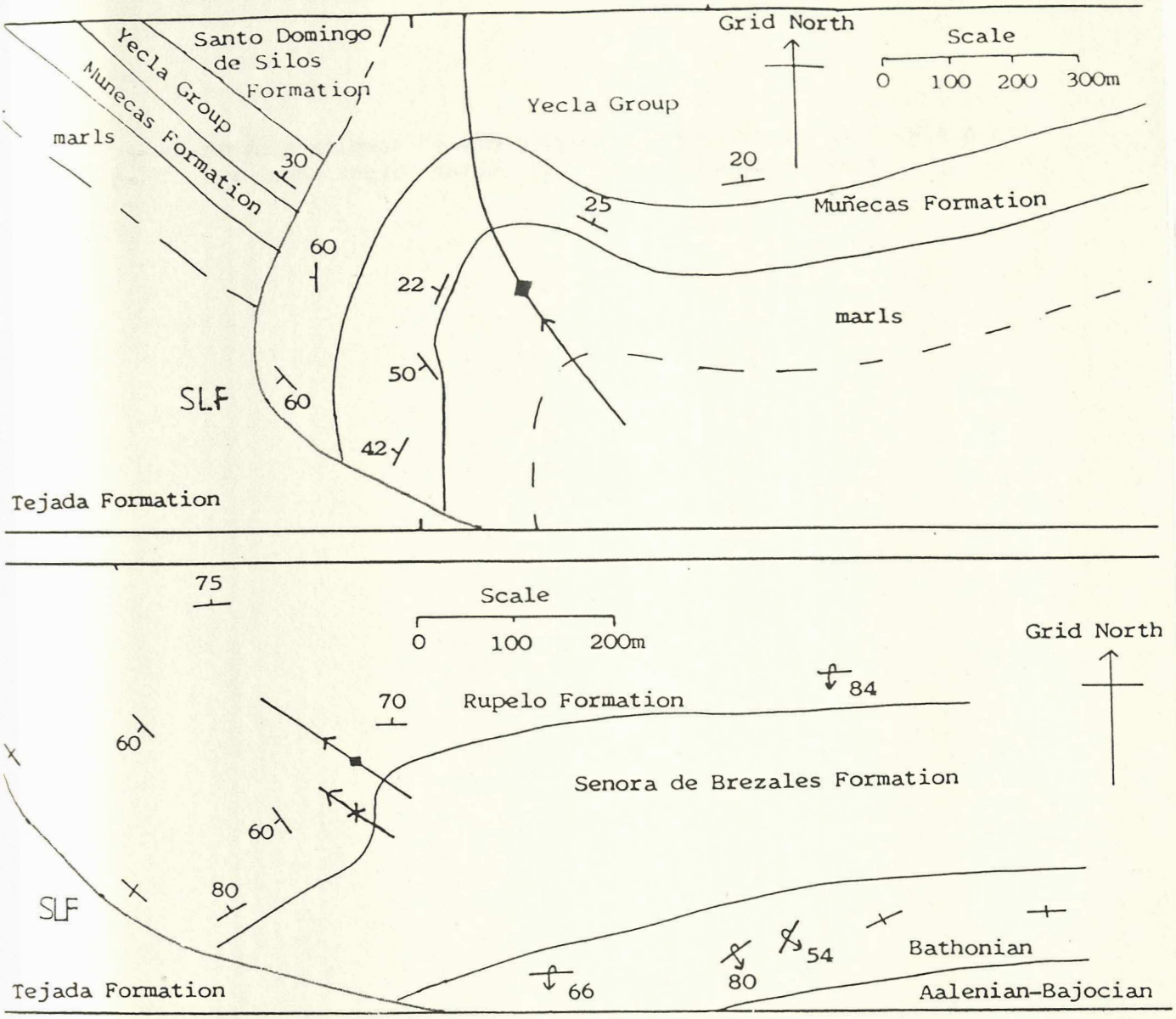

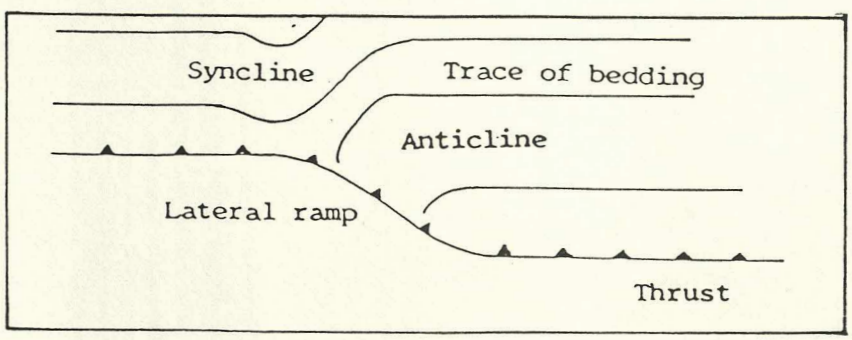

CROSS-SECTION

COMPLEX STRUCTURE AT THRUST TIPS AND RAMPS (after Vaughan 1986).

This interpretation is after Coward and Potts (1983) and Coward (1984) who describe similar structures from the Moine Thrust zone of NW Scotland. The folding is due to compression of the beds above the ramp as the ramp changes its geometry along the direction of transport.

Fig 8.113. Diagram showing the development of complex structures associated with thrust tip, Moine Thrust Zone, NW Scotland.

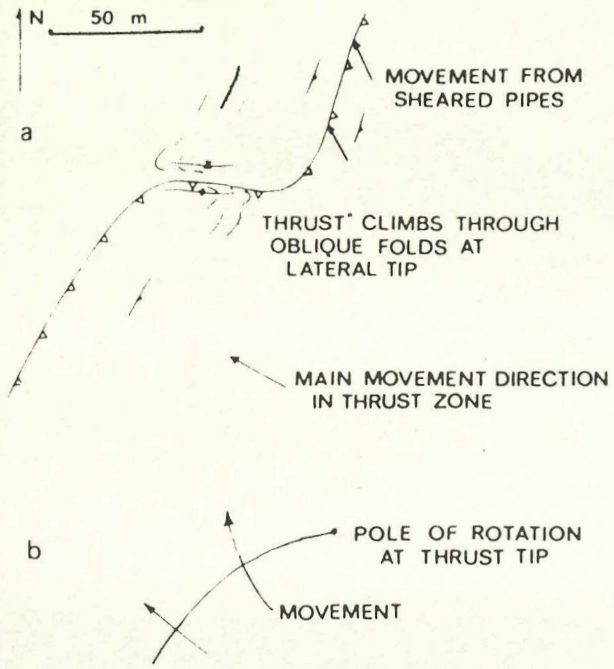

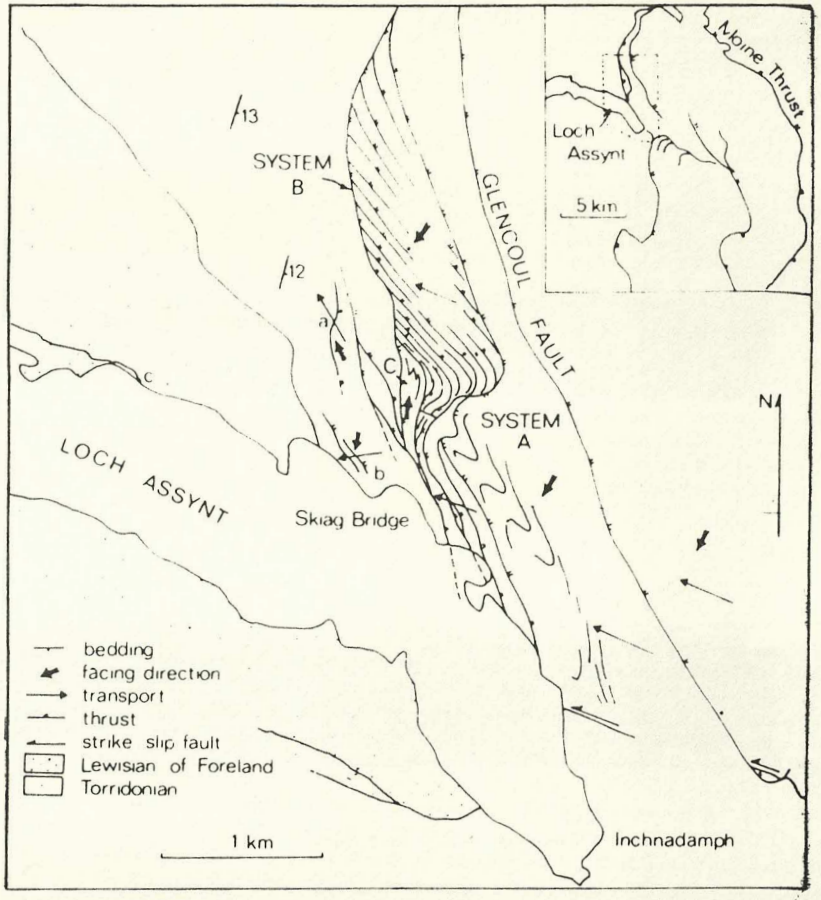

General map of NW Assynt, showing imbricate systems and locations referred to in the text. The facing direction relates to the oblique folds and thrusts.

Figs 8.114 & 8.115. Diagrams showing calculation of shortening across San Leonardo Fault Zone using balanced cross-sections (for unbalanced sections see enclosures). Although the reservations about layer-cake or template stratigraphy make the area-balancing method (Hossack, 1979) somewhat inappropriate, a line balance technique on an easily-recognisable marker horizon post-dating the major extension (eg base of Utrillas) still provides a useful first approximation to the magnitude of shortening. Note, however, reservations expressed in the text (see also fig 8.81) about the applicability of the thin-skinned model of thrust tectonics to a fractured and heavily extended terrane.

710393

727440

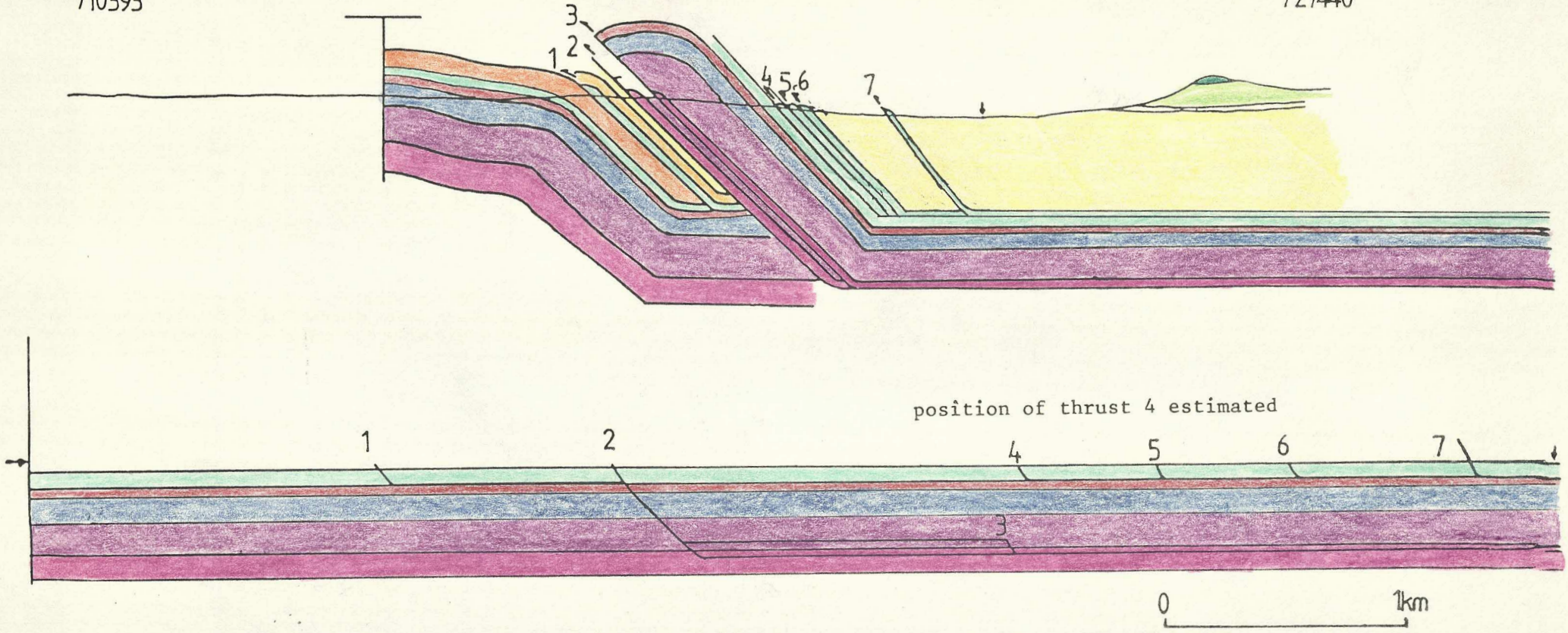

San Leonardo Fault Zone (West).
Construction of balanced cross-sections (line balance technique - assumptions as in Hossack, 1979).

Section length - 2.5km
Restored section length - 6.2km

Estimated minimum shortening - 3.7km

Figs 8.114 & 8.115. Diagrams showing calculation of shortening across San Leonardo Fault Zone using balanced cross-sections (for unbalanced sections see enclosures). Although the reservations about layer-cake or template stratigraphy make the area-balancing method (Hossack, 1979) somewhat inappropriate, a line balance technique on an easily-recognisable marker horizon post-dating the major extension (eg base of Utrillas) still provides a useful first approximation to the magnitude of shortening. Note, however, reservations expressed in the text (see also fig 8.81) about the applicability of the thin-skinned model of thrust tectonics to a fractured and heavily extended terrane.

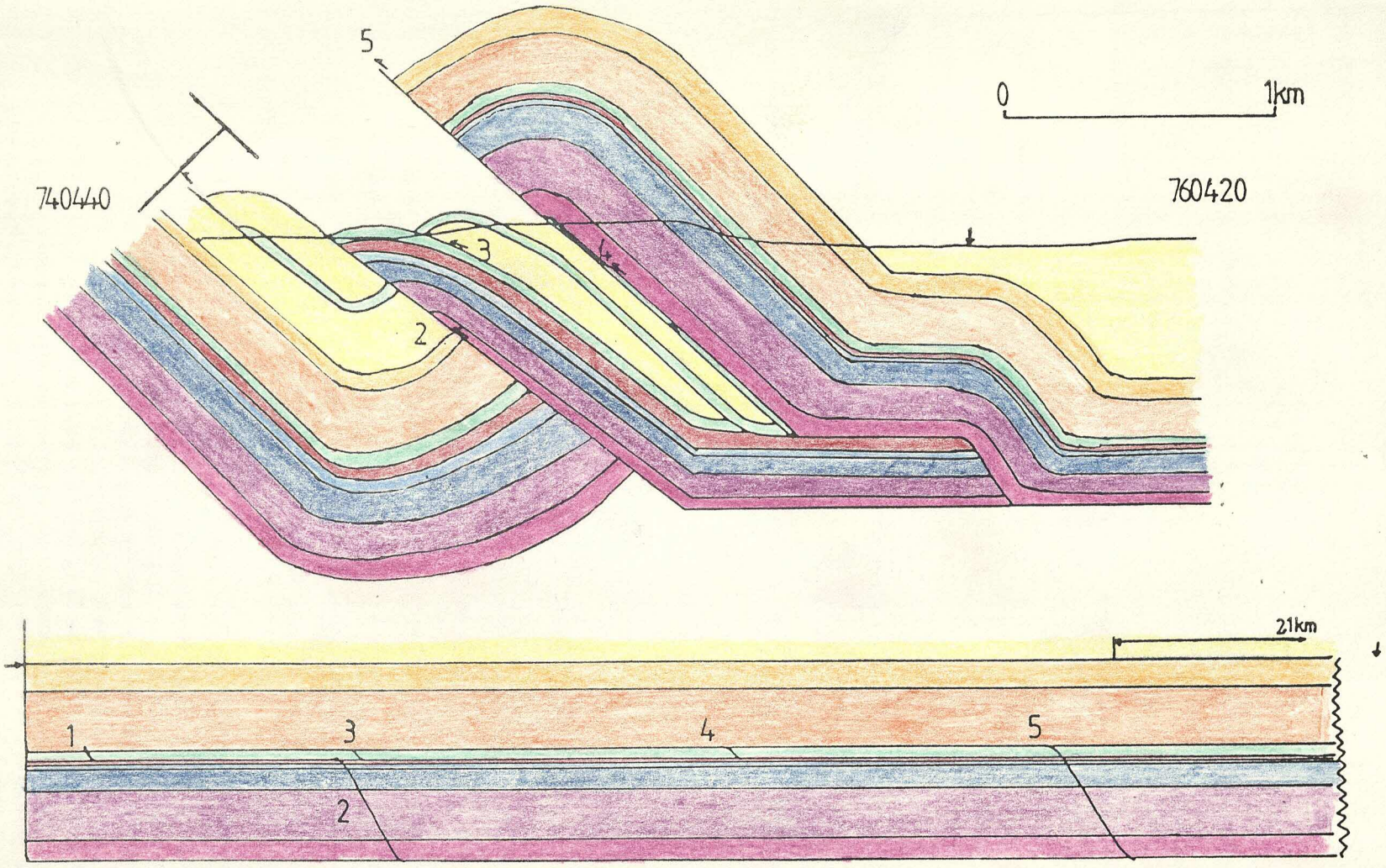

San Leonardo Fault Zone (West).
Construction of balanced cross-sections (line balance technique - assumptions as in Hossack, 1979).

Section length - 2.76km
Restored section length - 6.23km Estimated minimum shortening - 3.5km

Fig 8.116. Chadwick's (1985) method for the calculation of shortening using the principle of isostasy:
1) as applied to the Wessex Basin by Chadwick;
2) as applied to the W Cameros Basin.
Note that shortening in the W Cameros is an order of magnitude greater than for S England, indicating the greater intensity of inversion tectonics in N Spain.

SOUTHERN ENGLAND.

	Absolute uplift	≈0m
	Time since onset of compression	32 MY
H	Sea level change since onset of compression (eustatic)	−40m
E	Thickness of eroded strata (average, estimated)	340m
U	Uplift calculated from consideration of isostacy 96m	$\beta \approx 0.97$
	Wessex Basin: width	70km
	: shortening 0.03 x 70	2km

NORTHERN SPAIN.

	Time since onset of compression	32 MY
H	Sea level change since onset of compression (eustatic)	−40m
	Absolute uplift since onset of compression	950m
E	Thickness of eroded strata (average, estimated for Cameros)	1375m
U	Uplift calculated from consideration of isostacy 510m	
	Total calculated theoretical uplift	950+510 = 1460m
		$\beta \approx 0.75 - 0.80$
	W. Cameros Basin: width	35km
	: shortening	7 - 8.8km

Equation used for calculation of additional uplift from thickness of eroded strata:

$$U = E - \frac{(\rho_1 - \rho_2)}{\rho_2} - H$$

$\rho_1 = 3.3 g\ cm^{-3}$ – subcrustal density

$\rho_2 = 2.0 g\ cm^{-3}$ – sediment density

ESTIMATE OF SHORTENING:

ISOSTACY

(method of Chadwick, 1985)

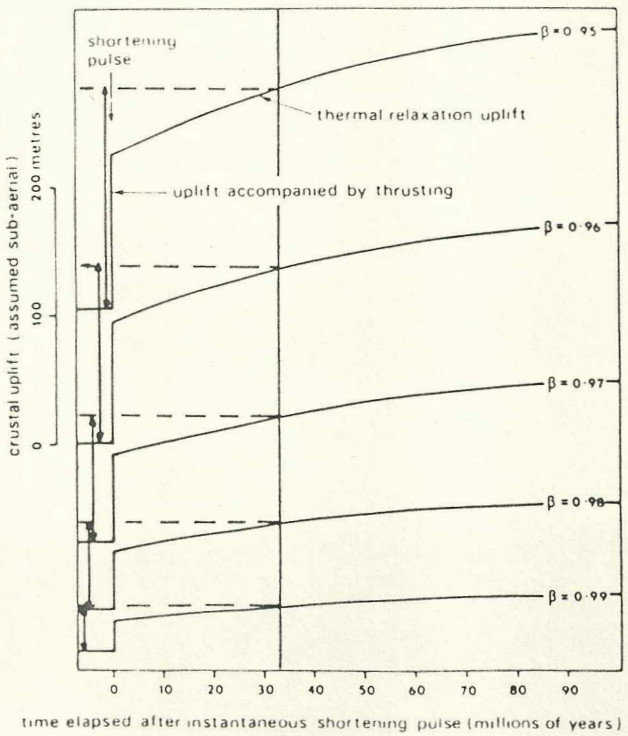

Predicted uplift curves of sub-aerial crust for various amounts of lithospheric shortening.

Fig 8.117. Interpretative sketch based upon the ideas of Hossack (pers. comm., 1986) showing model for thrusting in Central Interior N Spain, using the Sierra de la Demanda as an example, with thrusting utilising detachment both in the Keuper - Carniolas and in the Hercynian basement (eg on San Anton dolomite, see fig 2.2). Note that thrusting in the W Cameros must involve basement - as witnessed by involvement of Palaeozoic strata in the Moncalvillo anticline (see fig 1.6).

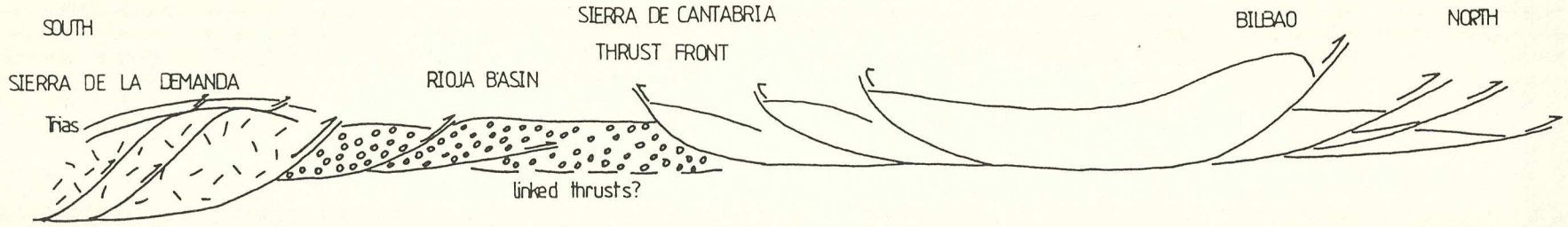

SCHEMATIC CROSS SECTION ACROSS THE RIOJA BASIN

(after Hossack, pers. comm., 1986)

Fig 8.118. Interpretative sketches showing the possible rôle of thrust "roll-back" as a mechanism for subsidence in extensional régimes: examples given for the Devonian basins of the Norwegian Caledonides (Hossack, 1984).

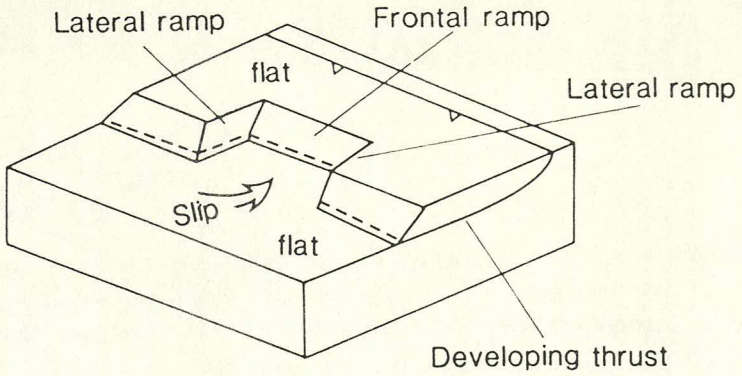

Thrust with the hanging-wall removed to show the foot-wall of the thrust with two opposed lateral ramps connected by faults and a frontal ramp. A younger thrust developing by branching off the foot-wall ramp produced a trailing edge branch-line in the ramp which is pecked.

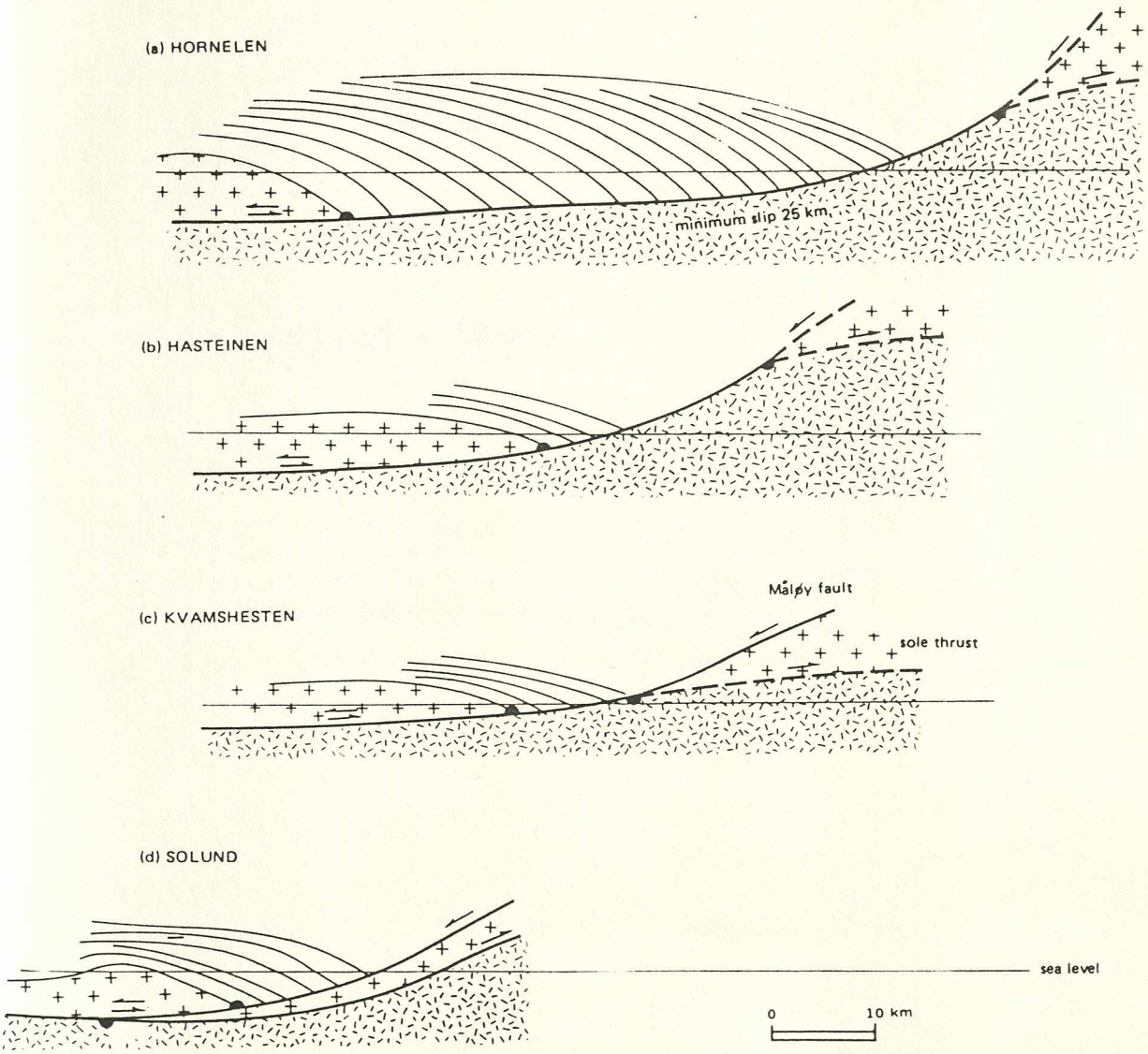

Longitudinal sections a–d, respectively, through the Devonian basins. The branch-line point of intersection between the sole thrust and the Måløy fault has been fixed in each section using the projection of the branch-line of Fig. 4 with each section. The minimum offset of 25 km on the fault beneath the Hornelen basin (A, Fig. 4) is suggested by the thickness of the onlapping Devonian sediments but the offset suggested by the metamorphic rocks in the hanging- and foot-walls is over 40 km.

Figs 8.119 - 8.121. Diagrams from Chadwick (1985) showing: the development of extensional systems from normal fault reactivation of thrusts; as applied to the Wessex Basin.

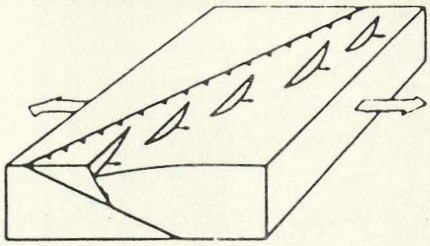

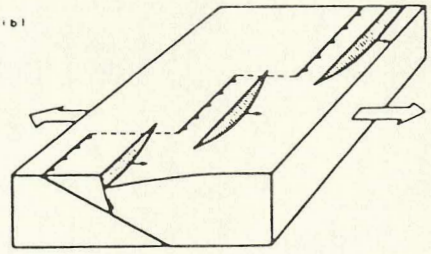

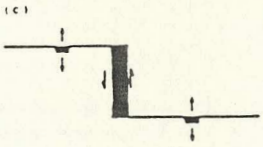

(*a*) Offset normal faults lying above a thrust which is oblique to the direction of extension; (*b*) offset normal faults lying above an offset thrust; (*c*) sinistral ground movement across a dextrally offsetting transfer zone.

Chadwick (1985)

transfer faults

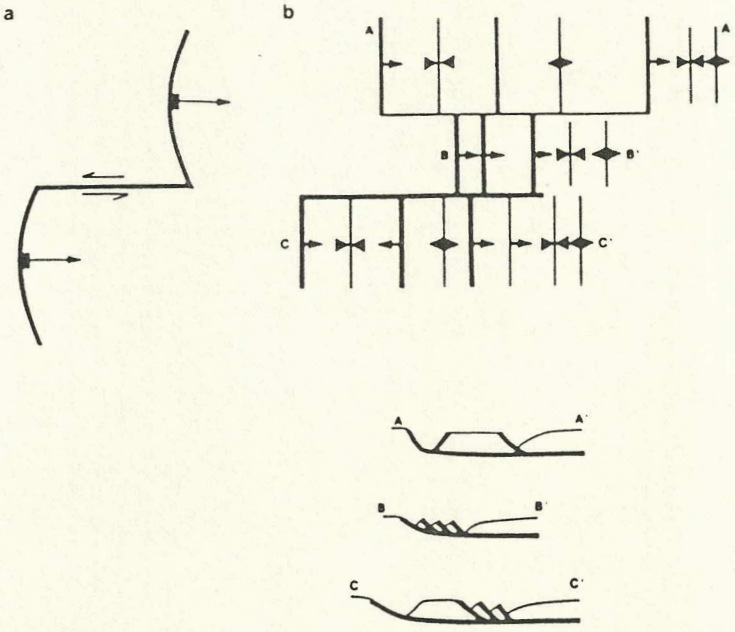

(*a*) Plan of a simple transfer fault connecting two normal listric faults. (*b*) Plan of two transfer faults separating three zones of different deformation style, sections A–A′, B–B′ and C–C′.

Gibbs (1984)

Figs 8.119 - 8.121. Diagrams from Chadwick (1985) showing: the development of extensional systems from normal fault reactivation of thrusts; as applied to the Wessex Basin.

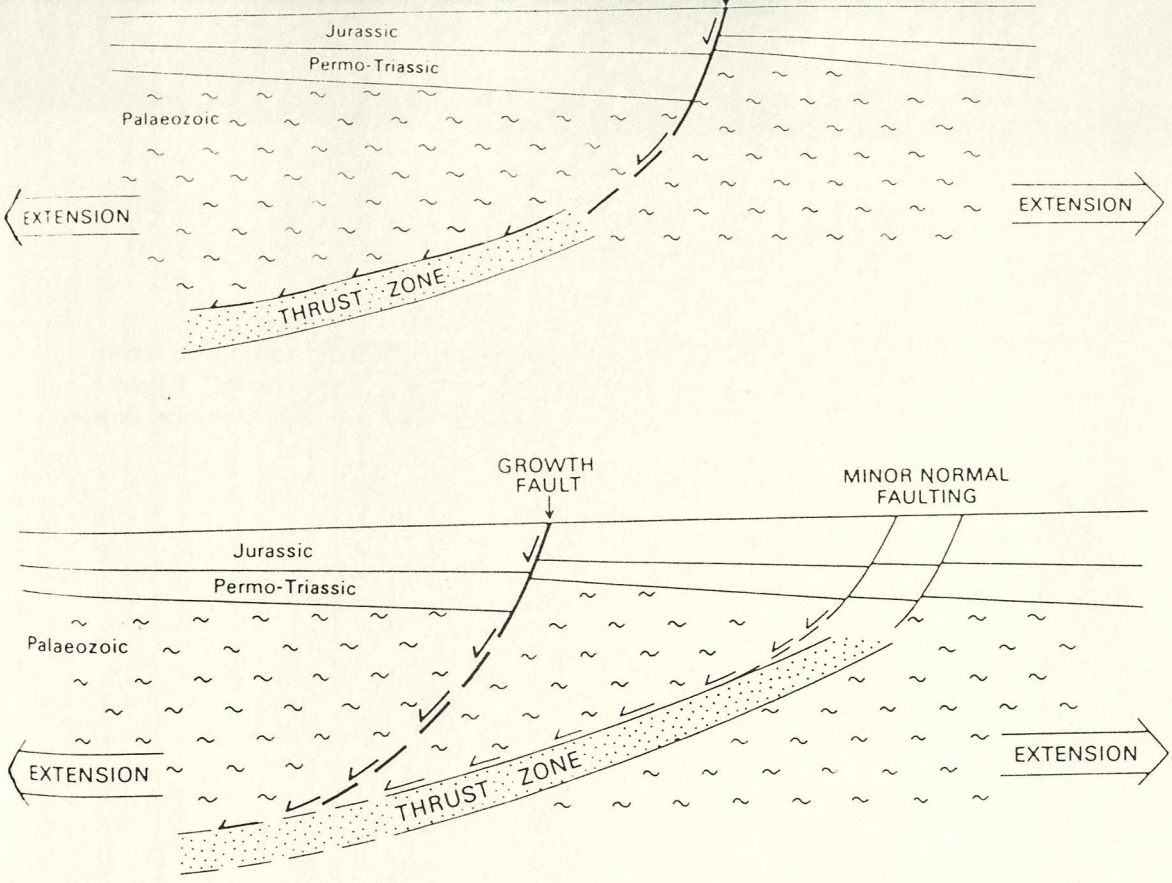

(a) Reactivation and reversal of a listric Variscan thrust zone to explain Mesozoic growth on the Mere Fault; (b) Reactivation and reversal of a listric Variscan thrust zone to explain Mesozoic growth on the Vale of Pewsey Fault.

Roll-back of Hercynian thrusts → Mesozoic listric extensional faults.

WESSEX BASIN

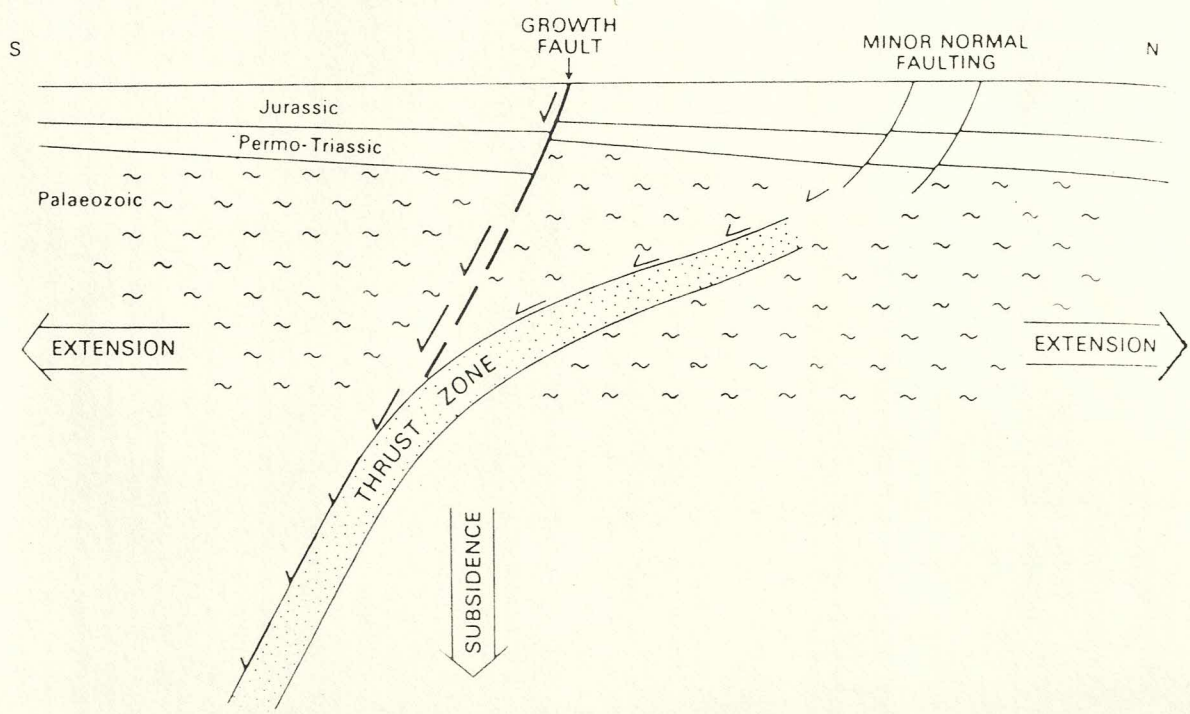

(c) Reactivation and reversal of a Variscan thrust zone steepening with depth, to explain Mesozoic growth on the Vale of Pewsey Fault.

Roll-back of steeper faults → basement involvement.

Figs 8.119 - 8.121. Diagrams from Chadwick (1985) showing: the development of extensional systems from normal fault reactivation of thrusts; as applied to the Wessex Basin.

SOUTHERN ENGLAND: CONTROL OF BASEMENT STRUCTURE ON BASIN DEVELOPMENT.

cf CAMEROS ?

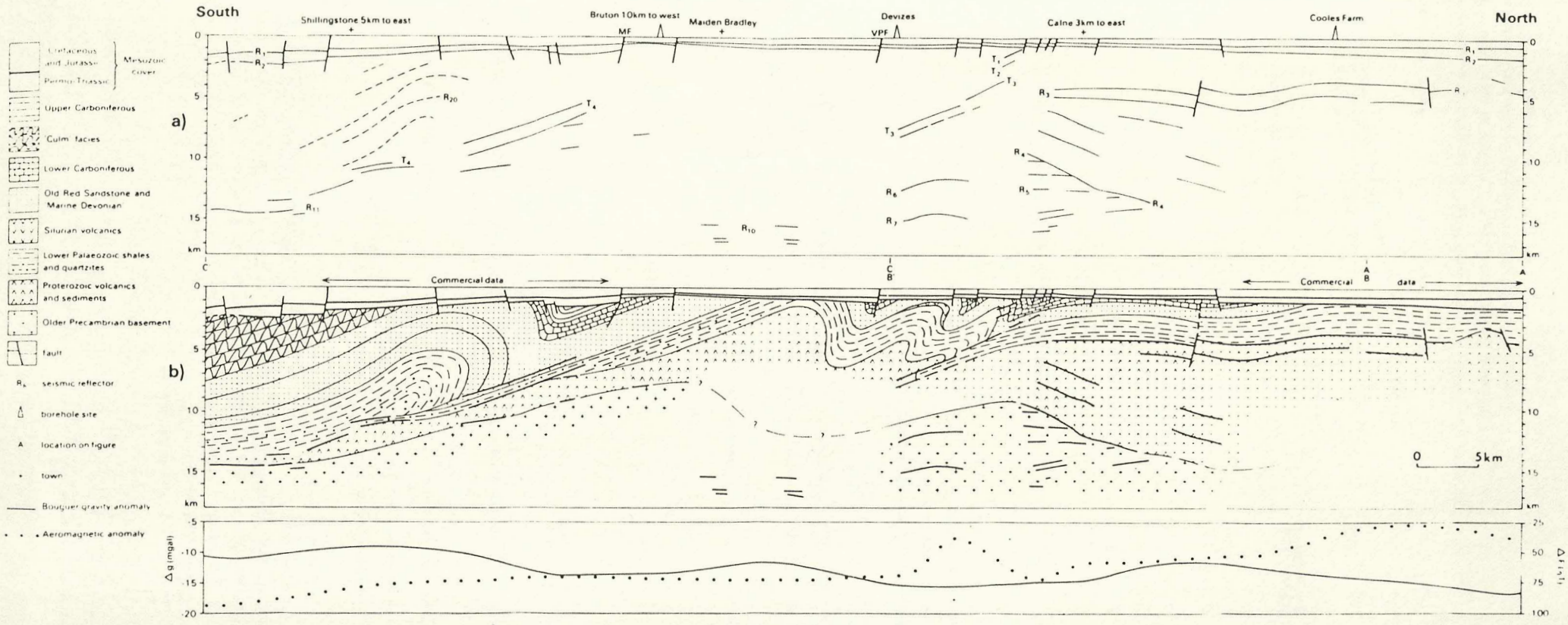

N–S depth sections showing (a) principal reflectors identified from seismic reflection sections and (b) geological interpretation of reflection events with Bouguer gravity and aeromagnetic anomalies.

Figs 8.122 - 8.124. Diagrams from Chadwick (1985) showing the subsequent inversion on compression by inverse reactivation of the normal faults; the rôle of transfer structures; as applied to the Wessex Basin.

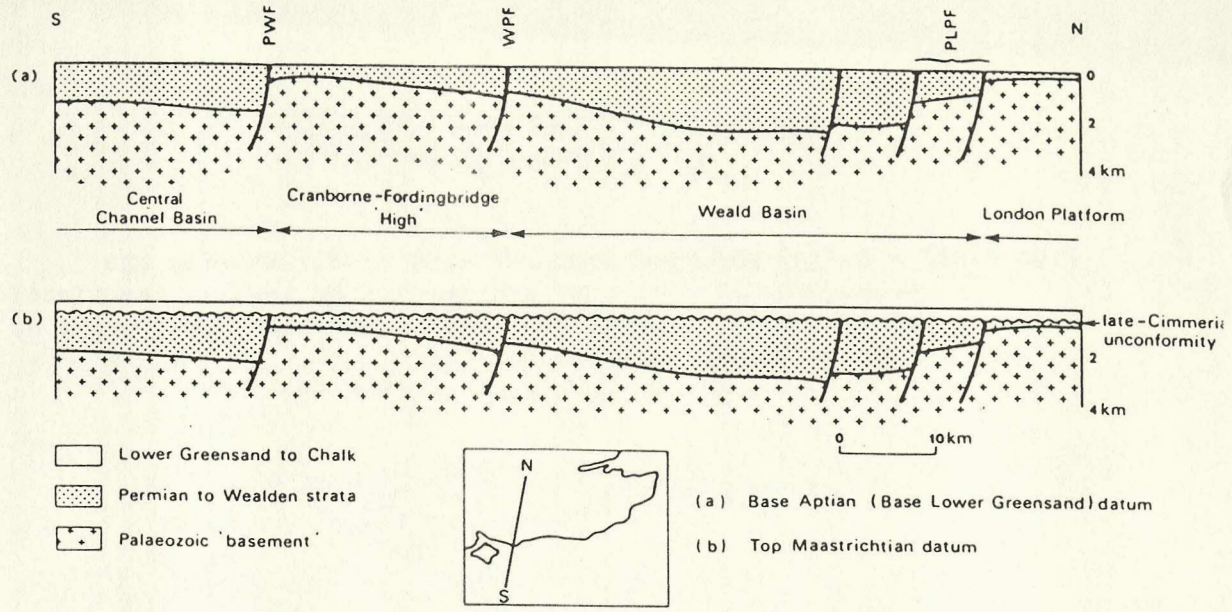

Simplified cross-sections across southern England: (*a*) restored to base Lower Greensand/Gault datum; (*b*) restored to top Chalk datum.

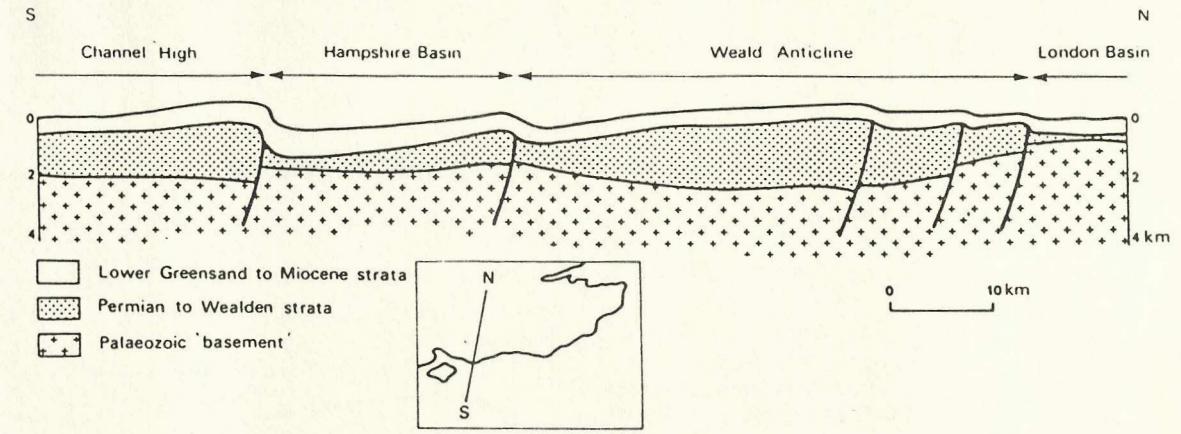

Simplified cross-section across southern England, post-inversion.

Wessex Basin

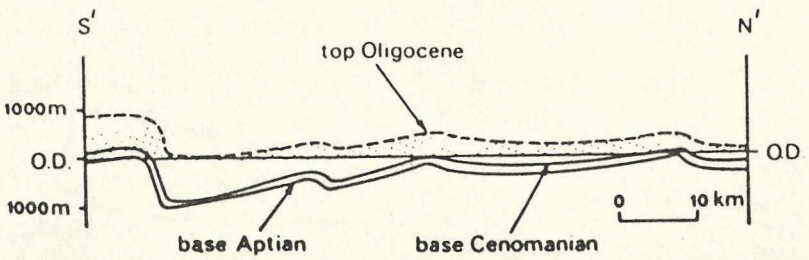

Chadwick (1985)

Section S'–N' through the post-Aptian sediments of the Wessex Basin, showing the effects of Cenozoic folding. Stippled area denotes strata (mostly removed by erosion) elevated above sea-level by inversion.

Figs 8.122 - 8.124. Diagrams from Chadwick (1985) showing the subsequent inversion on compression by inverse reactivation of the normal faults; the rôle of transfer structures; as applied to the Wessex Basin.

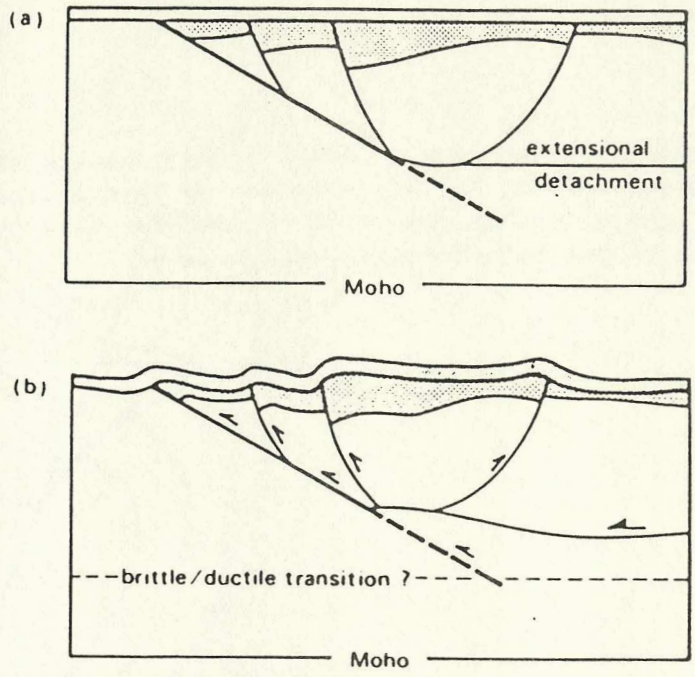

The effect of horizontal shortening on a two-layer crustal section: (*a*) before shortening; (*b*) after shortening.

basin inversion

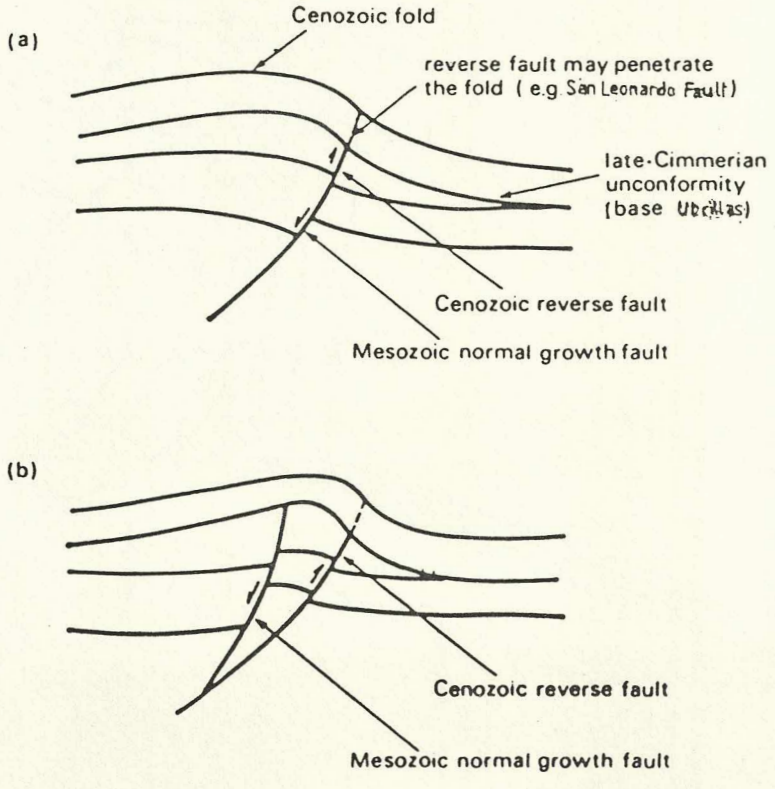

Schematic sections to show modes of Cenozoic inversion of Mesozoic structures.

after Chadwick (1985)

Figs 8.122 - 8.124. Diagrams from Chadwick (1985) showing the subsequent inversion on compression by inverse reactivation of the normal faults; the rôle of transfer structures; as applied to the Wessex Basin.

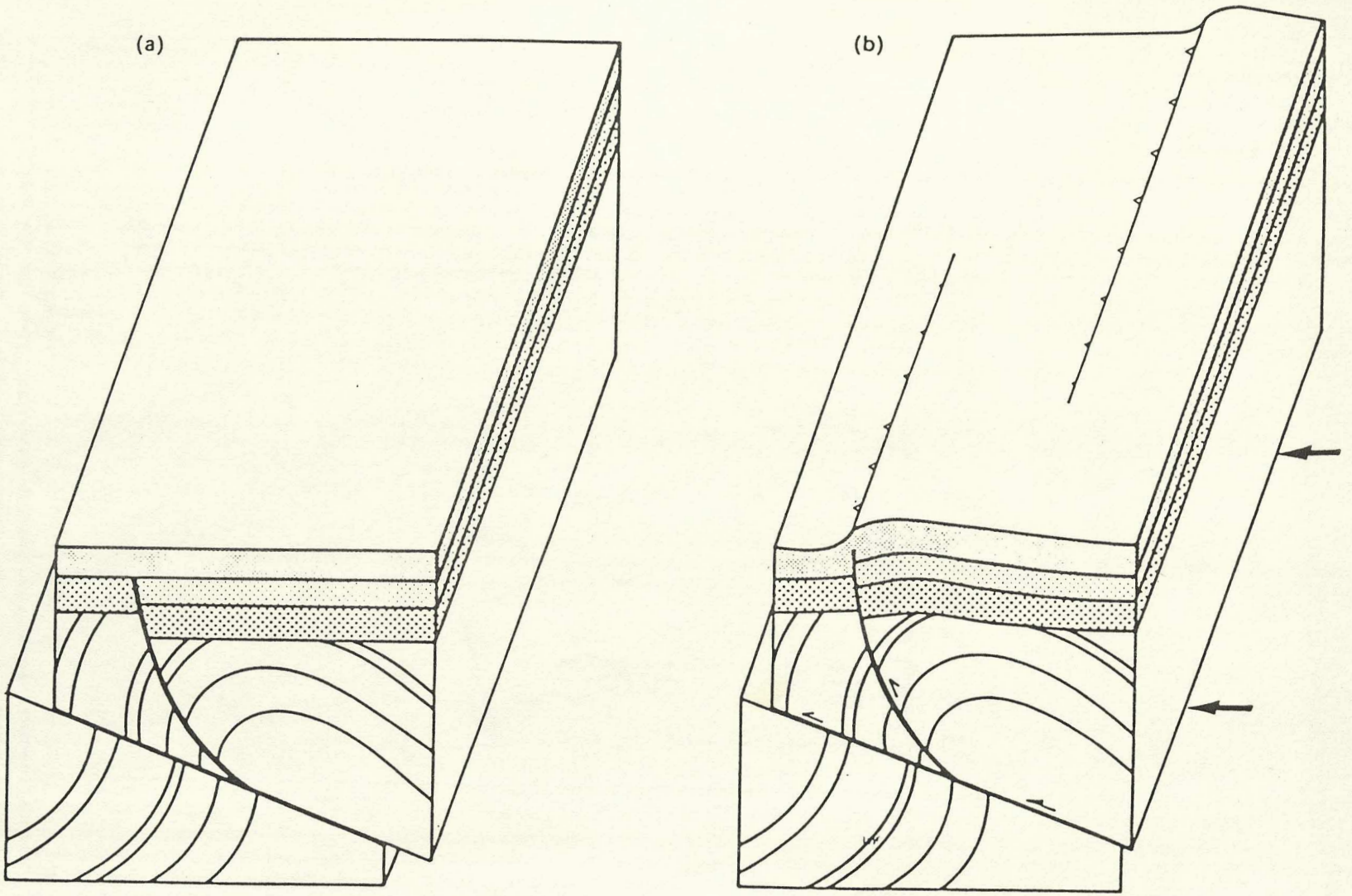

Schematic block diagram of normal faults offset by a transfer zone reactivated in a reverse sense and forming folds in the overlying strata: (*a*) before compression; (*b*) after compression.

Chadwick (1985)

Figs 8.125 & 8.126. Map and cross-sections of parts of the Wessex Basin showing the local development of thrust splays as a result of contractional reactivation of normal faults. After Stonely (1982).

offset monoclines in Weald (NNE transfer faults)

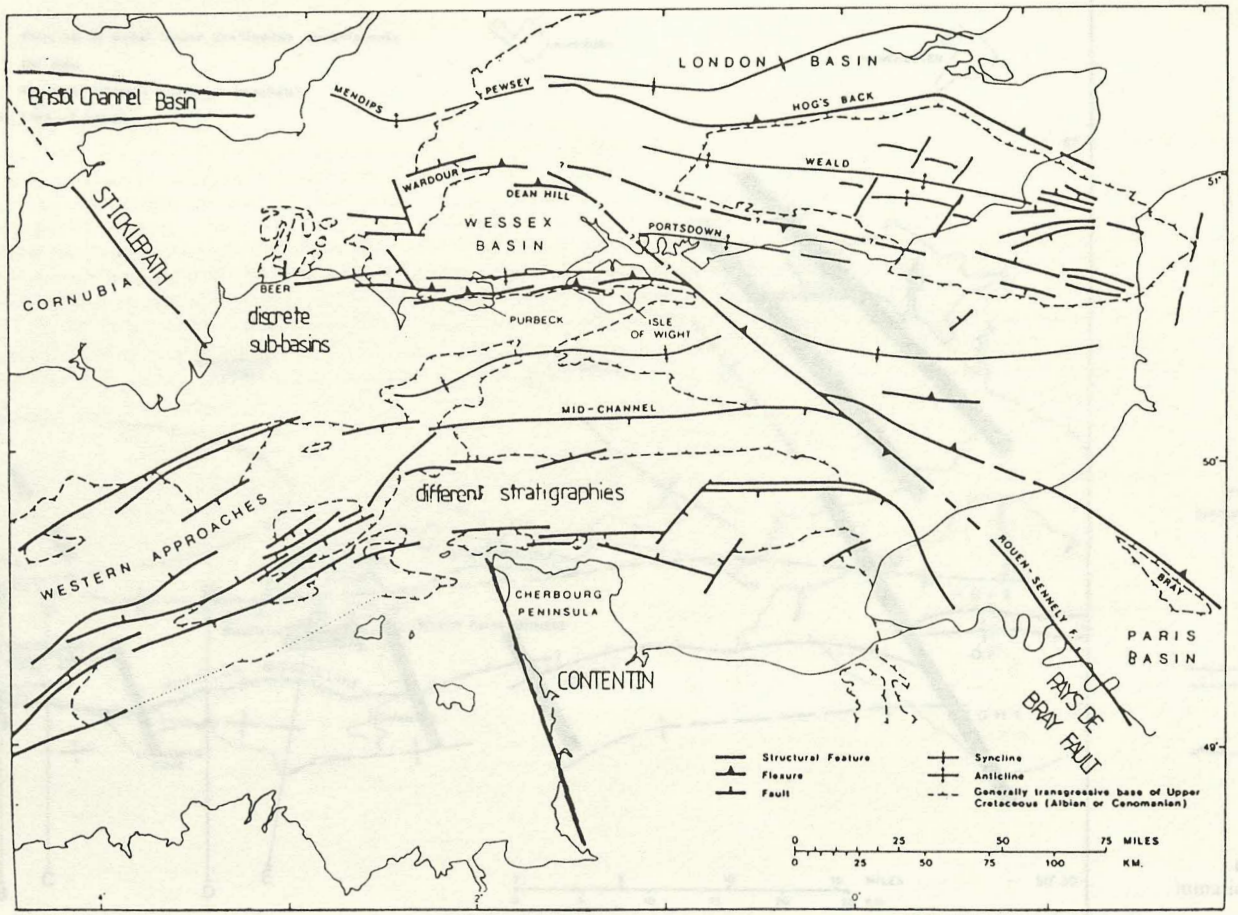

Mesozoic-Tertiary structural features of the Wessex Basin and neighbouring areas

change in orientation due to swinging round of Hercynian thrust direction from NW to NE

E-W faults: reactivated Hercynian thrusts
NW-SE faults: Mesozoic transfers reactivated Oligocene
→mosaic of sub basins

WESSEX BASIN – OFFSET MONOCLINES offsets interpreted as along NW trending "transfer" structures parallel to Pays de Bray Fault

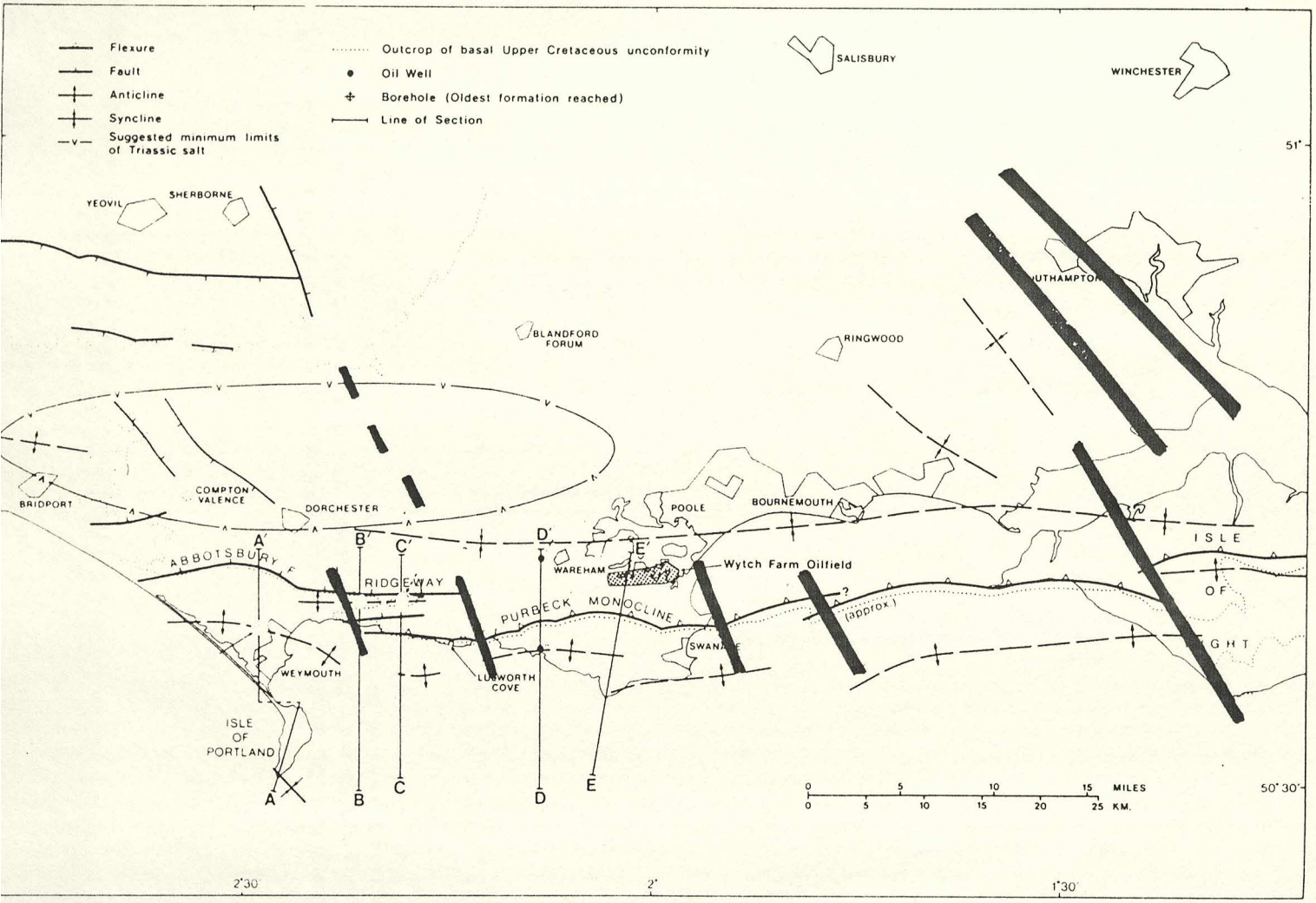

The South Dorset–Isle of Wight belt of structural disturbance.

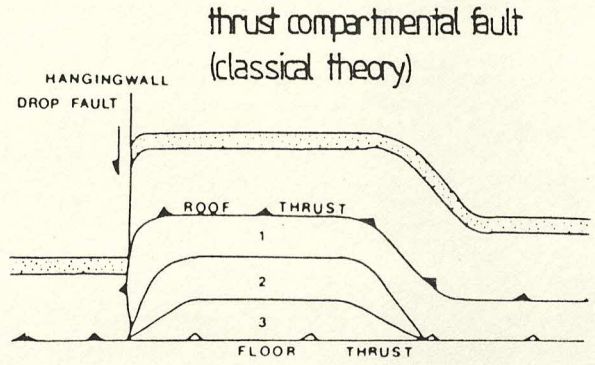

Location of a hangingwall drop fault in a vertical lateral c
mination wall. The thrust transport direction is out of the page.

Figs 8.125 & 8.126. Map and cross-sections of parts of the Wessex Basin showing the local development of thrust splays as a result of contractional reactivation of normal faults. After Stonely (1982).

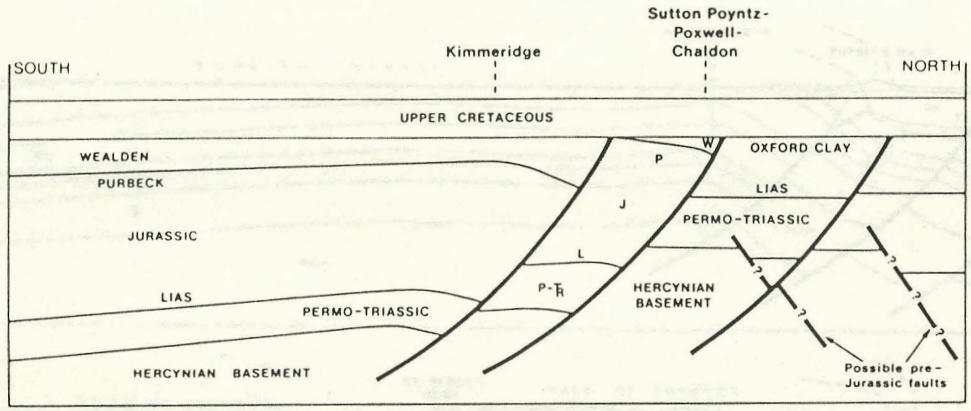

Diagram showing the generalized interpreted profile across south Dorset at the close of the Cretaceous. Not to scale.

Wessex Basin: Austrian Inversion

SOUTHERN ENGLAND — POST INVERSION ie POST PYRENEAN.

Note: contractional faults; local thrust splays high in structural pile.

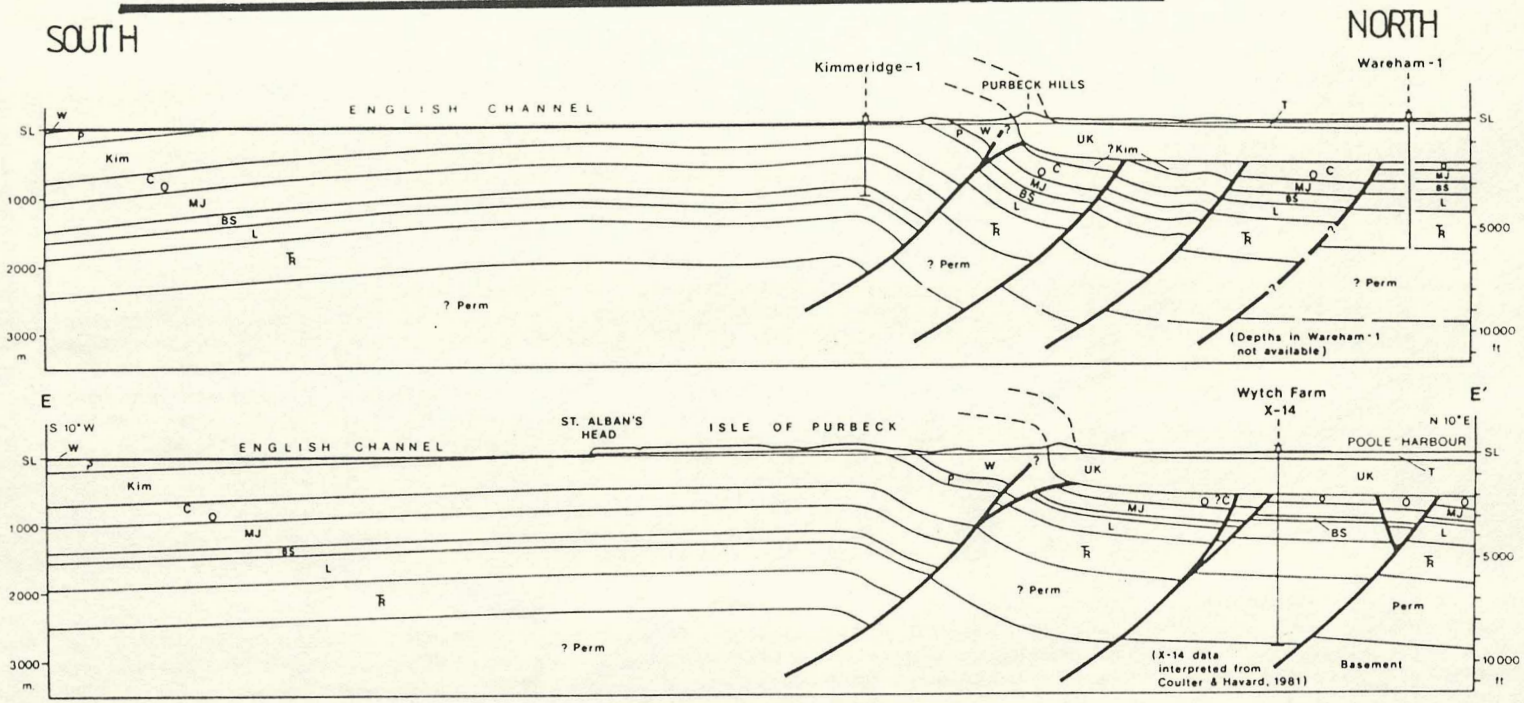

Interpretive cross-sections A–A′, B–B′, C–C′, D–D′ and E–E′ across southern Dorset. Natural scale. Abbreviations: T = Tertiary, UK = Upper Cretaceous, W = Wealden, P = Portland & Purbeck, Kim = Kimmeridge Clay, C = Corallian, O = Oxford Clay, MJ = Middle Jurassic, BS = Bridport Sands (shown as a separate unit because of their diachronous nature), L = Lias, TR = Triassic, Perm = Permian.

Fig 8.127. Structural map of NW Santander, after Hines (1986). Note: E - W structures - developed as a result of reactivation of E-W trending Hercynian thrusts.

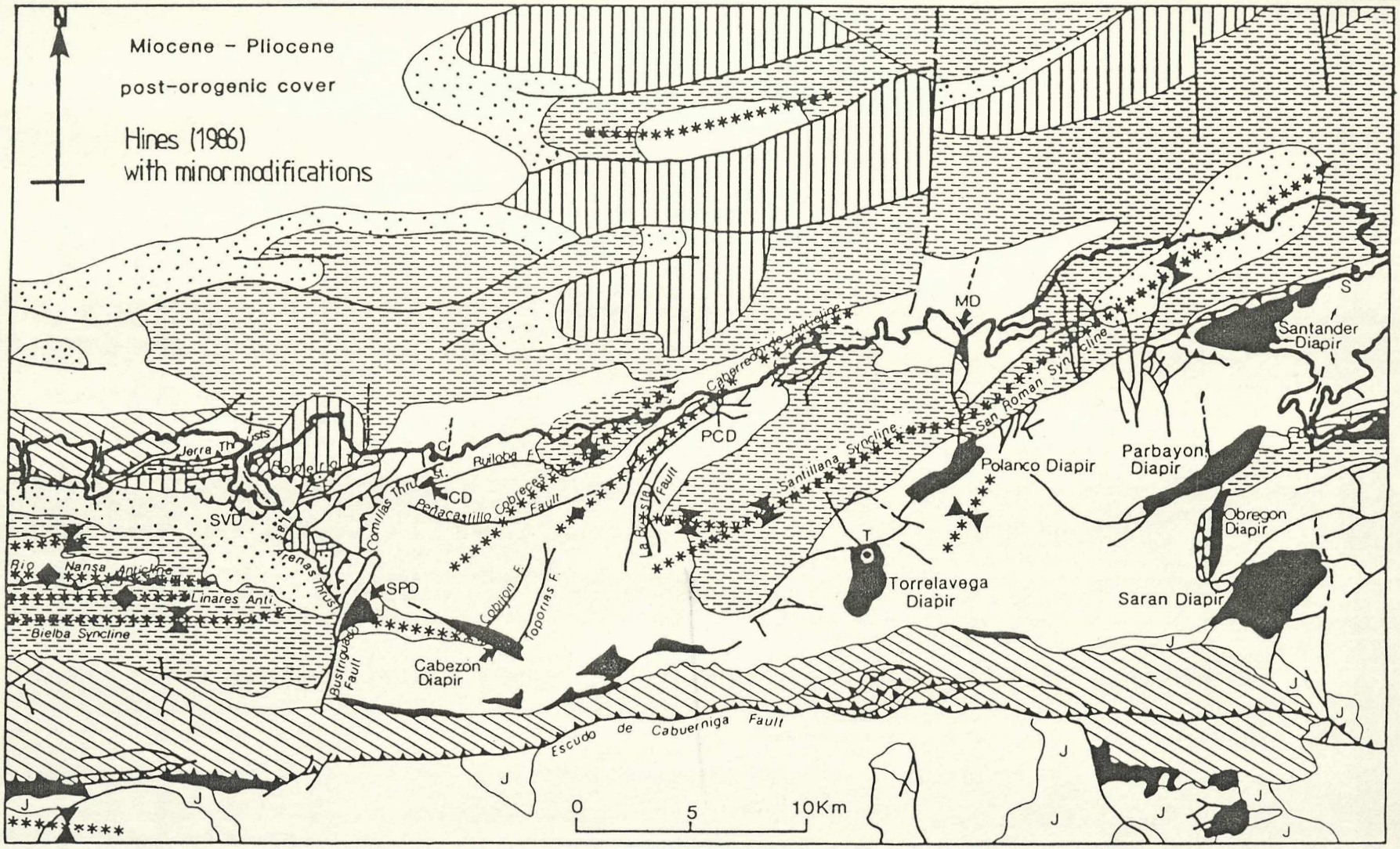

STRUCTURAL MAP OF NORTH-WEST SANTANDER

- Basement
- Keuper Diapir
- J Jurassic
- Lower Cretaceous
- Upper Cretaceous
- Paleocene-Middle Eocene
- Upper Eocene- Oligocene
- Fault
- Thrust
- Anticline
- Syncline
- Plunging fold
- Town

Structural map of northwest Santander. Offshore geology from Boillot et al., (1976). Diapirs : CD-Comillas Diapir, MD-Miengo Diapir, PCD-Punta Calderon Diapir, SPD-San Pedro Diapir, SVD-San Vicente de la Barquera Diapir.
Towns : C-Comillas, S-Santander, T-Torrelavega.

Fig 9.1. Classical view of lacustrine facies distributions, as shown in Picard & High (1981). Concentric arrangement of facies belts. In fact, all of the lake basins given show a marked asymmetry, suggesting that tectonic influences on lacustrine sedimentation patterns are actually very significant.

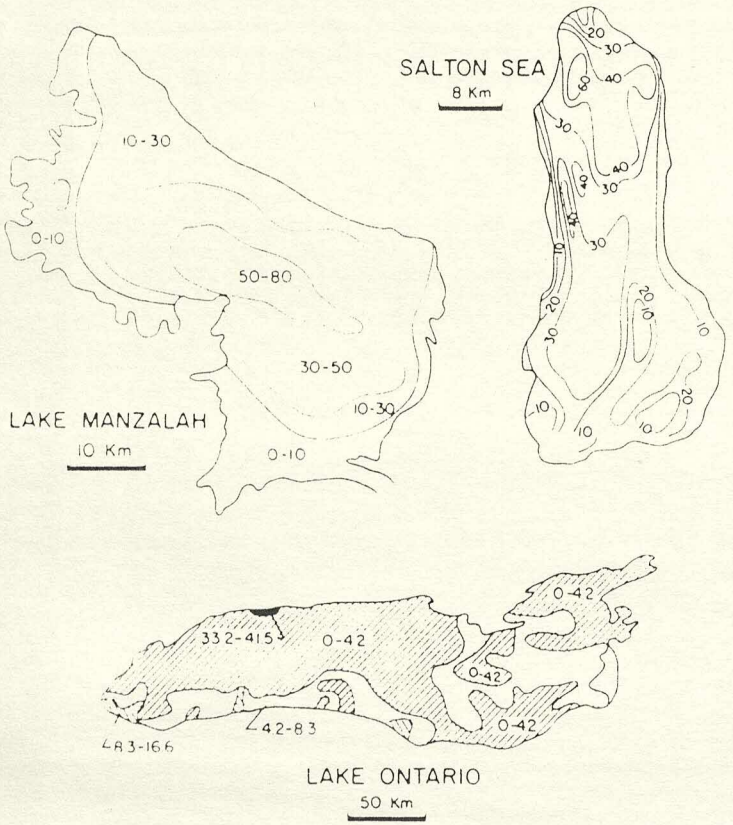

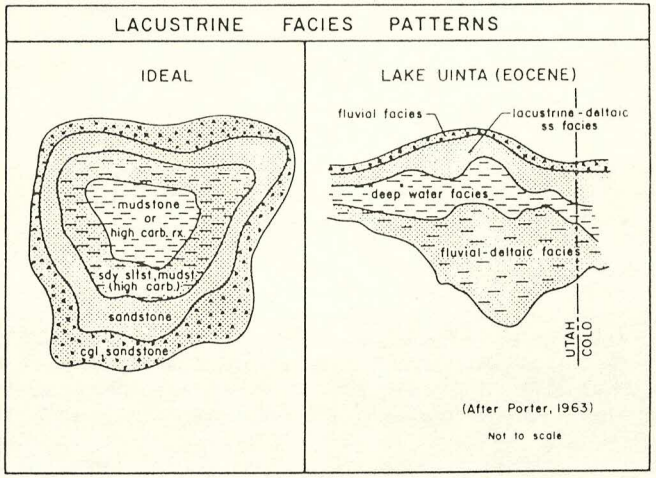

Fig. 8. – Distribution of carbonate sediments in some modern lakes: Lake Manzalah (El-Wakeel and Wahby, 1970); Salton Sea (Arnal, 1961); Lake Ontario (Thomas, Kemp, and Lewis, 1972). See Fig. 3 for Gnadensee

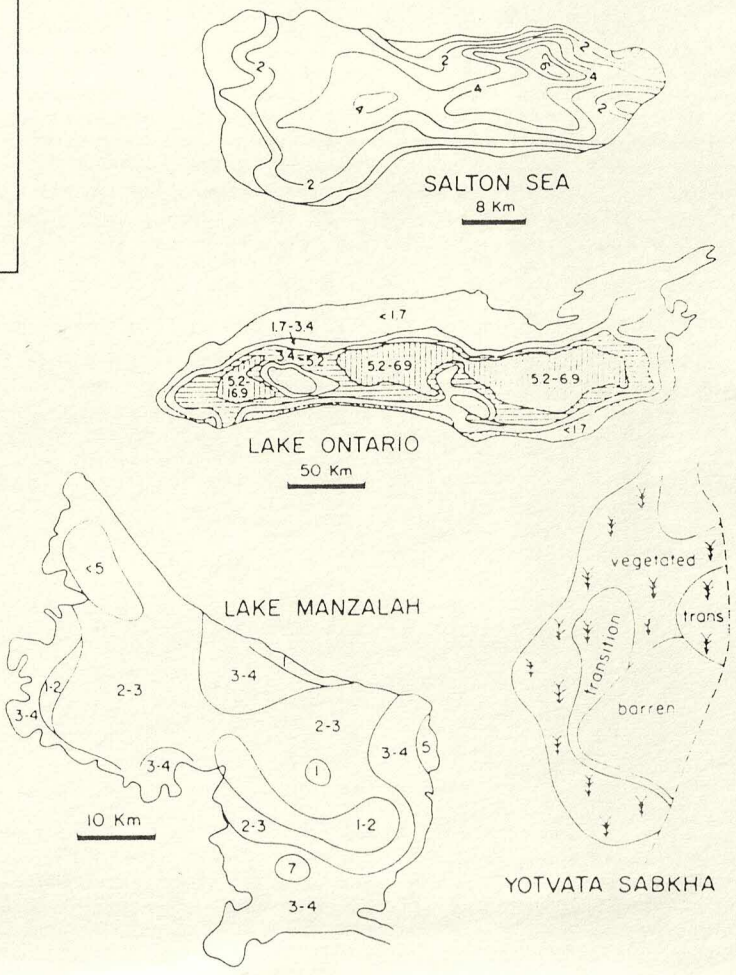

Fig. 9. – Distribution of organic sediments in some modern lakes: Salton Sea (Arnal, 1961); Lake Ontario (Thomas, Kemp and Lewis, 1972); Lake Manzalah (El-Wakeel and Wahby, 1970); Yotvata Sabkha (Amiel and Friedman, 1971)